SIGNALING EVENTS IN REGULATING LEAF SENESCENCE

EDITED BY: Yongfeng Guo, Salma Balazadeh and Nam-Chon Paek

PUBLISHED IN: Frontiers in Plant Science

frontiers Research Topics

ISSN 1664-8714
ISBN 978-2-88974-687-3
DOI 10.3389/978-2-88974-687-3

About Frontiers

Frontiers is more than just an open-access publisher of scholarly articles: it is a pioneering approach to the world of academia, radically improving the way scholarly research is managed. The grand vision of Frontiers is a world where all people have an equal opportunity to seek, share and generate knowledge. Frontiers provides immediate and permanent online open access to all its publications, but this alone is not enough to realize our grand goals.

Frontiers Journal Series

The Frontiers Journal Series is a multi-tier and interdisciplinary set of open-access, online journals, promising a paradigm shift from the current review, selection and dissemination processes in academic publishing. All Frontiers journals are driven by researchers for researchers; therefore, they constitute a service to the scholarly community. At the same time, the Frontiers Journal Series operates on a revolutionary invention, the tiered publishing system, initially addressing specific communities of scholars, and gradually climbing up to broader public understanding, thus serving the interests of the lay society, too.

Dedication to Quality

Each Frontiers article is a landmark of the highest quality, thanks to genuinely collaborative interactions between authors and review editors, who include some of the world's best academicians. Research must be certified by peers before entering a stream of knowledge that may eventually reach the public - and shape society; therefore, Frontiers only applies the most rigorous and unbiased reviews.
Frontiers revolutionizes research publishing by freely delivering the most outstanding research, evaluated with no bias from both the academic and social point of view. By applying the most advanced information technologies, Frontiers is catapulting scholarly publishing into a new generation.

What are Frontiers Research Topics?

Frontiers Research Topics are very popular trademarks of the Frontiers Journals Series: they are collections of at least ten articles, all centered on a particular subject. With their unique mix of varied contributions from Original Research to Review Articles, Frontiers Research Topics unify the most influential researchers, the latest key findings and historical advances in a hot research area! Find out more on how to host your own Frontiers Research Topic or contribute to one as an author by contacting the Frontiers Editorial Office: frontiersin.org/about/contact

SIGNALING EVENTS IN REGULATING LEAF SENESCENCE

Topic Editors:
Yongfeng Guo, Tobacco Research Institute, Chinese Academy of Agricultural Sciences (CAAS), China
Salma Balazadeh, Leiden University, Netherlands
Nam-Chon Paek, Seoul National University, South Korea

Citation: Guo, Y., Balazadeh, S., Paek, N.-C., eds. (2022). Signaling Events in Regulating Leaf Senescence. Lausanne: Frontiers Media SA. doi: 10.3389/978-2-88974-687-3

Table of Contents

frontiers in Plant Science

EDITORIAL
published: 23 February 2022
doi: 10.3389/fpls.2022.860923

Editorial: Signaling Events in Regulating Leaf Senescence

Yongfeng Guo[1]*, *Salma Balazadeh*[2] *and Nam-Chon Paek*[3]

[1] *Tobacco Research Institute, Chinese Academy of Agricultural Sciences (CAAS), Qingdao, China,* [2] *Institute of Biology, Leiden University, Leiden, Netherlands,* [3] *Department of Agriculture, Forestry and Bioresources, Seoul National University, Seoul, South Korea*

Keywords: leaf senescence, signals, transcription factor, senescence-associated genes (SAGs), jasmonic acid (JA)

Editorial on the Research Topic

Signaling Events in Regulating Leaf Senescence

Leaf senescence is a critical stage in plant life cycles and is of great importance in agriculture (Woo et al., 2019; Guo et al., 2021). Initiation and progression of leaf senescence occur under the finely-tuned control of a complex network of signaling events that can be triggered by a variety of signals and environmental cues. Senescence-regulating signals, including age, reproductive growth, phytohormones, abiotic/biotic stresses, and small peptides, as reported recently (Zhang et al., 2021), are often perceived by membrane-localized receptors and transduced into the cells to trigger differential expression of thousands of genes, especially senescence-associated genes (SAGs), many of which function in regulating leaf senescence (Ahmad and Guo, 2019). During the past two decades, a significant number of genes that are involved in senescence regulation have been characterized (Woo et al., 2019; Guo et al., 2021), including transcription factors that are potentially responsible for regulating the massive switch in gene expression during leaf senescence (Kim et al., 2016; Li et al., 2018; Li et al.). The big picture of regulatory networks of leaf senescence, however, remains to be unraveled.

Three of the articles included in this Research Topic are related to senescence- regulating signals. Research progress on senescence regulation by light and circadian clock was summarized in a mini-review by Lee et al.. Involvement of Phytochrome-Interacting Factors (PIFs) from light signaling and core clock components in senescence processes suggested important roles of light as senescence-suppressing and circadian clock as senescence-inducing signals (Lee et al.). ABA has been shown to be a senescence-promoting signal in a number of plant species (Guo et al., 2021). A sharp increase in abscisic acid (ABA) content was detected during winter in senescing leaves and in rhizomes of yellow flag (*Iris pseudacorus*) plants growing in a natural wetland, suggesting a major role of ABA in regulating cold-induced leaf senescence in this wetland plant (Caselles et al.). In studying phytotoxic effects of tropospheric ozone (O_3) on the foliage of hybrid poplar, Turc et al. found that precocious senescence and hypersensitive response-like lesions were induced on leaves after O_3 exposure. Higher O_3 tolerance was observed in younger leaves than older leaves (Turc et al.), confirming the role of O_3 as a senescence-promoting signal.

As critical regulators of gene expression change during leaf senescence, a large number of transcription factors have been characterized to be involved in senescence regulation (Guo, 2013; Woo et al., 2019). In this collection of articles, one NAC and two WRKY transcription factors were studied for their regulatory roles in leaf senescence (Kan et al.; Li et al.; Qiao et al.). The Arabidopsis NAC075 transcription factor was found to function as a negative regulator of leaf senescence. Loss-of-function promoted, while overexpression of *NAC075* delayed senescence of Arabidopsis leaves. Further study

OPEN ACCESS

Edited and reviewed by:
Brad M. Binder,
The University of Tennessee, Knoxville, United States

***Correspondence:**
Yongfeng Guo
guoyongfeng@caas.cn

Specialty section:
This article was submitted to Plant Physiology, a section of the journal Frontiers in Plant Science

Received: *24 January 2022*
Accepted: *31 January 2022*
Published: *23 February 2022*

Citation:
Guo Y, Balazadeh S and Paek N-C (2022) Editorial: Signaling Events in Regulating Leaf Senescence. Front. Plant Sci. 13:860923. doi: 10.3389/fpls.2022.860923

suggested that NAC075 directly suppresses the expression of the antioxidant enzyme gene *CAT2*, thereby promoting the accumulation of reactive oxygen species (ROS) to control leaf senescence (Kan et al.). Similarly, the rice WRKY transcription factor OsWRKY93 was identified as a negative regulator of dark-induced leaf senescence and susceptibility to *Magnaporthe oryzae* infection. CRISPR/Cas9-edited mutants of *OsWRKY93* showed early senescence and higher disease sensitivity while enhanced expression of this gene led to delayed senescence and resistance to *M. oryzae* infection (Li et al.). The wheat WRKY family protein, TaWRKY13-A, on the other hand, acted as a positive regulator of leaf senescence (Qiao et al.). VIGS-silencing of *TaWRKY13-A* led to delayed senescence in leaves whereas overexpression of this gene accelerated the onset of leaf senescence. Moreover, the function of TaWRKY13-A in regulating leaf senescence seemed to be related to the jasmonic acid (JA) signaling pathway (Qiao et al.).

Transcription factors often function in activating the expression of *SAG*s, which leads to the execution of senescence via various biochemical and physiological processes (Guo, 2013; Woo et al., 2019). Some of the SAGs might be involved in protein degradation, such as the Ring/U-box protein AtUSR1, which was shown to be involved in age-dependent and dark-induced leaf senescence in Arabidopsis (Zhang et al.). AtUSR1 was identified as a positive regulator of senescence that functions downstream of the MYC2-mediated JA signaling pathway. MeJA treatment promoted *AtUSR1* expression in a MYC2-dependent manner. While the *myc2* mutation alone caused a delay in leaf senescence, overexpression of *AtUSR1* in the *myc2* background led to precocious senescence (Zhang et al.). Some other senescence-regulating genes encode for catalytic enzymes in various metabolic and biochemical processes. Functional inactivation of UDP-N-acetylglucosamine pyrophosphorylase 1 (UAP1) induced defense-related lesion-mimic spots and early senescence in rice leaves. UAP2 showed similar catalytic activities as UAP1 and overexpression of *UAP2* rescued the *uap1* mutant phenotype. It was suggested that UAP1 and UAP2 play key roles in rice leaf senescence in a synergetic manner (Wang et al.). Another rice gene, *CYP71P1*, was identified via map-based cloning of the causal gene of two lesion mimic mutants (*msl-1* and *msl-2*) obtained from ethyl methyl sulfonate mutagenesis. CYP71P1 is a cytochrome P450 monooxygenase and was shown to be involved in the regulation of leaf senescence and cell death (Zheng et al.). Also identified via map-based cloning, ACCELERATED CELL DEATH 6 (ACD6) is a transmembrane ankyrin repeat protein functioning in sequential and monocarpic senescence in Arabidopsis (Jasinski et al.). The results of ^{15}N partitioning experiments showed that N remobilization efficiency was significantly lower in the *acd6* mutant than the wild type. ACD6 did not affect nitrate uptake efficiency but enhanced nitrogen remobilization to seeds (Jasinski et al.).

Interestingly, most of the senescence regulators described in this Research Topic are also involved in stress responses. OsWRKY93, ACD6, UAP1, and UAP2 are involved in disease resistance (Li et al.; Jasinski et al.; Wang et al.). NAC075, OsWRKY93, AtUSR1, and CYP71P1 are regulators of ROS homeostasis (Kan et al.; Li et al.; Zhang et al.; Zheng et al.). Both AtUSR1 and TaWRKY13-A function through the JA signaling pathway (Zhang et al.; Qiao et al.), which is related to biotic and abiotic stress responses (Wang et al., 2021). All these results indicate extensive cross talk between leaf senescence and stress responses.

AUTHOR CONTRIBUTIONS

All authors contributed to this manuscript and approved the final version.

FUNDING

YG was supported by the Agricultural Science and Technology Innovation Program of China, Chinese Academy of Agricultural Sciences (ASTIP-TRI02), and Funds for Special Projects of the Central Government in Guidance of Local Science and Technology Development (21-1-1-1-zyyd-nsh).

ACKNOWLEDGMENTS

We would like to thank all authors of the articles published in this Research Topic for their contributions, the reviewers and editors for their help in evaluating the manuscripts, and the members of the editorial office for their managerial support.

REFERENCES

Ahmad, S., and Guo, Y. (2019). Signal transduction in leaf senescence: progress and perspective. *Plants (Basel)* 8, 405. doi: 10.3390/plants8100405

Guo, Y. (2013). Towards systems biological understanding of leaf senescence. *Plant Mol. Biol.* 82, 519–528. doi: 10.1007/s11103-012-9974-2

Guo, Y., Ren, G., Zhang, K., Li, Z., Miao, Y., et al. (2021). Leaf senescence: progression, regulation, and application. *Mol. Hortic.* 1, 5. doi: 10.1186/s43897-021-00006-9

Kim, H. J., Nam, H. G., and Lim, P. O. (2016). Regulatory network of NAC transcription factors in leaf senescence. *Curr. Opin. Plant Biol.* 33, 48–56. https://doi.org/10.1016/j.pbi.2016.06.002

Li, Z., Woo, H. R., and Guo, H. (2018). Genetic redundancy of senescence-associated transcription factors in Arabidopsis. *J. Exp. Bot.* 69, 811–823. doi: 10.1093/jxb/erx345

Wang, Y., Mostafa, S., Zeng, W., and Jin, B. (2021). Function and mechanism of jasmonic acid in plant responses to abiotic and biotic stresses. *Int. J. Mol. Sci.* 22, 8568. doi: 10.3390/ijms22168568

Woo, H. R., Kim, H. J., Lim, P. O., and Nam, H. G. (2019). Leaf senescence: systems and dynamics aspects. *Ann. Rev. Plant Biol.* 70, 347–376. doi: 10.1146/annurev-arplant-050718-095859

Zhang, Z., Liu, C., Li, K., Li, X., Xu, M., and Guo, Y. (2021). CLE14 functions as a "brake signal" to suppress age-dependent and stress-induced leaf senescence

by promoting JUB1-mediated ROS scavenging in Arabidopsis. *Mol. Plant*. 15, 179–188. doi: 10.1016/j.molp.2021.09.006

Conflict of Interest: The authors declare that the research was conducted in the absence of any commercial or financial relationships that could be construed as a potential conflict of interest.

Publisher's Note: All claims expressed in this article are solely those of the authors and do not necessarily represent those of their affiliated organizations, or those of the publisher, the editors and the reviewers. Any product that may be evaluated in this article, or claim that may be made by its manufacturer, is not guaranteed or endorsed by the publisher.

frontiers in Plant Science

ORIGINAL RESEARCH
published: 16 December 2020
doi: 10.3389/fpls.2020.608589

Ring/U-Box Protein AtUSR1 Functions in Promoting Leaf Senescence Through JA Signaling Pathway in Arabidopsis

*Zenglin Zhang, Mengmeng Xu and Yongfeng Guo**

Tobacco Research Institute, Chinese Academy of Agricultural Sciences, Qingdao, China

Leaf senescence is regulated by a large number of internal and environmental factors. Here, we report that AtUSR1 (U-box Senescence Related 1) which encodes a plant Ring/U-box protein, is involved in age-dependent and dark-induced leaf senescence in Arabidopsis. Expression of *AtUSR1* gene in leaves was up-regulated in darkness and during aging. Plants of *usr1*, an *AtUSR1* gene knock-down mutant, showed a significant delay in age-dependent and dark-induced leaf senescence and the delayed senescence phenotype was rescued when the *AtUSR1* gene was transferred back to the mutant plants. Meanwhile, overexpression of *AtUSR1* caused accelerated leaf senescence. Furthermore, the role of AtUSR1 in regulating leaf senescence is related to MYC2-mediuated jasmonic acid (JA) signaling pathway. MeJA treatments promoted the accumulation of *AtUSR1* transcripts and this expression activation was dependent on the function of MYC2, a key transcription factor in JA signaling. Dual-luciferase assay results indicated that MYC2 promoted the expression of *AtUSR1*. Overexpression of *AtUSR1* in *myc2* mutant plants showed precocious senescence, while *myc2* mutation alone caused a delay in leaf senescence, suggesting that AtUSR1 functions downstream to MYC2 in the JA signaling pathway in promoting leaf senescence.

Keywords: MYC2, JA, leaf senescence, AtUSR1, ring/U-box

OPEN ACCESS

Edited by:
Alejandro Ferrando, Universitat Politècnica de València, Spain

Reviewed by:
Krzysztof Zienkiewicz, Nicolaus Copernicus University in Toruń, Poland
Yasuhito Sakuraba, The University of Tokyo, Japan

***Correspondence:**
Yongfeng Guo
guoyongfeng@caas.cn

Specialty section:
This article was submitted to Plant Physiology, a section of the journal Frontiers in Plant Science

Received: *21 September 2020*
Accepted: *17 November 2020*
Published: *16 December 2020*

Citation:
Zhang Z, Xu M and Guo Y (2020) Ring/U-Box Protein AtUSR1 Functions in Promoting Leaf Senescence Through JA Signaling Pathway in Arabidopsis. Front. Plant Sci. 11:608589. doi: 10.3389/fpls.2020.608589

INTRODUCTION

As a process of programmed cell death, leaf senescence is important in plants' development and response to environmental stresses (Guo and Gan, 2005; Kim et al., 2018). Under harsh environmental conditions, in order to complete their life cycle, stressed plants often endeavor to reallocate nutrients to reproductive organs via the process of leaf senescence (Sedigheh et al., 2011). Leaf senescence can be induced by a large number of endogenous and environmental factors including age, plant hormones, light conditions, abiotic stresses, and pathogen infection. Once senescence is initiated, significant changes in gene expression, metabolic, and physiological activities take place and the execution of leaf senescence eventually leads to programmed cell death (Quirino et al., 2000; Khanna-Chopra, 2012; Guo, 2013). During senescence, visible leaf yellowing can be observed as the result of chloroplast degeneration which is associated with drastic metabolic reprogramming including degradation of macromolecules, enhanced reactive oxygen species (ROS), and occurrence of membrane ion leakage (Ansari et al., 2014; Gan, 2018). During senescence, the expression of genes related to photosynthesis is down-regulated, whereas genes involved in senescence execution generally have increased expression. Genes encoding components of

protein degradation pathways, for example, comprise a significant proportion of *Senescence Associated Genes* (*SAG*s; Guo et al., 2004; Lim et al., 2007; Gregersen et al., 2008; Zhang et al., 2010). As an essential part of protein degradation, the ubiquitin/26S proteasome pathway is not only important in targeting and degrading proteins, but also involved in regulation of the senescence process. Mutation in several components in the ubiquitin/proteasome system led to altered leaf senescence (Woo et al., 2001; So et al., 2019; Shim et al., 2020), suggesting a regulatory role of the ubiquitin pathway in leaf senescence. As a critical component of the ubiquitin pathway, E3 ubiquitin ligase is involved in polyubiquitination of target proteins and participates in various plant development processes including senescence. In rice, RING-type ubiquitin ligase GW2 acts as a positive regulator of leaf senescence by affecting chlorophyll degradation (Shim et al., 2020). Senescence-associated E3 ubiquitin ligase1/Plant U-box44 (SAUL1/PUB44) regulates dark-induced leaf senescence in Arabidopsis by affecting stability of the chloroplast-localized Abscisic acid (ABA)-responsive factor Senescence-Associated Protein (CSAP; So et al., 2019). RING-type E3 ligases SEVEN IN ABSENTIA OF ARABIDOPSIS THALIANA1 (SINAT1), SINAT2, and SINAT6 control autophagosome formation and leaf senescence via controlling stability of the autophagy-related protein ATG13 in Arabidopsis (Qi et al., 2020). U-box E3 ubiquitin ligases PUB12 and PUB13 play multiple functions in immunity, flowering, and senescence. Loss-of-function mutations of PUB12 and PUB13 led to early senescence phenotypes in Arabidopsis under stress conditions (Zhou et al., 2015). BIG BROTHER (BB) also encodes an E3 ligase and is involved in organ size and leaf senescence. Arabidopsis plants overexpressing *BB* displayed early senescence, while *bb* mutants showed delayed senescence phenotypes (Vanhaeren et al., 2017). In rice, dark-induced senescence results in releasing of cytochrome f (Cyt f) from chloroplasts into the cytoplasm, where Cyt f functions to activate caspase-3-like activities by interacting with E3-ubiquitin ligases and RPN9b, the subunit of the ubiquitin proteasome system, ultimately resulting in programmed cell death (PCD) process (Wang et al., 2014).

Phytohormones play very important roles during leaf senescence. ABA, ethylene, jasmonic acid (JA), and salicylic acid (SA) promote senescence, while cytokinins and auxin inhibit this process (Zhang and Guo, 2018; Woo et al., 2019). As a positive regulator of leaf senescence, JA accumulation increases during senescence (He et al., 2002; Hu et al., 2017). Activation of the JA biosynthetic gene *LIPOXYGENASE2* (*LOX2*) by transcription factor TEOSINTE BRANCHED/ CYCLOIDEA/PCF4 (TCP4) resulted in early senescence (Suraneni et al., 2010). JA-biosynthetic enzyme 3-ketoacyl-CoA thiolase 2 (KAT2) participates in the catabolism associated with senescence, as well in the early events required for leaf senescence (Castillo and Leon, 2008). As a JA receptor, CORONATINE INSENSITIVE 1 (COI1) is an F-box protein forming complexes with JASMONATE ZIM-domain proteins (JAZ) to mediate their degradation via the 26S proteasome pathway (Xie et al., 1998; Thines et al., 2007; Shan et al., 2011; Kim et al., 2013). The JA-insensitive *coi1-1* mutant displays delayed leaf senescence in *Arabidopsis* (Castillo and Leon, 2008). In the rice (*Oryza sativa*) genome, there are three COI homologs named *OsCOI1a*, *OsCOI1b*, and *OsCOI2*, respectively. *oscoi1b-1* mutant plants displayed delayed leaf senescence under dark and natural conditions. *35S*:*OsCOI1a* or *35S*:*OsCOI1b* could rescue the delayed senescence phenotype of *coi1-1* in *Arabidopsis*, indicating that both OsCOI1a and OsCOI1b play a role in promoting leaf senescence in rice (Lee et al., 2015). JAZs function as negative regulators of the JA signaling pathway via repressing transcriptional activation activities of downstream transcription factors (Chini et al., 2007; Song et al., 2011). JAZ proteins form complex with NOVEL INTERACTOR of JAZs (NINJA)/TOPLESS to restrain JA response by directly regulating various transcription factors (Pauwels et al., 2010; Causier et al., 2012; Kim et al., 2013). JAZ4 and JAZ8 were reported to inhibit JA–induced senescence through interacting with transcription factor WRKY57, which was proposed to play as a balance internode between JA and auxin signaling in regulating senescence (Jiang et al., 2014). JA also interacts with ethylene in regulating senescence in which JAZ proteins interact with ETHYLENE-INSENSITIVE3(EIN3) and ETHYLENE-INSENSITIVE3-LIKE 1(EIL1), two of the key components of the ethylene signaling pathway (Zhu et al., 2011). Furthermore, crosstalk between JA and SA in regulating leaf senescence has been reported. Senescence regulating TF *WRKY53* was found to be antagonistically regulated by JA and SA signals (Miao and Zentgraf, 2007). Among the proteins inhibited by JAZ complexes, MYC2, MYC3, MYC4, and MYC5 displayed accelerated protein degradation under dark or shade conditions but were stabilized in light and after JA treatments (Zhu et al., 2015; Yu et al., 2016). These MYC transcription factors have been shown to be involved in multiple JA response processes via regulating expression of JA responsive genes (Figueroa and Browse, 2012; Zhu et al., 2015; Hu et al., 2017). Recently, It was reported that JA inducible gene *DNA binding-with-one-finger 2.1*(*Dof2.1*) functions in enhancing JA-induced leaf senescence via a MYC2–Dof2.1–MYC2 feed-forward loop (Zhuo et al., 2020).

Dark-induced leaf senescence has been widely studied, in which Ethylene, JA, and Nitric oxide (NO) all play regulatory roles (Fujiki et al., 2001). NO was shown to be involved in regulating dark-induced senescence via ETHYLENE INSENSITIVE 2(EIN2) of the ethylene signaling pathway (Niu and Guo, 2012; Liu and Guo, 2013). It has been shown that endogenous JA content and expression of JA biosynthetic genes increased during dark-induced senescence (Hu et al., 2017; Huang et al., 2017). JAZ7 was reported to regulate dark-induced senescence by interacting with COI1 and MYC2. In *Arabidopsis,* knock-out mutant of *JAZ7* displayed accelerated senescence (Yu et al., 2016). Previous study has demonstrated that MYC2 regulated JA-induced leaf senescence in Arabidopsis by binding to the promoter and activating the expression of SENESCENCE-ASSOCIATED GENE 29(*SAG29*). On the other hand, the bHLH transcription factors (TF) including bHLH03, bHLH13, bHLH14, and bHLH17 repressed the senescence process via antagonistically binding to the promoter and repressing the expression of *SAG29*, resulting in fine-tuned control of JA-induced leaf senescence which assists plants in adapting various environmental changes (Qi et al., 2015). Additionally, ROS plays

important roles in JA-induced leaf senescence. JA enhances the accumulation of H_2O_2 and reduced H_2O_2 content suppresses JA-induced leaf senescence. Results from a recent study revealed that MYC2 was involved in JA-induced H_2O_2 accumulation through down-regulating the expression of *CATALASE 2* (*CAT2*) by directly binding to its promoter (Zhang Y. et al., 2020).

Leaf senescence is regulated by a large number of different signals with complex cross-talks among different signaling pathways. Identification and characterization of key senescence regulators that modulate different signaling pathways are therefore of great significance in understanding the molecular mechanisms underlying leaf senescence. In this study, we identified a novel senescence regulator, Ring/U-box protein AtUSR1. Expression of *AtUSR1* was induced by age, darkness, and several plant hormones including JA and ABA. Functional analyses revealed that AtUSR1 plays a positive role in regulating leaf senescence, potentially through regulating the JA signaling pathway. Further study demonstrated that MYC2 can regulate *AtUSR1* expression and AtUSR1 likely functions downstream of the JA-MYC2 signaling pathway in regulating leaf senescence.

MATERIALS AND METHODS

Plant Materials, Growth Conditions, and Stress Treatments

Arabidopsis thaliana ecotype Col-0 was used in this study. The *usr1* (*Salk_095353*) and *myc2* [*Salk_017005*, also referred as *jin1-9* (Lorenzo et al., 2004; Jung et al., 2015)] mutant lines were obtained from the Arabidopsis Biological Resource Center (ABRC). Mutants homozygous were obtained by genotyping. Arabidopsis seeds were sterilized in 70% ethanol for 3 min, then washed 3 times by sterile water, and placed on 0.5 × Murashige and Skoog (MS) medium plates, stratified at 4°C for 3 day in the dark, then transferred into continuous light conditions for germination. Plants were grown in soil at 22–24°C under continuous light (100 μmol m^{-2} s^{-1}) conditions in a growth room.

For dark treatments of detached leaves, the fifth or sixth leaves from 30-day-old plants were detached and treated in the dark for designated time on filter papers soaked with treatment buffer (3 mM MES, 0.5 × MS, pH 5.8). For dark-induced senescence of attached leaves, fully expanded non-senescence leaves were wrapped with aluminum foil for 6 days.

For hormone treatments, fully expanded non-senescence leaves of 4-week-old plants were detached and immersed in hormone treatment solutions (3 mM MES, 0.5 × MS, pH 5.8) with or without phytohormones (10 μM ABA, 50 μM MeJA, 50 μM IAA, or 10 μM 1-aminocyclopropane-1-carboxylic acid (ACC)) for designated time.

Generation of Constructs and Transgenic Plants

To generate the *35S*::*AtUSR1* construct, full-length coding sequence (CDS) of *AtUSR1* was polymerase chain reaction (PCR)-amplified and cloned into the pEarleyGate202 (Earley et al., 2006) vector with via gateway cloning methods according to the manufacturer's instructions (Invitrogen). To obtain the *AtUSR1* complementation construct, *AtUSR1* genomic DNA including the promoter region was PCR-amplified using primers proUSR1-gate-F and AtUSR1gateOER and subcloned into pEarleyGate302 (Earley et al., 2006). To obtain the *proUSR1*::*GUS* construct, the promoter of *AtUSR1* was obtained using primers proUSR1-Glucuronidase (GUS)-F/R, then subcloned into pCAMBIA3301-GUS vector (Abdollahi et al., 2007)at the restriction enzymes digest sites HindIII and NcoI. To generate Dual-luciferase assay constructs, the promoter of *AtUSR1* was amplified using primers proUSR1-pGreenHindIIIF and proUSR1-pGreenBamH1R, then subcloned into the pGreenII 0800-LUC vector at the HindIII and BamH1 sites. Transgenic plants were obtained via the floral-dip method (Clough and Bent, 1998). T3 generation of overexpression plants were used for phenotyping analysis. Primers used in this study are listed in **Supplementary Table 1**.

β-Glucuronidase Staining Assay

Histochemical staining was carried out as described previously (Jefferson et al., 1987). Briefly, the sixth leaves of 4-week-old transgenic plants harboring the *proUSR1*::*GUS* construct were incubated in the 5-bromo-4-chloro-3-indolyl-β-D-glucuronide solution (0.5 g/mL of 5-bromo-4-chloro-3-indolyl-β-D-glucuronide, 0.5 mM of potassium ferricyanide, 0.5 mM of potassium ferrocyanide, and 0.1 M of sodium phosphate, pH 7.4) at 37°C for 12 h. Subsequently, the leaves were decolorized in 100% (v/v) ethanol.

Nitro-Blue Tetrazolium Chloride Staining Assay and H_2O_2 Measurement

Nitro-blue tetrazolium (NBT) chloride staining was carried out as previously described (Zhang Z. et al., 2020). Briefly, the fifth leaves of 4-week-old plants were detached and incubated in the NBT staining buffer (0.5 mg/mL NBT in 10 mM potassium phosphate buffer, pH 7.6) overnight, then decolorized in the fixative solution (ethanol: acetic acid: glycerol, 3:1:1) and kept in the ethanol: glycerol (4:1) solution at 4°C. Quantitative H_2O_2 measurement was performed according to the methods described previously (Lee et al., 2012).

Chlorophyll, *Fv*/*Fm*, and Membrane Leakage Rate Measurement

Chlorophyll was extracted from leaves at different growth stages using 95% ethanol, and chlorophyll content was determined by detecting the absorbance at 665 nm and 649 nm using a UV2400 UV/VIS spectrophotometer as previously described (Zhang and Guo, 2018). The photochemical efficiency of photosystem II (PSII; *Fv*/*Fm*) was measured using a Chlorophyll Fluorescence Imaging System (Technologica, United Kingdom). Measurements of relative electrolyte leakage were carried out using a bench-top conductivity meter (CON500, CLEAN Instruments). Detached leaves were collected and washed three times using deionized water and immersed in water. Initial conductivity data was collected using the conductor

followed by a final conductivity data reading after boiling in 100°C for 10 min to maximum membrane disruption. Total membrane ion leakage was calculated as following: initial conductivity/final conductivity × 100%. Membrane leakage rate was described in the form of percentage of initial conductivity over final conductivity, with 100% ion leakage meaning complete disruption of the membrane system.

qRT-PCR Analysis

Total RNA was extracted using TRIzol following the manufacturer's instructions (Invitrogen). The first-strand cDNA was obtained by the Transgene Kit (Transgene Company), which includes the elimination of contaminant genomic DNA. qRT-PCR was carried out using the SYBR Premix Ex Taq (Takara). Each reaction was designed with three technical replicates. Data analysis was done using the $2^{-\Delta\Delta Ct}$ method (Livak and Schmittgen, 2001). The Ct was calculated using the *ACTIN2* gene as an internal control. Three biological replicates were performed for each genotype. Primers used are listed in **Supplementary Table 1**.

Dual-Luciferase Assay

For dual-luciferase assay, the pGreenII 0800-LUC vector (Hellens et al., 2000) harboring a firefly luciferase (LUC) gene driven by the *AtUSR1* promoter was generated. The Renilla luciferase (REN) gene driven by the *CaMV35S* promoter was used as an internal control. *35S::AtUSR1* was inserted into the effector plasmid. The reporter and effector plasmids were co-transformed into Arabidopsis mesophyll protoplasts isolated from young and senescence leaves of 4-week–old plants according to the methods described previously (Zhuo et al., 2020). Dual-luciferase assay was performed according to the manufacturer (Promega), Briefly, the luciferase extracted by Passive Lysis buffer (PLB), then value of firefly and REN was obtained in an muti-mode microplate reader (TECAN, Infinite M200 PRO).

Accession Numbers

The accession numbers for the genes mentioned in this article are listed as follows: *AtUSR1*(At1g14200), *MYC2* (At1g32640), *MYC3*(At5g46760), *MYC4*(At4g17880), *MYC5*(At5g46830), *WRKY57*(At1g69310), *JAZ7*(At2g34600), *SAG12*(At5g45890), *SAG13*(At2g29350), *RBCS3B*(At5g38410), *LOX2*(At3g45140), and *ACTIN2*(At3g18780).

RESULTS

Expression of *AtUSR1* Is Associated With Leaf Senescence

To identify new regulators of leaf senescence, the GENEVESTIGATOR database[1] was analyzed and a RING/U-box gene named *AtUSR1* (*U-box Senescence Related 1,* At1g14200), was identified to have enhanced expression in senescing leaves. Results of qRT-PCR analysis showed that *AtUSR1* was significantly up-regulated in senescing leaves (**Figure 1A**). Within an individual leaf, significant increase of *AtUSR1* expression was observed from the base to the tip where senescence has been initiated (**Figure 1B**). Expression of SENESCENCE-ASSOCIATED GENE 12 (*SAG12*) was used as an indicator of senescence progress in these analyses. Different from the expression of *SAG12*that was not detected until the last stage of leaf senescence, the expression peak of *AtUSR1* appeared at the early senescence stage. Under darkness, the level of *AtUSR1* transcripts in detached leaves increased gradually and reached a peak at 12 h after dark treatments (**Figure 1C**).

At different leaf developmental stages, as indicated by GUS staining of *proAtUSR1*::*GUS* transgenic plants, higher promoter activities of *AtUSR1* were detected in yellowing leaves with dark blue staining, whereas less *AtUSR1* promoter activities were detected in younger leaves with light blue staining (**Figure 1D**).

We further analyzed the effect of phytohormones on the expression of *AtUSR1*. No obvious difference was detected when leaves were treated with ACC or IAA, while significant increase of *AtUSR1* expression was observed when leaves were treated with JA or ABA (**Figure 1E**).

Leaf Senescence Is Delayed in the *usr1* Mutant

To investigate the function of AtUSR1 in leaf senescence, we obtained an AtUSR1 knock-down mutant (*usr1*) in which a T-DNA fragment is inserted in the 5′UTR region of this gene (**Supplementary Figure 1A**). The *AtUSR1* expression level was significantly lower in *usr1* than in WT Col-0 (**Supplementary Figure 1B**). A complementation assay was carried out in which the full length genomic DNA of *AtUSR1* (*proAtUSR1*::*AtUSR1*) was used to transform the *usr1* mutant to generate complementation plants. Under our growth conditions, older leaves from 6-week-old Col-0 plants started to exhibit visible yellowing, while the counterpart leaves from *usr1* plants were still green. The complementation plants displayed similar senescence progress to Col-0 (**Figures 2A,B**), indicating that the *proUSR1*::*AtUSR1* transgene was able to rescue the delayed senescence phenotype of *usr1* plants.

Total chlorophyll contents of the 4th and 7th leaves of *usr1* plants were significantly higher than that of Col-0 (**Figure 2C**). As an indicator of photosynthetic efficiency, the *Fv/Fm* ratio in *usr1* leaves was significantly higher than Col-0 (**Figure 2D**). Meanwhile, the complementation plants displayed similar chlorophyll contents and *Fv/Fm* values to Col-0 (**Figures 2C,D**). Similarly, the *usr1* mutant displayed lower transcripts of the senescence marker genes *SAG12* and *SAG13* but higher expression of the photosynthetic gene *RBCS* compared with Col-0 and the complementation plants (**Figure 2E**).

In this study, *proUSR1::USR1/usr1* transgenic plants displayed an slightly early senescence phenotype compared with WT (**Figure 2**). One possibility is that multiple copies of the T-DNA insertion led to higher expression of *AtUSR1* than WT (**Supplementary Figure 1**).

[1]https://www.genevestigator.com/gv/index.jsp

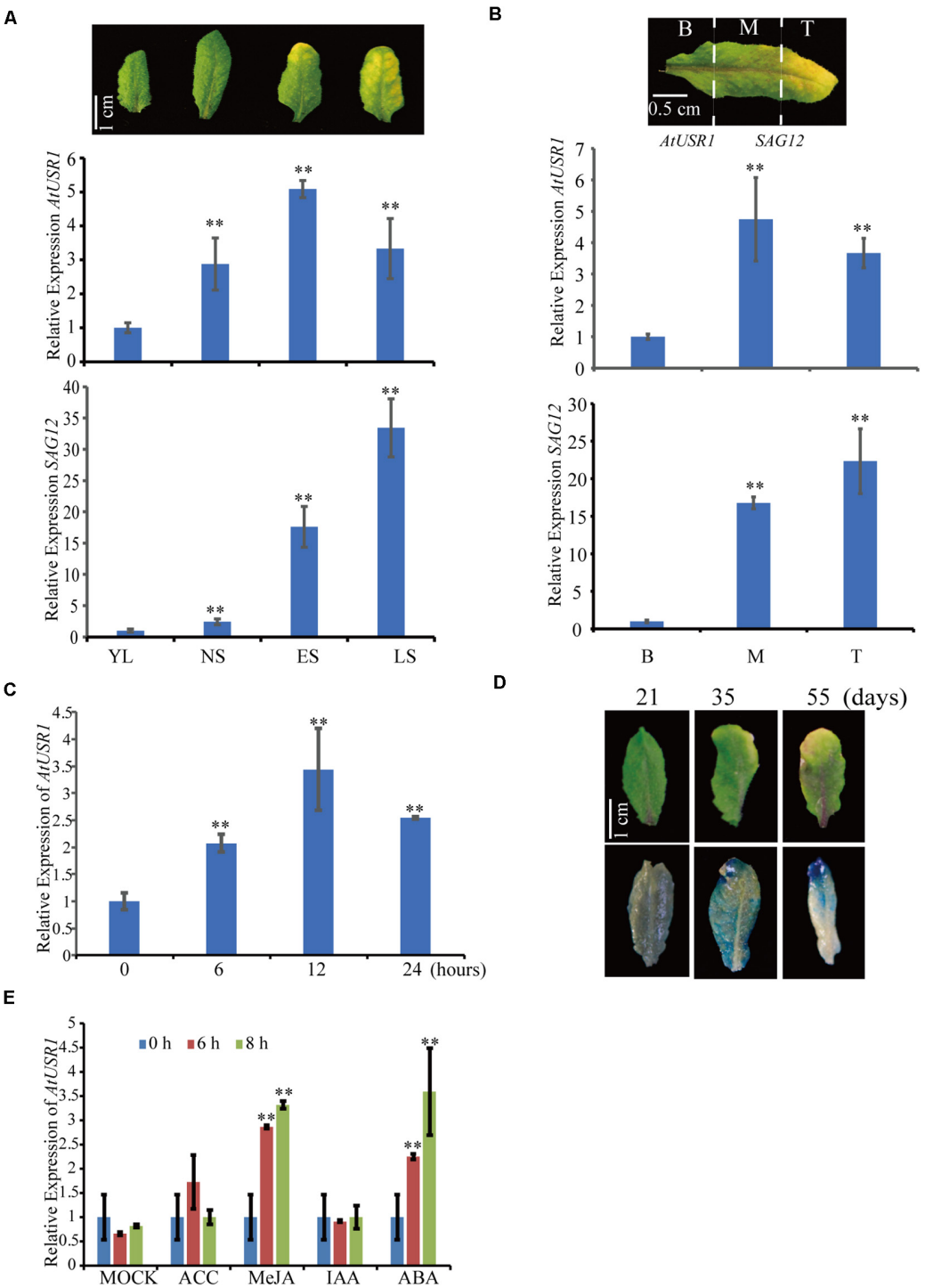

FIGURE 1 | The expression pattern of *AtUSR1*. **(A)** The transcript level of *AtUSR1* was enhanced in an age dependent manner and reached its peak at the ES stage. According to the description of Guo and Gan (2006), gene expression was detected at four different stages of leaf senescence in Arabidopsis. YL, young leaves; NS, fully expanded mature leaves without senescence symptoms; ES, early senescent leaves; and LS, late senescent leaves. The relative values of gene expression (*AtUSR1* and *SAG12*) were calculated based on comparison with gene expression from YL, which was set as 1. **(B)** The expression pattern of *AtUSR1* in indifferent parts of a yellowing leaf; B, Base; M, Middle; and T, Tip. **(C)** The expression pattern of *AtUSR1* under dark conditions. The relative values of gene expression were calculated based on comparison with gene expression from **B**, which was set as 1. **(D)** Histochemical staining of GUS activity detection in leaves at different timepoints as indicated. **(E)** The expression of *AtUSR1* was induced by MeJA and ABA treatments. * and ** indicate significant difference at $0.01 < P < 0.05$ and $P < 0.01$ levels using student's *t*-test. Data are shown as the mean ± SD from three independent experiments. Significance analysis was only performed on *AtUSR1* expression.

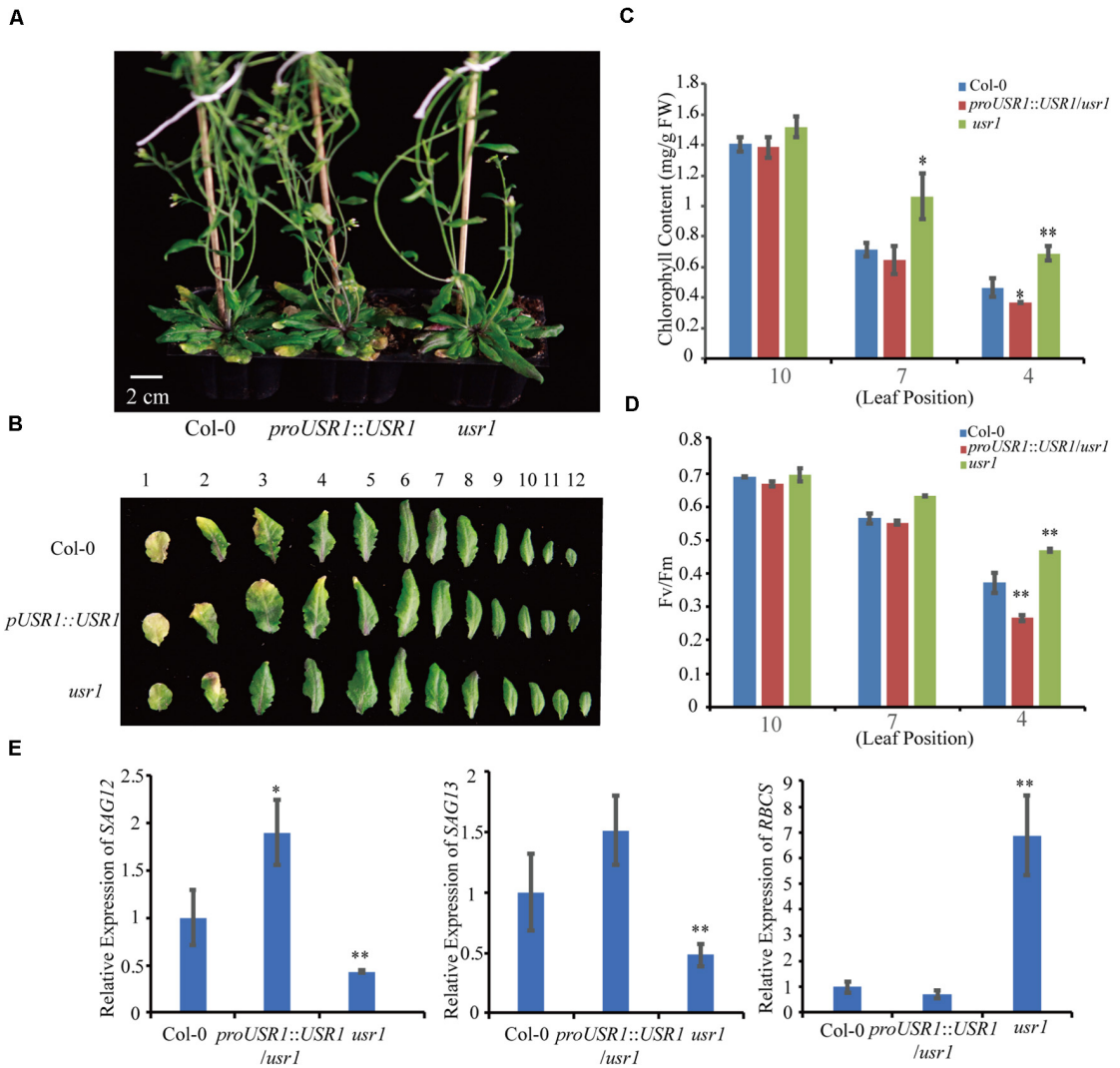

FIGURE 2 | The *usr1* mutant plants show delayed leaf senescence. **(A)** The senescence phenotype of plants with different genotype as indicated after grown under continuously light for 40 days. *usr1* mutant shows delayed leaf senescence and complementation plants *proUSR1*::*USR1*/*usr1* rescued the delayed leaf senescence phenotype of *usr1* plants. **(B)** Senescence phenotypes of detached 1st–12th leaves of different genotypes as indicated. **(C,D)** Chlorophyll content and *Fv/Fm* detection of leaves from different leaf positions in Col-0, *usr1*, and *proUSR1*::*USR1*/*usr1* plants as indicated. **(E)** Expression of *SAGs* genes including *SAG12*, *SAG13*, and *RBCS* in plants of different genotypes as indicated. Single and double asterisk indicate significant difference at $0.01 < P < 0.05$ and $P < 0.01$ levels using student's *t*-test. Data are shown as the mean ± SD from three independent experiments.

Overexpression of *AtUSR1* Accelerates Leaf Senescence

To further understand the role of AtUSR1 in leaf senescence, transgenic plants harboring *35S*::*AtUSR1* were generated and two representative lines (*35S*::*AtUSR1#1, 35S*::*AtUSR1#6*) were used for further characterization (**Supplementary Figure 2**). Under continuous light, 5-week-old plants of *35S*::*AtUSR1#1* and *35S*::*AtUSR1#6* displayed a premature leaf senescence phenotype compared with Col-0 (**Figures 3A,B**). Consistent with the visible phenotype, chlorophyll levels, and *Fv/Fm* ratios of both *AtUSR1* overexpression lines were lower than Col-0 (**Figures 3C,D**). The expression of *SAG12* and *SAG13* was significantly increased while the expression of *RBCS* was reduced in *AtUSR1* overexpression plants compared with Col-0 (**Figure 3E**). Together, these results suggested that AtUSR1 acted as a positive regulator of leaf senescence.

AtUSR1 Promotes Dark-Induced Senescence

Since *AtUSR1* expression was induced by both senescence and darkness, we studied the role of AtUSR1 in dark-induced senescence. After incubated under dark conditions for 5 days, detached leaves of the *usr1* mutant retained green color while the *35S*::*AtUSR1*#1 and *35S*::*AtUSR1*#6 leaves showed accelerated leaf yellowing compared to that of Col-0 (**Figure 4A**). Total chlorophyll levels and *Fv/Fm*

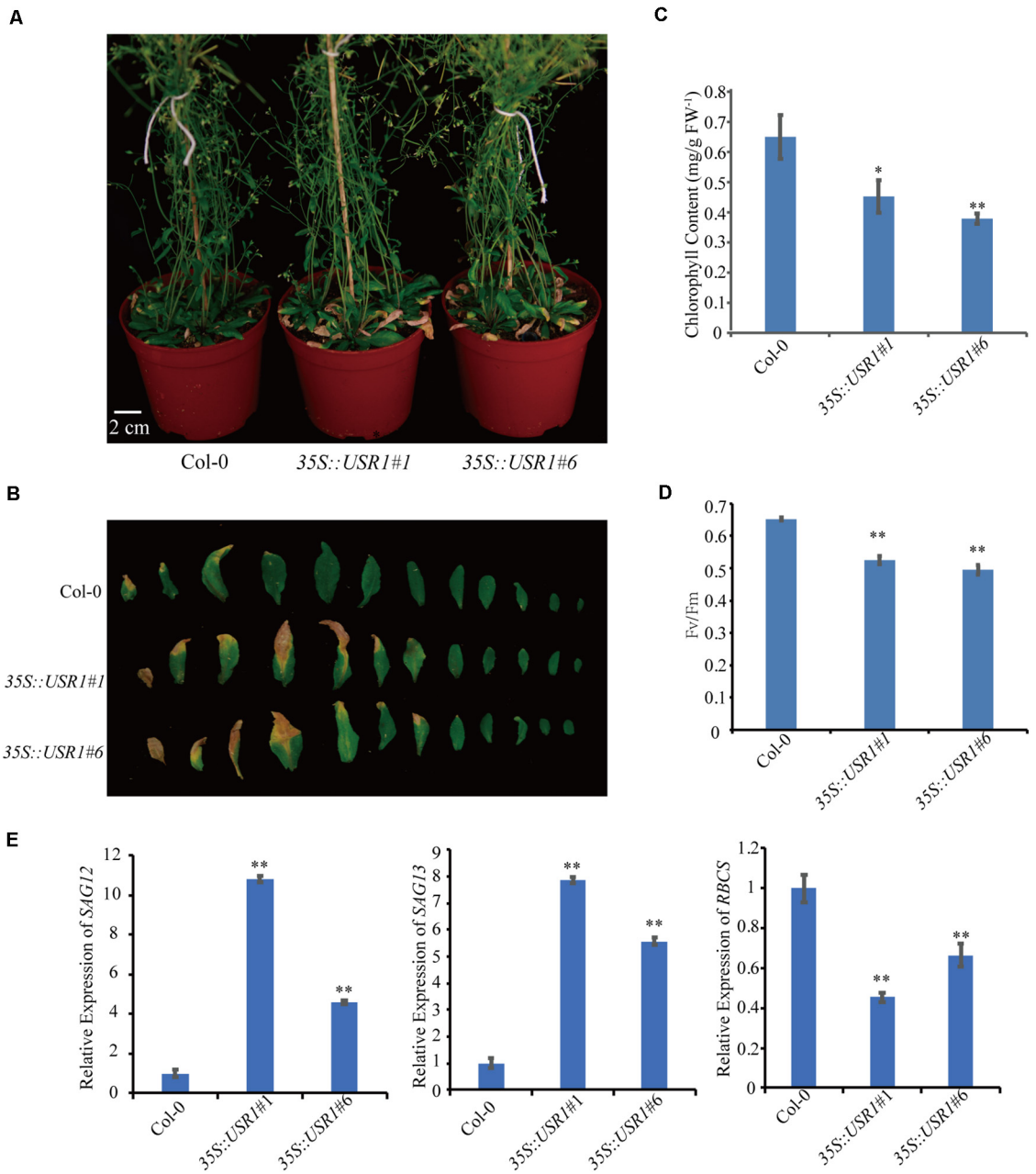

FIGURE 3 | *AtUSR1* overexpression accelerates leaf senescence. **(A)** The precocious senescence phenotype of *AtUSR1* overexpression lines after grown under continuously light condition for 40 days. **(B)** The phenotype of 1st–12th leaves detached from plants with different genotypes. **(C,D)** Chlorophyll content and *Fv/Fm* detection at different leaf positions in Col-0, two independent *AtUSR1* overexpression plants as indicated. **(E)** Expression pattern of *SAG12*, *SAG13*, and *RBCS* in plants overexpressing *AtUSR1* and in Col-0. Single and double asterisk indicate significant difference at $0.01 < P < 0.05$ and $P < 0.01$ levels using student's *t*-test. Data are shown as the mean ± SD from three independent experiments.

ratios of the *AtUSR1*-overexpressing lines were significantly lower than the *usr1* mutant after the dark treatment (**Figures 4B,C**).

We also studied dark-induced senescence of attached leaves from Col-0, *AtUSR1* overexpression, and *usr1* plants. Fully expanded non-senescence leaves were wrapped with aluminum foil for dark treatments. 6 days after treatments, the wrapped leaves of *usr1* plants stayed green while dark-treated leaves of the *35S::AtUSR1* lines displayed senescence symptoms compared with Col-0 (**Supplementary Figure 2A**). Compared to Col-0, chlorophyll content was higher in leaves of *usr1* and lower in *35S::AtUSR1* leaves while membrane leakage rates were lower in *usr1* leaves and higher in *35S::AtUSR1* leaves (**Supplementary Figures 2B,C**). The above described

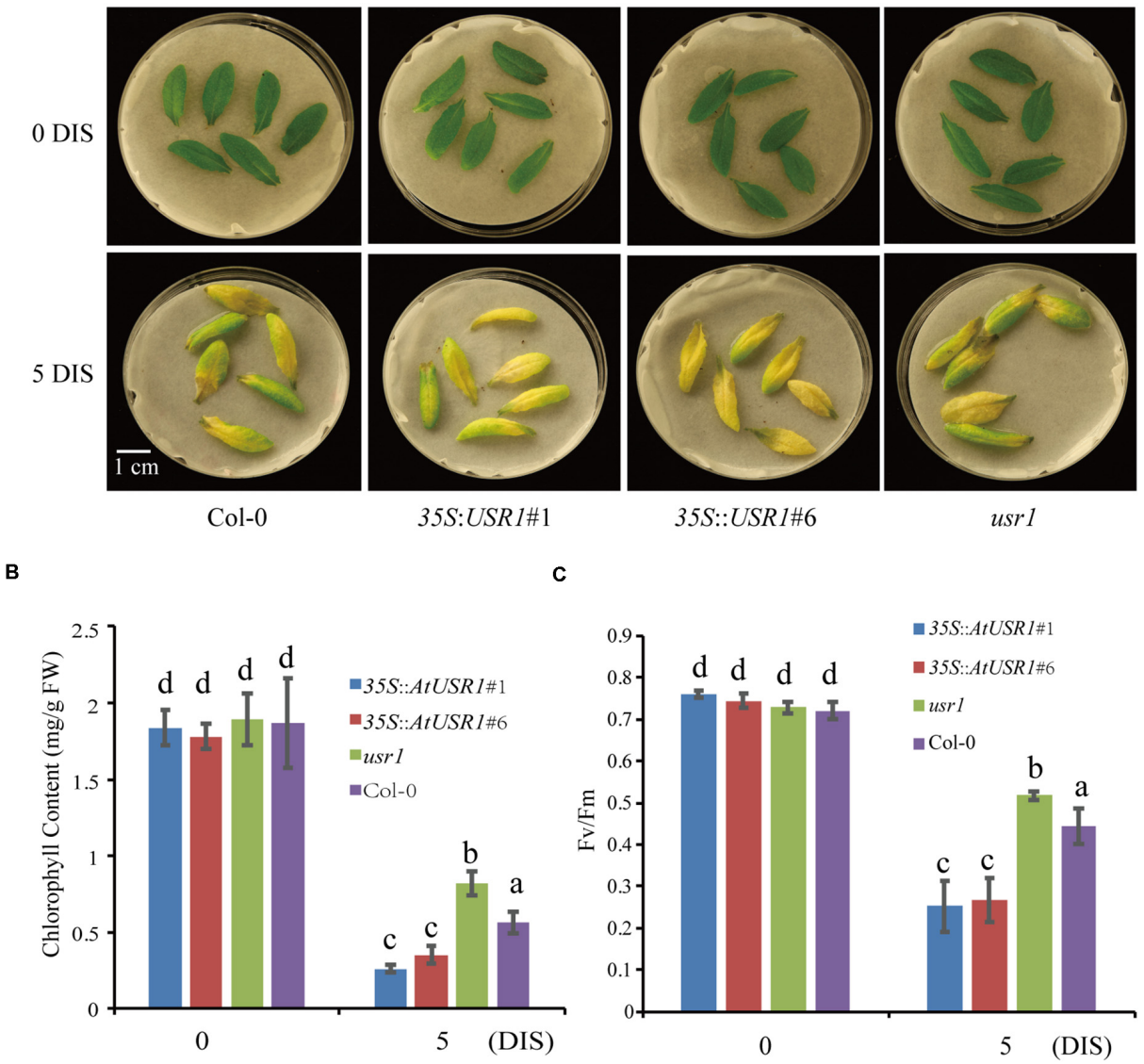

FIGURE 4 | AtUSR1 is involved in dark-induced leaf senescence. **(A)** *AtUSR1* Overexpression lines displayed precocious leaf senescence while the *usr1* mutant showed delayed senescence under dark conditions. **(B,C)** Total chlorophyll content and *Fv/Fm* of different genotypes as indicated. The data in **(B,C)** different letters above columns indicate significant differences according to Duncan's multiple range test ($P < 0.05$). Data are shown as the mean ± SD from three independent experiments.

results suggested that AtUSR1 positively regulates dark-induced senescence as well.

AtUSR1 Affects ROS Homeostasis

Reactive oxygen species play important roles in senescence as well as stress responses (Sedigheh et al., 2011; Jajic et al., 2015). Cellular levels of ROS in fully expanded non-senescence leaves with different genotypes were measured by NBT staining and H_2O_2 quantification. The results showed that leaves of the *35S::AtUSR1* lines displayed stronger while the *usr1* mutant showed weaker NBT staining compared with Col-0, suggesting that AtUSR1 rendered plant accumulating more ROS in leaves (**Figure 5A**). Leaves from *35S::AtUSR1*#1 to *35S::AtUSR1*#6 lines contained significantly higher amount of H_2O_2 while the *usr1* mutant had lower levels of H_2O_2 accumulation compared with Col-0 (**Figure 5B**).

AtUSR1 Is Involved in JA-Mediated Senescence

Jasmonic acid is a senescence-promoting signal in both age-dependent and dark-induced senescence (Yu et al., 2016; Hu et al., 2017). Our data indicated that *AtUSR1* expression

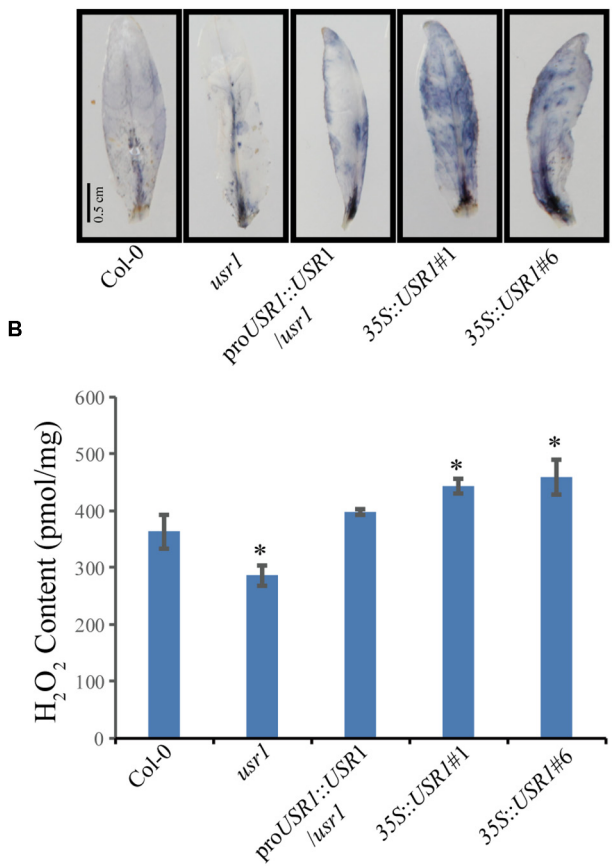

FIGURE 5 | AtUSR1 affects ROS accumulation. **(A)** The NBT staining results of leaves from different genotypes. **(B)** Accumulation of H_2O_2 in detached leaves of different genotypes as indicated. *Indicate significant difference at $0.01 < P < 0.05$ levels using student's *t*-test. Data are shown as the mean ± SD from three independent experiments.

was up-regulated by JA treatments (**Figure 1E**). We therefore tested the role of AtUSR1 in JA-induced senescence. After treated with exogenous MeJA for 5 days, detached leaves from *35S::AtUSR1* plants were completely yellow, while *usr1* leaves remained mostly green and leaves of Col-0 were in-between (**Figure 6A**). Chlorophyll content and *Fv/Fm* ratio data also indicated that the *usr1* mutation delayed while *AtUSR1* overexpression accelerated JA-induced senescence on detached leaves (**Figures 6B,C**).

AtUSR1 Functions Downstream to MYC2 in Regulating Leaf Senescence

Previous studies have demonstrated that MYC2 plays an essential role in JA-induced senescence (Yu et al., 2016). Transcription factor MYC2 binds to the G-box motif (CACGTG) and its variants such as E-box (CANNTG), G/A box (CACGAG), and G/C box (CACGCG) to regulate expression of target genes (Dombrecht et al., 2007; Zhuo et al., 2020). Interestingly, using PLACE[2], we have identified a E-box [CAN(A)N(T)TG] motif in the promoter region of *AtUSR1* (−130 bp to −124 bp upstream of the translation start site).

We then examined the expression of *AtUSR1* in the *myc2* mutant under MeJA treatments. Detached fully expanded leaves were treated with MeJA for 8 h, after which *AtUSR1* expression was observed to be significantly increased in Col-0 but this increase was significantly reduced in the *myc2* mutant (**Figure 7A**), suggesting that the JA-induction of *AtUSR1* expression is partially MYC2-dependent.

We further analyzed the MYC2 regulation of *AtUSR1* expression via a dual-luciferase assay. In the reporter construct, the *Firefly luciferase* gene was driven by the *AtUSR1* promoter containing the E-box sequence and the REN gene was used as an internal reference (**Figure 7B**). The reporter construct was used in co-transfecting of Col-0 protoplasts together with an effector construct in which *MYC2* was under the control of the 35S promoter. The ratio of Firefly/Renilla activities was significantly higher when the effector construct harboring *35S::MYC2* was co-transformed with the reporter construct containing the *AtUSR1* promoter. The increase in Firefly/Renilla ratio was not detected when the E-box on the *AtUSR1* promoter was replaced by a mutated sequence (**Figure 7C**). These results suggest that MYC2 could regulate the expression of *AtUSR1* and this regulation is dependent on the E-box on its promoter.

Next, we studied the role of MYC2 in JA-regulated expression of *AtUSR1* using the same dual luciferase strategy. The *35S::MYC2* effector construct was co-transfected with a reporter construct in which firefly LUC was driven by the *AtUSR1* promoter. In the same reporter construct, Renilla LUC driven by the *35S* promoter was used as an internal control. This combination was co-transfected into Col-0 protoplasts with or without JA treatments. The results indicated that Firefly/Renilla was significantly higher under JA treatments compared with the mock. The increase of Firefly/Renilla caused by JA treatments disappeared when *myc2* mutant protoplasts were transfected, suggesting that the MeJA induction of *AtUSR1* promoter activities was affected in the *myc2* mutant (**Figure 7D**).

Mutation of *MYC2* has been reported to delay JA-induced chlorophyll degradation (Zhu et al., 2015). To further study the relationship between *AtUSR1* and MYC2 in JA-induced senescence, we obtained *myc2* mutant plants harboring *35S::AtUSR1* (referred to as *myc2*/*35S::AtUSR1*) and senescence phenotypes of detached leaves were examined in presence of MeJA. Similar to *35S::AtUSR1* leaves that displayed early senescence phenotypes compared to Col-0, leaves of *myc2*/*AtUSR1OE* plants also showed precocious senescence, rescuing the delayed senescence phenotype of the *myc2* mutant (**Figure 7E**). Moreover, the effects of *myc2* mutation on chlorophyll content and *Fv/Fm* of MeJA-treated leaves were reduced by *AtUSR1* overexpression (**Figures 7F,G**). The above-described results suggested that AtUSR1 acted downstream to MYC2 in mediating JA-induced senescence.

[2]https://www.dna.affrc.go.jp/PLACE/?action=newplace

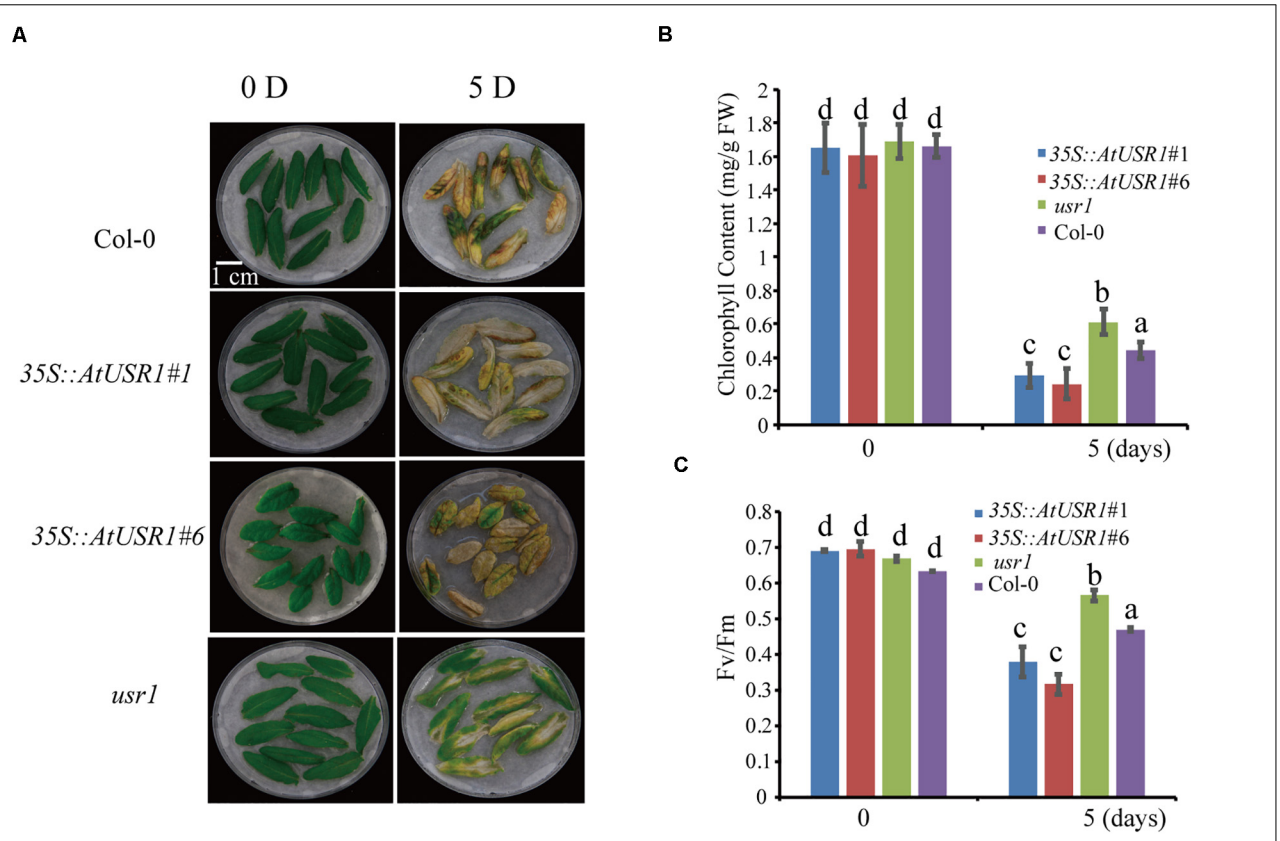

FIGURE 6 | AtUSR1 plays as positive role in JA mediated leaf senescence. **(A)** *AtUSR1* overexpression enhanced JA-induced leaf senescence while *usr1* mutation delayed this process. Detached Sixth leaves of different genotypes were treated with 50 μM MeJA for 5 days. **(B,C)** Total chlorophyll content and *Fv/Fm* in the leaf samples of different genotypes as indicated. The data in **(B,C)** different letters above columns indicate significant differences according to Duncan's multiple range test ($P < 0.05$). Data are shown as the mean ± SD from three independent experiments.

DISCUSSION

As the last stage of development, leaf senescence is a crucial process that influences photosynthetic capacity and reallocation of nutrients from senescing leaves into young leaves and reproductive organs (Ahmad and Guo, 2019; Krieger-Liszkay et al., 2019). Timely senescence is essential for plants' reproductive success. Precocious or early senescence caused by harsh growth conditions, on the other hand, compromises crop yield in an agricultural setting (Wu et al., 2012; Bengoa Luoni et al., 2019). Initiation and progression of leaf senescence can be affected by a large number of endogenous and environmental factors including developmental stage, age, phytohormones, environmental cues such as temperature, darkness, and pathogens (Bresson et al., 2018). All these factors and related signaling pathways form a complex network in fine-tuning the initiation and progression of leaf senescence. Identifying senescence-regulating genes and clarifying their functions are of great importance in devising genetic strategies of manipulating senescence for improving crop yield and production traits (Jing and Nam, 2012).

A large number of genes undergo substantial changes in expression during senescence, including genes related to protein degradation, nutrient remobilization, chlorophyll metabolism, and transcription regulation (Sato et al., 2009; Goud and Kachole, 2011; Izumi and Ishida, 2011; Sakuraba et al., 2012; Tamary et al., 2019). Also included are regulators involved in signaling transduction in response to phytohormones such as ethylene, JA, ABA, auxin, and cytokinins (Jan et al., 2019).

Here we report the function of a ring/u-box protein AtUSR1 in promoting leaf senescence mediated by the JA-MYC2 pathway. Firstly, the expression of *AtUSR1* was age-dependent and was induced by darkness, JA, and ABA treatments (**Figure 1**). Interestingly, different from the expression of *SAG12* that was not detected until the last stage of leaf senescence, the expression peak of *AtUSR1* appeared at the early senescence stage indicating that *AtUSR1* plays potential roles in the initial of senescence stage. Leaves of *usr1* plants showed an obvious delayed senescence phenotype and *proAtUSR1*::*AtUSR1* was able to rescue the mutant phenotype (**Figure 2**). Overexpression of *AtUSR1* caused early leaf senescence (**Figure 3**). In addition, results from dark treatments of *usr1* and *35S*::*AtUSR1* plants indicated that AtUSR1 functioned in accelerating dark-induced senescence as well (**Figure 4**). Further study demonstrated that *AtUSR1*overexpression promoted JA-induced senescence and knocking-down of *AtUSR1* delayed this process (**Figure 6**).

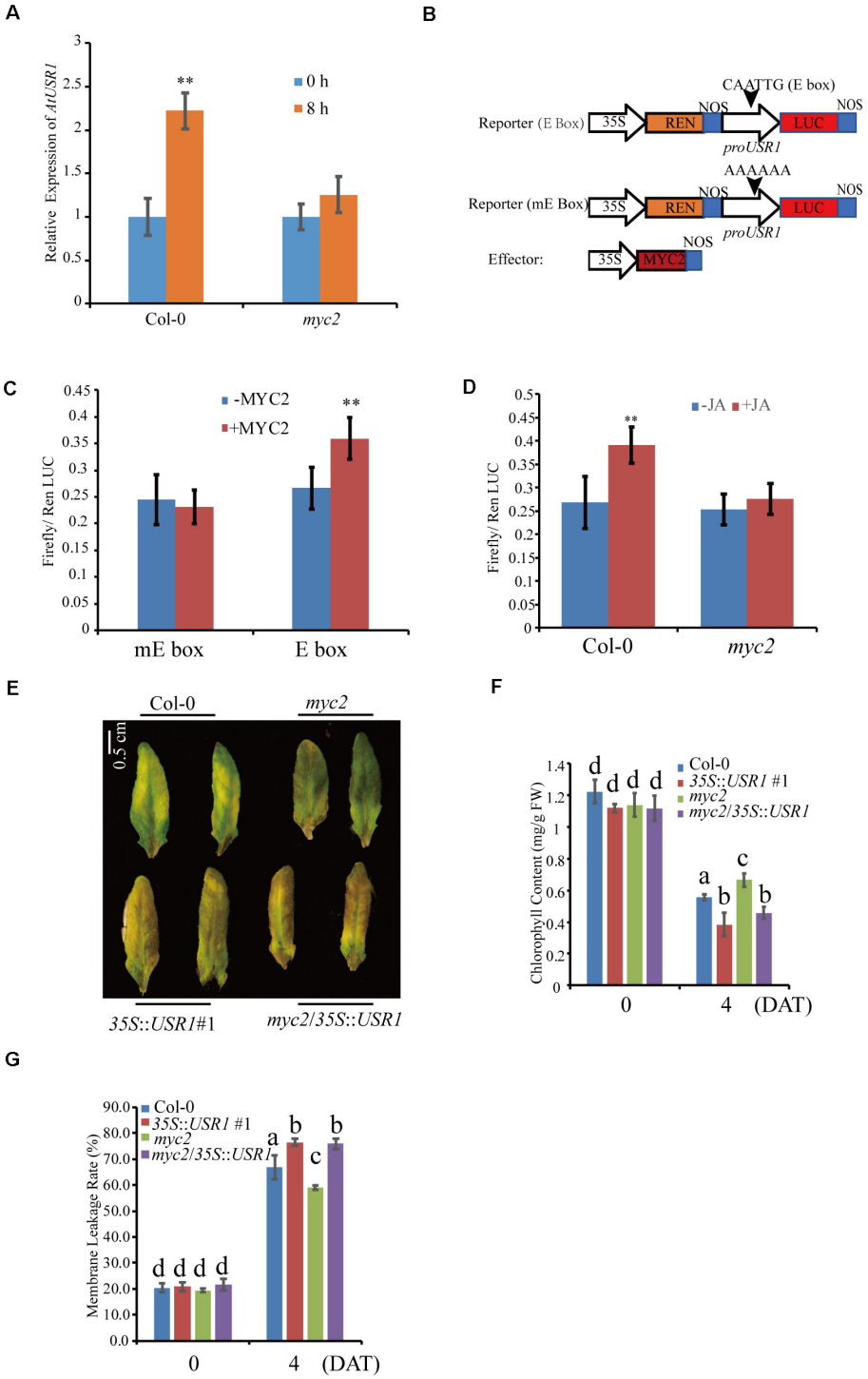

FIGURE 7 | AtUSR1 functions downstream to MYC2. **(A)** The expression pattern of *AtUSR1* in Col-0 and the *myc2* mutant under 100 μM MeJA treatments. **(B)** Schematic diagram of the reporter and effector constructs used in the dual luciferase assay. **(C)** MYC2 increased the activities of the *AtUSR1* promoter. The promoter of *AtUSR1* containing an E-box (CAGCGT) or a mutant version of the E-box (AAAAAA) fused with LUC was co-transformed with an effecter construct with or without *35S::MYC2* into Col-0 protoplasts. Ren LUC activity acted as internal control. The experiments presented here were done only with Col-0 plants (labeled as –MYC2). **(D)** MeJA induced the expression of *AtUSR1* and this induction was MYC2-dependent. The reporter construct (*proAtUSR1::LUC*) was transformed into protoplasts of Col-0 or *myc2*, respectively. Ren Luc acted as an internal control. **(E)** The cross line myc2/35S::USR1 rescued the delayed senescence phenotype of *myc2* under MeJA treatments. **(F)** Chlorophyll contents in different genotypes as indicated. **(G)** Membrane leakage rates in different genotypes as indicated. **Indicate significant difference at $P < 0.01$ levels using student's *t*-test. Data are shown as the mean ± SD from three independent experiments. The data in **(F,G)** different letters above columns indicate significant differences according to Duncan's multiple range test ($P < 0.05$).

In this study, we demonstrated that AtUSR1 acts downstream of MYC2 in JA-induced leaf senescence. Firstly, MeJA treatments enhanced *AtUSR1* expression in a MYC2-dependent manner (**Figure 7A**). Results of dual luciferase assays indicated that MYC2 could regulate *AtUSR1* expression (**Figures 7C,D**). In the presence of JA, JAZ proteins undergo degradation via ubiquitin pathways mediated by the F-box protein COI1. MYC2 is thus released from the JAZ-MYC2 complex and function to activate the expression of downstream genes including *AtUSR1*, that functions in promoting leaf senescence (**Figure 7**). In the absence of JA, the JAZ-MYC2 complexes inhibit the activity of MYC2 and *AtUSR1* transcription is compromised.

We also found that AtUSR1 affects ROS homeostasis. ROS over-accumulated in *35S::AtUSR1* leaves and the *usr1* mutant had less ROS (**Figure 5**). ROS are known to be involved in multiple biological processes in plants such as leaf senescence, stress response, and hypersensitive response (Sedigheh et al., 2011; Jajic et al., 2015). Since ROS can interplay with other signaling molecules in regulating plant development and stress responses (Hoque et al., 2012; Li et al., 2018), it's reasonable to hypothesize that AtUSR1 could also be involved in multiple signaling pathways. Significant overlap of gene expression changes exists between natural senescence, treatments of senescence-promoting phytohormones and stress conditions (Guo, 2013). AtUSR1 can potentially function as an internode factor that can be affected by multiple senescence-promoting signaling pathways induced by age, darkness, and JA.

DATA AVAILABILITY STATEMENT

The original contributions presented in the study are included in the article/**Supplementary Material**, further inquiries can be directed to the corresponding author/s.

AUTHOR CONTRIBUTIONS

YG conceived the project. ZZ and YG designed the research, performed data analysis, and wrote the manuscript. ZZ and MX performed experiments. All authors contributed to the article and approved the submitted version.

FUNDING

This work was supported by the Agricultural Science and Technology Innovation Program, Chinese Academy of Agricultural Sciences (ASTIP-TRI02).

SUPPLEMENTARY MATERIAL

The Supplementary Material for this article can be found online at: https://www.frontiersin.org/articles/10.3389/fpls.2020.608589/full#supplementary-material

Supplementary Figure 1 | Genotyping of the *usr1* mutant. **(A)** The Gene structure of *AtUSR1* and the *usr1* (*Salk_095353*) T-DNA insertion in the 5′UTR region. **(B)** Transcript levels of *AtUSR1 in Col-0, usr1* mutant, and complementation plants harboring *proAtUSR1::USR1/usr1*.

Supplementary Figure 2 | Expression of *AtUSR1* in two independent overexpression lines.

Supplementary Figure 3 | Phenotype of attached leaves under dark conditions. **(A)** Fully expanded leaves were wrapped with aluminum foil for 6 days. **(B)** Chlorophyll contents of different genotypes as indicated. **(C)** Membrane leakage rates of different genotypes as indicated.

Supplementary Table 1 | Primers used in this study.

REFERENCES

Abdollahi, M. R., Moieni, A., Mousavi, A., Salmanian, A. H., Jalali Javaran, M., and Majdi, M. (2007). Effect of integrated bombardment and *Agrobacterium* transformation system on transient GUS expression in hypocotyls of rapeseed (*Brassica napus* L. cv. PF704) microspore-derived embryos. *Pak. J. Biol. Sci.* 10, 3141–3145. doi: 10.3923/pjbs.2007.3141.3145

Ahmad, S., and Guo, Y. (2019). Signal transduction in leaf senescence: progress and perspective. *Plants* 8:405. doi: 10.3390/plants8100405

Ansari, M. I., Hasan, S., and Jalil, S. U. (2014). Leaf senescence and GABA shunt. *Bioinformation* 10, 734–736. doi: 10.6026/97320630010734

Bengoa Luoni, S., Astigueta, F. H., Nicosia, S., Moschen, S., Fernandez, P., and Heinz, R. (2019). Transcription factors associated with leaf senescence in crops. *Plants* 8:411. doi: 10.3390/plants8100411

Bresson, J., Bieker, S., Riester, L., Doll, J., and Zentgraf, U. (2018). A guideline for leaf senescence analyses: from quantification to physiological and molecular investigations. *J. Exp. Bot.* 69, 769–786. doi: 10.1093/jxb/erx246

Castillo, M. C., and Leon, J. (2008). Expression of the beta-oxidation gene *3-ketoacyl-CoA thiolase 2 (KAT2)* is required for the timely onset of natural and dark-induced leaf senescence in *Arabidopsis*. *J. Exp. Bot.* 59, 2171–2179. doi: 10.1093/jxb/ern079

Causier, B., Ashworth, M., Guo, W., and Davies, B. (2012). The TOPLESS interactome: a framework for gene repression in Arabidopsis. *Plant Physiol.* 158, 423–438. doi: 10.1104/pp.111.186999

Chini, A., Fonseca, S., Fernandez, G., Adie, B., Chico, J. M., Lorenzo, O., et al. (2007). The JAZ family of repressors is the missing link in jasmonate signalling. *Nature* 448, 666–671. doi: 10.1038/nature06006

Clough, S. J., and Bent, A. F. (1998). Floral dip: a simplified method for *Agrobacterium*-mediated transformation of *Arabidopsis thaliana*. *Plant J.* 16, 735–743. doi: 10.1046/j.1365-313x.1998.00343.x

Dombrecht, B., Xue, G. P., Sprague, S. J., Kirkegaard, J. A., Ross, J. J., Reid, J. B., et al. (2007). MYC2 differentially modulates diverse jasmonate-dependent functions in *Arabidopsis*. *Plant Cell* 19, 2225–2245. doi: 10.1105/tpc.106.048017

Earley, K. W., Haag, J. R., Pontes, O., Opper, K., Juehne, T., Song, K., et al. (2006). Gateway-compatible vectors for plant functional genomics and proteomics. *Plant J.* 45, 616–629. doi: 10.1111/j.1365-313X.2005.02617.x

Figueroa, P., and Browse, J. (2012). The Arabidopsis *JAZ2* promoter contains a G-Box and thymidine-rich module that are necessary and sufficient for jasmonate-dependent activation by MYC transcription factors and repression by JAZ proteins. *Plant Cell Physiol.* 53, 330–343. doi: 10.1093/pcp/pcr178

Fujiki, Y., Yoshikawa, Y., Sato, T., Inada, N., Ito, M., Nishida, I., et al. (2001). Dark-inducible genes from *Arabidopsis thaliana* are associated with leaf senescence and repressed by sugars. *Physiol. Plant.* 111, 345–352. doi: 10.1034/j.1399-3054.2001.1110312.x

Gan, S. (2018). Concepts and types of senescence in plants. *Methods Mol. Biol.* 1744, 3–8. doi: 10.1007/978-1-4939-7672-0_1

Goud, P. B., and Kachole, M. S. (2011). Role of chloroplastidial proteases in leaf senescence. *Plant Signal. Behav.* 6, 1371–1376. doi: 10.4161/psb.6.9.16316

Gregersen, P. L., Holm, P. B., and Krupinska, K. (2008). Leaf senescence and nutrient remobilisation in barley and wheat. *Plant Biol.* 10(Suppl. 1), 37–49. doi: 10.1111/j.1438-8677.2008.00114.x

Guo, Y. (2013). Towards systems biological understanding of leaf senescence. *Plant Mol. Biol.* 82, 519–528.

Guo, Y., Cai, Z., and Gan, S. (2004). Transcriptome of Arabidopsis leaf senescence. *Plant Cell Environ.* 27, 521–549.

Guo, Y., and Gan, S. (2005). Leaf senescence: signals, execution, and regulation. *Curr. Top. Dev. Biol.* 71, 83–112.

Guo, Y., and Gan, S. (2006). AtNAP, a NAC family transcription factor, has an important role in leaf senescence. *Plant J.* 46, 601–612. doi: 10.1111/j.1365-313X.2006.02723.x

He, Y., Fukushige, H., Hildebrand, D. F., and Gan, S. (2002). Evidence supporting a role of jasmonic acid in Arabidopsis leaf senescence. *Plant Physiol.* 128, 876–884. doi: 10.1104/pp.010843

Hellens, R. P., Edwards, E. A., Leyland, N. R., Bean, S., and Mullineaux, P. M. (2000). pGreen: a versatile and flexible binary Ti vector for *Agrobacterium*-mediated plant transformation. *Plant Mol. Biol.* 42, 819–832. doi: 10.1023/a:1006496308160

Hoque, T. S., Uraji, M., Ye, W., Hossain, M. A., Nakamura, Y., and Murata, Y. (2012). Methylglyoxal-induced stomatal closure accompanied by peroxidase-mediated ROS production in Arabidopsis. *J. Plant Physiol.* 169, 979–986. doi: 10.1016/j.jplph.2012.02.007

Hu, Y., Jiang, Y., Han, X., Wang, H., Pan, J., and Yu, D. (2017). Jasmonate regulates leaf senescence and tolerance to cold stress: crosstalk with other phytohormones. *J. Exp. Bot.* 68, 1361–1369. doi: 10.1093/jxb/erx004

Huang, H., Liu, B., Liu, L., and Song, S. (2017). Jasmonate action in plant growth and development. *J. Exp. Bot.* 68, 1349–1359. doi: 10.1093/jxb/erw495

Izumi, M., and Ishida, H. (2011). The changes of leaf carbohydrate contents as a regulator of autophagic degradation of chloroplasts via Rubisco-containing bodies during leaf senescence. *Plant Signal. Behav.* 6, 685–687. doi: 10.4161/psb.6.5.14949

Jajic, I., Sarna, T., and Strzalka, K. (2015). Senescence, stress, and reactive oxygen species. *Plants* 4, 393–411. doi: 10.3390/plants4030393

Jan, S., Abbas, N., Ashraf, M., and Ahmad, P. (2019). Roles of potential plant hormones and transcription factors in controlling leaf senescence and drought tolerance. *Protoplasma* 256, 313–329.

Jefferson, R. A., Kavanagh, T. A., and Bevan, M. W. (1987). GUS fusions: beta-glucuronidase as a sensitive and versatile gene fusion marker in higher plants. *EMBO J.* 6, 3901–3907.

Jiang, Y., Liang, G., Yang, S., and Yu, D. (2014). *Arabidopsis* WRKY57 functions as a node of convergence for jasmonic acid- and auxin-mediated signaling in jasmonic acid-induced leaf senescence. *Plant Cell* 26, 230–245. doi: 10.1105/tpc.113.117838

Jing, H. C., and Nam, H. G. (2012). Leaf senescence in plants: from model plants to crops, still so many unknowns. *J. Integr. Plant Biol.* 54, 514–515. doi: 10.1111/j.1744-7909.2012.01148.x

Jung, C., Zhao, P., Seo, J. S., Mitsuda, N., Deng, S., and Chua, N. H. (2015). PLANT U-BOX PROTEIN10 regulates MYC2 stability in Arabidopsis. *Plant Cell* 27, 2016–2031. doi: 10.1105/tpc.15.00385

Khanna-Chopra, R. (2012). Leaf senescence and abiotic stresses share reactive oxygen species-mediated chloroplast degradation. *Protoplasma* 249, 469–481. doi: 10.1007/s00709-011-0308-z

Kim, J., Dotson, B., Rey, C., Lindsey, J., Bleecker, A. B., Binder, B. M., et al. (2013). New clothes for the jasmonic acid receptor COI1: delayed abscission, meristem arrest and apical dominance. *PLoS One* 8:e60505. doi: 10.1371/journal.pone.0060505

Kim, J., Kim, J. H., Lyu, J. I., Woo, H. R., and Lim, P. O. (2018). New insights into the regulation of leaf senescence in Arabidopsis. *J. Exp. Bot.* 69, 787–799. doi: 10.1093/jxb/erx287

Krieger-Liszkay, A., Krupinska, K., and Shimakawa, G. (2019). The impact of photosynthesis on initiation of leaf senescence. *Physiol. Plant.* 166, 148–164. doi: 10.1111/ppl.12921

Lee, S., Seo, P. J., Lee, H. J., and Park, C. M. (2012). A NAC transcription factor NTL4 promotes reactive oxygen species production during drought-induced leaf senescence in Arabidopsis. *Plant J.* 70, 831–844. doi: 10.1111/j.1365-313X.2012.04932.x

Lee, S. H., Sakuraba, Y., Lee, T., Kim, K. W., An, G., Lee, H. Y., et al. (2015). Mutation of *Oryza sativa* CORONATINE INSENSITIVE 1b (OsCOI1b) delays leaf senescence. *J. Integr. Plant Biol.* 57, 562–576. doi: 10.1111/jipb.12276

Li, Z., Wang, F., Zhao, Q., Liu, J., and Cheng, F. (2018). Involvement of NADPH oxidase isoforms in the production of O2- manipulated by ABA in the senescing leaves of early-senescence-leaf (esl) mutant rice (*Oryza sativa*). *PLoS One* 13:e0190161. doi: 10.1371/journal.pone.0190161

Lim, P. O., Kim, H. J., and Nam, H. G. (2007). Leaf senescence. *Annu. Rev. Plant Biol.* 58, 115–136. doi: 10.1146/annurev.arplant.57.032905.105316

Liu, F., and Guo, F. Q. (2013). Nitric oxide deficiency accelerates chlorophyll breakdown and stability loss of thylakoid membranes during dark-induced leaf senescence in Arabidopsis. *PLoS One* 8:e56345. doi: 10.1371/journal.pone.0056345

Livak, K. J., and Schmittgen, T. D. (2001). Analysis of relative gene expression data using real-time quantitative PCR and the 2(-Delta Delta C(T)) Method. *Methods* 25, 402–408. doi: 10.1006/meth.2001.1262

Lorenzo, O., Chico, J. M., Sanchez-Serrano, J. J., and Solano, R. (2004). *JASMONATE-INSENSITIVE1* encodes a MYC transcription factor essential to discriminate between different jasmonate-regulated defense responses in Arabidopsis. *Plant Cell* 16, 1938–1950. doi: 10.1105/tpc.022319

Miao, Y., and Zentgraf, U. (2007). The antagonist function of *Arabidopsis* WRKY53 and ESR/ESP in leaf senescence is modulated by the jasmonic and salicylic acid equilibrium. *Plant Cell* 19, 819–830. doi: 10.1105/tpc.106.042705

Niu, Y. H., and Guo, F. Q. (2012). Nitric oxide regulates dark-induced leaf senescence through *EIN2* in *Arabidopsis*. *J. Integr. Plant Biol.* 54, 516–525. doi: 10.1111/j.1744-7909.2012.01140.x

Pauwels, L., Barbero, G. F., Geerinck, J., Tilleman, S., Grunewald, W., Perez, A. C., et al. (2010). NINJA connects the co-repressor TOPLESS to jasmonate signalling. *Nature* 464, 788–791. doi: 10.1038/nature08854

Qi, H., Li, J., Xia, F. N., Chen, J. Y., Lei, X., Han, M. Q., et al. (2020). Arabidopsis SINAT proteins control autophagy by mediating ubiquitylation and degradation of ATG13. *Plant Cell* 32, 263–284. doi: 10.1105/tpc.19.00413

Qi, T., Wang, J., Huang, H., Liu, B., Gao, H., Liu, Y., et al. (2015). Regulation of jasmonate-induced leaf senescence by antagonism between bHLH subgroup IIIe and IIId factors in Arabidopsis. *Plant Cell* 27, 1634–1649. doi: 10.1105/tpc.15.00110

Quirino, B. F., Noh, Y. S., Himelblau, E., and Amasino, R. M. (2000). Molecular aspects of leaf senescence. *Trends Plant Sci.* 5, 278–282.

Sakuraba, Y., Schelbert, S., Park, S. Y., Han, S. H., Lee, B. D., Andres, C. B., et al. (2012). STAY-GREEN and chlorophyll catabolic enzymes interact at light-harvesting complex II for chlorophyll detoxification during leaf senescence in *Arabidopsis*. *Plant Cell* 24, 507–518. doi: 10.1105/tpc.111.089474

Sato, Y., Morita, R., Katsuma, S., Nishimura, M., Tanaka, A., and Kusaba, M. (2009). Two short-chain dehydrogenase/reductases, NON-YELLOW COLORING 1 and NYC1-LIKE, are required for chlorophyll b and light-harvesting complex II degradation during senescence in rice. *Plant J.* 57, 120–131. doi: 10.1111/j.1365-313X.2008.03670.x

Sedigheh, H. G., Mortazavian, M., Norouzian, D., Atyabi, M., Akbarzadeh, A., Hasanpoor, K., et al. (2011). Oxidative stress and leaf senescence. *BMC Res. Notes* 4:477. doi: 10.1186/1756-0500-4-477

Shan, X., Li, C., Peng, W., and Gao, B. (2011). New perspective of jasmonate function in leaf senescence. *Plant Signal. Behav.* 6, 575–577. doi: 10.4161/psb.6.4.14899

Shim, K. C., Kim, S. H., Jeon, Y. A., Lee, H. S., Adeva, C., Kang, J. W., et al. (2020). A RING-type E3 ubiquitin ligase, OsGW2, controls chlorophyll content and dark-induced senescence in rice. *Int. J. Mol. Sci.* 21:1704. doi: 10.3390/ijms21051704

So, W. M., Kim, S. Y., Hyoung, S., and Shin, J. S. (2019). The novel protein CSAP accelerates leaf senescence and is negatively regulated by SAUL1 in the dark. *Plant Cell Rep.* 39, 325–334. doi: 10.1007/s00299-019-02493-z

Song, S., Qi, T., Huang, H., Ren, Q., Wu, D., Chang, C., et al. (2011). The jasmonate-ZIM domain proteins interact with the R2R3-MYB transcription factors MYB21 and MYB24 to affect jasmonate-regulated stamen development in *Arabidopsis*. *Plant Cell* 23, 1000–1013. doi: 10.1105/tpc.111.083089

Suraneni, M. V., Schneider-Broussard, R., Moore, J. R., Davis, T. C., Maldonado, C. J., Li, H., et al. (2010). Transgenic expression of 15-lipoxygenase 2 (15-LOX2) in mouse prostate leads to hyperplasia and cell senescence. *Oncogene* 29, 4261–4275. doi: 10.1038/onc.2010.197

Tamary, E., Nevo, R., Naveh, L., Levin-Zaidman, S., Kiss, V., Savidor, A., et al. (2019). Chlorophyll catabolism precedes changes in chloroplast structure and proteome during leaf senescence. *Plant Direct* 3:e00127. doi: 10.1002/pld3.127

Thines, B., Katsir, L., Melotto, M., Niu, Y., Mandaokar, A., Liu, G., et al. (2007). JAZ repressor proteins are targets of the SCF(COI1) complex during jasmonate signalling. *Nature* 448, 661–665. doi: 10.1038/nature05960

Vanhaeren, H., Nam, Y. J., De Milde, L., Chae, E., Storme, V., Weigel, D., et al. (2017). Forever young: the role of ubiquitin receptor DA1 and E3 ligase BIG BROTHER in controlling leaf growth and development. *Plant Physiol.* 173, 1269–1282. doi: 10.1104/pp.16.01410

Wang, H., Zhu, X., Li, H., Cui, J., Liu, C., Chen, X., et al. (2014). Induction of caspase-3-like activity in rice following release of cytochrome-f from the chloroplast and subsequent interaction with the ubiquitin-proteasome system. *Sci. Rep.* 4:5989. doi: 10.1038/srep05989

Woo, H. R., Chung, K. M., Park, J. H., Oh, S. A., Ahn, T., Hong, S. H., et al. (2001). ORE9, an F-box protein that regulates leaf senescence in Arabidopsis. *Plant Cell* 13, 1779–1790. doi: 10.1105/tpc.010061

Woo, H. R., Kim, H. J., Lim, P. O., and Nam, H. G. (2019). Leaf senescence: systems and dynamics aspects. *Annu. Rev. Plant Biol.* 70, 347–376.

Wu, X. Y., Kuai, B. K., Jia, J. Z., and Jing, H. C. (2012). Regulation of leaf senescence and crop genetic improvement. *J. Integr. Plant Biol.* 54, 936–952. doi: 10.1111/jipb.12005

Xie, D. X., Feys, B. F., James, S., Nieto-Rostro, M., and Turner, J. G. (1998). *COI1*: an *Arabidopsis* gene required for jasmonate-regulated defense and fertility. *Science* 280, 1091–1094. doi: 10.1126/science.280.5366.1091

Yu, J., Zhang, Y., Di, C., Zhang, Q., Zhang, K., Wang, C., et al. (2016). JAZ7 negatively regulates dark-induced leaf senescence in *Arabidopsis*. *J. Exp. Bot.* 67, 751–762. doi: 10.1093/jxb/erv487

Zhang, A., Lu, Q., Yin, Y., Ding, S., Wen, X., and Lu, C. (2010). Comparative proteomic analysis provides new insights into the regulation of carbon metabolism during leaf senescence of rice grown under field conditions. *J. Plant Physiol.* 167, 1380–1389. doi: 10.1016/j.jplph.2010.05.011

Zhang, Y., Ji, T. T., Li, T. T., Tian, Y. Y., Wang, L. F., and Liu, W. C. (2020). Jasmonic acid promotes leaf senescence through *MYC2*-mediated repression of *CATALASE2* expression in Arabidopsis. *Plant Sci.* 299:110604. doi: 10.1016/j.plantsci.2020.110604

Zhang, Z., and Guo, Y. (2018). Hormone treatments in studying leaf senescence. *Methods Mol. Biol.* 1744, 125–132. doi: 10.1007/978-1-4939-7672-0_11

Zhang, Z., Li, W., Gao, X., Xu, M., and Guo, Y. (2020). DEAR4, a member of DREB/CBF family, positively regulates leaf senescence and response to multiple stressors in *Arabidopsis thaliana*. *Front. Plant Sci.* 11:367. doi: 10.3389/fpls.2020.00367

Zhou, J., Lu, D., Xu, G., Finlayson, S. A., He, P., and Shan, L. (2015). The dominant negative ARM domain uncovers multiple functions of PUB13 in *Arabidopsis* immunity, flowering, and senescence. *J. Exp. Bot.* 66, 3353–3366. doi: 10.1093/jxb/erv148

Zhu, X., Chen, J., Xie, Z., Gao, J., Ren, G., Gao, S., et al. (2015). Jasmonic acid promotes degreening via MYC2/3/4- and ANAC019/055/072-mediated regulation of major chlorophyll catabolic genes. *Plant J.* 84, 597–610. doi: 10.1111/tpj.13030

Zhu, Z., An, F., Feng, Y., Li, P., Xue, L., Mu, A., et al. (2011). Derepression of ethylene-stabilized transcription factors (EIN3/EIL1) mediates jasmonate and ethylene signaling synergy in *Arabidopsis*. *Proc. Natl. Acad. Sci. U.S.A.* 108, 12539–12544. doi: 10.1073/pnas.1103959108

Zhuo, M., Sakuraba, Y., and Yanagisawa, S. (2020). A jasmonate-activated MYC2-Dof2.1-*MYC2* transcriptional loop promotes leaf senescence in Arabidopsis. *Plant Cell* 32, 242–262. doi: 10.1105/tpc.19.00297

Conflict of Interest: The authors declare that the research was conducted in the absence of any commercial or financial relationships that could be construed as a potential conflict of interest.

frontiers in Plant Science

ORIGINAL RESEARCH
published: 07 January 2021
doi: 10.3389/fpls.2020.611170

ACCELERATED CELL DEATH 6 Acts on Natural Leaf Senescence and Nitrogen Fluxes in *Arabidopsis*

*Sophie Jasinski, Isabelle Fabrissin, Amandine Masson, Anne Marmagne, Alain Lécureuil, Laurence Bill and Fabien Chardon**

Institut Jean-Pierre Bourgin, INRAE, AgroParisTech, Université Paris-Saclay, Versailles, France

As the last step of leaf development, senescence is a molecular process involving cell death mechanism. Leaf senescence is trigged by both internal age-dependent factors and environmental stresses. It must be tightly regulated for the plant to adopt a proper response to environmental variation and to allow the plant to recycle nutrients stored in senescing organs. However, little is known about factors that regulate both nutrients fluxes and plant senescence. Taking advantage of variation for natural leaf senescence between *Arabidopsis thaliana* accessions, *Col-0* and *Ct-1*, we did a fine mapping of a quantitative trait loci for leaf senescence and identified *ACCELERATED CELL DEATH 6* (*ACD6*) as the causal gene. Using two near-isogeneic lines, differing solely around the *ACD6* locus, we showed that *ACD6* regulates rosette growth, leaf chlorophyll content, as well as leaf nitrogen and carbon percentages. To unravel the role of *ACD6* in N remobilization, the two isogenic lines and *acd6* mutant were grown and labeled with ^{15}N at the vegetative stage in order to determine ^{15}N partitioning between plant organs at harvest. Results showed that N remobilization efficiency was significantly lower in all the genotypes with lower *ACD6* activity irrespective of plant growth and productivity. Measurement of N uptake at vegetative and reproductive stages revealed that *ACD6* did not modify N uptake efficiency but enhanced nitrogen translocation from root to silique. In this study, we have evidenced a new role of ACD6 in regulating both sequential and monocarpic senescences and disrupting the balance between N remobilization and N uptake that is required for a good seed filling.

Keywords: aging, nitrogen remobilization, nitrogen uptake, seed filling, *Arabidopsis thaliana*, quantitative trait loci, natural variation

OPEN ACCESS

Edited by:
Yongfeng Guo, Tobacco Research Institute (CAAS), China

Reviewed by:
Ying Miao, Fujian Agriculture and Forestry University, China
Uwe Ludewig, University of Hohenheim, Germany

****Correspondence:***
Fabien Chardon
fabien.chardon@inrae.fr

Specialty section:
This article was submitted to Plant Physiology, a section of the journal Frontiers in Plant Science

Received: *28 September 2020*
Accepted: *23 November 2020*
Published: *07 January 2021*

Citation:
Jasinski S, Fabrissin I, Masson A, Marmagne A, Lécureuil A, Bill L and Chardon F (2021) ACCELERATED CELL DEATH 6 Acts on Natural Leaf Senescence and Nitrogen Fluxes in Arabidopsis. Front. Plant Sci. 11:611170. doi: 10.3389/fpls.2020.611170

INTRODUCTION

Leaf senescence constitutes the final stage of leaf development. The most obvious visible symptoms of leaf senescence is yellowing due to chlorophyll degradation. However, during this last developmental stage, other macromolecules are degraded, including macromolecules that have been accumulated through carbon fixation during the photosynthetic period of the leaf. The salvaged nutrient of dying leaf tissues may be remobilized to newly developing organs such as younger leaves, flowers, and seeds (Himelblau and Amasino, 2001). Hence, senescence, although deteriorative by nature, contributes to the growth, reproductive success, and general fitness of plants. Consequently, the onset, rate, and progression of leaf senescence must be tightly regulated

to ensure plant survival via the efficient recycling of nutrients for the next generation (i.e., seeds), especially in annual plants.

Leaf senescence is primarily driven by the developmental age but is also regulated by a complex network of internal and environmental signals that are integrated into the age information through intricate regulatory pathways. All phytohormones known to date play a role in leaf senescence regulation. Cytokinins, giberrelins, and auxins delay leaf senescence, whereas ethylene, jasmonic acids, abscisic acid, salicylic acid (SA), brassinosteroids, and strigolactones induce leaf senescence (Jibran et al., 2013; Schippers et al., 2015; Yamada and Umehara, 2015). Other important determinants of leaf senescence are sugar sensing and signaling (Wingler, 2018), as well as the communication between source and sink, corresponding to the demand for nutrients in the sink tissue and the capacity of a source to provide these nutrients (Schippers et al., 2015; Kumar et al., 2019). This source–sink communication is required to adjust the remobilization rate of nutrients. Last but not least, the environment plays a major role in leaf senescence regulation. Darkness, shade, temperature, soil salinity, drought, nutrient limitation, and pathogen infection can all affect senescence for instance (Lim et al., 2007; Schippers et al., 2015; Santos Matos, 2020).

Over the past decade, in an attempt to understand the complex process of leaf senescence, many genetic and molecular studies, together recently with "omics" studies, have been performed in plants, allowing the identification of key regulators as well as intertwined networks involved in leaf senescence regulation (Lim et al., 2007; Guiboileau et al., 2010; Schippers et al., 2015). Multiple layers of regulation, including chromatin, transcriptional, posttranscriptional, translational, and posttranslational regulations, controlled the leaf senescence process (Kim et al., 2018; Woo et al., 2019). All these studies allowed the identification of many transcription factors and gene-regulatory networks. Yet, how these gene networks are coordinated and how this coordination impacts plant fitness and then adaptation of plants to their environment remain poorly understood.

The study of natural variation is a strategy of choice to unravel the role of a trait in plant adaptation and evolution. With this aim, studies have been conducted in *Arabidopsis*, highlighting strong variation in the onset, progression, and intensity of senescence in accessions from different geographic origins (Levey and Wingler, 2005; Luquez et al., 2006; Balazadeh et al., 2008). The genetic basis of this variation was investigated in *Arabidopsis* using recombinant inbred line (RIL) or genome-wide association (GWA) populations for quantitative trait loci (QTL) analysis (Diaz et al., 2006; Luquez et al., 2006; Masclaux-Daubresse et al., 2007; Wingler et al., 2010; Chardon et al., 2014; Lyu et al., 2019). Similar strategies based on the natural variation were carried out to study leaf senescence in various crops such as rice, wheat, sorghum maize, and barley (Wehner et al., 2015; Kamal et al., 2019; Sekhon et al., 2019; Zhao et al., 2019). Recently, the investigation of 259 natural *Arabidopsis* accessions in a GWA study allowed the identification of a new leaf senescence regulator, *Genetic Variants in Leaf Senescence 1* (*GVS1*; Lyu et al., 2019). Interestingly, *GVS1* is also involved in sensitivity to oxidative stress (Lyu et al., 2019), suggesting a link between leaf senescence and oxidative stress. In nature, plants are challenged by many biotic and abiotic stresses, which generate reactive oxygen species and consequently oxidative stress damages. Many studies have previously shown significant overlap, at the molecular level, between senescence and plant defense regulatory pathways (Guo and Gan, 2012). In the same vein, the phytohormones mentioned above regarding leaf senescence regulation are also key players in plant stress responses. This highlights the existence of a crosstalk between senescence and oxidative stress.

During senescence, nitrogen remobilization will allow the seeds to be filled with proteins, which also relies on nitrogen uptake. Similarly to senescence, nitrogen remobilization and uptake are both regulated by genetic and environmental factors (Diaz et al., 2008; Chardon et al., 2010; Masclaux-Daubresse and Chardon, 2011). However, how leaf senescence and nitrogen fluxes are related to each other, in particular to ensure correct seed filling with proteins, is unknown. The links between leaf senescence, yield, and seed filling have been investigated in three *Arabidopsis*-RIL populations, revealing that leaf senescence is negatively correlated to final rosette weight, yield, and seed nitrogen content in the *Ct-1* × *Col-0* population (Chardon et al., 2014). In this population, early senescence decreased the nitrogen remobilization efficiency from the rosette to the reproductive organs and altered seed nitrogen content.

In order to better understand the link between leaf senescence and nitrogen fluxes in the *Ct-1* × *Col-0* population, we aimed to identify the gene underlying the major leaf senescence QTL mapped in this population and to explore its role in nitrogen fluxes. With this objective, we fine mapped the QTL to a single gene, named *ACCELERATED CELL DEATH 6* (*ACD6*), and studied its impact on leaf-aging senescence and its capacity to modulate N mobilization and N uptake during seed filling.

MATERIALS AND METHODS

Plant Material and Growth Condition

The *acd6-2* (SALK_045869, N545869) and *acl1-1* (GK-108H02, N410358) mutants were ordered from the NASC. Both T-DNA mutants were genotyped with gene-specific primers (**Supplementary Table S1**) flanking the T-DNA insertion site and the T-DNA-specific primers LB-Salk2 (5′-GCTTTCTTCCCTTCCTTTCTC-3′) or gabi_o8409 (5′-ATATTGACCATCATACTCATTGC-3′) for Salk or Gabi mutant, respectively.

The HIF434 was developed from the F8 RIL434 that still segregates in a 5.9-Mb genomic region on chromosome 4 (Tuinstra et al., 1997; Loudet et al., 2005). Several plants were sown and genotyped individually for the appropriate markers across the segregating region, and three independently fixed plants for each allele (named *HIF434-Ct* and *HIF434-Col*, composing the HIF) were chosen and allowed to self-fertilize. In order to identify recombinants (rHIFs) within the segregating interval, 276 F9 plants were genotypically screened. Seventy-seven recombinants were identified and genotyped with

microsatellites or indel markers to identify recombination events within the candidate region. Once recombinants had been identified, microsatellites, indel, or dCAPS markers were used to refine and localize recombination breakpoints to smaller intervals when needed. All the markers used are listed in **Supplementary Table S2**. Twenty-three rHIFs were then tested for the segregation of the leaf senescence phenotype by progeny of fixed-progeny testing. For fixed-progeny testing, for each rHIF, 24 plants were grown and genotyped to isolate individuals fixed for the parental alleles at the remaining heterozygous interval. Three plants fixed for each parental allele were then self-fertilized, and their seed were sawn (four replicates/line) for leaf senescence phenotyping. For progeny testing, for each rHIF, 48 plants were grown and phenotyped for leaf senescence as well as genotyped within the heterozygous interval. The advanced rHIF line 434 (*arHIF434*), which segregates solely for the 7.875-kb candidate region, was obtained from a cross between two different rHIFs lines (rHIF434.40.23.38 and rHIF434.40.23.35; **Figure 1C**) with adequate genotypes (rHIFs recombined immediately to the north or immediately to the south of the *SEN.4* final interval and with adequate genotype elsewhere), as described by Loudet et al. (2005).

For leaf senescence, plants were grown on soil in greenhouse under natural light supplemented with sodium lamps to provide a 16-h photoperiod. For ^{15}N labeling experiments, plant were grown on sand in a growth chamber in short-day condition (8 h light at 140 μmol photons m^{-2} s^{-1}, 21 and 17°C day/night temperatures; relative humidity of 65%) until bolting and then transferred to the growth chamber under long-day conditions (16 h light).

RT-PCR

Three plants per genotype (*Col-0*, *acl1-1*, and *acd6-2*) were grown in greenhouse under long-day condition. At 4 weeks old, the fourth rosette leaves were pooled for total RNA extraction using the RNeasy Plant Mini Kit (Qiagen) following the manufacturer's protocol. DNAse treatment was performed on columns. Five hundred nanograms of total RNA was reverse transcribed by the RevertAid M-MuLV Reverse Transcriptase (Fermentas) with an oligo (dT) primer according to the manufacturer's protocol. Complementary DNA (cDNA) was diluted five times, and 2.5 μl was used as template in a 20-μl PCR reaction. PCR primers specific for *ACD6* (ACD6-F1 and SeqACD6-R5), *ACL1* (ACL1-For1 and ACL1-Rev1), and *ACTIN* (ActQ1F and ActQ2R) were used. All sequence primers are described in **Supplementary Table S1**.

qRT-PCR

Three plants per genotype (*Col-0*, *acl1-1*, and *acd6-2*) in two independent cultures were grown in greenhouse under long day condition. At 5 weeks old, the sixth rosette leaves were pooled for total RNA extraction using the RNeasy Plant Mini Kit (Qiagen) following the manufacturer's protocol. DNAse treatment was performed on columns. Two hundred fifty nano grams of total RNA was reverse transcribed by the RevertAid M-MuLV Reverse Transcriptase (Fermentas) with an oligo (dT) primer according to the manufacturer's protocol. For the qRT-PCR, the 10-μl reaction mixture contained 2.5 μl of cDNA, 0.3 μl of each primer (10 μM), 5 μl of a Takyon Rox SYBR MasterMix dTT Blue solution (UF-RSMT-B0710, Eurogentec, Liège, Belgium) containing the Taq polymerase, the deoxyribonucleotide triphosphates (dNTPs), and the Sybr Green in a reaction buffer, and 2.2 μl of water. The reverse transcription quantitative PCRs (RT-qPCRs) were run on a CFX 96 thermocycler (Biorad) using a first step at 95°C for 3 min and then 40 cycles of 10 s at 95°C, 10 s at 58°C, and 30 s at 72°C. A final step consisted in an increase of 0.1°C s^{-1} to 95°C. The primers used for RT-qPCR are listed in **Supplementary Table S1**. All primers presented an efficiency of 100 ± 5%. *PP2AA3* (AT1G13320) and *APC2* (AT2G04660) were used as reference genes for the calculation of *ACD6* relative expression.

Leaf Senescence Phenotyping

Leaf senescence was scored at different time points during plant growth as the ratio of the number of yellow rosette leaves on total number of rosette leaves at bolting.

Leaf Chlorophyll, Nitrogen, and Carbon Percentage Measurement

Sampling and measurements were done at the same time of the day to avoid circadian effects. The leaves emerging after the cotyledons were numbered continuously from old to young, starting at the two first leaves and ending before the emergence of the cauline leaves, which are recognizable by their small and pointed leaf blade and lack of petioles (Steynen et al., 2001). Chlorophyll content was determined using a Dualex Scientific™ clamp (Force A, Orsay, France). Measurements were taken in the middle of each leaf blade. For each time point during the lifespan of plants, four rosettes for each genotype were harvested. For N and C percentage measurements, leaves were gathered and ground in powder after drying, by groups of 10 leaves: old leaves (OL), ranks 1–10; mature leaves (ML), ranks 11–20; young leaves (YL), ranks 21–30; and new leaves (NL), ranks 31 to >40. A subsample of 1,000–2,000 μg was carefully weighed in tin capsules to determine total C and N percentages of samples using an elemental analyzer (FLASH 2000 Organic Elemental Analyzer, Thermo Fisher Scientific, Courtabeuf, France).

^{15}N Labeling for Uptake Experiment

Seeds were sown in sand and watered with a 10-mM nitrate solution. Plants were grown in the growth chamber in short days (16 h light, 21 and 17°C day/night temperatures). The vegetative ^{15}N uptake time point occurred 40 days after sowing (DAS) when plants were still vegetative. Plants for the postflowering time ^{15}N uptake were transferred in long days (16 h light, 21 and 17°C day/night temperatures). The postflowering ^{15}N uptake time point occurred 72 DAS, 2 weeks after flower buds emergence. At the time point, the unlabeled watering solution was replaced by an ^{15}N-containing solution (10% enrichment). All the pots were watered during 24 h, using an equal volume of labeled solutions. Cutting the rosettes stopped ^{15}N uptake. Roots,

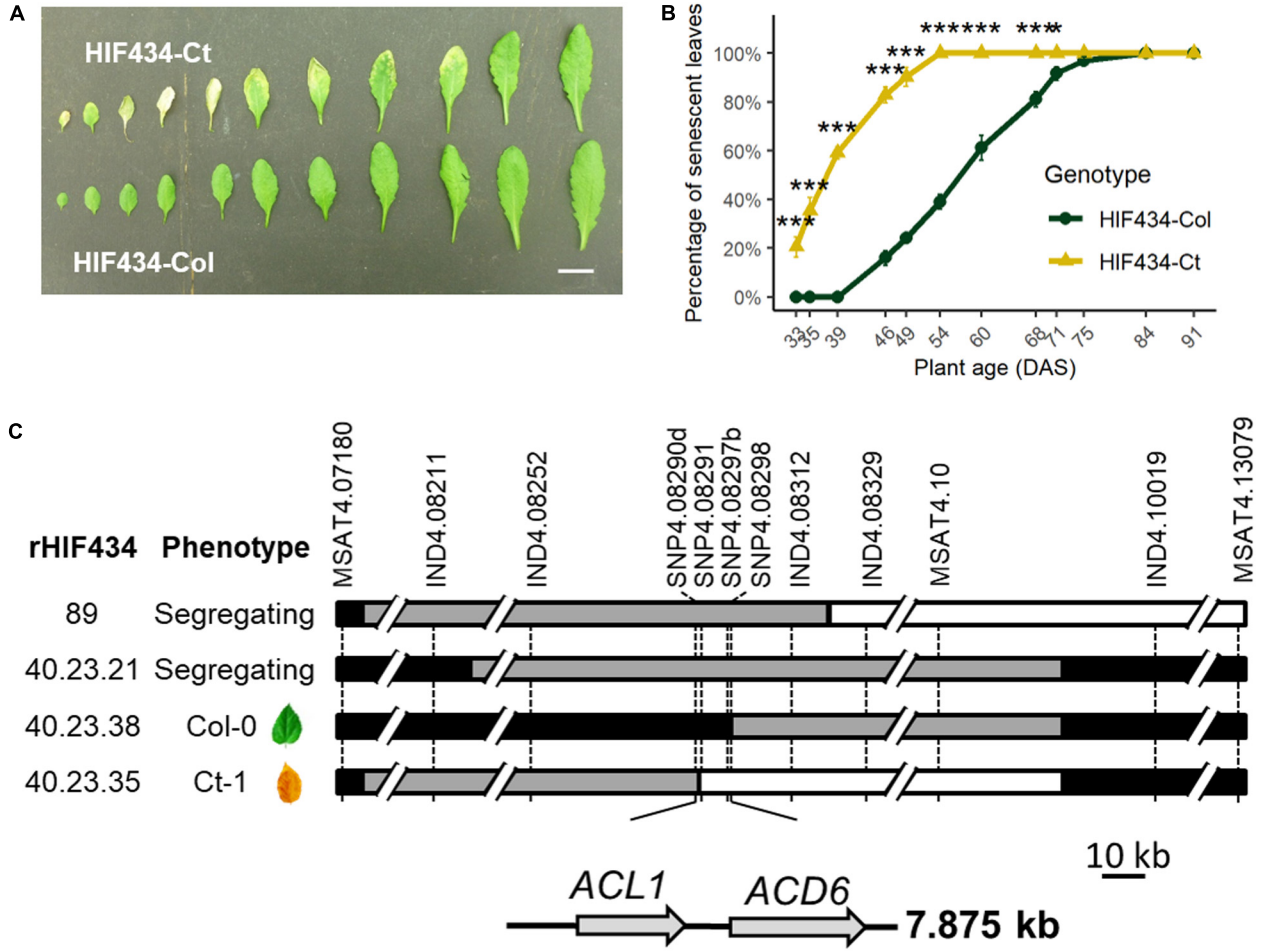

FIGURE 1 | Fine mapping of *SEN.4* locus. **(A)** Rosette leaves (rank 4–14) of 7-week-old plants. Upper row: *HIF434-Ct*; lower row: *HIF434-Col*. Scale bar corresponds to 2 cm. **(B)** Percentage of senescent leaves in *HIF434-Ct* (yellow triangle line) and *HIF434-Col* (dark green circle line) during the reproductive phase. Flowering transition occurred on average at 23.6 days after sowing (DAS) for *HIF434-Col* and 24.6 DAS for *HIF434-Ct*. Stars indicate significant difference between the two genotypes (Student's test, $n = 12$, $^{*}p < 0.05$, $^{***}p < 0.001$). **(C)** The genotype of the most informative recombinants (rHIFs) used to delineate the final 7.875 kb candidate interval is represented with horizontal bars (black for *Col-0* allele, white for *Ct-1* allele, gray for heterozygous). Dashed vertical bars represent markers used for genotyping between 7.180 and 13.08 Mb on chromosome 4. The phenotype of each rHIF progeny is indicated (phenotype).

rosettes, and siliques were then dried, and their dry weight (DW) was determined.

^{15}N Labeling for Remobilization Experiment

Seeds were sown in sand and watered with a 10-mM nitrate solution. Plants were grown in the growth chamber in short days (8 h light, 21 and 17°C day/night temperatures). Around 40 days after sowing (about 1 week before bolting), 1 ml of a 10-mM nitrate solution containing 10% of ^{15}N NO_3 was dropped to the sand closed to the rosette. After 24 h, plants were rinsed in clear water to eliminate the remaining ^{15}N NO_3. About 10 days after ^{15}N labeling, plants were transferred into long-day condition (16 h light, 21 and 17°C day/night temperatures). Plants were harvested at the end of their cycle, at maturity, when all seeds were matured and the rosette dried. Samples were separated as (i) rosette, (ii) stem (stem + cauline leaves + empty-dry siliques), and (iii) seeds (total seeds). The roots were not harvested because a large part of the root system was lost in the sand during harvesting. The DW of rosette, stem, and seeds were determined.

Determination of ^{15}N Abundance

For all the experiments, unlabeled samples were harvested in order to determine the ^{15}N natural abundance. After drying and weighting each plant, the material was ground to obtain a homogeneous fine powder. A subsample of 1,000–2,000 µg was carefully weighed in tin capsules to determine the total C and N percentages and ^{15}N abundance using an elemental analyzer (FLASH 2000 Organic Elemental Analyzer, Thermo Fisher Scientific, Courtabeuf, France) coupled to an isotope ratio mass spectrometer (delta V isotope ratio mass spectrometer, Thermo Fisher Scientific, Courtabeuf, France) calibrated using international reference (caffeine, IAEA-600, Vienna, Austria). The ^{15}N abundance was calculated as atom percent and defined

as A% = 100 × (^{15}N)/(^{15}N + ^{14}N) for labeled plant samples and for unlabeled plant controls ($A\%_{control}$ was ca. 0.3660). The ^{15}N enrichment (E%) of the plant material was then defined as ($A\%_{sample}$ - $A\%_{control}$)/100. The absolute quantity of N and ^{15}N contained in the sample were defined as QtyN = DW × N% and Qty^{15}N = DW × E% × N%, respectively. Different parameters used to evaluate harvest index (HI), N fluxes components were defined as follows:

$$HI = DWseeds/(DWrosette + DWStem + DWseeds),$$

$$\text{N allocation in rosette} = QtyNrosette/(QtyNrosette + QtyNstem + QtyNseeds),$$

$$\text{N allocation in stem} = QtyNstem/(QtyNrosette + QtyNstem + QtyNseeds),$$

$$\text{N allocation in seeds (NHI)} = QtyNseeds/(QtyNrosette + QtyNstem + QtyNseeds),$$

$$^{15}\text{N allocation in rosette} = Qty^{15}Nrosette/(Qty^{15}Nrosette + Qty^{15}Nstem + Qty^{15}Nseeds),$$

$$^{15}\text{N allocation in stem} = Qty^{15}Nstem/(Qty^{15}Nrosette + Qty^{15}Nstem + Qty^{15}Nseeds),$$

$$^{15}\text{N allocation in seeds } (^{15}\text{NHI}) = Qty^{15}NSeeds/(Qty^{15}Nrosette + Qty^{15}Nstem + Qty^{15}Nseeds),$$

$$NRE = {}^{15}NHI/HI,$$

$$NUpE = [(Qty^{15}Nrosette + Qty^{15}Nstem + Qty^{15}Nseeds)/E\%]/(DWrosette + DWStem + DWseeds)$$

Statistical Analyses

Analysis of variance followed by Tukey's honestly significant difference (HSD) test as well as two−sample t tests were used in this study. All statistical analyses were performed using the free software environment R Version 4.0.2.[1] The least-square means were calculated using the R package emmeans.

[1]https://www.r-project.org/

RESULTS

ACD6 Is the Gene Underling the *SEN.4* Leaf Senescence QTL

In a previous study, five QTLs for leaf senescence were mapped in the *Arabidopsis Ct-1* × *Col-0* population (Chardon et al., 2014). The parental accessions were highly contrasted for leaf senescence, *Ct-1* displaying earlier leaf senescence than *Col-0*. In order to gain insight into the leaf senescence molecular process, the QTLs on chromosome 4 (*Ct_Senes_4* and referred as *SEN.4* hereafter), explaining the most important variation (29%), were fine mapped. The *Ct-1* allele displayed an earlier leaf senescence than the *Col-0* allele at *SEN.4*.

The phenotypic effect linked to *SEN.4* was confirmed using specific near-isogenic lines differing for a small genomic region spanning a few megabases around the QTL. Near-isogenic lines for this QTL were obtained by producing a heterogeneous inbred family (HIF), which is easily generated taking advantage of the residual heterozygosity still segregating in RILs (Tuinstra et al., 1997; Loudet et al., 2005). RIL434, segregating only around *SEN.4* but fixed as homozygous for all the tested markers in the rest of chromosome 4 and elsewhere in the genome, was used to generate HIF434. Plants bearing the *Ct-1* allele ("*HIF434-Ct*") displayed an earlier senescence than plants bearing the *Col-0* allele ("*HIF434-Col*") (**Figures 1A**, B), validating the QTL location.

HIF434 was further used for fine mapping *SEN.4*. Using additional genetic markers, the heterozygous region of *HIF434* was mapped to a 5.9-Mb interval between markers at positions 7.180000 and 13.079020 Mb on chromosome 4. Screening of 276 progeny plants from a *HIF434-Het* individual (heterozygous over the 5.9 Mb region) resulted in the isolation of 77 recombination events in this interval. Phenotyping of the progeny of 24 recombinants (rHIF, see section "Materials and Methods") reduced the region of interest to a 117.5-kb interval between markers at positions 8.211624 and 8.329176 Mb. A second screening of 1,288 plants resulted in the isolation of 34 new recombinants. Phenotyping of 10 of them reduced the region of interest to a 7.875-kb interval between markers at positions 8.290453 and 8.298328 Mb on chromosome 4 (**Figure 1C**).

To further confirm this result, an "advanced rHIF cross" (arHIF; see section "Materials and Methods" and Loudet et al., 2008) was designed to obtain the *arHIF434* line, which segregated only for this 7.875 kb region (**Supplementary Figure 1A**). Like the original HIF, the progeny of this line segregated for leaf senescence with *arHIF434-Ct* displaying an earlier leaf senescence compared to *arHIF434-Col*, confirming the presence of *SEN.4* within this 7.875-kb interval (**Supplementary Figures 1B,C**).

Two predicted genes, *ACD6* (*At4g14400*) and *ACL1* encoding an *ACD6*-like ankyrin repeat family protein (*At4g14390*), are present in this 7.875-kb interval (**Figure 1C** and **Supplementary Figure 1A**). To investigate the possible role of these two genes in leaf senescence variation between *Ct-1* and *Col-0* accessions, T-DNA insertion mutants in *ACL1* (named *acl1-1*) and *ACD6* (*acd6-2*), both available in the *Col-0* genetic background, were

analyzed. Molecular characterization of the mutants revealed that *acl1-1* contained an inverted tandem insertion at the 739th base of the second exon (accompanied with a 54-bp deletion) and *acd6-2* carried a T-DNA insertion in the third intron of *ACD6* (**Figure 2A**).

Reverse transcription PCR (RT-PCR) using primers specific to *ACD6* (**Supplementary Table S1**) showed that there is no *ACD6* expression in leaves of *acd6-2* mutant, whereas *ACD6* is strongly expressed in Col-0 and *acl1-1* mutant at the same developmental stage (**Figure 2B**). Using primers specific to *ACL1* (**Supplementary Table S1**), no expression of the gene was detected in *Col-0* leaves by RT-PCR, in accordance with an extremely low expression level in rosette leaves as referred in eFP Browser (Winter et al., 2007).

Phenotypic analysis for leaf senescence revealed that *acl1-1* homozygous mutant displayed a leaf senescence kinetic similar to the wild type during plant development (**Figure 2C**), validating that *ACL1* is not involved in the leaf senescence phenotype. By contrast, *acd6-2* homozygous mutants displayed a delayed leaf senescence compared to wild type (**Figure 2C**), demonstrating that modification in *ACD6* is responsible for the leaf senescence variation observed at *SEN.4* locus.

Alignment of *ACD6* coding sequences from both *Ct-1* and *Col-0* accessions showed 34 single-nucleotide polymorphisms (SNPs) leading to 20 amino acid changes between both accessions and the lack of the last amino acid in *Ct-1* compared to *Col-0* (**Supplementary Figure 2**). Two amino acids changes were located in the second ankyrin motif and one was in the eighth one. Five amino acids changes were in transmembrane domains. *Ct-1* and *Col-0* differed at amino acids 566 and 634, showed to be both necessary and sufficient for variation in late-onset leaf necrosis between accessions carrying *ACD6-Est-1* and *ACD6-Col-0* alleles (Todesco et al., 2010). In our study, *Ct-1* displayed the *ACD6-Est-1* allele and Col-0 the *ACD6-Col-0* allele described by Todesco et al. (2010). In addition, we did not detect any variation in *ACD6* transcript levels in the sixth rosette leaf between the two *arHIF434*, at the same stage of development (**Supplementary Figure 3A**). However, *arHIF434-Ct* plants had higher levels of *SAG12* messenger RNA (mRNA) and lower levels of *RBSC1A* mRNA, confirming that the senescence process was enhanced in *arHIF434-Ct* leaves compared to the *arHIF434-Col* ones (**Supplementary Figures 3B,C**). The *arHIF434-Ct* plants showed a higher relative expression of *PR1* than *arHIF434-Col* plants, indicating an enhancement of SA signaling in *arHIF434-Ct* leaves (**Supplementary Figure 3D**). These results suggested that *ACD6* expression was not the source of the early senescence in *arHIF434-Ct*, and they supported that the two modifications at amino acid 566 and 634 were responsible for the leaf senescence variation observed between plants carrying either the *Ct-1* or the *Col-0 ACD6* alleles, although a role of other amino acids cannot be ruled out.

ACD6 Activity Regulates Leaf Senescence Kinetics

The chlorophyll content of the different rosette leaves were monitored for both *arHIF434* lines during the entire life span of plants (**Figure 3**). In both genotypes, the chlorophyll content increased with leaf rank. The start of its decrease marked the onset of leaf senescence. In *arHIF434-Col* oldest leaves (rank <10), the chlorophyll content decrease was concurrent with the flower bud emergence, corresponding to a direct effect of the monocarpic leaf senescence. However, in the *arHIF434-Ct* oldest leaves (rank <10), the chlorophyll content decreased before the flower bud emergence, even though this decrease was more pronounced after the floral transition. The significant difference in chlorophyll content between the two genotypes before and after the flower bud emergence indicated that *SEN4* QTL regulated both sequential and monocarpic senescence.

The N and C percentages were measured in four group of leaves: (1) old leaves (OL), ranks 1–10; (2) mature leaves (ML), ranks 11–20; (3) young leaves (YL), ranks 21–30; and (4) new leaves (NL), ranks 31 to >40. Independently of the genotype, the average N percentage was higher in the OL, ML, and YL than in NL (**Figure 4A**). In contrast, the average C percentage increased from OL to NL (**Figure 4B**). There was no significant variation in the average N percentage between the two *arHIF434* lines irrespective of the leaf group (**Figure 4A**). However, the average C percentage was lower in *arHIF434-Ct* than in *arHIF434-Col* in the OL and ML groups, which corresponded to the most senescent leaves (**Figure 4B**). Such differences in element composition between the two genotypes could be due to the effect of *ACD6* on leaf growth or nutrient mobilization.

The N and C percentages showed different kinetics during plant development (**Figures 4C,D**). The N percentage decreased slowly with plant age, starting on average from 7.5% to reach a plateau at 4.5% (**Figure 4C**). We noticed a genetic variation in the N percentage kinetic only for OL, in which the decrease in N percentage was faster in *arHIF434-Ct* than in *arHIF434-Col*. The C percentages varied among groups of leaves from 32.3% on average for OL to 38.1% on average for NL. In all leaf groups, the C percentage slightly decreased with plant age in *arHIF434-Ct*, while it increased in *arHIF434-Col* (**Figure 4D**). The genetic differences in C and N percentage kinetics revealed that *SEN.4* QTL affected the nutrient remobilization from senescing leaves to new organs.

ACD6 Activity Modulates Rosette Biomass

In a previous study, Chardon et al. (2014) showed that leaf senescence was negatively correlated with rosette, stem, and seed biomass in the *Ct-1* × *Col-0* population and that the *metaQTL4.2* (overlapping the *SEN.4* QTL) had a positive effect on leaf senescence and a negative effect on rosette, stem, and seed biomass. Furthermore, Todesco et al. (2010) have previously shown that a hyperactive allele of *ACD6* reduces leaf biomass.

In order to investigate the role of *ACD6*, not only during vegetative growth but also during all plant development, the overall DW average variations in three plant compartments, rosette, stem, and seeds (one parameter of plant fitness) were analyzed at maturity in four genotypes (*arHIF434-Ct*, *arHIF434-Col*, *Col-0*, and *acd6-2* mutant) displaying different ACD6

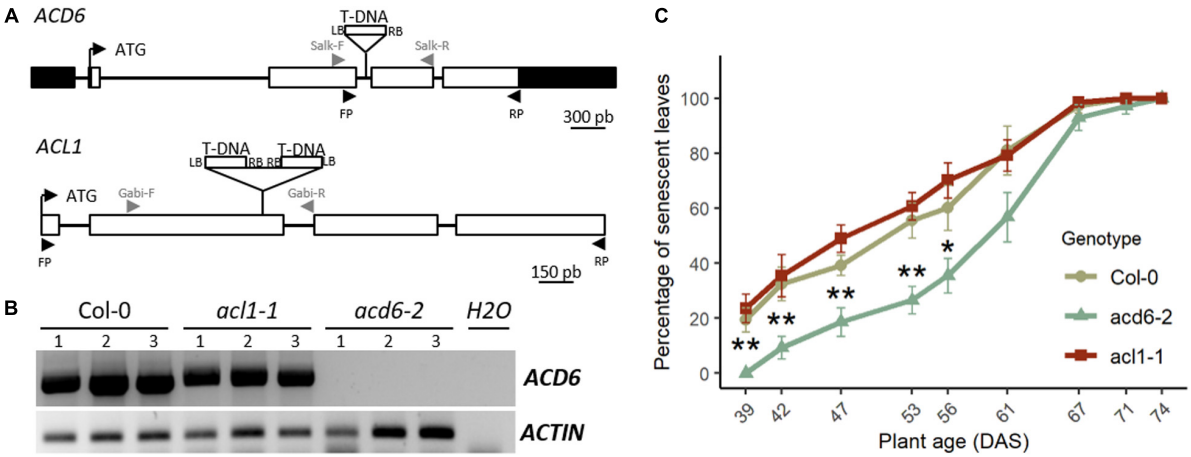

FIGURE 2 | *acd6-2* mutant displays a delayed leaf senescence. **(A)** Structure of the *ACL1* and *ACD6* genes with positions of the T-DNA insertions in *acl1-1* and *acd6-2* mutants is indicated. White boxes represent exons, lines indicate intron, and black boxes represent 5′ and 3′ untranslated regions (UTRs). LB, left border of T-DNA; RB, right border of T-DNA. Gray arrowheads correspond to primers used to genotype mutants. Black arrowheads correspond to primers used for RT-PCR. **(B)** Reverse transcription PCR (RT-PCR) analysis of *ACD6* expression in the fourth leaf of 4-week-old plants of wild type (*Col-0*), *acl1-1*, and *acd6-2*. For each genotype, three different plants (1, 2, and 3) were analyzed. *ACTIN* was used as a constitutively expressed gene control. Primers used for RT-PCR are indicated by black arrowheads in panel **(A)**. **(C)** Percentage of senescent leaves in *Col-0* (khaki round line), *acd6-2* (green triangle line), and *acl1-1* (burgundy square line). Stars indicate significant difference between *Col-0* and *acd6-2* (Student's test, $7 \leq n \leq 8$, $^{*}p < 0.05$, $^{**}p < 0.01$).

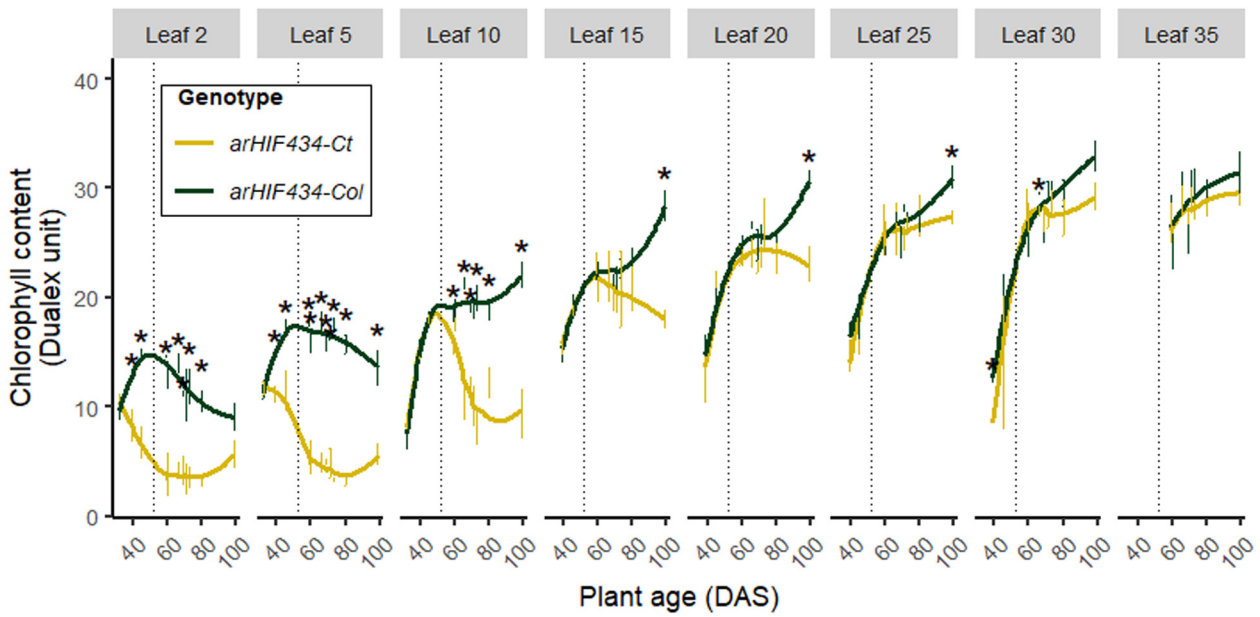

FIGURE 3 | ACD6 activity affects kinetics of chlorophyll content. Yellow and green colors indicate values for *arHIH434-Ct* and *arHIF434-Col*, respectively. Kinetics of chlorophyll content among several leaf ranks in the two *arHIF434* genotypes. Points indicate the average of chlorophyll content (±SE). Stars indicate significant difference between the two genotypes (Student's test, $4 \leq n \leq 8$, $p \leq 0.05$). Vertical dotted lines show the flower bud emergence at 52 days after sowing (DAS).

activity (**Figure 5**). *arHIF434-Ct* displayed a reduced rosette DW compared to *arHIF434-Col*. Conversely, *acd6-2* mutant showed an increased rosette DW compared to *Col-0* (**Figure 5A**). This result was in accordance with *Ct-1* and *acd6-2* alleles being hyperactive and hypomorphic alleles, respectively, compared to *Col-0* allele. *arHIF434-Ct* displayed a reduced stem DW compared to *arHIF434-Col*, but no significant difference in stem DW was observed between *Col-0* and *acd6-2* (**Figure 5B**). No significant difference in seed DW was observed between the two *arHIF434* genotypes, neither between *Col-0* and *acd6-2* (**Figure 5C**). As a result, the harvest index (HI), measured as the seed DW divided by total plant DW, was higher in *arHIF434-Ct* compared to *arHIF434-Col* and lower in *acd6-2* compared to *Col-0* (**Figure 5D**). It is important to mention

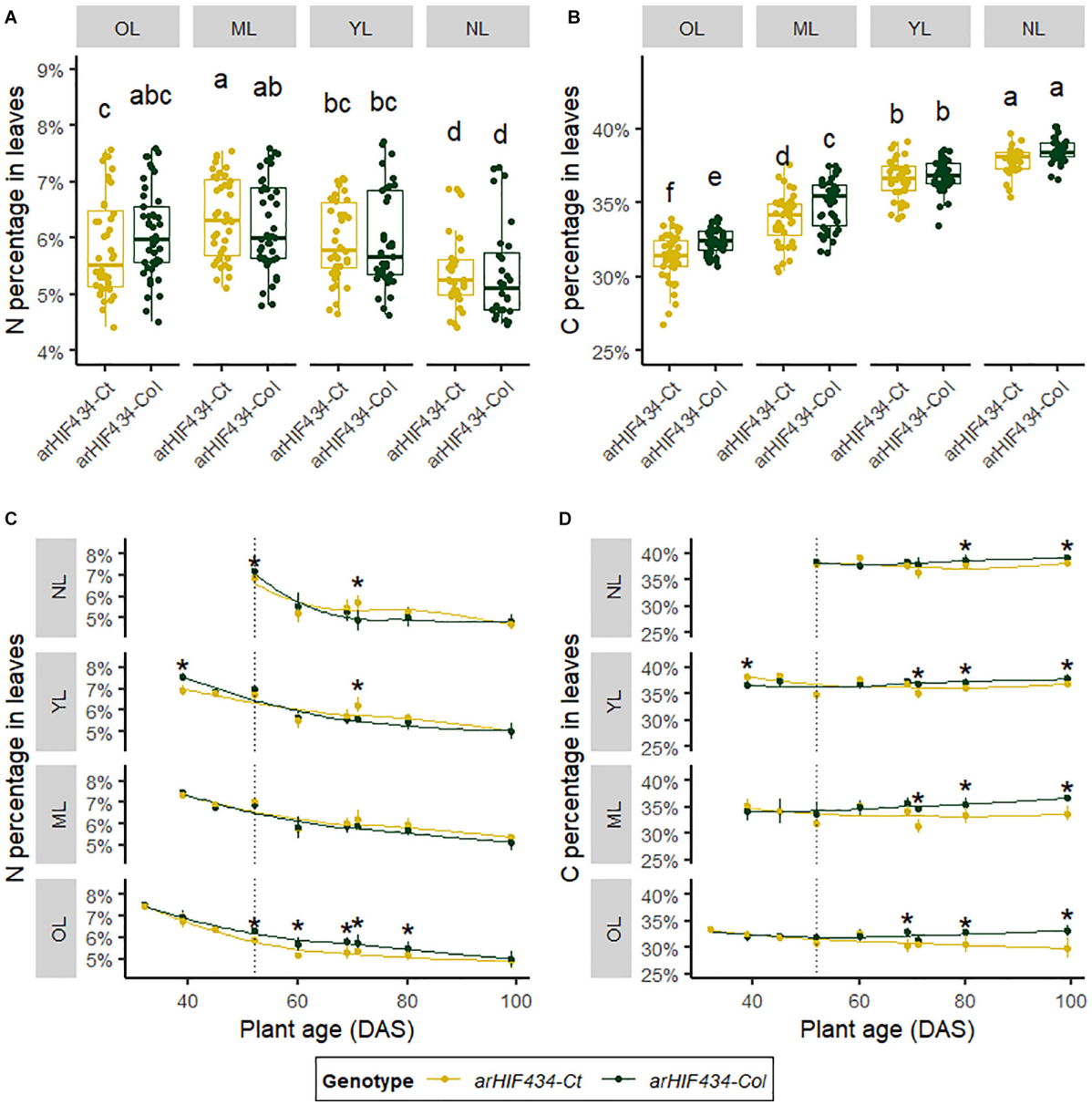

FIGURE 4 | ACD6 activity acts on mobilization of nitrogen and carbon depending on rosette leaf rank. Yellow and green colors indicate values for *arHIH434-Ct* and *arHIF434-Col*, respectively. **(A)** Nitrogen and **(B)** carbon percentages in the groups of leaves in the two *arHIF434* genotypes. Leaves were gathered by groups of 10 leaves: old leaves (OL), ranks 1–10; mature leaves (ML), ranks 11–20; young leaves (YL), ranks 21–30; and new leaves (NL), ranks 31 to >40. Different letters indicate significant difference (Tukey's test, $30 \leq n \leq 48$, $p \leq 0.05$). Kinetics of nitrogen **(C)** and carbon **(D)** percentages in the two *arHIF434* genotypes for the four groups of leaves during plant development. Stars indicate significant difference between the two genotypes (Student's test, $4 \leq n \leq 8$, $p < 0.05$). Vertical dotted lines in panels **(C,D)** show the flower bud emergence at 52 days after sowing (DAS).

that no major flowering time difference was observed between *arHIF434-Ct* and *arHIF434-Col*, neither between *Col-0* and *acd6-2* (result not shown).

ACD6 Enhances Nitrogen Remobilization to Seeds

N partitioning between plant organs at the end of the plant's life was investigated (**Figure 6A**). *arHIF434-Ct* and *Col-0* plants allocated more nitrogen to their seeds compared to *arHIF434-Col* and *acd6-2* plants, respectively, even though the difference is not significant between Col-0 and *acd6-2*. However, we did not find a clear impact of *ACD6* on seed quality (**Supplementary Figure 4**). In addition, the proportion of N in rosette was lower in *arHIF434-Ct* and *Col-0* compared to *arHIF434-Col* and *acd6-2* plants, respectively (**Figure 6**). Similarly, *arHIF434-Ct* showed lower C percentage in rosette than *arHIF434-Col* (**Supplementary Figure 4**).

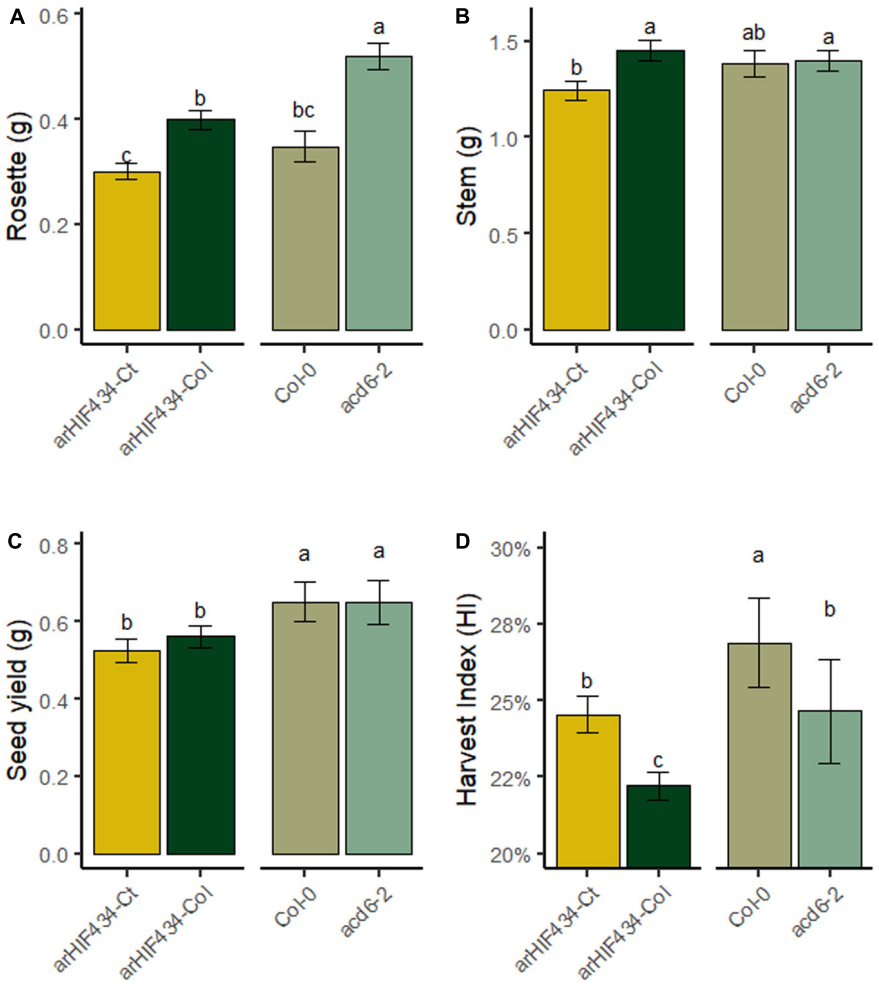

FIGURE 5 | ACD6 activity impacts harvest index by modulating rosette biomass. The dry weight (DW) of **(A)** rosette, **(B)** stem, and **(C)** seeds was measured at harvest and **(D)** the harvest index calculated as the seed DW divided by total plant DW for the four genotypes (*arHIF434-Ct*, *arHIF434-Col*, *Col-0*, and *acd6-2*). Least-square means from two independent experiments ± SE are shown ($n \geq 11$ for each genotype). Different letters indicate significant difference (Tukey's test, $p \leq 0.05$).

These modifications of N partitioning in plants, and the strong variation in nutrient mobilization in rosette (**Figures 4A,C**), suggested together that ACD6 activity modifies N fluxes in plants.

To better understand the observed differences in N allocation, ^{15}N labeling experiments were performed. The ^{15}N labeling was applied before bolting, allowing to measure N remobilization from rosette leaves to inflorescence stems and seeds, with the proportion of ^{15}N found in the different plant parts (Havé et al., 2016). In both genetic backgrounds (*arHIF434* and *Col-0*), the most active allele of *ACD6* enhanced the proportion of ^{15}N in seeds (^{15}NHI) and reduced the proportion of ^{15}N in rosette compared to the less active allele (**Figure 6B**). We concluded that ACD6 enhanced plant capacity to remobilize N from rosette to seeds. The N remobilization efficiency (NRE), measured as ^{15}NHI on HI ratio, was higher in *arHIF434-Ct* and *Col-0* compared to *arHIF434-Col* and *acd6-2* plants, respectively (**Figure 6C**). These results demonstrated that ACD6 activity modulates N remobilization efficiency in plants; the more the ACD6 activity, the higher the level of remobilization.

ACD6 Does Not Affect Nitrate Uptake Efficiency but Enhances N Translocation to Silique

To complete our analysis of ACD6 effect on N fluxes in plants, nitrate uptake capacity of plants during the vegetative and reproductive phases was analyzed. After 24 h of ^{15}N labeling, whole plants were harvested, and ^{15}N content in roots and rosette was measured. The *arHIF434-Ct* and *Col-0* had absorbed less ^{15}N than *arHIF434-Col* and *acd6-2*, respectively (**Figure 7A**). Since the two last genotypes displayed higher plant weight than the two first ones (**Figure 7B**), the resulting nitrate uptake efficiencies (NUpE), computed as the ratio between ^{15}N quantity absorbed and the biomass of plant, were similar in all the genotypes (**Figure 7C**). Moreover, no variation in ^{15}N transfer between old

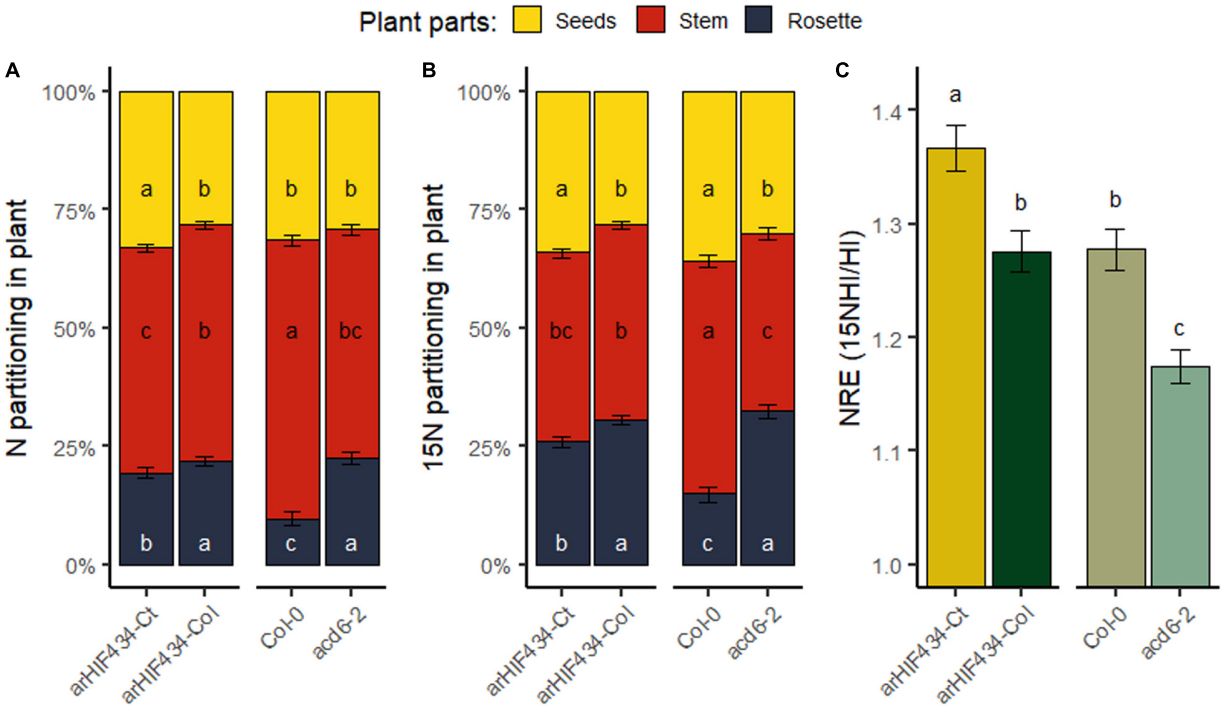

FIGURE 6 | ACD6 modulates N partitioning and N remobilization. **(A)** Proportion of total N in rosette, stem, and seeds in the four genotypes (*arHIF434-Ct*, *arHIF434-Col*, *Col-0*, and *acd6-2*). **(B)** Proportion of total ^{15}N in rosette, stem, and seeds in the four genotypes. **(C)** Nitrogen remobilization efficiency for the four genotypes. Least-square means from three independent experiments ± SE are shown. Different letters indicate significant difference between the genotypes (Tukey's test, $n \geq 18$, $p \leq 0.05$).

and new leaves was measured between the genotypes at this stage (**Supplementary Figure 5**). Then, we estimated the postflowering N uptake in the two *arHIF434* lines. Like for N uptake during the vegetative phase, *arHIF434-Ct* absorbed less ^{15}N than *arHIF434-Col* in 24 h (**Figure 7D**), but the NUpE of both genotypes were similar (**Figure 7E**) since *arHIF434-Ct* is smaller than *arHIF434-Col*. Interestingly, the proportion of ^{15}N stored in silique was more important in *arHIF434-Ct* than in *arHIF434-Col* (**Figure 7F**). Simultaneously, *arHIF434-Col* transferred more nitrate from the roots to inflorescence stems and rosette than *arHIF434-Ct*. We concluded that an enhanced ACD6 activity promoted the translocation of nitrogen from root to silique.

DISCUSSION

ACD6 Regulates Natural Senescence Process Before and After the Flowering Time

Leaf senescence is a crucial process for nutrient mobilization and recycling from old organs to support the growth of new organs. Previously, we detected a locus, *SEN.4*, involved in a large variation in leaf senescence between *Col-0* and *Ct-1* accessions (Chardon et al., 2014). Here, we fine mapped the locus to a small genomic region including two genes, *ACL1* and *ACD6* (**Figure 1C**). The first one is nearly not expressed in plant (eFP Browser, Winter et al., 2007). It was indeed undetectable in wild-type *Col-0* leaves. The latter is specifically expressed in leaves (eFP Browser, Winter et al., 2007). Furthermore, *ACD6* is expressed during the entire leaf lifespan but in an age-dependent manner (Andriankaja et al., 2012; Woo et al., 2016).The absence of *ACD6* gene expression in the corresponding *acd6-2* knockout mutant (**Figure 2B**) delays rosette leaf senescence. On the contrary, the senescence of the *acl1-1* mutant is not affected compared to *Col-0* (**Figure 2C**), in accordance with the phenotype of a KO mutant with artificial microRNA (Todesco et al., 2014). Together, the fine mapping and the phenotype of the mutants demonstrated that *ACD6* regulates the natural leaf senescence process and that its polymorphism is involved in the leaf senescence variation observed between *Col-0* and *Ct-1* accessions.

ACD6 gene encodes a protein with ankyrin and transmembrane domains (Lu et al., 2003). The spontaneous leaf necrosis phenotype of the gain of function mutant gave the name of the gene: *ACCELERATED CELL DEATH 6* (Lu et al., 2003). Little is known about the molecular function of ACD6 protein (Lu et al., 2005). Nevertheless, it has been demonstrated that the ACD6 protein plays a major role in plant response to biotic and abiotic stresses through the SA signaling pathway (Rate et al., 1999; Todesco et al., 2014; Pluhařová et al., 2019). During pathogen infection, the rise in SA levels in leaves triggers the cell death program and leaf necrosis. Todesco et al. (2010) revealed that the natural variation in *ACD6* expression affects both leaf initiation rate and late-onset leaf

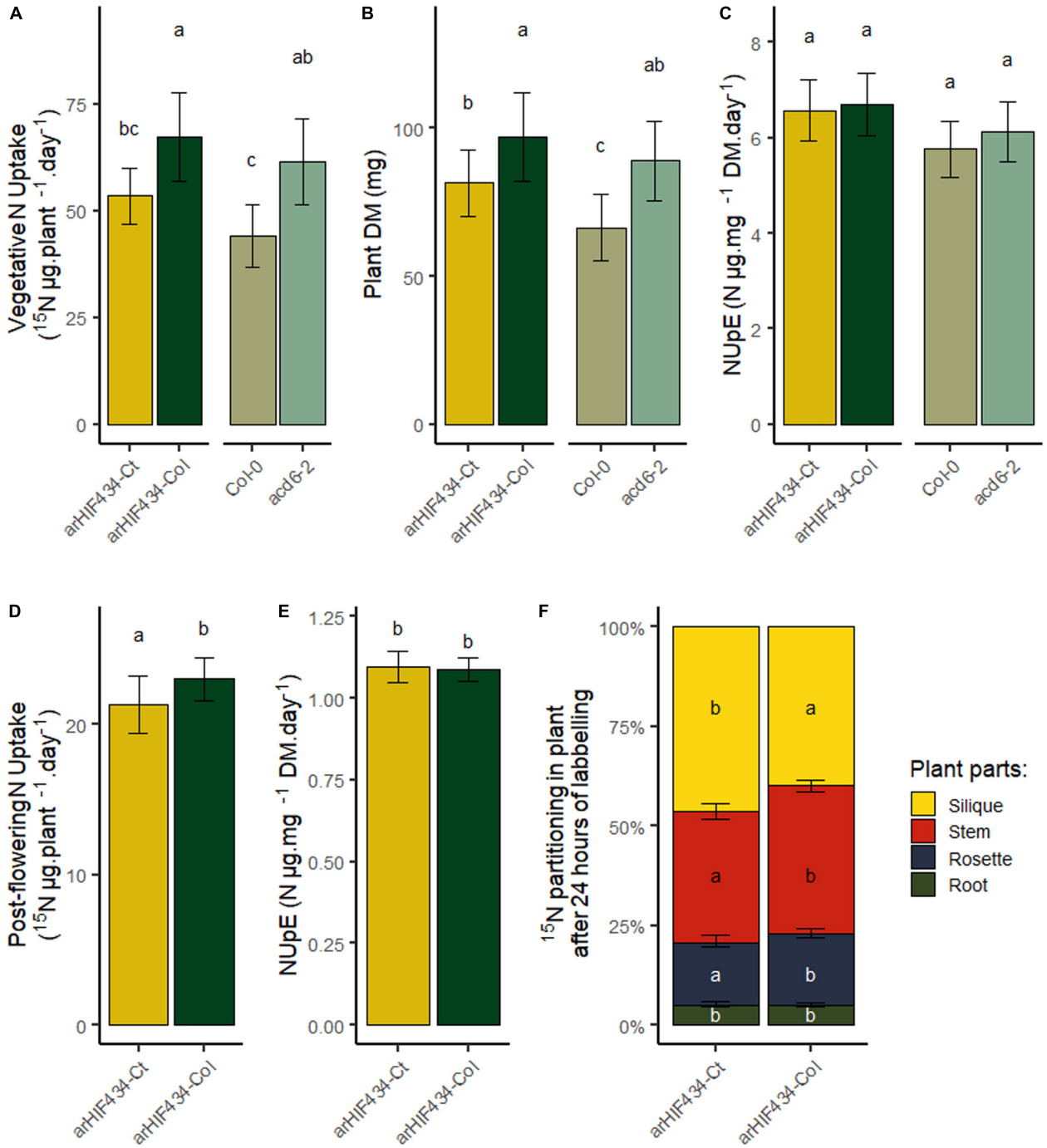

FIGURE 7 | ACD6 does not affect N nitrate uptake efficiency but enhances nitrogen translocation from root to silique. **(A)** Vegetative N uptake in the two *arHIF434* genotypes, *Col-0* and *acd6-2*, as quantity of ^{15}N absorbed during 24 h. **(B)** Plant dry matter in the four genotypes. **(C)** Vegetative N uptake efficiency of the four genotypes. **(D)** Postflowering N uptake in the two *arHIF434*, as quantity of ^{15}N absorbed during 24 h. **(E)** Postflowering N uptake efficiency in the two *arHIF434*. **(F)** Nitrogen translocation from the roots to the other plant parts. Least-square means from two independent experiments ± SE are shown (n = 15 for each genotype). Different letters indicate significant difference between the genotypes (Tukey's test, $p \leq 0.05$).

necrosis by using the diversity of *Arabidopsis* accessions. The hyperactive *ACD6* allele of *Est-1* accession, a closely related allele of *Ct-1*, reduced the leaf initiation and induced extensive and spontaneous necrosis development on fully expanded leaves. Interestingly, *ACD6* is also involved in the hybrid incompatibility generated by crossing two genotypes from the same species (Todesco et al., 2014; Świadek et al., 2017). Specific combinations of *ACD6* alleles caused natural hybrid necrosis resulting in

spontaneous activation of plant defenses associated with leaf cell death, reduced growth, accumulation of SA, and low fertility in hybrids. The geographic dispersion of natural *ACD6* alleles, sometimes incompatible, that enhances either plant defense or leaf growth support the hypothesis that the *ACD6* locus is involved in an adaptive trade-off in *Arabidopsis* (Todesco et al., 2014; Świadek et al., 2017). In this study, the analysis of four genotypes displaying three *ACD6* alleles—the hyperactive *Ct-1*, the *Col-0* or the hypomorphic *acd6-2* allele—was congruent with this role of *ACD6*. Indeed, the *Ct-1* hyperactive allele of *ACD6* promoted the natural leaf senescence but reduced the rosette and stem inflorescence DW compared to the *Col-0* allele (**Figures 1**, **5**). On the contrary, the *acd6-2* hypomorphic allele of *ACD6* slowed natural leaf senescence down but increased rosette DW (**Figures 2**, **5**).

During the *Arabidopsis* lifespan, two phases of senescence can be distinguished (Schippers et al., 2015). During the first one, occurring before the flower bud emergence, the sequential leaf senescence appears sequentially from the older basal rosette leaves to the younger apical ones. Then, the stem inflorescence development and seed production lead to the need of rosette compound recycling. Consequently, the development of seeds enhanced the senescence of all rosette leaves in *Arabidopsis*. Previous observations of *ACD6* allelic variation report leaf necrosis during vegetative stage. Following chlorophyll content kinetic before and after the flower bud emergence, we provided evidence that ACD6 regulates both the sequential and monocarpic senescence (**Figure 3**).

ACD6 Modulates Finely the Nitrogen Remobilization Efficiency

In plants, senescence is a dynamic process with several phases in which the nutrients, especially N-rich compounds, are remobilized from the senescing organs to the new ones (Malagoli et al., 2005; Diaz et al., 2008; Lemaître et al., 2008). It is a finely regulated genetic process involving a coordinated action at the cellular, tissue, organ, and organism levels (Lim et al., 2007). A complex network of regulatory pathways fine tunes the timing of the plant senescence in response to both external and internal clues, such as plant pathogen, nutrient starvation, and phytohormones, including abscisic acid, jasmonic acid, ethylene, and SA. For instance, SA levels in leaves participates to the natural senescence by regulating the expression of genes that are also modified by abiotic stresses (Morris et al., 2000; Lim et al., 2007). Following the N percentage in leaves and the N remobilization from the leaves to the seeds, we provided evidence that ACD6 acts on N mobilization during leaf senescence (**Figures 4A,C**). We showed that ACD6 also increased by 10% the N remobilization to seeds during the reproductive period (**Figure 6**). Other cellular processes have been previously shown to act simultaneously on leaf senescence and N remobilization to seeds. For instance, defect in the macroautophagy process, an intravesicular process for vacuolar bulk degradation of cytoplasmic components, enhanced leaf senescence but limited N remobilization efficiency. Knockout mutants of autophagy genes conserved only around 40% of their N remobilization efficiency in *Arabidopsis* when the plants were grown in low N condition (Guiboileau et al., 2012). Similarly, a maize mutant affected in the autophagy process displayed only 60% of the N remobilization efficiency of the wild type (Li et al., 2015). Moreover, cytosolic glutamine synthetases, key enzymes of ammonium assimilation during the N recycling process, are induced during leaf senescence (Diaz et al., 2008; Lothier et al., 2011) and act on N remobilization efficiency (Moison et al., 2018). The *gln1;1-gln1;2-gln1;3* triple mutant displayed a 12% reduction in N remobilization to seeds compared to wild type (Moison et al., 2018). In addition, environmental stresses may also have a large effect on N remobilization to seeds, which is increased by 38% under N limited condition or reduced by 45% under heat stress (Marmagne et al., 2020). In this context, we concluded that ACD6 has a major effect on natural senescence but plays a limited role on N remobilization efficiency compared to other cellular processes and environmental stresses.

Advantage and Limitation of a Fast Leaf Senescence Onto N Remobilization Capacity

ACCELERATED CELL DEATH 6 had a positive effect on leaf senescence as well as on N remobilization efficiency of plants although to a lesser extent (**Figures 4**, **6**). Yet, the effect of the locus onto the seed composition was very limited (**Supplementary Figure 4**). Our results highlighted two phenomena occurring during seed filling: (i) the negative impact of excessive leaf senescence on N mobilization process and (ii) the balance between N remobilization and uptake during the reproductive phase.

ACD6 induced a burst of SA levels in cells leading to a rapid cell death and resulting in leaf necrosis as reported by several authors (Lu et al., 2003; Todesco et al., 2014). In our conditions, the plants with a hyperactive *Ct-1 ACD6* allele showed a faster senescence of rosette than the *Col-0* plants (**Figures 1A,B**, **3A**). A fast senescence process might be an asset for the plant to isolate a pathogen infection from the healthy parts of the leaves and to activate concomitantly the plant defense system. An early onset of leaf senescence might also help in mobilizing leaf nutrients. However, even though all the leaves from the *Ct-1* plants senesced more rapidly than the leaves from the *Col-0* ones, we observed that *ACD6* effect on N mobilization (i.e., decrease of N percentage in leaves) varied among leaf ranks (**Figure 4C**). Indeed, the oldest leaves showed the strongest response to *ACD6* variation for N mobilization compared to the youngest and newest leaves. We noticed that variation in N mobilization is associated to the difference in sequential senescence in the old leaves (**Figure 4C**). Nevertheless, the strong mobilization of N induced by seed filling after flower bud emergence did not correlate with the difference in monocarpic senescence between the two genotypes (**Figure 3**). After flower bud emergence, N percentage decreased in medium, young, and new leaves, in contrast to the chlorophyll content (**Figure 3**), highlighting that the mobilization of N compounds occurs before the monocarpic senescence. Similarly to rice, mobilization of metabolites from the flag and second leaves occurs before chlorophyll decrease during grain filling (Ray and Choudhuri, 1981; Lee et al., 2017). We assumed that if leaf

senescence is early but too intense, the N mobilization process could be interrupted due to the rapid death of the leaves.

The N stored in seed is derived from direct N uptake from the soil and N recycling from other organs during the reproductive phase (Masclaux-Daubresse et al., 2010). Growing and storage organs are two elements that drive N transportation within plants (Yoneyama et al., 2003). Likewise, the source–sink relationship created by seed production is the main driver of N remobilization efficiency in *Arabidopsis* (Masclaux-Daubresse and Chardon, 2011). In the present study, the use of ^{15}N-labeled nitrate allowed us to estimate postflowering N uptake and remobilization of plants. We showed that *ACD6* acts on the N remobilization efficiency (**Figure 6**) but does not affect the N uptake efficiency, during neither vegetative nor reproductive stages (**Figures 7C,E**). However, *ACD6* impaired N fluxes and N translocation during the reproductive phase (**Figure 7F**). In particular, *ACD6* activity enhanced the translocation of nitrogen from root to silique. We assumed then that the death of several leaves, due to the action of *ACD6*, limits transitory storage of N in rosette. Following this hypothesis, the N requirements for seed filling are fulfilled by N uptake in hyperactive *Ct-1 ACD6* allele, reducing the strength of the sink for N remobilization. Consequently, the positive effect of *ACD6* onto N remobilization due to early leaf senescence is partially balanced by the negative and indirect effect of *ACD6* on N uptake. Similar compensatory phenomenon between N uptake and N mobilization have been observed in maize in which an accelerated leaf senescence results in a decrease in source–sink ratio and a reduction in the proportion of N in the grain that was taken up during grain filling (Rajcan and Tollenaar, 1999).

We observed that leaf senescence was negatively correlated to N percentage in seeds in different recombinant inbreed line populations, in particular the *Ct-1* × *Col-0* one (Chardon et al., 2014). Several hypotheses could explain the difference between the QTL effect on N percentage in seeds in the *Ct-1* × *Col-0* population and the lack of effect detected in the present study (**Supplementary Figure 4**). First, the genetic regulation of seed filling is complex, and different genes could be located in the same genomic region and act independently on leaf senescence and seed filling. Second, because seed filling is sensitive to the environment (Marmagne et al., 2020), the small environmental variations inherent to the different experiments may change the regulation of the seed filling process. Third, because the senescence process is also influenced by a range of environmental factors, such as low nutrient supply, photoperiod, temperature, and drought (Lim et al., 2007; Schippers et al., 2015; Santos Matos, 2020), small variations in the environment may affect the leaf senescence intensity promoted by the hyperactive *ACD6* allele. Several genetic analyses pointed out that both the onset and the duration of leaf senescence act on the grain filling in crop plants (Hafsi et al., 2000; Gregersen et al., 2013; Xie et al., 2016; Kitonyo et al., 2018). For instance, Xie et al. (2016) showed that a delayed but fast leaf senescence promoted grain-filling rates in bread wheat. These results were in accordance with our hypothesis that the duration and intensity of leaf senescence act on the N mobilization process. In addition to the trade-off opposing plant growth and plant defense associated to *ACD6* reported by Todesco et al. (2014), we bring here a new link showing the extra level of regulation of *ACD6* on leaf senescence and nutrient use efficiency.

DATA AVAILABILITY STATEMENT

The raw data supporting the conclusions of this article will be made available by the authors, without undue reservation.

AUTHOR CONTRIBUTIONS

SJ, IF, AmM, and AL performed the QTL fine mapping. SJ performed the phenotyping and molecular analysis of the T-DNA mutants, as well as the *ACD6* sequences analysis. FC and SJ did the chlorophyll measurement. AnM performed C and N percentage analyses and ^{15}N isotopic measurements. AnM and SJ performed the q-RT-PCR. FC carried out the statistical analysis. FC and SJ designed the research, analyzed the data, and wrote the manuscript. All authors read and approved the final manuscript.

FUNDING

This work was benefited from the support of IJPB's Plant Observatory Technological Platforms. The IJPB benefits from the support of Saclay Plant Sciences-SPS (ANR-17-EUR-0007).

ACKNOWLEDGMENTS

We thank Céline Masclaux-Daubresse and Mathilde Fagard for fruitful discussions. We thank Philippe Guerche for critical reading of the manuscript. We also thank Lilian Dahuron and Philippe Marechal for plant care.

SUPPLEMENTARY MATERIAL

The Supplementary Material for this article can be found online at: https://www.frontiersin.org/articles/10.3389/fpls.2020.611170/full#supplementary-material

Supplementary Figure 1 | *arHIF434-Ct* displays an earlier leaf senescence than *arHIF434-Col*. **(A)** *arHIF434* is represented with horizontal bars (black for *Col-0* allele, white for *Ct-1* allele, grey for heterozygous). Dashed vertical bars represent markers delimiting the candidate interval on chromosome 4. Numbers correspond to marker position (Mb). Position of *ACL1* and *ACD6* genes are shown above the arHIF. **(B)** Rosette leaves of 5-week-old plants. Upper rows: *arHIF434-Ct*, lower rows: *arHIF434-Col*. Scale bar corresponds to 1 cm. **(C)** Percentage of senescent leaves in *arHIF434-Ct* (yellow triangle line) and *arHIF434-Col* (dark green circle line) during the reproductive phase. Flowering transition occurred in average at 23.7 DAS for *arHIF434-Col* and 23.9 DAS for *arHIF434-Ct*.

Supplementary Figure 2 | Protein sequence alignment of ACD6 from *Col-0* and *Ct-1* accessions. Numbers indicate amino acid position from the first Methionine. Grey box correspond to ankyrin repeats and black lines to transmembrane domains as predicted using SMART website (http://smart.embl-heidelberg.de/). *Amino acids 566 and 634.

Supplementary Figure 3 | Expression of *ACD6* in *arHIF434-Ct* and *arHIF434-Col*. Plants were grown under long days (8 h light/16 h dark) for 35 d after sowing and then harvested. Transcript levels of *ACD6* **(A)**; *SAG12* **(B)**, and *RBCS1A* **(C)** marker genes of leaf senescence, and *PR1* **(D)** involved in SA signaling process, were monitored using RT–qPCR and specific primers (**Supplementary Table 1**). Expression of *ACD6* was normalized using *PP2AA3* and *APC2*. Expression of *PR1*, *SAG12* and *RBCS1A* were normalized using *PP2AA3*.

Supplementary Figure 4 | Effect of *ACD6* on N and C percentages in the different parts of the plants. N and C percentages in rosette **(A,B)**, stem **(C,D)**, and seeds **(E,F)**. N and C percentages for the four genotypes (*arHIF434-Ct*, *arHIF434-Col*, *Col-0* and *acd6-2*) are shown. Least-square means from 3 independent experiments ± s.e. are shown ($n \geq 18$ for each genotype). Different letters indicate significant difference (Tukey's test, p-value ≤ 0.05).

Supplementary Figure 5 | ACD6 does not affect N translocation (T1) and remobilization (T2) from old leaves to young leaves during the vegetative phase. The four genotypes (*arHIF434-Ct*, *arHIF434-Col*, *Col-0* and *acd6-2*) were grown on sand in short day conditions (8 hours). After 48h of labeling with $^{15}NO3$, lower (ranks 1 to 10) and upper (ranks > 10) leaves were harvested and grouped. Proportion of total ^{15}N was measured in the two groups of leaves, just after the labeling period (T1) to estimate the N translocation, and 7 days after (T2) to estimate the N remobilization from old leaves to young leaves during vegetative phase.

REFERENCES

Andriankaja, M., Dhondt, S., DeBodt, S., Vanhaeren, H., Coppens, F., DeMilde, L., et al. (2012). Exit from Proliferation during Leaf Development in Arabidopsis thaliana: A Not-So-Gradual Process. *Dev. Cell* 22, 64–78. doi: 10.1016/j.devcel.2011.11.011

Balazadeh, S., Parlitz, S., Mueller-Roeber, B., and Meyer, R. C. (2008). Natural developmental variations in leaf and plant senescence in Arabidopsis thaliana. *Plant Biol.* 10(Suppl 1), 136–147.doi: 10.1111/j.1438-8677.2008.00108.x

Chardon, F., Barthelemy, J., Daniel-Vedele, F., and Masclaux-Daubresse, C. (2010). Natural variation of nitrate uptake and nitrogen use efficiency in Arabidopsis thaliana cultivated with limiting and ample nitrogen supply. *J. Exp. Bot.* 61, 2293–2302. doi: 10.1093/jxb/erq059

Chardon, F., Jasinski, S., Durandet, M., Lécureuil, A., Soulay, F., Bedu, M., et al. (2014). QTL meta-analysis in Arabidopsis reveals an interaction between leaf senescence and resource allocation to seeds. *J. Exp. Bot.* 65, 3949–3962. doi: 10.1093/jxb/eru125

Diaz, C., Lemaître, T., Christ, A., Azzopardi, M., Kato, Y., Sato, F., et al. (2008). Nitrogen recycling and remobilization are differentially controlled by leaf senescence and development stage in Arabidopsis under low nitrogen nutrition. *Plant Physiol.* 147, 1437–1449. doi: 10.1104/pp.108.119040

Diaz, C., Saliba-Colombani, V., Loudet, O., Belluomo, P., Moreau, L., Daniel-Vedele, F., et al. (2006). Leaf yellowing and anthocyanin accumulation are two genetically independent strategies in response to nitrogen limitation in Arabidopsis thaliana. *Plant Cell Physiol.* 2006:225. doi: 10.1093/pcp/pci225

Gregersen, P. L., Culetic, A., Boschian, L., and Krupinska, K. (2013). Plant senescence and crop productivity. *Plant Mole. Biol.* 82, 603–622. doi: 10.1007/s11103-013-0013-8

Guiboileau, A., Sormani, R., Meyer, C., and Masclaux-Daubresse, C. (2010). Senescence and death of plant organs: Nutrient recycling and developmental regulation. *Comp. Rendus Biol.* 333, 382–391. doi: 10.1016/j.crvi.2010.01.016

Guiboileau, A., Yoshimoto, K., Soulay, F., Bataillé, M. P., Avice, J. C., and Masclaux-Daubresse, C. (2012). Autophagy machinery controls nitrogen remobilization at the whole-plant level under both limiting and ample nitrate conditions in Arabidopsis. *N. Phytol.* 194, 732–740. doi: 10.1111/j.1469-8137.2012.04084.x

Guo, Y., and Gan, S. S. (2012). Convergence and divergence in gene expression profiles induced by leaf senescence and 27 senescence-promoting hormonal, pathological and environmental stress treatments. *Plant, Cell Env.* 35, 644–655. doi: 10.1111/j.1365-3040.2011.02442.x

Hafsi, M., Mechmeche, W., Bouamama, L., Djekoune, A., Zaharieva, M., and Monneveux, P. (2000). Flag leaf senescence, as evaluated by numerical image analysis, and its relationship with yield under drought in durum wheat. *J. Agron. Crop Sci.* 185, 275–280. doi: 10.1046/j.1439-037X.2000.00436.x

Havé, M., Marmagne, A., Chardon, F., and Masclaux-Daubresse, C. (2016). Nitrogen remobilisation during leaf senescence: lessons from Arabidopsis to crops. *J. Exp. Bot.* 68:erw365. doi: 10.1093/jxb/erw365

Himelblau, E., and Amasino, R. M. (2001). Nutrients mobilized from leaves of Arabidopsis thaliana during leaf senescence. *J. Plant Physiol.* 158, 1317–1323. doi: 10.1078/0176-1617-00608

Jibran, R., Hunter, D. A., and Dijkwel, P. P. (2013). Hormonal regulation of leaf senescence through integration of developmental and stress signals. *Plant Mole. Biol.* 82, 547–561. doi: 10.1007/s11103-013-0043-2

Kamal, N. M., Gorafi, Y. S. A., Abdelrahman, M., Abdellatef, E., and Tsujimoto, H. (2019). Stay-green trait: A prospective approach for yield potential, and drought and heat stress adaptation in globally important cereals. *Int. J. Mole. Sci.* 20:5837. doi: 10.3390/ijms20235837

Kim, J., Kim, J. H., Lyu, J., Il, Woo, H. R., and Lim, P. O. (2018). New insights into the regulation of leaf senescence in Arabidopsis. *J. Exp. Bot.* 69, 787–799. doi: 10.1093/jxb/erx287

Kitonyo, O. M., Sadras, V. O., Zhou, Y., and Denton, M. D. (2018). Nitrogen supply and sink demand modulate the patterns of leaf senescence in maize. *Field Crops Res.* 225, 92–103. doi: 10.1016/j.fcr.2018.05.015

Kumar, R., Bishop, E., Bridges, W. C., Tharayil, N., and Sekhon, R. S. (2019). Sugar partitioning and source–sink interaction are key determinants of leaf senescence in maize. *Plant Cell Environ.* 42, 2597–2611. doi: 10.1111/pce.13599

Lee, S., Jeong, H., Lee, S., Lee, J., Kim, S. J., Park, J. W., et al. (2017). Molecular bases for differential aging programs between flag and second leaves during grain-filling in rice. *Sci. Rep.* 7, 1–16. doi: 10.1038/s41598-017-07035-9

Lemaître, T., Gaufichon, L., Boutet-Mercey, S., Christ, A., and Masclaux-Daubresse, C. (2008). Enzymatic and metabolic diagnostic of nitrogen deficiency in Arabidopsis thaliana Wassileskija accession. *Plant Cell Physiol.* 49, 1056–1065. doi: 10.1093/pcp/pcn081

Levey, S., and Wingler, A. (2005). Natural variation in the regulation of leaf senescence and relation to other traits in Arabidopsis. *Plant Cell Environ.* 28, 223–231. doi: 10.1111/j.1365-3040.2004.01266.x

Li, F., Chung, T., Pennington, J. G., Federico, M. L., Kaeppler, H. F., Kaeppler, S. M., et al. (2015). Autophagic recycling plays a central role in maize nitrogen remobilization. *Plant Cell* 27, 1389–1408. doi: 10.1105/tpc.15.00158

Lim, P. O., Kim, H. J., and Gil Nam, H. (2007). Leaf Senescence. *Ann. Rev. Plant Biol.* 58, 115–136. doi: 10.1146/annurev.arplant.57.032905.105316

Lothier, J., Gaufichon, L., Sormani, R., Lemaître, T., Azzopardi, M., Morin, H., et al. (2011). The cytosolic glutamine synthetase GLN1;2 plays a role in the control of plant growth and ammonium homeostasis in Arabidopsis rosettes when nitrate supply is not limiting. *J. Exp. Bot.* 62:1375–1390. doi: 10.1093/jxb/erq299

Loudet, O., Gaudon, V., Trubuil, A., and Daniel-Vedele, F. (2005). Quantitative trait loci controlling root growth and architecture in Arabidopsis thaliana confirmed by heterogeneous inbred family. *Theor. Appl. Genet.* 110, 742–753. doi: 10.1007/s00122-004-1900-9

Loudet, O., Michael, T. P., Burger, B. T., Le Mette, C., Mockler, T. C., Weigel, D., et al. (2008). A zinc knuckle protein that negatively controls morning-specific growth in Arabidopsis thaliana. *Proc. Natl. Acad. Sci. U S A* 105, 17193–17198. doi: 10.1073/pnas.0807264105

Lu, H., Liu, Y., and Greenberg, J. T. (2005). Structure-function analysis of the plasma membrane-localized Arabidopsis defense component ACD6. *Plant J.* 44, 798–809. doi: 10.1111/j.1365-313X.2005.02567.x

Lu, H., Rate, D. N., Song, J. T., and Greenberg, J. T. (2003). ACD6, a Novel Ankyrin Protein. Is a Regulator and an Effector of Salicylic Acid Signaling in the Arabidopsis Defense Response. *Plant Cell* 15, 2408–2420. doi: 10.1105/tpc.015412

Luquez, V. M. C., Sasal, Y., Medrano, M., Martín, M. I., Mujica, M., and Guiamét, J. J. (2006). Quantitative trait loci analysis of leaf and plant longevity in Arabidopsis thaliana. *J. Exp. Bot.* 57, 1363–1372. doi: 10.1093/jxb/erj112

Lyu, J., Il, Kim, J. H., Chu, H., Taylor, M. A., Jung, S., et al. (2019). Natural allelic variation of GVS1 confers diversity in the regulation of leaf senescence in Arabidopsis. *N. Phytol.* 221, 2320–2334. doi: 10.1111/nph.15501

Malagoli, P., Laine, P., Rossato, L., and Ourry, A. (2005). Dynamics of nitrogen uptake and mobilization in field-grown winter oilseed rape (Brassica napus) from stem extension to harvest: I. Global N flows between vegetative and reproductive tissues in relation to leaf fall and their residual N. *Ann. Bot.* 95, 853–861. doi: 10.1093/aob/mci091

Marmagne, A., Jasinski, S., Fagard, M., Bill, L., Guerche, P., Masclaux-Daubresse, C., et al. (2020). Post-flowering biotic and abiotic stresses impact nitrogen use efficiency and seed filling in Arabidopsis thaliana. *J. Exp. Bot.* 71:011. doi: 10.1093/jxb/eraa011

Masclaux-Daubresse, C., and Chardon, F. (2011). Exploring nitrogen remobilization for seed filling using natural variation in Arabidopsis thaliana. *J. Exp. Bot.* 62, 2131–2142. doi: 10.1093/jxb/erq405

Masclaux-Daubresse, C., Daniel-Vedele, F., Dechorgnat, J., Chardon, F., Gaufichon, L., and Suzuki, A. (2010). Nitrogen uptake, assimilation and remobilization in plants: Challenges for sustainable and productive agriculture. *Ann. Bot.* 105, 1141–1157. doi: 10.1093/aob/mcq028

Masclaux-Daubresse, C., Purdy, S., Lemaitre, T., Pourtau, N., Taconnat, L., Renou, J.-P., et al. (2007). Genetic Variation Suggests Interaction between Cold Acclimation and Metabolic Regulation of Leaf Senescence. *Plant Physiol.* 143, 434–446. doi: 10.1104/pp.106.091355

Moison, M., Marmagne, A., Dinant, S., Soulay, F., Azzopardi, M., Lothier, J., et al. (2018). Three cytosolic glutamine synthetase isoforms localized in different-order veins act together for N remobilization and seed filling in Arabidopsis. *J. Exp. Bot.* 69, 4379–4393. doi: 10.1093/jxb/ery217

Morris, K., Mackerness, S. A. H., Page, T., Fred John, C., Murphy, A. M., Carr, J. P., et al. (2000). Salicylic acid has a role in regulating gene expression during leaf senescence. *Plant J.* 23, 677–685. doi: 10.1046/j.1365-313X.2000.00836.x

Pluhařová, K., Leontovyčová, H., Stoudková, V., Pospíchalová, R., Maršík, P., Klouček, P., et al. (2019). "Salicylic Acid Mutant Collection" as a Tool to Explore the Role of Salicylic Acid in Regulation of Plant Growth under a Changing Environment. *Int. J. Mole. Sci.* 20, 1–15. doi: 10.3390/ijms20246365

Rajcan, I., and Tollenaar, M. (1999). Source:sink ratio and leaf senescence in maize. *Field Crops Res.* 60, 255–265. doi: 10.1016/s0378-4290(98)00143-9

Rate, D. N., Cuenca, J. V., Bowman, G. R., Guttman, D. S., and Greenberg, J. T. (1999). The gain-of-function Arabidopsis acd6 mutant reveals novel regulation and function of the salicylic acid signaling pathway in controlling cell death, defenses, and cell growth. *Plant Cell* 11, 1695–1708. doi: 10.1105/tpc.11.9.1695

Ray, S., and Choudhuri, M. A. (1981). Mobilization of Metabolites from Leaves to Grains as the Cause of Monocarpic Senescence in Rice. *Plant Physiol.* 68, 1345–1348. doi: 10.1104/pp.68.6.1345

Santos Matos, F. (2020). Ecophysiology Of Leaf Senescence. *Agron. Agricult. Sci.* 3, 1–6. doi: 10.24966/aas-8292/100020

Schippers, J. H. M., Schmidt, R., Wagstaff, C., and Jing, H. C. (2015). Living to die and dying to live: The survival strategy behind leaf senescence. *Plant Physiol.* 169, 914–930. doi: 10.1104/pp.15.00498

Sekhon, R. S., Saski, C., Kumar, R., Flinn, B. S., Luo, F., Beissinger, T. M., et al. (2019). Integrated Genome-Scale Analysis Identifies Novel Genes and Networks Underlying Senescence in Maize. *Plant cell* 31, 1968–1989. doi: 10.1105/tpc.18.00930

Steynen, Q. J., Bolokoski, D. A., and Schultz, E. A. (2001). Alteration in flowering time causes accelerated or decelerated progression through Arabidopsis vegetative phases. *Can. J. Bot.* 79, 657–665. doi: 10.1139/cjb-79-6-657

Świadek, M., Proost, S., Sieh, D., Yu, J., Todesco, M., Jorzig, C., et al. (2017). Novel allelic variants in ACD6 cause hybrid necrosis in local collection of Arabidopsis thaliana. *N. Phytolog.* 213, 900–915. doi: 10.1111/nph.14155

Todesco, M., Balasubramanian, S., Hu, T. T., Traw, M. B., Horton, M., Epple, P., et al. (2010). Natural allelic variation underlying a major fitness trade-off in Arabidopsis thaliana. *Nature* 465, 632–636. doi: 10.1038/nature09083

Todesco, M., Kim, S. T., Chae, E., Bomblies, K., Zaidem, M., Smith, L. M., et al. (2014). Activation of the Arabidopsis thaliana Immune System by Combinations of Common ACD6 Alleles. *PLoS Genetics* 10:e1004459. doi: 10.1371/journal.pgen.1004459

Tuinstra, M. R., Ejeta, G., and Goldsbrough, P. B. (1997). Heterogeneous inbred family (HIF) analysis: a method for developing near-isogenic lines that differ at quantitative trait loci. *Theor. Appl. Genet.* 95, 1005–1011. doi: 10.1007/s001220050654

Wehner, G. G., Balko, C. C., Enders, M. M., Humbeck, K. K., and Ordon, F. F. (2015). Identification of genomic regions involved in tolerance to drought stress and drought stress induced leaf senescence in juvenile barley. *BMC Plant Biol.* 15:0524. doi: 10.1186/s12870-015-0524-3

Wingler, A. (2018). Transitioning to the next phase: The role of sugar signaling throughout the plant life cycle. *Plant Physiol.* 176, 1075–1084. doi: 10.1104/pp.17.01229

Wingler, A., Purdy, S. J., Edwards, S. A., Chardon, F., and Masclaux-Daubresse, C. (2010). QTL analysis for sugar-regulated leaf senescence supports flowering-dependent and -independent senescence pathways. *N. Phytol.* 185, 420–433. doi: 10.1111/j.1469-8137.2009.03072.x

Winter, D., Vinegar, B., Nahal, H., Ammar, R., Wilson, G. V., and Provart, N. J. (2007). An "Electronic Fluorescent Pictograph" browser for exploring and analyzing large-scale biological data sets. *PLoS One* 2:e718. doi: 10.1371/journal.pone.0000718

Woo, H. R., Kim, H. J., Lim, P. O., and Nam, H. G. (2019). Leaf Senescence: Systems and Dynamics Aspects. *Ann. Rev. Plant Biol.* 70, 347–376. doi: 10.1146/annurev-arplant-050718-095859

Woo, H. R., Koo, H. J., Kim, J., Jeong, H., Yang, J. O., Lee, I. H., et al. (2016). Programming of plant leaf senescence with temporal and inter-organellar coordination of transcriptome in arabidopsis. *Plant Physiol.* 171, 452–467. doi: 10.1104/pp.15.01929

Xie, Q., Mayes, S., and Sparkes, D. L. (2016). Early anthesis and delayed but fast leaf senescence contribute to individual grain dry matter and water accumulation in wheat. *Field Crops Res.* 187, 24–34. doi: 10.1016/j.fcr.2015.12.009

Yamada, Y., and Umehara, M. (2015). Possible roles of strigolactones during leaf senescence. *Plants* 4, 664–677. doi: 10.3390/plants4030664

Yoneyama, T., Ito, O., and Engelaar, W. M. H. G. (2003). Uptake, metabolism and distribution of nitrogen in crop plants traced by enriched and natural 15N: Progress over the last 30 years. *Phytochem. Rev.* 2, 121–132. doi: 10.1023/B:PHYT.0000004198.95836.ad

Zhao, Y., Qiang, C., Wang, X., Chen, Y., Deng, J., Jiang, C., et al. (2019). New alleles for chlorophyll content and stay-green traits revealed by a genome wide association study in rice (Oryza sativa). *Sci. Rep.* 9, 1–11. doi: 10.1038/s41598-019-39280-5

Conflict of Interest: Since August 2019, the co-author AmM has been employed by Frontiers Media SA. AmM declared their affiliation with Frontiers and the handling editor states that the process nevertheless met the standards of a fair and objective review.

The remaining authors declare that the research was conducted in the absence of any commercial or financial relationships that could be construed as a potential conflict of interest.

frontiers in Plant Science

ORIGINAL RESEARCH
published: 24 February 2021
doi: 10.3389/fpls.2021.634040

Transcription Factor NAC075 Delays Leaf Senescence by Deterring Reactive Oxygen Species Accumulation in *Arabidopsis*

Chengcheng Kan[1,2†], Yi Zhang[1†], Hou-Ling Wang[1], Yingbai Shen[2], Xinli Xia[1,2], Hongwei Guo[1,3] and Zhonghai Li[1*]*

[1] Beijing Advanced Innovation Center for Tree Breeding by Molecular Design, Beijing Forestry University, Beijing, China, [2] National Engineering Laboratory for Tree Breeding, College of Biological Sciences and Technology, Beijing Forestry University, Beijing, China, [3] Key Laboratory of Molecular Design for Plant Cell Factory of Guangdong Higher Education Institutes, Department of Biology, Southern University of Science and Technology (SUSTech), Shenzhen, China

OPEN ACCESS

Edited by:
Yongfeng Guo, Tobacco Research Institute (CAAS), China

Reviewed by:
Pyung Ok Lim, Daegu Gyeongbuk Institute of Science and Technology (DGIST), South Korea
Xin Zhou, Shanghai Normal University, China

***Correspondence:**
Hongwei Guo
guohw@sustech.edu.cn
Zhonghai Li
lizhonghai@bjfu.edu.cn

[†] These authors have contributed equally to this work

Specialty section:
This article was submitted to Plant Physiology, a section of the journal Frontiers in Plant Science

Received: *26 November 2020*
Accepted: *22 January 2021*
Published: *24 February 2021*

Citation:
Kan C, Zhang Y, Wang H-L, Shen Y, Xia X, Guo H and Li Z (2021) Transcription Factor NAC075 Delays Leaf Senescence by Deterring Reactive Oxygen Species Accumulation in Arabidopsis. Front. Plant Sci. 12:634040. doi: 10.3389/fpls.2021.634040

Leaf senescence is a highly complex genetic process that is finely tuned by multiple layers of regulation. Among them, transcriptional regulation plays a critical role in controlling the initiation and progression of leaf senescence. Here, we found that the NAC transcription factor NAC075 functions as a novel negative regulator of leaf senescence. Loss of function of NAC075 promotes leaf senescence in an age-dependent manner, whereas constitutive overexpression of *NAC075* delays senescence in *Arabidopsis*. Transcriptome analysis revealed that transcript levels of antioxidant enzymes such as catalase (CAT), ascorbate peroxidase (APX), and superoxide dismutase (SOD) are significantly suppressed in *nac075* mutants compared with wild-type plants. Electrophoretic mobility shift assay (EMSA) and chromatin immunoprecipitation (ChIP) analyses revealed that NAC075 directly binds the promoter of *catalase 2* (*CAT2*). Moreover, genetic analysis showed that overexpression of *CAT2* suppresses the overproduction of reactive oxygen species (ROS) and the early senescence phenotypes of *nac075* mutants, suggesting that CAT2 acts downstream of NAC075 to delay leaf senescence by repressing ROS accumulation. Collectively, our findings provide a new regulatory module involving NAC075-CAT2-ROS in controlling leaf senescence in *Arabidopsis*.

Keywords: leaf senescence, NAC transcription factor, reactive oxygen species, catalase, *Arabidopsis thaliana*

INTRODUCTION

Leaf senescence is a universal biological phenomenon in nature that contributes to the recycling of nutrients (Guo and Gan, 2005; Hughes and Reynolds, 2005). Senescence is the last stage of leaf development, accompanied by the hydrolysis of a series of macromolecules and the disassembly of chloroplasts and mitochondria, which ultimately leads to leaf death (Buchanan-Wollaston et al., 2005; Mao et al., 2017; Woo et al., 2019). Among them, yellowing of leaves from tip to base due to the loss of chlorophyll is the most striking marker of leaf senescence (Guo and Gan, 2005; Li et al., 2019; Woo et al., 2019). During leaf senescence, nutrients released by the catabolism

of macromolecular substances such as proteins, lipids, and nucleic acids are transferred to active growing organs such as new buds and developing fruits and seeds, or stored for use in the next growing season (Guo and Gan, 2005; Lim et al., 2007; Woo et al., 2019). Efficient senescence is essential for maximizing viability in the next generation or season, while premature senescence induced by a variety of environmental factors declines crop plants' yield and quality (Breeze et al., 2011). Thus, the appropriate onset and progression of leaf senescence are essential for plant fitness, suggesting that senescence evolves as a life history strategy. Significant advances in understanding the regulatory mechanisms of leaf senescence will provide valuable clues for the manipulation of traits of agronomical important plants.

Leaf senescence is a highly complex and orderly dynamic regulation process and is strictly controlled by multiple layers of regulation, including chromatin-mediated, transcriptional, post-transcriptional, translational, and post-translational regulation (Woo et al., 2013, 2019; Kim et al., 2016, 2018). Leaf senescence is not a passive but a highly coordinated process that is regulated by a number of senescence-associated genes (*SAG*s), whose transcripts increase as leaves age. The onset, development, and completion of leaf senescence involve extensive regulation of gene expression (Woo et al., 2013). Genome-wide transcriptional analysis revealed that the leaf senescence process is accompanied by differential expression of thousands of *SAG*s (Breeze et al., 2011; Woo et al., 2016). At the transcription level, transcription factors (TFs) act as core control elements to drive the drastic changes in *SAG*s expression during leaf senescence. The dynamic activation of TFs is triggered by internal signals such as plant hormones or environmental factors such as high salt (Guo and Gan, 2005; Guo, 2013; Li et al., 2018). Significant advances in dissecting the regulatory mechanisms underpinning leaf senescence have benefited from the identification and functional assessment of hundreds of SAGs and their corresponding mutants. Previous studies have identified numerous TFs that participate in the process of leaf senescence in *Arabidopsis*, including NAC (NAM, ATAF1, 2, and CUC2), WRKY, MYB, and bZIP families' TFs, which play important roles in regulating leaf senescence (Lim et al., 2007; Balazadeh et al., 2008; Woo et al., 2019). As one of the largest TF families in plants, NAC TFs receive widespread attention due to their important role in regulating leaf senescence process in a variety of plant species (Kim et al., 2016). The regulatory roles of a number of NAC TFs in leaf senescence have been characterized in *Arabidopsis*. For instance, ORE1 (ANAC092), AtNAP (ANAC029), ATAF1 (ANAC002), JUB1 (ANAC042/ANAC2), VNI2 (ANAC083), and ANAC017/082/090 act as positive or negative regulators of leaf senescence (Guo and Gan, 2006; Balazadeh et al., 2010; Yang et al., 2011; Wu et al., 2012; Jensen et al., 2013; Garapati et al., 2015; Kim et al., 2018). Recent findings revealed that the molecular network of NAC TFs regulates leaf senescence by integrating internal developmental signals and numerous environmental signals (Kim et al., 2016). Although a growing body of evidence indicates that NAC TFs play important roles in leaf senescence, little is known regarding their importance and underlying regulatory mechanisms.

In this study, we found that NAC TF NAC075 functions as a negative regulator of leaf senescence. Mutation of NAC075 evidently hastens leaf senescence, whereas overexpression of *NAC075* markedly prolongs leaf longevity. Biochemical and genetic evidence shows that NAC075 delays leaf senescence by directly upregulating *CAT2* expression and suppressing the accumulation of reactive oxygen species (ROS) in *Arabidopsis*.

MATERIALS AND METHODS

Plant Materials and Growth Conditions

The *Arabidopsis thaliana* ecotype Columbia (Col-0) is the parent strain for all mutants and transgenic lines used in this study. The transfer DNA (T-DNA) insertional mutant *nac075* (SALK_132120C) was obtained from the Nottingham Arabidopsis Stock Centre (NASC). The *nac075 CAT2ox* was generated by genetic cross, and the homozygous plants were identified through PCR-based genotyping. Seeds were surface-sterilized and plated on Murashige and Skoog (MS) medium (4.3 g/L MS salts, 1% sucrose, pH 5.7–5.8, and 8 g/L agar). After stratifying at 4°C for 3 days to improve germination uniformity, the plates were transferred to an environmentally controlled growth room (PAR of 100–150 μE m^{-2} s^{-1}) for 4 days. For plant leaf senescence phenotypic analysis, light-grown seedlings were transferred to soil and grown at 22°C under long-day conditions (16-h light/8-h dark).

Plasmid Construction and Generation of Transgenic Plants

To construct *ProNAC075:GUS*/Col-0, a 3-kb genomic promoter sequence was amplified and inserted into pCambia1391 vector (GenBank Accession-AF234308). To generate *35S:GFP-NAC075*/Col-0, the full-length *NAC075* CDS sequence was amplified and then inserted into pEGAD vector (Cutler et al., 2000). To generate inducible overexpressing lines, the full-length *NAC075* CDS fused with 3xFLAG was into pER8 vector (Zuo et al., 2000). All constructs were transformed into *Agrobacterium tumefaciens* cells (strain GV3101), which was used to transform Col-0 plants by the floral dip method (Clough and Bent, 1998). Primers used for PCR are listed in **Supplementary Table 1**.

RNA Isolation and Real-Time PCR Analysis

Total RNA was isolated by using plant RNA extraction kits (ER301; TransGen Biotech, China), and the complementary DNA was produced using TransScript All-in-One First-Strand cDNA Synthesis kit (AT341; TransGen Biotech). Transcript levels were detected with TransStart Green qPCR SuperMix (AQ111; TransGen Biotech) by using Applied Biosystems 7500 Real-Time PCR System (Life Technologies, Carlsbad, California, United States). Ubiquitin-conjugating enzyme 21 (*UBC21*, AT5G25760) was used as an internal control to normalize the gene expression level. The primers used in this study are listed in **Supplementary Table 1**.

Measurement of Chlorophyll Contents and Maximal Photochemical Efficiencies of PSII

Chlorophyll contents were measured in the third and fourth rosette leaves of *Arabidopsis* using a chlorophyll meter Konica Minolta SPAD502 Plus (Sakura-machi, Hino-shi Tokyo, Japan), and three biological replicates were performed. Maximal photochemical efficiencies of Photosystem II (PSII, Fv/Fm) were measured by using a MultiSpeQ instrument (East Lansing, MI, United States).

GUS Staining

GUS (β-Glucuronidase) staining was performed as described previously (Jefferson, 1989). Plant tissues were incubated with GUS staining solution (100 mM Na_3PO_4, pH 7.0, 1 mM EDTA, 1 mM potassium ferrocyanide, 1 mM potassium ferricyanide, 1% Triton X-100, and 1 mg/ml 5-bromo-4-chloro-3-indolyl-β-D-glucuronide) for 8 to 12 h at 37°C in the dark, followed by decolonization using 95% ethanol.

Detection of Hydrogen Peroxide and Superoxide

The third and fourth leaves (18-day-old) were vacuum-infiltrated with diaminobenzidine tetrahydrochloride (DAB) solution (1 mg/ml 3,3'-diaminobenzidine-4HCl, pH 3.8) and NBT (nitroblue-tetrazole) solution (0.5 mg/ml NBT, 10 mM potassium phosphate, pH 7.8, and 10 mM sodium azide) to detect hydrogen peroxide and superoxide, respectively, incubated in the dark for 8–10 h, and decolorized in 95% ethanol. The intensity of brown and blue coloration indicates H_2O_2 and O^{2-} contents, respectively.

Trypan Blue Staining

Trypan blue staining was performed as described previously with minor modifications (Kim et al., 2009). Briefly, the third and fourth rosette leaves were soaked in trypan blue staining solution (10 g phenol, 10 ml glycerol, 10 ml lactic acid, 10 ml ddH_2O_2, and 0.02 g trypan blue) and stained in a boiling water bath for 3–5 min. Three leaves were completely submerged in trypan blue staining solution. After leaving overnight at room temperature, the leaves were carefully clamped into the decolorizing solution (2.5 g/ml chloral hydrate).

RNA-Sequencing Analysis

The third and fourth rosette leaves of 24-day-old Col-0 and *nac075* mutant plants were collected and ground into a powder in liquid nitrogen. Total RNA was extracted using an RNeasy Plant kit (Qiagen), and the quality and quantity of RNA were detected using an IMPLEN NanoPhotometer (GmbH). RNA-seq data were generated with an Illumina HiSeq 2000 system at Biomarker Ltd. (Beijing, China). Raw reads (fastq format) were trimmed and filtered through in-house perl scripts (Biomarker Ltd. China). The reads were then mapped to *Arabidopsis* reference genome using Hisat2 algorithm. DEGs were filtered using the following criteria: $|\text{Log2 (fold change)}| > 1.0$, $P < 0.05$. Gene ontology (GO) enrichment analysis was performed by using the GO database[1]. Default parameters were used for all bioinformatics software. Raw RNA-seq reads are available at the National Center for Biotechnology Information[2].

Electrophoretic Mobility Shift Assay (EMSA)

The full-length coding region of NAC075 was produced by quantitative RT-PCR (qRT-PCR) and used for developing the DNA constructs to pET32a for the expression of recombinant proteins in *Escherichia coli* BL21 (DE3). Purification of NAC075 protein was conducted according to the protocol included with the His-Trap HP pre-packed minicolumns (GE Healthcare Life Sciences, Uppsala, Sweden). EMSA was performed according to the user guide from the LightShift Chemiluminescent EMSA Kit (Lot#20148, Thermo Scientific). Briefly, the binding reaction was performed in a total volume of 20 μl by incubation of an appropriate amount of NAC075 proteins with 20 fm of biotin-labeled probe DNA and 1 μg of poly (dI–dC) in a reaction buffer (25 mM HEPES-KOH, pH 7.5, 100 mM KCl, 0.1 mM EDTA, 10% [v/v] glycerol, and 1 mM DTT) at room temperature for 30 min. The binding reaction products were resolved on a 6% polyacrylamide gel run in 0.5 × TBE buffer. 5'-biotin-labeled oligonucleotide of *CAT2* was synthesized and used as probes in EMSA (**Supplementary Table 1**).

Chromatin Immunoprecipitation (ChIP) Assays

ChIP experiments were performed as described previously with minor modifications (Saleh et al., 2008). Briefly, 5 g of 4-week-old *35S:GFP-NAC075* leaves was collected into 50-ml Falcon tubes with 37 ml of cross-linked buffer (10 mM Tris–HCl, pH 8.0, 0.4 M sucrose, 1 mM EDTA, 1 mM PMSF, and 1% formaldehyde). Next, 2 M glycine was added for 5 min to quench the cross-linking reaction. The leaves were then washed three times with sterile deionized water, frozen in liquid nitrogen, and quickly ground into a powder. Next, the ground powder was added into 25 ml of nuclear separation buffer and vortexed to isolate chromatin DNA. The sonicated chromatin supernatant (300 μl) was diluted and 50 μl of salmon sperm DNA/protein A agarose beads (Upstate) was added for pre-clearing at 4°C for 1 h with gentle rotation (12 rpm). The solutions were then transferred into two new tubes. Add 10 μl of anti-GFP monoclonal antibody with a dilution of 1:150 (v/v) to one tube, but not the other (as a negative control). After incubation at 4°C overnight, beads were washed with low-salt wash buffer, high-salt wash buffer, and Tris–EDTA (TE) buffer, followed by followed by Proteinase K (10 mg/ml; Sigma-Aldrich) treatment and reverse cross-linking with 5 M NaCl. DNA was extracted with phenol/chloroform/isoamyl alcohol (25:24:1), and then ethanol precipitated with 2 μl of 20 mg/ml glycogen. The purified DNA was resuspended in 20 μl of distilled water and stored at -20°C. All oligonucleotide sequences used here are listed in **Supplementary Table 1**.

[1] http://geneontology.org/

[2] https://www.ncbi.nlm.nih.gov/sra/?term=PRJNA689040

Plant Hormone-Induced Leaf Senescence

The third and fourth leaves (20-day-old) detached from Col-0, *nac075*, and *NAC075ox* plants were treated with 5 mM MES (Mock), 10 μM ACC, 50 mM MeJA, 1 mM SA, 50 μM ABA, 10 mM H_2O_2, or 100 mM NaCl in dark conditions for 3 days, respectively.

Induction of *NAC075* Gene Expression by Treatment With β-Estradiol

The 28-day-old *pER8-FLAG-NAC075* transgenic plants were sprayed with 50 μM β-estradiol. After treatment for 0.5, 1, and 4 h, the third and fourth rosette leaves were detached and used for RNA extraction and qRT-PCR analysis.

RESULTS

Transcript Level of *NAC075* Increases as Leaf Ages

Previous studies have shown that NAC TF NAC075 is related to leaf senescence (Woo et al., 2016; Li et al., 2020), but the underlying regulatory mechanism remains unclear. Toward this end, we firstly performed Real-Time Quantitative Reverse Transcription PCR (qRT-PCR) to examine the transcript levels of *NAC075* in *Arabidopsis* leaves at young, mature, early, and late stage of senescence (**Figure 1A**). Time-course analysis of mRNA level monitored by qRT-PCR revealed that the transcript level of *NAC075* gradually increased during leaf development and senescence (**Figure 1A**). *SAG12*, a widely used marker gene of leaf senescence (Noh and Amasino, 1999; Pontier et al., 1999), was specifically expressed in the senescing leaves (**Supplementary Figure 1A**). We also measured the transcript levels of *AtNAP* and *ORE1*, two well-known positive regulators of leaf senescence (Guo and Gan, 2006; Kim et al., 2009), and found that their expressions also increased as leaves age (**Supplementary Figures 1B,C**). To further verify the age-dependent regulation of *NAC075* mRNA *in planta*, we generated transgenic *Arabidopsis* expressing GUS (β-glucuronidase gene) driven by *NAC075* promoter containing a 3-kb fragment upstream promoter of the start codon (*ProNAC075:GUS*/Col-0). Histochemical staining assay of rosette leaves of 30-day-old *ProNAC075:GUS*/Col-0 plants revealed that the old yellowing leaves displayed higher GUS activity than that in young green leaves (**Figure 1B**), indicative of an increase in *NAC075* expression level during the leaf senescence process.

We next performed qRT-PCR to investigate the influences of other senescence-regulating signals such as plant hormones, ROS, and salt stress on the transcription of *NAC075*. We found that treatment with the ethylene precursor ACC (1-aminocyclopropane-1-carboxylate), methyl jasmonate (MeJA), salicylic acid (SA), abscisic acid (ABA), H_2O_2, and salt evidently increased the expression levels of NAC075 compared to the mock-treated plants (**Figure 1C**). Among them, treatment with ABA greatly enhanced *NAC075* transcription (**Figure 1C**), suggesting that NAC075 may be involved in ABA-induced leaf senescence process.

NAC075 Negatively Regulates Leaf Senescence

To investigate the function of NAC075 in leaf senescence, we examined the senescence-associated phenotypes of *nac075* knockout mutant carrying a T-DNA insert in the third intron of *NAC075* (**Supplementary Figure 2A**) and the transgenic plants overexpressing *NAC075* (*NAC075ox*) (**Figure 2A**). Genotyping analysis demonstrated that *nac075* mutant is a null allele (**Supplementary Figure 2B**), which was confirmed further by gene expression analysis (**Supplementary Figure 2C**). We performed qRT-PCR to detect the *NAC075* transcription in three *NAC075ox* lines (#1, #2, and #3), and selected *NAC075ox* #2 with the highest expression level for subsequent experiments (**Supplementary Figure 3**). We found that *nac075* mutant

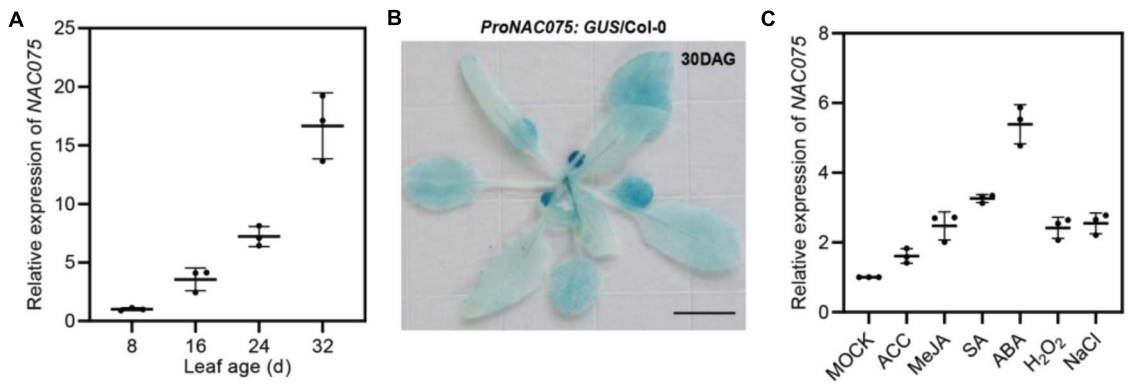

FIGURE 1 | NAC075 transcription factor is a senescence-associated gene that is induced by age, plant hormones, ROS, and salinity. **(A)** qRT-PCR analyses of *NAC075* expression in the third or fourth rosette leaves at the indicated leaf age. Data are represented as means ± SD (n = 3). **(B)** GUS staining of rosette leaves of 30-day-old plants harboring the GUS transgene driven by the promoter of *NAC075* (*ProNAC075:GUS*/Col-0). Scale bar, 1 cm. **(C)** qRT-PCR analyses of *NAC075* expression in the leaves of 20-day-old Col-0 plants upon treatment with 5 mM MES (Mock), 10 μM ACC, 50 mM MeJA, 1 mM SA, 50 μM ABA, 10 mM H_2O_2, or 100 mM NaCl for 6 h. Data are represented as means ± SD (n = 3).

exhibited an early-senescence phenotype in comparison to Col-0 plants under long-day conditions (**Figure 2A**), while *NAC075ox* plant displayed a delayed senescence phenotype (**Figure 2A**), suggesting that NAC075 is a negative regulator of leaf senescence. Interestingly, the *nac075* mutants also displayed early silique senescence (**Supplementary Figure 4**), suggesting that NAC075 is also involved in silique development. Next, we examined the senescence characteristics of single leaf at different ages. Leaf yellowing occurred in the third or fourth rosette leaves of *nac075* mutant plants at 24 days after emergence (DAE), whereas the leaves of Col-0 and *NAC075ox* plants remained green. At 28 DAE, the third and fourth rosette leaves of *nac075* mutants were completely yellowed, which was not observed in Col-0 and *NAC075ox* plants (**Figure 2B**). At 32 DAE, the leaves of Col-0 plant began to turn yellow, while the leaves of *NAC075ox* plants remained green. Leaf yellowing caused by chloroplast decomposition and chlorophyll loss are typical characteristics of leaf senescence (Woo et al., 2001). We also monitored the chlorophyll contents, and photochemical efficiency of photosystem II (PSII; Fv/Fm) decreased more quickly and evidently in *nac075* mutant than in Col-0 (**Figures 2C–E**). The *NAC075ox* plants displayed delayed leaf senescence phenotypes, with elevated chlorophyll content and Fv/Fm compared with Col-0, demonstrating further that NAC075 is a negative regulator of leaf senescence. We also found that aging-induced cell death was accelerated in the *nac075* mutants, which was delayed in *NAC075ox* plants, as shown by the earlier emergence of trypan blue-stained cells in 16 and 24-day-old leaves (**Figure 2F**). Thus, NAC075 is a negative regulator of aging-induced cell death and senescence in *Arabidopsis* leaves.

Given that *NAC075* transcription was induced by multiple plant hormones and stresses (**Figure 1C**), we examined whether NAC075 is involved in the leaf senescence process triggered by these factors. To this end, the third or fourth rosette leaves of 20-day-old Col-0, *nac075* mutants, and *NAC075ox* plants were treated with darkness, plant hormones, ROS, and salt. We found that the leaves of *NAC075ox* plants exhibited the delayed senescence phenotypes upon treatment with these factors (**Supplementary Figure 5**), suggesting that NAC075 delays the leaf senescence process caused by numerous factors. In contrast, the senescence phenotype of *nac075* leaves was not evidently different from that of the wild-type Col-0, indicative of the existence of the functional redundancy among NAC TFs (**Supplementary Figure 5**).

NAC075 Regulates Genes Involved in ROS Scavenging Processes

To elucidate the underlying mechanisms of NAC075 in the regulation of leaf senescence, we performed genome-wide mRNA expression analysis of wild-type and mutant leaves at the presenescent stage (24-day-old) to identify the candidate

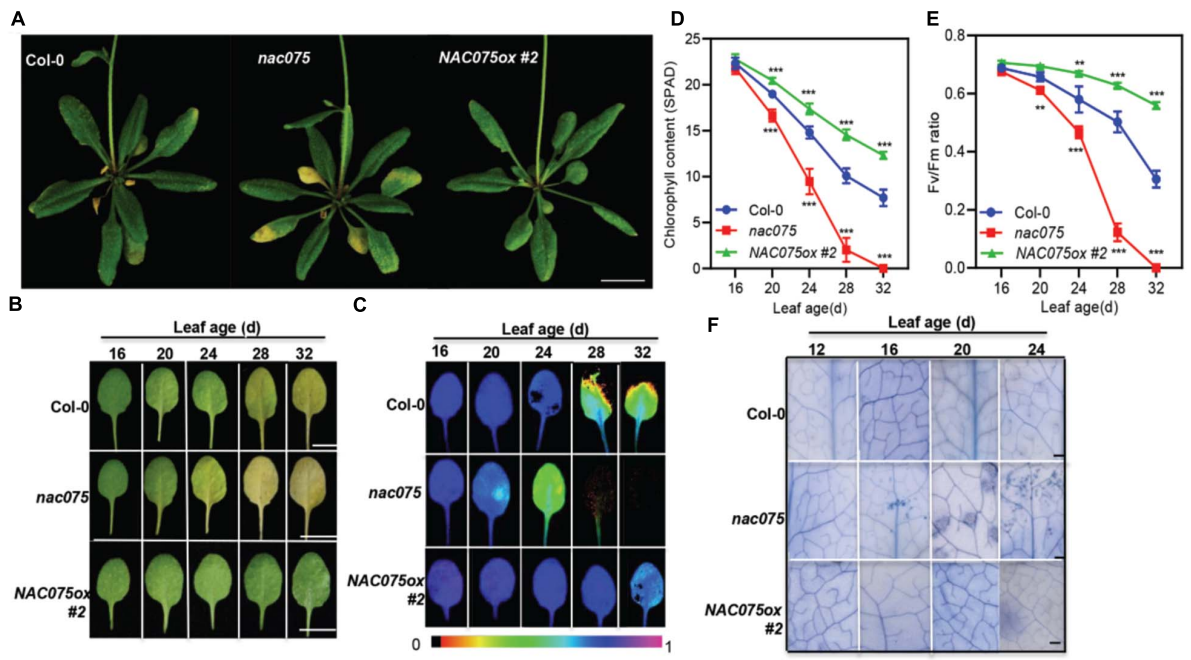

FIGURE 2 | Age-dependent senescence symptoms in the *nac075* mutants and *NAC075ox* plants. **(A)** The senescence phenotypes of 30-day-old Col-0, *nac075* mutants, and *NAC075ox* plants. Early onset of leaf senescence in *nac075* mutant was observed compared with Col-0 plants grown under long-day condition. Scale bar, 1 cm. **(B)** The age-dependent leaf senescence phenotype of Col-0, *nac075* mutants, and *NAC075ox* plants. Photographs show the third or fourth rosette leaves at the indicated days after emergence (DAE). Scale bar, 1 cm. **(C)** Analysis of Fv/Fm in Col-0, *nac075* mutants, and *NAC075ox* plants as leaves age. Image generation was performed by IMAGING-PAM. Image processing was performed by Imaging Win software. **(D,E)** Chlorophyll content **(D)** and Fv/Fm **(E)** in Col-0, *nac075* mutants and *NAC075ox* plants as leaves age. Error bars indicate SD ($n = 3$). Student's *t* test, $^{**}P < 0.01$, $^{***}P < 0.001$. **(F)** Trypan blue staining of leaves at the indicated leaf age. In each plant leaf, dead or dying leaf areas formed blue-colored patches of cells by trypan blue staining. Bar = 500 μm.

target genes. We compared the transcriptomes of wild-type leaves with those of *nac075* mutants and identified 2225, 2241, and 2156 differentially expressed genes (DEGs) in three biological replicates, respectively (**Figure 3A**). Out of them, 1721 genes (491 up-regulated genes and 1211 down-regulated genes) exhibited overlapping differential expression in three biological replicate samples (**Figure 3B**), suggesting substantial regulation by NAC075.

Next, in order to determine the cellular processes associated with the DEGs, we carried out enrichment analysis of GO biological processes (GOBPs) by subjecting the sequences to GO annotations (Young et al., 2010). Interestingly, the GOBP-association analysis revealed that responses to stimulus or chemical (such as salt stresses) and responses to oxygen-containing compounds (such as oxidative/ROS) are the top senescence-promoting processes regulated by NAC075 among

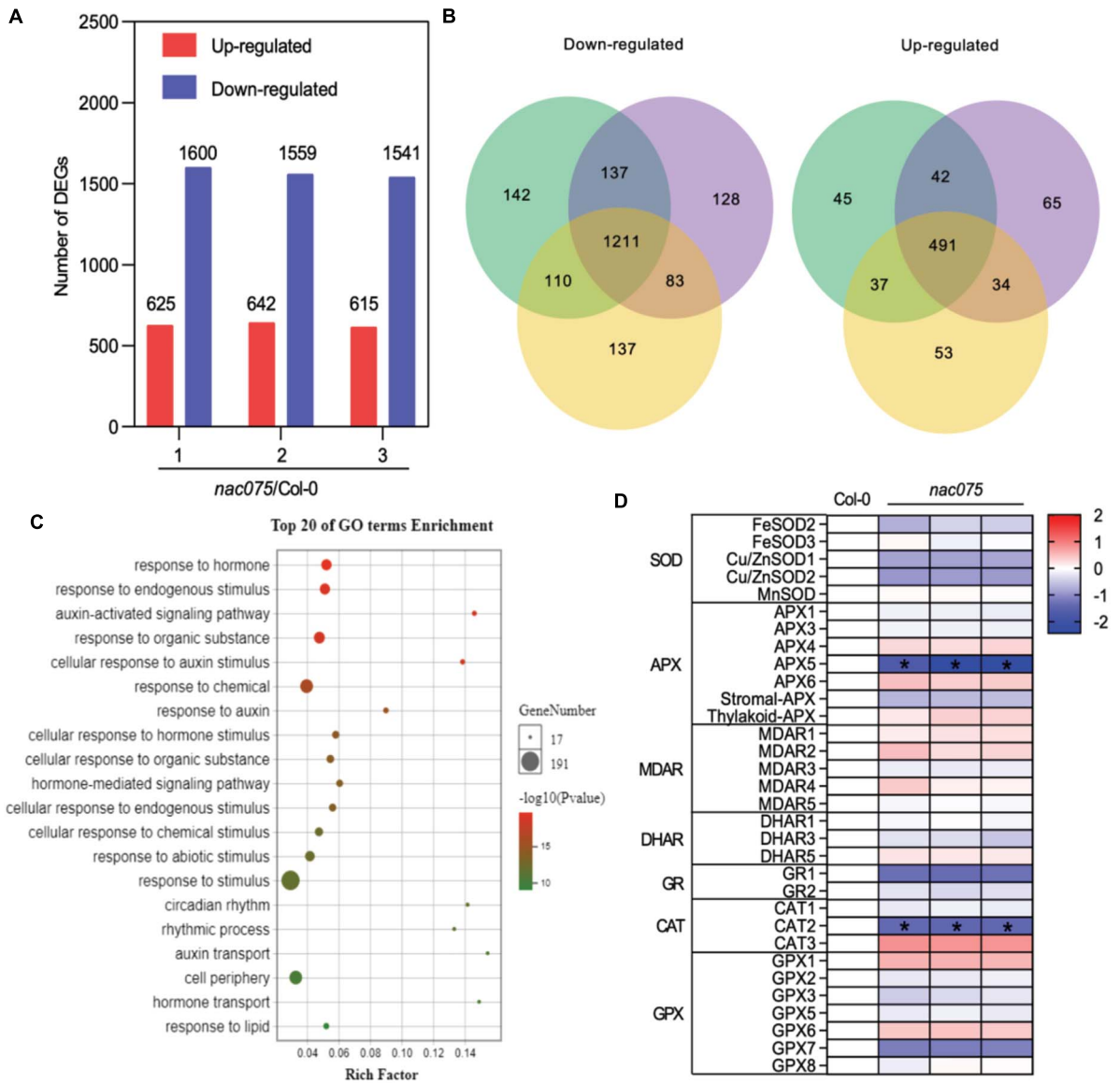

FIGURE 3 | Genome-wide transcriptome analysis of *nac075* mutant plants. **(A)** The number of up-regulated and down-regulated genes in three biological replicates of *nac075* mutant plant rosette leaves vs. Col-0 with RNA-seq. Red represents up-regulated genes, and blue represents down-regulated genes. **(B)** Schematic of the Venn diagram analysis of common down-regulated and up-regulated genes [DEG; | Log2 (FC)| $>$ 1, FDR $<$ 0.05] in three *nac075* mutant plant leaves relative to the Col-0 control. **(C)** GO bubble diagram of down-regulated genes among the DEGs in three *nac075* rosette leaf samples. The bubble size represents the number of DEGs, and the bubble color represents the *P*-value. The rich factor equals the number of DEGs in a certain signaling pathway. **(D)** Heat map showing ROS-related genes in *nac075* mutant plant rosette leaves compared to Col-0. Means of three experiments are shown. The log2 fold change scale is indicated on the right side of the heat map. SOD, superoxide dismutase; APX, ascorbate peroxidase; MDAR, monodehydroascorbate reductase; DHAR, dehydroascorbate reductase; GR, glutathione reductase; CAT, catalase; GPX, glutathione peroxidate.

all processes (**Figure 3C**). Overproduction of ROS caused by various stresses has been demonstrated as potentially critical for induction and maintenance of senescence in animals and plants (Woo et al., 2013). Therefore, we performed GO analysis on seven types of ROS-clearance genes in *DEG*s. The heat map showed that several ROS-clearance genes, such as *APX5* and *CAT2*, were down-regulated in mutants (**Figure 3D**), which is consistent with the early-senescence phenotype of *nac075* mutants (**Figure 2**). Collectively, these data suggest that NAC075 delays leaf senescence process through negatively regulating senescence-promoting processes such as responses to oxidative/ROS stress.

NAC075 Directly Binds the *CAT2* Promoter to Activate Its Transcription

The above data pushed us to explore whether NAC075 directly regulates expressions of genes related to ROS clearance. Interestingly, transcripts of *CATALASE2* (*CAT2*), an important ROS scavenging enzyme, were significantly decreased in the leaves of *nac075* mutants in comparison with Col-0 (**Figure 4A**), which is consistent with the transcriptome data (**Supplementary Dataset 1**). To examine whether *CAT2* is a direct target of NAC075, we firstly identified the NAC075 binding sites (NBSs) in the promoter regions of *CAT2*. Based on a previous study (Lindemose et al., 2014), two NBSs (TG/ACGT) were identified and then used for ChIP assay using 35-day-old *Pro35S:NAC075-GFP*/Col-0 (*NAC075ox*) transgenic plants. ChIP-qPCR analysis showed that NAC075 is significantly enriched in TACGT regions, indicating that NAC075 binds to these regions *in vivo* (**Figure 4B**). We next performed EMSAs to examine the *in vitro* binding activity of NAC075. The results revealed that NAC075 protein tagged with His (NAC075-His) was capable of binding probes containing P2, while it was unable to bind probes containing P1 (**Figure 4C**). Using unlabeled probes as competitors, competitive binding assays were carried out to confirm the binding specificity by adding an excess of unlabeled competitor DNA fragments (**Figure 4C**), suggesting further that NAC075 directly binds the promoter of *CAT2*. To further investigate the regulatory roles of NAC075 on *CAT2*, we generated inducible overexpressing plants *pER8-FLAG-NAC075*. Upon treatment with β-estradiol, *NAC075* transcripts increased (**Figure 4D**). As expected, expression levels of *CAT2* also increased (**Figure 4D**). Collectively, the above data reveal that NAC075 can directly bind the promoter of *CAT2* and regulate its expression.

Overexpression of *CAT2* Suppresses the Early Senescence Phenotype of *nac075* Mutants

To further explore the genetic regulatory relationship between NAC075 and CAT2 in leaf senescence, we generated *nac075 CAT2ox* plants by crossing the *CAT2ox* (Guo et al., 2017) transgenic plants to *nac075* mutant. Under long-day conditions, plants with the combined *nac075 CAT2ox* genotype showed an obvious delayed senescence phenotype compared with *nac075* mutant plants, indicating that the accelerated leaf senescence phenotype of *nac075* mutant plants was effectively suppressed by CAT2 (**Figure 5A**). Moreover, DAB staining showed that H_2O_2 levels in the *nac075 CAT2ox* and *CAT2ox* plants was significantly lower than that of *nac075* and Col-0 plants (**Figure 5B**). This indicates that overexpression of *CAT2* suppresses the elevated H_2O_2 levels in *nac075* mutant plants, which is in line with the observation that *CAT2* is the downstream target gene of NAC075. Similarly, higher chlorophyll content and Fv/Fm further confirmed the delayed senescence phenotype of *nac075 CAT2ox* plants (**Figures 5C,D**). Taken together, these results reveal that overexpression of *CAT2* suppresses the early senescence phenotype in *nac075* mutant plants by reducing H_2O_2 accumulation. Therefore, a regulatory module is proposed, which is the NAC075-CAT2 pathway modulates leaf senescence by regulating ROS levels (**Figure 5E**).

DISCUSSION

Leaf senescence is a process of programmed cell death (PCD), which not only is affected by various internal and external factors but also involves highly complex regulatory processes with the coordinated actions of multiple pathways (Lim et al., 2007; Woo et al., 2013, 2019). Deep dissection of the molecular mechanism underlying the leaf senescence may provide a theoretical basis for crop genetic breeding. As leaf senescence involves extensive transcriptional reprogramming, the dynamic activation of transcription factors is considered as a key mechanism that controls the age-dependent expression of thousands of *SAG*s (Woo et al., 2013). Transcriptome profiling has revealed that a number of NAC genes showed enhanced expression during leaf senescence in *Arabidopsis*, indicating that they play important roles in the senescence process (Kim et al., 2016). Genetic analyses reveal that a number of NAC TFs function as positive (ANAC016, ANAC029/AtNAP, ANAC046, ANAC059/ORS1, and ANAC092/ORE1) (Guo and Gan, 2006; Balazadeh et al., 2010, 2011; Kim et al., 2013; Oda-Yamamizo et al., 2016) or negative (ANAC042/JUB1, ATAF1/ANAC002 and ANAC083/VNI2) regulators of leaf senescence (Yang et al., 2011; Wu et al., 2012; Garapati et al., 2015). Recently, ANAC017, ANAC082, and ANAC090, referred to as a "NAC troika," are responsible for governing the positive-to-negative regulatory shift and function as negative regulators of leaf senescence in *Arabidopsis* (Kim et al., 2018). Here, our study revealed that NAC TF NAC075 acts as a novel negative regulator in the age-dependent leaf senescence.

Our data demonstrated that NAC075 is a functional *SAG* whose transcription level increases with age (**Figure 1A**). To this end, we screened knockout lines and generated overexpression transgenic plants to investigate its function in leaf senescence. Loss of function of NAC075 significantly accelerated leaf senescence, whereas overexpression of *NAC075* delayed leaf senescence (**Figure 2A**), further supporting its negative function in regulating leaf senescence. In addition, overexpression of *NAC075* also evidently suppressed numerous plant hormones or stress-induced leaf senescence. We also found that NAC75 and other NAC TFs may have functional redundancy in regulating

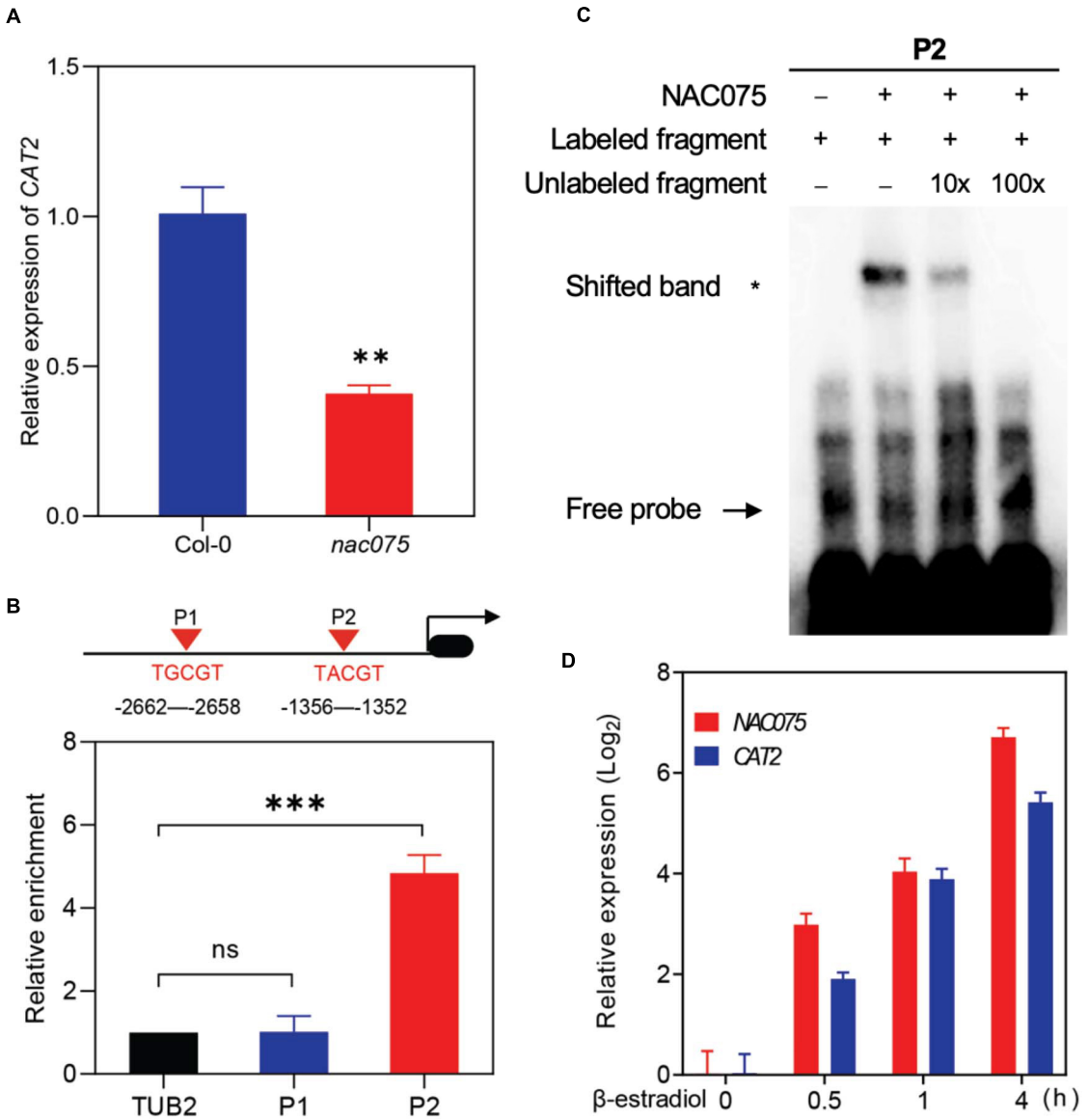

FIGURE 4 | *CAT2* is a direct target of NAC075. **(A)** Relative expression level of *CAT2* in the third and fourth rosette leaves of 25-day-old Col-0 and *nac075* mutant plants. Data are means ± SD, $n = 3$. **(B)** NAC075 directly binds to the promoter of *CAT2*. Schematic diagram indicates the locations of two putative NAC075 binding sites (P1 and P2) in the *CAT2* promoter (top). ChIP-qPCR was performed to examine the relative NAC075 binding to the *CAT2* promoter (bottom). An anti-GFP monoclonal antibody was used for DNA immunoprecipitation from 28-day-old *Pro35S:NAC075-GFP*/Col-0 transgenic plants. The relative enrichment of NAC075 binding to *CAT2* promoter was normalized to *TUBULIN2* (*TUB2*). Student's *t*-test, $^{**}P < 0.01$, $^{***}P < 0.001$, ns, not significant. Data are means ± SD of three independent biological replicates. **(C)** EMSA assay of the binding of NAC075 to the *CAT2* promoter *in vitro*. Biotin-labeled probe was used to EMSA experiment and non-labeled fragments were used as competitors. The + and − symbols represent the presence and absence of components. Three biological replicates were performed with similar results. **(D)** qRT-PCR analysis of *NAC075* and *CAT2* expressions in the *pER8-FLAG-NAC075* plants treated with 50 mM β-estradiol for the indicated time points. Data are represented as means ± SD, $n = 3$.

leaf senescence and will construct multiple mutants to verify this possibility in the future. RNA-seq profiling analysis revealed that most of the *DEG*s are enriched in response to stimulus, and a large portion of ROS-clearance genes were significantly downregulated in *nac075* mutant plants (**Figures 3C,D**). Consequently, we observed that the ROS content in *nac075* mutant plants was increased compared with the wild type (**Figure 5B**). This indicates that NAC075 functions during leaf senescence likely by regulating the expression of ROS-clearance genes. Accordingly, we found that ROS scavenging enzyme *CAT2* is one of the putative target genes of NAC075. H_2O_2 is a well-defined inducers of leaf senescence and *CAT2* is a key gene responsible for removing H_2O_2 (Vandenabeele et al., 2004; Hieno et al., 2019). Our ChIP-qPCR and EMSA experiments demonstrated that NAC075 bound directly to the *CAT2* promoter, indicating that *CAT2* is a direct target of NAC075 (**Figures 4C,D**). In

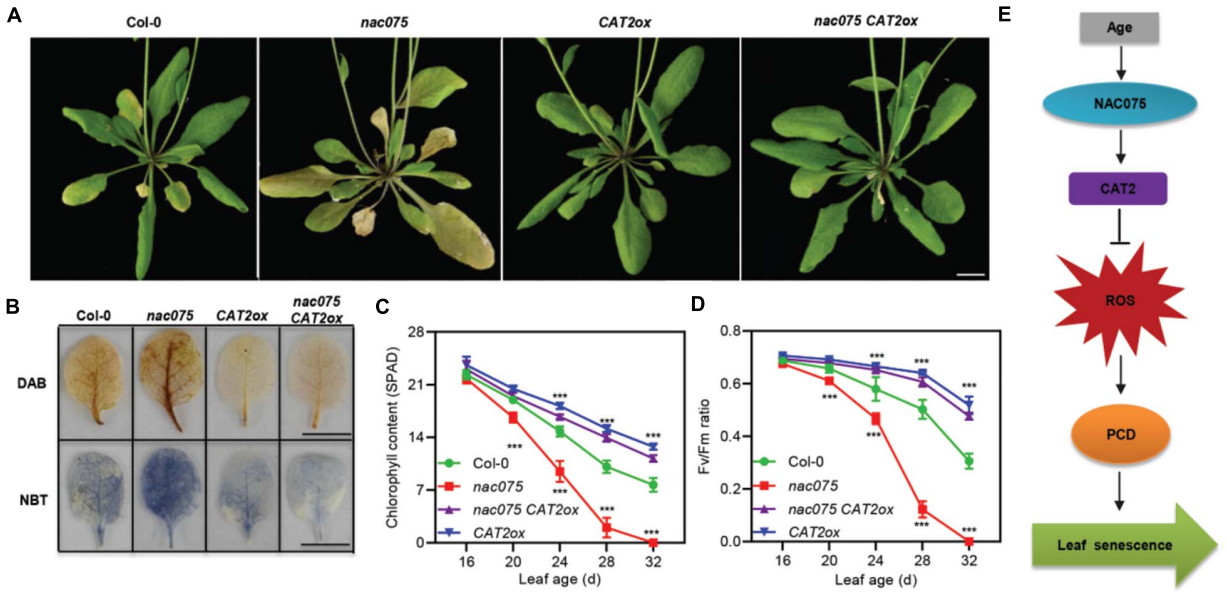

FIGURE 5 | Overexpression of *CAT2* suppresses the early senescence phenotype of *nac075* mutant plants. **(A)** Leaf senescence phenotype of 32-day-old Col-0, *nac075*, *nac075 CAT2ox*, and *CAT2ox* plants. The scale bar represents 1 cm. **(B)** DAB and NBT staining were used to detect H_2O_2 and O_2^- accumulation, respectively, in the third or fourth leaves of Col-0, *nac075*, *nac075 CAT2ox*, and *CAT2ox* plants. The brown and blue color represent H_2O_2 and O_2^- accumulation, respectively. Scale bar, 1 cm. **(C,D)** Measurements of chlorophyll contents **(C)** and photochemical efficiency (Fv/Fm) **(D)** in Col-0, *nac075*, *nac075 CAT2ox*, and *CAT2ox* plants as leaves age. Data are represented as means ± SD, $n = 3$. The experiment was performed three times with similar results. Student's *t*-test, $^{***}P < 0.001$. **(E)** A proposed model illustrates the transcription factor NAC075 that delays leaf senescence by deterring reactive oxygen species accumulation in *Arabidopsis*. NAC075 promotes *CAT2* transcription by directly binding to its promoter, which is able to suppress ROS overproduction. Decreased ROS levels are capable of reducing programmed cell death, thereby delaying leaf senescence.

addition, *CAT2* overexpression suppresses the early senescence phenotype of *nac075* mutant plants (**Figure 5B**), providing genetic evidence for the importance of *CAT2* transcription promotion by NAC075 to leaf senescence and ROS accumulation. Based on these results, we conclude that NAC075 suppresses ROS production and leaf senescence by inducing *CAT2* expression. Currently, the upstream TFs regulating age-dependent NAC075 transcription are unclear.

It is reported that increased ROS levels due to decreased antioxidant capacity is highly correlated with leaf senescence (Rogers and Munne-Bosch, 2016). A number of studies have previously reported that NAC TFs regulate leaf senescence by modulating ROS levels, such as JUB1 (ANAC042) (Wu et al., 2012), ATAF1 (ANAC002) (Garapati et al., 2015), ORS1 (ANAC059) (Balazadeh et al., 2011), NTL4 (NAC53) (Lee et al., 2012), ANAC017 (Kim et al., 2018), and ANAC032 (Mahmood et al., 2016). Previous studies reveal that the expressions of JUB1 and ORS1 are induced by H_2O_2 (Balazadeh et al., 2011; Wu et al., 2012), while our work found that NAC075 is not response to ROS, suggesting that NAC075 acts as an upstream negative regulator of ROS accumulation but is not induced by ROS.

Based on our data, we proposed a NAC075-CAT2-ROS model to clarify how NAC075 is responsible for delaying leaf senescence (**Figure 5E**). In this model, *NAC075* transcription is induced by age. Elevated ROS levels lead to PCD and accelerate the senescence process of leaves (Lee et al., 2012; Wu et al., 2012; Rogers and Munne-Bosch, 2016), whereas NAC075 is able to deter the accumulation of ROS by promoting *CAT2* transcription and thereby delay leaf senescence. It is reported that NAC075 is involved in the secondary cell wall formation and the regulation of flowering (Sumire and Nobutaka, 2016). Transcriptome analysis also shows that NAC075 is involved in an array of biotic and abiotic stresses as well as the signal transduction process of plant hormones. Given that the downstream regulatory networks dictated by NAC075 in these processes are still unclear, our finding of the regulatory role of NAC075 in ROS scavenging in leaf senescence offers a potential mechanism for these processes as well.

DATA AVAILABILITY STATEMENT

The datasets presented in this study can be found in online repositories. The name of the repository and accession number can be found below: National Center for Biotechnology Information (NCBI), https://www.ncbi.nlm.nih.gov/, PRJNA689040.

AUTHOR CONTRIBUTIONS

ZL and HG conceived the project and designed the experiments. YS and XX designed part of the experiments. CK carried out most of the experiments. YZ conducted ChIP and EMSA assays. H-LW analyzed the RNA-seq data. ZL and CK wrote the manuscript with input from all co-authors. All authors contributed to the article and approved the submitted version.

FUNDING

This work was supported by the National Natural Science Foundation of China (31970196 to ZL, 32011540381 to ZL, 31570286 to HG, 31900173 to HW, and 31770649 to XX), the National Key Research and Development Program of China (No. 2019YFA0903904 to HG), Shenzhen Science and Technology Program (KQTD20190929173906742 to HG), Chinese Postdoctoral Science Foundation (2019M650514 to YZ and 2019M650516 to HW), and the startup funding for plant aging research from "Beijing Advanced Innovation Center for Tree Breeding by Molecular Design, Beijing Forestry University."

ACKNOWLEDGMENTS

We thank the lab members for their helpful suggestions and discussions. T-DNA mutant lines were purchased from the NASC.

SUPPLEMENTARY MATERIAL

The Supplementary Material for this article can be found online at: https://www.frontiersin.org/articles/10.3389/fpls.2021.634040/full#supplementary-material

Supplementary Figure 1 | Transcript level of *SAG12*, *AtNAP* and *ORE1* increases as leaf ages.

Supplementary Figure 2 | PCR genotyping of the *nac075* mutants.

Supplementary Figure 3 | Overexpression of *NAC075* delayed leaf senescence.

Supplementary Figure 4 | The age-dependent pods senescence phenotype of 30-d-old Col-0 and *nac075* mutants.

Supplementary Figure 5 | Senescence phenotypes of Col-0, *nac075* mutants and *NAC075ox* plants.

Supplementary Table 1 | Primers used in this study.

Supplementary Dataset 1 | The differential expressed genes in *nac075* mutant.

REFERENCES

Balazadeh, S., Kwasniewski, M., Caldana, C., Mehrnia, M., Zanor, M. I., Xue, G. P., et al. (2011). ORS1, an H2O2-responsive NAC transcription factor, controls senescence in *Arabidopsis thaliana*. *Mol. Plant* 4, 346–360. doi: 10.1093/mp/ssq080

Balazadeh, S., Riano-Pachon, D. M., and Mueller-Roeber, B. (2008). Transcription factors regulating leaf senescence in *Arabidopsis thaliana*. *Plant Biol.* 10(Suppl. 1), 63–75. doi: 10.1111/j.1438-8677.2008.00088.x

Balazadeh, S., Siddiqui, H., Allu, A. D., Matallana-Ramirez, L. P., Caldana, C., Mehrnia, M., et al. (2010). A gene regulatory network controlled by the NAC transcription factor ANAC092/AtNAC2/ORE1 during salt-promoted senescence. *Plant J.* 62, 250–264. doi: 10.1111/j.1365-313x.2010.04151.x

Breeze, E., Harrison, E., Mchattie, S., Hughes, L., Hickman, R., Hill, C., et al. (2011). High-resolution temporal profiling of transcripts during Arabidopsis leaf senescence reveals a distinct chronology of processes and regulation. *Plant Cell* 23, 873–894. doi: 10.1105/tpc.111.083345

Buchanan-Wollaston, V., Page, T., Harrison, E., Breeze, E., Lim, P. O., Nam, H. G., et al. (2005). Comparative transcriptome analysis reveals significant differences in gene expression and signalling pathways between developmental and dark/starvation-induced senescence in Arabidopsis. *Plant J.* 42, 567–585. doi: 10.1111/j.1365-313x.2005.02399.x

Clough, S. J., and Bent, A. F. (1998). Floral dip: a simplified method for agrobacterium-mediated transformation of *Arabidopsis thaliana*. *Plant J.* 16, 735–743. doi: 10.1046/j.1365-313x.1998.00343.x

Cutler, S. R., Ehrhardt, D. W., Griffitts, J. S., and Somerville, C. R. (2000). Random GFP: : cDNA fusions enable visualization of subcellular structures in cells of Arabidopsis at a high frequency. *Proc. Natl. Acad. Sci. U. S. A.* 97, 3718–3723. doi: 10.1073/pnas.97.7.3718

Garapati, P., Xue, G. P., Munne-Bosch, S., and Balazadeh, S. (2015). Transcription factor ATAF1 in Arabidopsis promotes senescence by direct regulation of key chloroplast maintenance and senescence transcriptional cascades. *Plant Physiol.* 168, 1122–1139. doi: 10.1104/pp.15.00567

Guo, P., Li, Z., Huang, P., Li, B., Fang, S., Chu, J., et al. (2017). A tripartite amplification loop involving the transcription factor WRKY75, salicylic acid, and reactive oxygen species accelerates leaf senescence. *Plant Cell* 29, 2854–2870. doi: 10.1105/tpc.17.00438

Guo, Y. (2013). Towards systems biological understanding of leaf senescence. *Plant Mol. Biol.* 82, 519–528. doi: 10.1007/s11103-012-9974-2

Guo, Y., and Gan, S. (2005). Leaf senescence: signals, execution, and regulation. *Curr. Top. Dev. Biol.* 71, 83–112. doi: 10.1016/s0070-2153(05)71003-6

Guo, Y., and Gan, S. (2006). AtNAP, a NAC family transcription factor, has an important role in leaf senescence. *Plant J.* 46, 601–612. doi: 10.1111/j.1365-313x.2006.02723.x

Hieno, A., Naznin, H. A., Inaba-Hasegawa, K., Yokogawa, T., Hayami, N., Nomoto, M., et al. (2019). Transcriptome analysis and identification of a transcriptional regulatory network in the response to H2O2. *Plant Physiol.* 180, 1629–1646. doi: 10.1104/pp.18.01426

Hughes, K. A., and Reynolds, R. M. (2005). Evolutionary and mechanistic theories of aging. *Annu. Rev. Entomol.* 50, 421–445. doi: 10.1146/annurev.ento.50.071803.130409

Jefferson, R. A. (1989). The GUS reporter gene system. *Nature* 342, 837–838. doi: 10.1038/342837a0

Jensen, M. K., Lindemose, S., De Masi, F., Reimer, J. J., Nielsen, M., Perera, V., et al. (2013). ATAF1 transcription factor directly regulates abscisic acid biosynthetic gene NCED3 in *Arabidopsis thaliana*. *FEBS Open Bio* 3, 321–327. doi: 10.1016/j.fob.2013.07.006

Kim, H. J., Nam, H. G., and Lim, P. O. (2016). Regulatory network of NAC transcription factors in leaf senescence. *Curr. Opin. Plant Biol.* 33, 48–56. doi: 10.1016/j.pbi.2016.06.002

Kim, H. J., Park, J. H., Kim, J., Kim, J. J., Hong, S., Kim, J., et al. (2018). Time-evolving genetic networks reveal a NAC troika that negatively regulates leaf senescence in Arabidopsis. *Proc. Natl. Acad. Sci. U. S. A.* 115, E4930–E4939.

Kim, J. H., Woo, H. R., Kim, J., Lim, P. O., Lee, I. C., Choi, S. H., et al. (2009). Trifurcate feed-forward regulation of age-dependent cell death involving miR164 in Arabidopsis. *Science* 323, 1053–1057. doi: 10.1126/science.1166386

Kim, Y. S., Sakuraba, Y., Han, S. H., Yoo, S. C., and Paek, N. C. (2013). Mutation of the Arabidopsis NAC016 transcription factor delays leaf senescence. *Plant Cell Physiol.* 54, 1660–1672. doi: 10.1093/pcp/pct113

Lee, S., Seo, P. J., Lee, H. J., and Park, C. M. (2012). A NAC transcription factor NTL4 promotes reactive oxygen species production during drought-induced leaf senescence in Arabidopsis. *Plant J.* 70, 831–844. doi: 10.1111/j.1365-313x.2012.04932.x

Li, W., Li, X., Chao, J., Zhang, Z., Wang, W., and Guo, Y. (2018). NAC family transcription factors in Tobacco and their potential role in regulating leaf senescence. *Front. Plant Sci.* 9:1900. doi: 10.3389/fpls.2018.01900

Li, X., Ahmad, S., Ali, A., Guo, C., Li, H., Yu, J., et al. (2019). Characterization of somatic embryogenesis receptor-like kinase 4 as a negative regulator of leaf senescence in Arabidopsis. *Cells* 8:50. doi: 10.3390/cells8010050

Li, Z., Zhang, Y., Zou, D., Zhao, Y., Wang, H. L., Zhang, Y., et al. (2020). LSD 3.0: a comprehensive resource for the leaf senescence research community. *Nucleic Acids Res.* 48, D1069–D1075.

Lim, P. O., Kim, H. J., and Nam, H. G. (2007). Leaf senescence. *Annu. Rev. Plant Biol.* 58, 115–136.

Lindemose, S., Jensen, M. K., Van De Velde, J., O'shea, C., Heyndrickx, K. S., Workman, C. T., et al. (2014). A DNA-binding-site landscape and regulatory network analysis for NAC transcription factors in *Arabidopsis thaliana*. *Nucleic Acids Res.* 42, 7681–7693. doi: 10.1093/nar/gku502

Mahmood, K., El-Kereamy, A., Kim, S. H., Nambara, E., and Rothstein, S. J. (2016). ANAC032 positively regulates age-dependent and stress-induced senescence in *Arabidopsis thaliana*. *Plant Cell Physiol.* 57, 2029–2046. doi: 10.1093/pcp/pcw120

Mao, C., Lu, S., Lv, B., Zhang, B., Shen, J., He, J., et al. (2017). A rice NAC transcription factor promotes leaf senescence via ABA biosynthesis. *Plant Physiol.* 174, 1747–1763. doi: 10.1104/pp.17.00542

Noh, Y. S., and Amasino, R. M. (1999). Identification of a promoter region responsible for the senescence-specific expression of SAG12. *Plant Mol. Biol.* 41, 181–194.

Oda-Yamamizo, C., Mitsuda, N., Sakamoto, S., Ogawa, D., Ohme-Takagi, M., and Ohmiya, A. (2016). The NAC transcription factor ANAC046 is a positive regulator of chlorophyll degradation and senescence in Arabidopsis leaves. *Sci. Rep.* 6:23609.

Pontier, D., Gan, S., Amasino, R. M., Roby, D., and Lam, E. (1999). Markers for hypersensitive response and senescence show distinct patterns of expression. *Plant Mol. Biol.* 39, 1243–1255.

Rogers, H., and Munne-Bosch, S. (2016). Production and scavenging of reactive oxygen species and redox signaling during leaf and flower senescence: similar but different. *Plant Physiol.* 171, 1560–1568. doi: 10.1104/pp.16.00163

Saleh, A., Alvarez-Venegas, R., and Avramova, Z. (2008). An efficient chromatin immunoprecipitation (ChIP) protocol for studying histone modifications in Arabidopsis plants. *Nat. Protoc.* 3, 1018–1025. doi: 10.1038/nprot.2008.66

Sumire, F., and Nobutaka, M. (2016). ANAC075, a putative regulator of vascular-related NAC-DOMAIN7, is a repressor of flowering. *Plant Biotechnol.* 33, 255–265. doi: 10.5511/plantbiotechnology.16.0215b

Vandenabeele, S., Vanderauwera, S., Vuylsteke, M., Rombauts, S., Langebartels, C., Seidlitz, H. K., et al. (2004). Catalase deficiency drastically affects gene expression induced by high light in *Arabidopsis thaliana*. *Plant J.* 39, 45–58. doi: 10.1111/j.1365-313x.2004.02105.x

Woo, H. R., Chung, K. M., Park, J. H., Oh, S. A., Ahn, T., Hong, S. H., et al. (2001). ORE9, an F-box protein that regulates leaf senescence in Arabidopsis. *Plant Cell* 13, 1779–1790. doi: 10.1105/tpc.13.8.1779

Woo, H. R., Kim, H. J., Lim, P. O., and Nam, H. G. (2019). Leaf senescence: systems and dynamics aspects. *Annu. Rev. Plant Biol.* 70, 347–376. doi: 10.1146/annurev-arplant-050718-095859

Woo, H. R., Kim, H. J., Nam, H. G., and Lim, P. O. (2013). Plant leaf senescence and death - regulation by multiple layers of control and implications for aging in general. *J. Cell. Sci.* 126, 4823–4833. doi: 10.1242/jcs.109116

Woo, H. R., Koo, H. J., Kim, J., Jeong, H., Yang, J. O., Lee, I. H., et al. (2016). Programming of plant leaf senescence with temporal and inter-organellar coordination of transcriptome in Arabidopsis. *Plant Physiol.* 171, 452–467. doi: 10.1104/pp.15.01929

Wu, A., Allu, A. D., Garapati, P., Siddiqui, H., Dortay, H., Zanor, M. I., et al. (2012). JUNGBRUNNEN1, a reactive oxygen species-responsive NAC transcription factor, regulates longevity in Arabidopsis. *Plant Cell* 24, 482–506. doi: 10.1105/tpc.111.090894

Yang, S.-D., Seo, P. J., Yoon, H.-K., and Park, C.-M. (2011). The Arabidopsis NAC transcription factor VNI2 integrates abscisic acid signals into leaf senescence via the COR/RD genes. *Plant Cell* 23, 2155–2168. doi: 10.1105/tpc.111.084913

Young, M. D., Wakefield, M. J., Smyth, G. K., and Oshlack, A. (2010). Gene ontology analysis for RNA-seq: accounting for selection bias. *Genome Biol.* 11:R14.

Zuo, J., Niu, Q. W., and Chua, N. H. (2000). Technical advance: an estrogen receptor-based transactivator XVE mediates highly inducible gene expression in transgenic plants. *Plant J.* 24, 265–273. doi: 10.1046/j.1365-313x.2000.00868.x

Conflict of Interest: The authors declare that the research was conducted in the absence of any commercial or financial relationships that could be construed as a potential conflict of interest.

frontiers in Plant Science

ORIGINAL RESEARCH
published: 22 March 2021
doi: 10.3389/fpls.2021.643011

OsWRKY93 Dually Functions Between Leaf Senescence and in Response to Biotic Stress in Rice

Yanyun Li[1], Shuting Liao[1], Pengying Mei[1], Yueyun Pan[1], Yu Zhang[2], Xiangzi Zheng[2], Yakun Xie[2] and Ying Miao[1]**

[1] *Fujian Provincial Key Laboratory of Plant Functional Biology, Fujian Agriculture and Forestry University, Fuzhou, China,*
[2] *College of Life Sciences, Fujian Agriculture and Forestry University, Fuzhou, China*

Cross talking between natural senescence and cell death in response to pathogen attack is an interesting topic; however, its action mechanism is kept open. In this study, 33 *OsWRKY* genes were obtained by screening with leaf aging procedure through RNA-seq dataset, and 11 of them were confirmed a significant altered expression level in the flag leaves during aging by using the reverse transcript quantitative PCR (RT-qPCR). Among them, the *OsWRKY2*, *OsWRKY14*, *OsWRKY26*, *OsWRKY69*, and *OsWRKY93* members exhibited short-term alteration in transcriptional levels in response to *Magnaporthe grisea* infection. The CRISPR/Cas9-edited mutants of five genes were developed and confirmed, and a significant sensitivity to *M. oryzae* infection was observed in *CRISPR OsWRKY93-edited* lines; on the other hand, a significant resistance to *M. oryzae* infection was shown in the enhanced expression *OsWRKY93* plants compared to mock plants; however, enhanced expression of other four genes have no significant affection. Interestingly, ROS accumulation was also increased in *OsWRKY93* enhanced plants after flg22 treatment, compared with the controls, suggesting that *OsWRKY93* is involved in PAMP-triggered immune response in rice. It indicated that *OsWRKY93* was involved in both flag leaf senescence and in response to fungi attack.

Keywords: *OsWRKY93*, rice, flag leaf, senescence, biotic stress

OPEN ACCESS

Edited by:
Nam-Chon Paek,
Seoul National University,
South Korea

Reviewed by:
Guodong Ren,
Fudan University, China
Qian Qian,
Chinese Academy of Agricultural Sciences, China

****Correspondence:***
Yakun Xie
yakun.xie@fafu.edu.cn
Ying Miao
ymiao@fafu.edu.cn;
ymiao2013@hotmail.com

Specialty section:
This article was submitted to Plant Physiology, a section of the journal Frontiers in Plant Science

Received: *17 December 2020*
Accepted: *11 February 2021*
Published: *22 March 2021*

Citation:
Li Y, Liao S, Mei P, Pan Y, Zhang Y, Zheng X, Xie Y and Miao Y (2021) OsWRKY93 Dually Functions Between Leaf Senescence and in Response to Biotic Stress in Rice. Front. Plant Sci. 12:643011. doi: 10.3389/fpls.2021.643011

INTRODUCTION

Rice is the main food crop of the developing world. However, the increase of yield is seriously restricted by flag leaf senescence in rice. The flag leaf, the uppermost leaf in the rice plant, is thought to contribute highly to what is accumulated in grain (Ghosh et al., 1990; Li et al., 1998). Delaying the senescence of rice leaves and prolonging the photosynthesis time are beneficial for increasing the rice yield, and the yield can increase by about 2% after flag leaf senescence is delayed for 1 day (Ma and Lu, 1990). Therefore, studying the mechanism of flag leaf senescence is essential to improving the yield of rice grain.

Leaf senescence is the final stage of leaf development. As an organ level senescence, leaf senescence is a crucial means for plants to reallocate nutrients and valuable substances from senescent leaves to reproducing seeds, eventually maximizing reproductive success (Himelblau and Amasino, 2001). Leaf senescence is a strictly organized process finely governed by developmental age. However, leaf senescence is also influenced by various internal and environmental signals that

are integrated with age information (Lim et al., 2007). The internal factors that affect leaf senescence include developmental cues and reproductive development as well as phytohormones (Gan and Amasino, 1995; Pic et al., 2002; Riefler et al., 2006). The environmental cues include various stresses such as extreme temperatures, nutrient deficiency, drought, radiation, and infection from pathogens. Interestingly, the leaf transcriptome varies immensely accompanying the onset and progression of leaf senescence. It was previously reported that 20 different families of transcription factors that are transcriptionally up-regulated in senescent leaves remarkably contain several large groups such as NAC, WRKY, C2H2-type zinc finger, AP2/EREBP, and MYB proteins (Guo and Gan, 2005).

Among these large groups, WRKY proteins are plant specific transcription factors that are especially believed to play central roles in regulating senescence. All WRKY proteins contain at least one WRKY domain that is composed of a zinc finger structure and a 60-amino acid region with WRKYGQK at the N-terminal end. The WRKY domain is a DNA-binding domain that binds directly to various W-box variants (Eulgem et al., 2000; Yu et al., 2001). To date, many WRKY TFs regulating leaf senescence have been characterized in *Arabidopsis*. *WRKY6* is highly induced during leaf senescence (Robatzek and Somssich, 2001). *WRKY45* positively regulates age-triggered leaf senescence through interacting with a DELLA protein, RGL1 (Chen L. et al., 2017). Another well-known WRKY member, *WRKY53* plays a regulatory role in the early events of leaf senescence (Hinderhofer and Zentgraf, 2001; Miao et al., 2004). Overexpression of *WRKY75* accelerates age-dependent leaf senescence (Guo et al., 2017). In rice, WRKY family has over 102 members (Xie et al., 2005). However, relatively few *OsWRKY* members involved in leaf senescence have been examined. For instance, overexpressing *OsWRKY5* promotes leaf senescence under natural and dark-induced senescence conditions (Kim et al., 2019). Heterologous expression of *OsWRKY23* promotes dark-induced leaf senescence in Arabidopsis (Jing et al., 2009). *OsWRKY42* enhances leaf senescence by repressing the expression of *OsMT1d* to induce reactive oxygen species (ROS) in rice (Han et al., 2014).

The WRKY family is also known for being the key player in plant biotic stress response. The initial study investigated the expression of WRKY TFs in rice response to *M. oryzae* and found that 15 *OsWRKYs* were induced upon pathogen infection (Ryu et al., 2006). Subsequent research revealed more details about the involvement of many *OsWRKYs* in plant defense. At least nine *OsWRKYs* have been identified to regulate rice response to *M. oryzae* positively. For example, overexpression of *OsWRKY31*, *OsWRKY45*, *OsWRKY47*, *OsWRKY53*, or *OsWRKY67* in rice plants enhances resistance to *M. oryzae* (Chujo et al., 2007; Shimono et al., 2007; Zhang et al., 2008; Wei et al., 2013; Vo et al., 2018). On the contrary, several *OsWRKY* members function as negative regulators of the rice response to *M. oryzae* infection. For instance, through suppressing JA signaling-related genes, *OsWRKY42* negatively regulate rice response to *M. oryzae* (Cheng et al., 2015). Overexpression of *OsWRKY28* or *OsWRKY76* in rice plants resulted in increased susceptibility to *M. oryzae* (Chujo et al., 2013; Yokotani et al., 2013).

In this study, the transcriptome analysis shows that 33 *OsWRKY* members in rice flag leaves are differentially expressed during plant aging. Besides, RT-qPCR analysis displayed that the expression of five *OsWRKY* genes were altered in Guy11-treated rice plants. The Crispr/Cas9-edited mutants of five *OsWRKY* genes were developed and confirmed. Genetic analysis reveals that enhanced expression of *OsWRKY93* resulted in an enhanced resistance to *M. oryzae* infection in rice. This finding suggests that *OsWRKY93* plays a role in the defense response and is also associated with the regulation of flag leaf senescence in rice. All in all, this study provides a new candidate gene for in depth understanding of the regulatory mechanisms of pathogen induced leaf senescence, helping in breeding high yield and disease resistant crops.

MATERIALS AND METHODS

Plant Materials and Growth Conditions

The rice (*Oryza sativa* L. subsp. *japonica*) of the Kitaake accession was used for generating *OsWRKY2, OsWRKY14, OsWRKY26, OsWRKY69,* and *OsWRKY93* transgenic plants with increased *OsWRKY2, OsWRKY14, OsWRKY26, OsWRKY69,* and *OsWRKY93* expression level via a transcriptional activator containing four copies of VP16 (i.e., VP64), and named $OsWRKY_{VP64}$ (Sadowski et al., 1988; Yaghmai and Cutting, 2002). Rice plants were grown in the growth chamber at 30°C for 12 h (day) and 20°C for 12 h (night) or under outdoor conditions (natural long-day conditions) in Fuzhou Fujian Province, China, from April to September.

Identification of CRISPR/Cas9-Edited Mutants

The *OsWRKY2*, *OsWRKY14*, *OsWRKY26*, *OsWRKY69*, and *OsWRKY93* CRISPR transgenic plants were produced by the Biogle company (Hangzhou, China). Genomic DNA from individual transgenic plants was isolated using Edwards buffer (Edwards et al., 1991) for PCR analysis. The PCR products were amplified with *OsWRKY93*-specific primers and were sequenced directly. The *OsWRKY93*-specific primers were designed for amplifying targeted regions of *OsWRKY93* (**Supplementary Table S2**).

Pathogen Inoculation

M. oryzae strain Guy11 was used in this study. At the three-leaf stage, rice seedlings were spray-inoculated with the spore suspension of *M. oryzae* (1×10^5 spores/ml in water containing 0.02% Tween 20). Subsequently, the inoculated plants were incubated in the dark at high humidity for 24 h and transferred to a growth chamber at 24°C with 12 h of light and 12 h of darkness. The disease lesions in the infected leaves were observed, and were scanned at 0, 1, 3, 4 days post-inoculation (dpi).

Darkness Treatment

Kitaake, NIP, *oswrky93-1* mutant and the T2 generation $OsWRKY93_{vp64}$ plants were cultured in soil for 39 days after

germination. The fully expanded part of the sixth leaves were cut into 1–2 cm pieces and pooled, and then the leaf pieces were suspended in 3mM MES (pH5.8) buffer and cultured in the dark at 28°C for 0, 24, 36, 48, 60, 72, 84, and 96 h. The color changes of leaves were observed and photographed. Three biological replicates were used.

Chlorophyll Measurements

The chlorophyll content of flag leaves were measured using a chlorophyll meter (DUALEX SCIENTIFIC). For measurement 3–4 points in the central region of the leaf were picked up.

Reverse Transcription Quantitative PCR

Three-leaf stage rice seedlings were spray-inoculated with Guy11 (1×10^5 spores/ml) and water, and leaf samples were collected at 0, 24, 48, 72, 96, and 108 hrs post-inoculation (hpi). Two biological replicates were tested, and each biological replicate contains leaves from three independent plants. Total RNA was extracted from those leaf samples using TRIzol reagent (Invitrogen), followed by cDNA synthesis with RevertAid Reverse Transcriptase (Thermo Fisher Scientific). Quantitative PCR was performed using TransStart Green qPCR SuperMix Kit (TransGen Biotech, China) and the indicated primers (**Supplementary Table S1**). The rice actin1 (*OsACTIN1*) gene was selected as an internal control.

ROS Assay

Oxidative bursts were measured using a luminal-based assay with leaf discs from 5-week-old plants. The leaf discs were incubated in sterile water overnight, and then water was replaced with 20 μM luminal and 2.5 μg/ml peroxidase. To measure ROS, leaf discs were treated with 1 μM flg22 or water (Ctrl). Immediately, the luminescence was measured at 3 min intervals with a Varioskan LUX Multimode Microplate Reader (Thermo Fisher Scientific). Then 3–5 replications were carried out for each sample.

RESULTS

Expression Patterns of *OsWRKYs* in Rice Flag Leaves During Natural Senescence

To monitor the transcriptional changes in rice flag leaves during natural senescence, a genome-wide transcriptome analysis was carried out in flag leaf tissue of the *Nipponbare* through massive RNA sequencing. For generation of RNA-seq libraries, six flag leaf samples were taken. The first sample of the flag leaf was collected at the heading stage when the flag leaf was fully expanded [0 weeks after heading (WAH) and named 0W]; chlorophyll content is higher in 1w than 0w, and then it is gradually decreased from 1w to 5w; the following five flag leaf samples were collected every week (named 1W, 2W, 3W, 4W, and 5W, respectively, 0W used as control). The onset of leaf senescence coincides with the start of Chlorophyll (Chl) degradation, while the initiation of leaf senescence is before Chl degradation. Therefore, the senescence initiation of flag leaves started at the time period between 0W and 2W (**Supplementary Figure S1**). Through RNA-Seq analysis, the expression patterns of 102 *OsWRKY* family members in rice flag leaves during aging stages were investigated (**Supplementary Dataset S1**). EdgeR program was used for differential expression analysis of *OsWRKY* genes between any of the six samples (Nikolayeva and Robinson, 2014). In comparison with the control (0W), a differential expression profile of a total thirty-three *OsWRKY* genes were exhibited during natural senescence of flag leaves (**Figure 1** and **Supplementary Dataset S1**).

To further confirm the differential expression of thirty-three *OsWRKY* genes during natural senescence according to transcriptome data (**Figure 2** and **Supplementary Dataset S1**), all of 33 *OsWRKY* genes were checked by RT-qPCR, the transcript levels of eight OsWRKYs (*OsWRKY2*, *OsWRKY10*, *OsWRKY14*, *OsWRKY29, OsWRKY47*, *OsWRKY49*, *OsWRKY72,* and *OsWRKY73*) were immediately up-regulated in 1W-vs-0W comparison, while that of three OsWRKYs (*OsWRKY69*, *OsWRKY93*, *OsWRKY26*) were slightly down-regulated in 1W-vs-0W comparison then up-regulated in 2W vs. 0W again (**Figure 2**), suggesting that they are senescence-related *OsWRKY* genes. Among the 11 *OsWRKY* genes, *OsWRKY2*, *OsWRKY69,* and *OsWRKY93* shared a similar expression pattern in rice flag leaves that the transcript level increased and peaked at the second week after heading (2W) and declined afterward compared with the 0W control. The expression of *OsWRKY10* and *OsWRKY14* reached the highest level at 1W and remained relatively high afterward. The level of *OsWRKY26* mRNA was slightly increased at 1W and then stayed low level at 2W and

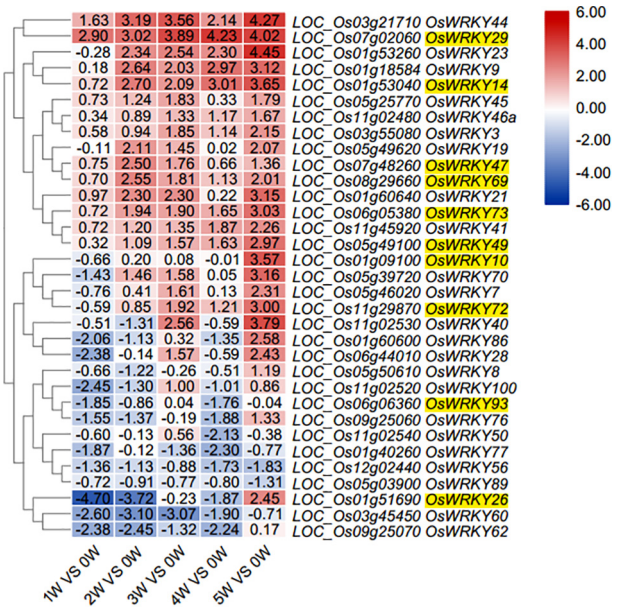

FIGURE 1 | Heat map diagram of relative gene expression levels of 33 *OsWKRYs* from total 102 *WRKYs* (**Supplementary Dataset S1**) in rice flag leaves at six stages during aging. Developmental stages comprising six stages of flag leaf (0, 1, 2, 3, 4, and 5 weeks after heading). Expression values were scaled by Log2Fold change ≥ 1 and FDR < 0.05 normalized to 0W stage of flag leaf development. 10 *OsWRKY* candidates are indicated with yellow highlight.

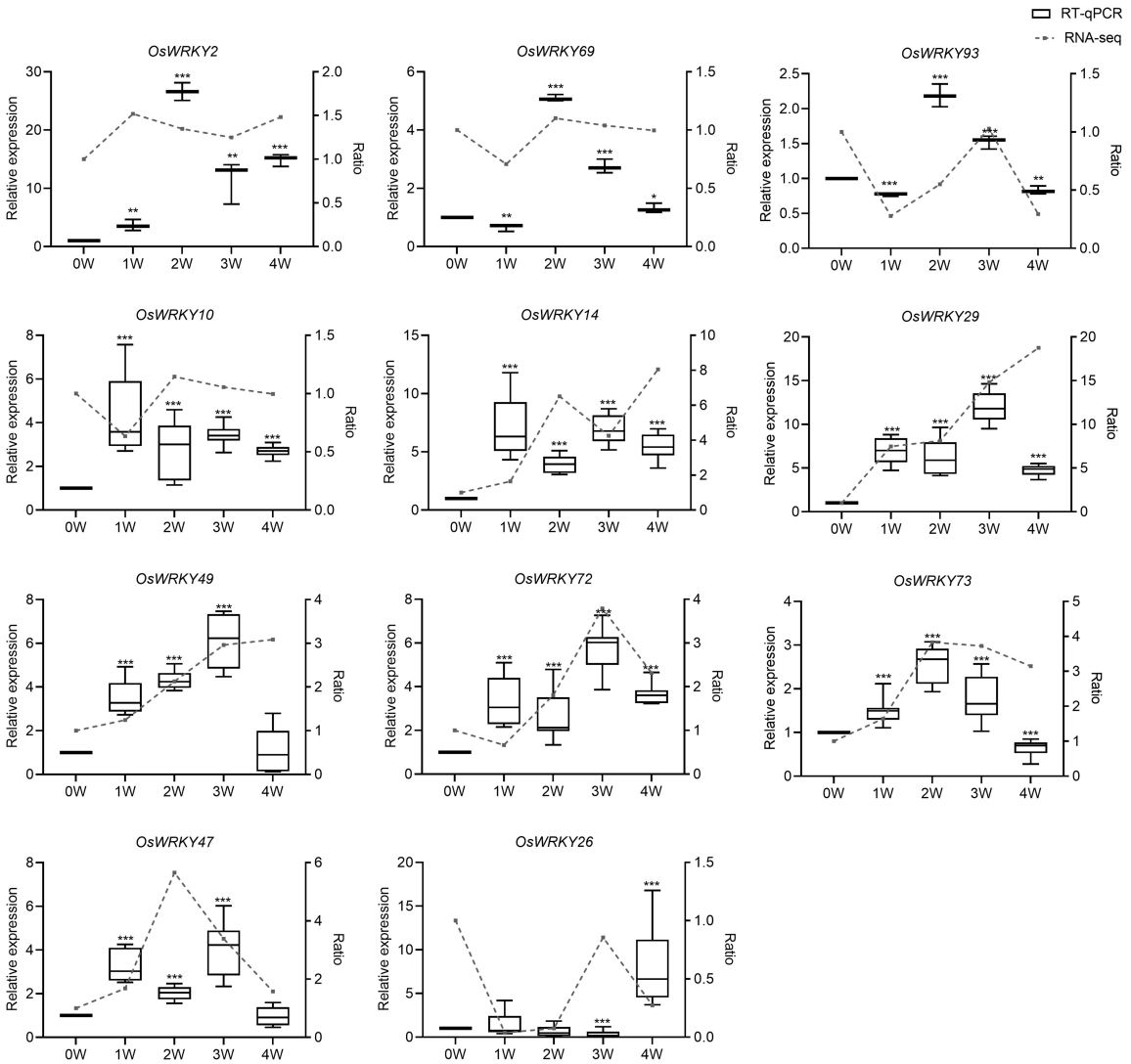

FIGURE 2 | Analyses of several *OsWRKYs* expression level in rice flag leaves during natural senescence. The expression level was assessed by RT-qPCR. All values were normalized to *OsACTIN* expression. Box-and-whisker plots show the median value (horizontal lines), interquartile range (boxes), and minimum and maximum values (whiskers). Three biological replicates and three technique replicates were used. The broken-line graphs indicate expression profiles of 11 *OsWRKYs* from RNA-seq dataset. Asterisks indicate significant differences relative to the 0W controls calculated using the Student *t*-test: $^{*}P < 0.05$; $^{**}P < 0.01$; and $^{***}P < 0.001$. The leaf *Y*_axis denotes relative expression by RT-qPCR. The right *y*-axis denotes ratio of the fold change of RPKM compared with 0W by RNA-seq. 0W means 0 week after heading.

3W and suddenly highly increased at 4W. At 3 weeks after heading, the expression of *OsWRKY29*, *OsWRKY47*, *OsWRKY49*, and *OsWRKY72* was significantly higher than other controls and began to decrease later (**Figure 2**). Overall, the results of RT-qPCR were similarly consistent with the RNA-seq data except *OsWRKY26* and *OsWRKY47* (**Figure 2** broken line).

Expression Profiles of *OsWRKYs* in Response to Pathogen Infection

In nature, plants are often attacked by various pathogens, leading to senescence and even death of plants. In this case, plants will initiate a series of immune defense responses to fight back. A number of WRKY family TFs are involved in regulation of both leaf senescence and pathogen defense response, evidently through the ROS and SA pathways, both of which play an important role in leaf senescence and defense responses induced by pathogens (Zhang et al., 2020). To investigate whether these 11 *OsWRKYs* are induced by infection from pathogens, we performed RT-qPCR (**Figure 3**). For pathogen treatment, three-leaf-stage rice seedlings were spray-inoculated with *Magnaporthe oryzae* strain Guy11. The infected leaf samples were collected every 24 h for near 5 days. The defense-related gene, *OsNAC4*, was used as a positive marker control, showing increased transcript levels in the infected leaves (Kaneda et al., 2009). Among 11 *OsWRKYs*, *OsWRKY2*, *OsWRKY14*,

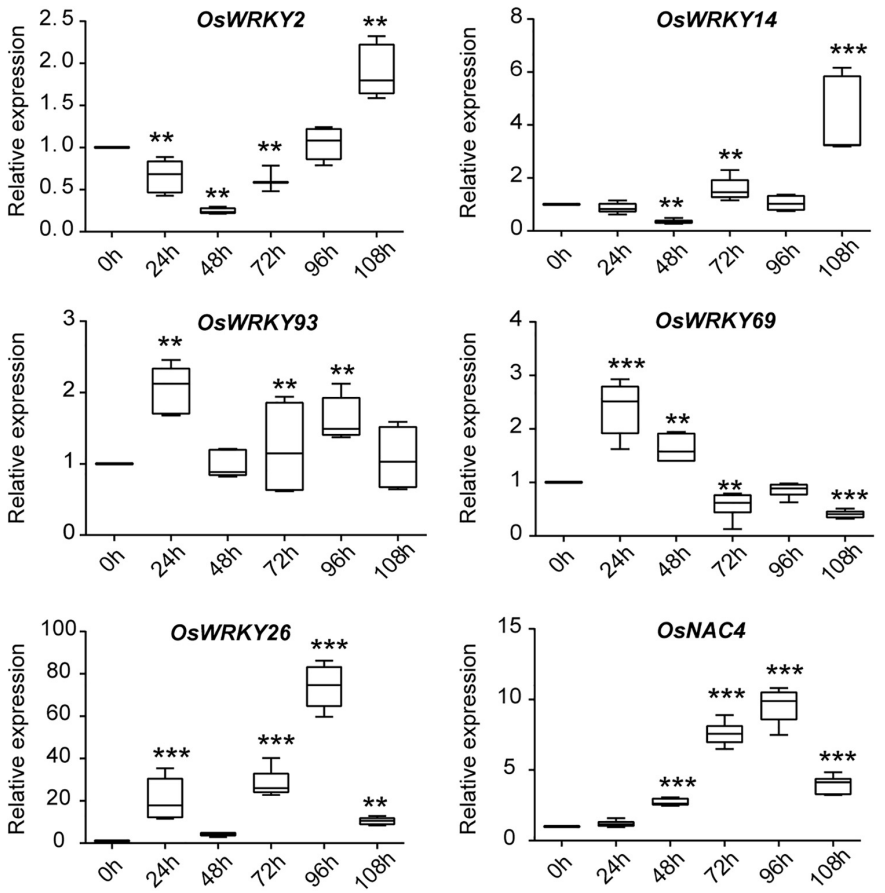

FIGURE 3 | Expression analysis of five *OsWRKY* genes and the defense-related marker gene Os*NAC4* in response to *M. oryzae* infection. qRT-PCR analysis of five *OsWRKYs* and *OsNAC4* in WT at 0, 24, 48, 72, 96, and 108 h after pathogen treatment. The *Y*-axis represents the relative expression level normalized to *OsACTIN*. Box-and-whisker plots show median value (line within box), interquartile range (boxes), and minimum and maximum values (whiskers). Three biological replicates and three technique replicates were used. Asterisk indicate significant differences (**$P < 0.01$, and ***$P < 0.001$) based on Student *t*-test compared to 0 h.

OsWRKY26, *OsWRKY69,* and *OsWRKY93* were induced by *M. oryzae* infection. For instance, *OsWRKY69* and *OsWRKY93* had slightly elevated mRNA levels in infected plants, and they were exclusively expressed at the early stage of infection. On the contrary, *OsWRKY2* and *OsWRKY14* were up-expressed at the late stage after infection. Specifically, the expression of *OsWRKY26* was strongly up-regulated at 96 h after inoculation with Guy11. Taken together, the five *OsWRKYs* appear to play roles in *M. oryzae* mediated resistance.

We summarized the expression profiles of five *OsWRKYs* genes both after pathogen infection and during plant aging and showed that *OsWRKY2* was down-regulated, which might mean no resistance and no senescence; *OsWRKY14* was down-regulated after infection but up-regulated during plant aging, which might imply senescence but no resistance; *OsWRKY26* was both up-regulated, which might mean both resistance and senescence. Both *OsWRKY69* and *OsWRKY93* showed up-resistance after infection but down-regulation during plant aging, which might mean resistance but no senescence (**Table 1**). Therefore, *OsWRKY69* and *OsWRKY93* were our favorite candidates for breeding of high yield and disease-resistant rice.

Evaluation of Disease Resistance of *OsWRKY93* Transgenic Lines to *Magnaporthe oryzae* Guy11

We showed that five *OsWRKYs* were induced in response to Guy11 treatment. In order to genetically evaluate five OsWRKYs protein functions, five $OsWRKY_{VP64}$ transgenic lines were generated to explore the potential functions in rice disease resistance (see section "Materials and Methods"). We

TABLE 1 | Summary of the expression profiles of five *OsWRKYs* genes after pathogen infection and during plant aging.

Genes	Expression profile response to *M. oryzae*	Expression profile during aging
OsWRKY2	Down	Down
OsWRKY14	Down	Up
OsWRKY26	Up	Up
OsWRKY69	Up	Down
OsWRKY93	Up	Down

first detected their transcript levels of five *OsWRKY* genes by RT-qPCR. The results showed that five *OsWRKYs* genes all increased their transcript levels in the transgenic lines (*OsWRKYs* $_{VP64}$) compared with WT Kitaake (**Figure 4A** and **Supplementary Figure S2**). We then inoculated the three-leaf-stage *OsWRKYs*$_{VP64}$ plants with *Magnaporthe oryzae* Guy11 using the spray-inoculation method. Surprisingly, we found that only *OsWRKY93*$_{VP64}$ plants showed a significant enhanced resistance to blast disease (**Figure 4B**). However, the other four of them have no significant alteration of disease resistance to *Magnaporthe oryzae* Guy11 in the transgenic lines (OsWRKYs$_{VP64}$) compared with WT Kitaake (**Supplementary Figure S3**).

In order to further confirm the role of *OsWRKY93* in disease resistance, we generated *oswrky93* mutants using CRISPR/Cas9 system in *Nipponbare* (**Figure 4C**). We found one mutant line *oswrky93-1* that carries a one-base insertion in the first exon of the *OsWRKY93* gene (**Figure 4D**). In contrast to *Nipponbare* plants, the CRISPR/Cas9-edited *oswrky93* mutants are more susceptible to *M. oryzae*, showing more disease lesions and less healthy leaf area (**Figure 4E**), suggesting that *oswrky93-1* plants exhibited elevated susceptibility to *M. oryzae*. Together with the results from the above analysis, these data imply the contribution of *OsWRKY93* to rice defense against *M. oryzae* infection.

Detection of ROS Production in *OsWRKY93* Transgenic Lines

Reactive oxygen species (ROS) burst is a common feature in plant response to a number of biotic stresses, and flg22 has been shown to trigger ROS production in *Arabidopsis* (Mersmann et al., 2010). To examine whether enhanced-expression or knockout of *OsWRKY93* affect ROS production after flg22 treatment, we collected leaves from the *OsWRKY93*$_{VP64}$, *oswrky93-1* and WT plants and measured immediately the ROS level after flg22 treatment. In our experiments, ROS production was increased in *OsWRKY93*$_{VP64}$ activation plants after treatment with flg22, and the flg22-induced ROS generation was twofold higher, compared to the Kitaake plants control and water treatment (**Figure 5A**). As expected, no constitutive ROS production was observed in *oswrky93-1* mutant plants (**Figure 5B**). Given these facts, we concluded that overexpressing *OsWRKY93* enhances PAMP-triggered immune response in rice.

Detection of Darkness-Induced Leaf Senescence Phenotype in *OsWRKY93* Transgenic Lines

In order to further evaluate the potential role of *OsWRKY93* in leaf senescence, the OsWRKY93$_{vp64}$, *oswrky93-1* mutant and two ecotypes of rice (Kitaake and NIP) plants were used for phenotype observation. The plants grown in the soil during the period of 39 days after germination did not show any visibly different phenotypes among enhanced-expression or knockout of *OsWRKY93* and WT. However, the results of detached leaves after darkness treatment showed that the enhanced OsWRKY93 level clearly delayed leaf senescence after darkness treatment for 84 h in OsWRKY93$_{vp64}$ line compared to Kitaake (**Figure 6A**), while knockout of *OsWRKY93* apparently promoted leaf senescence after darkness treatment for 72 h in the *oswrky93-1* line compared to NIP (**Figure 6B**). Therefore, *OsWRKY93* plays function in darkness induced leaf senescence, although there is no visible senescence phenotype in the seedling stage of *oswrky93* mutants.

In view of these facts, OsWRKY93 is a new candidate protein for in-depth understanding of the regulatory mechanisms of pathogen-induced cell death and leaf senescence, helping in breeding high-yield and disease-resistant crops.

DISCUSSION

Plant breeders are facing a serious challenge in rice production, that is, the premature senescence of leaves, in particular, flag leaves, which causes yield loss. There are, however, quite few studies that investigate the molecular mechanism of flag leaf senescence in rice. In this paper, we have identified 11 *OsWRKYs* that were differentially expressed during the senescence of flag leaves through RNA-Seq together with the RT-qPCR analysis. Importantly, we also surveyed the responses of 11 *OsWRKY* genes to *M. oryzae* to explore the correlation between leaf senescence and plant defense. Finally, we genetically identified OsWRKY93 as a new candidate protein for in-depth understanding of the regulatory mechanisms of pathogen-induced leaf senescence, helping in breeding high-yield and disease-resistant crops.

Our experimental results demonstrate that five senescence-inducible genes, *OsWRKY2*, *OsWRKY14*, *OsWRKY26*, *OsWRKY69,* and *OsWRKY93,* were induced in response to *M. oryzae* infection, implying that part of OsWRKY TFs connect leaf senescence and plant defense. In light of the fact that numerous studies have shown that the WRKY family plays a central role in leaf senescence as well as biotic stress tolerance (Bakshi and Oelmüller, 2014), it's not surprising that some WRKY members might have dual functions between them, such as WRKY53, WRKY6, WRKY22, and WRKY70 in *Arabidopsis* (Robatzek and Somssich, 2002; Miao and Zentgraf, 2007; Rushton et al., 2010; Zhou et al., 2011; Hu et al., 2012; Chen J. et al., 2017; Zhou et al., 2018; Ramos et al., 2021). In this study, the transcript levels of *OsWRKY93* increased as leaf senescence progressed, suggesting that *OsWRKY93* is involved in the onset of flag leaf senescence. Gain-of *OsWRKY93* delays a dark-induced leaf senescence, contrary to the loss-of *OsWRKY93*, and promotes a dark-induced leaf senescence (**Figure 6**). We further showed that rice transgenic plants overexpressing *OsWRKY93* displayed an enhanced resistance to *M. oryzae* and the knockout *oswrky93-1* mutants are more susceptible to *M. oryzae*. In addition, we also found that the *OsWRKY93*$_{VP64}$ lines accumulated ROS highly in response to flg22 treatments (**Figure 5A**). In contrast, enhanced ROS production couldn't be detected in the *oswrky93-1* mutant plants (**Figure 5B**). These results clearly indicate that the senescence-inducible gene *OsWRKY93* is also a positive regulator of the defense response in rice. These results also corroborate the findings of the previous study on *OsWRKY23*. As described in that paper, *OsWRKY23*

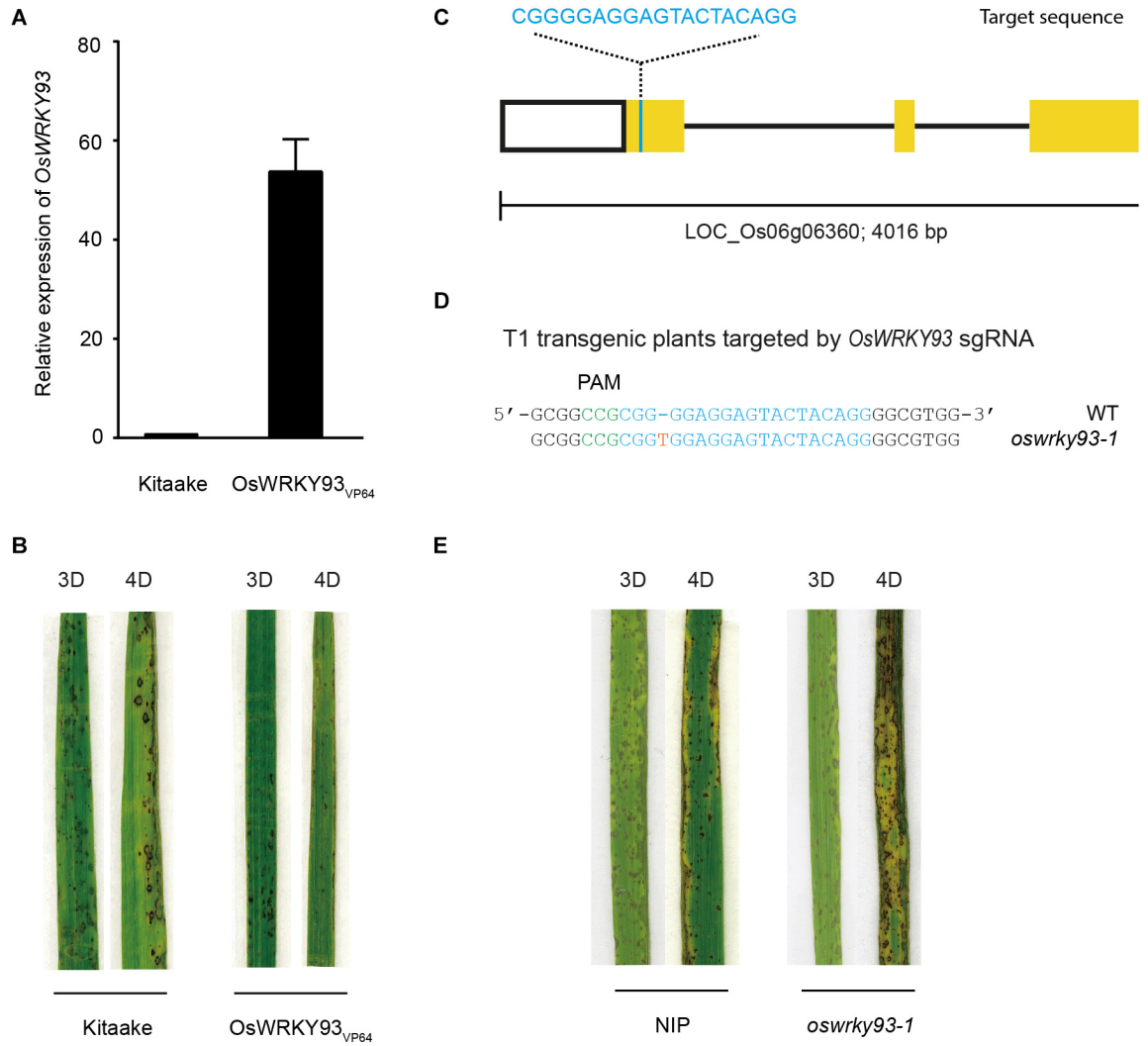

FIGURE 4 | Generation and analysis of the *OsWRKY93* transgenic lines. **(A)** Real-time quantitative PCR experiments showing expression changes of *OsWRKY93* in Kitaake and the OsWRKY93$_{VP64}$. **(B)** Representative leaves of Kitaake and the OsWRKY93$_{VP64}$ 3 and 4 days after inoculation with *M. oryzae*. Pathogen infection assays were performed on three biological replicates. **(C)** Schematic diagram for the CRISPR-edited mutant of *OsWRKY93*. Yellow boxes and black lines represent exons and introns, respectively. The sgRNA target is cyan. **(D)** Sequence of the *oswrky93-1* mutant identified from transgenic plants of the *OsWRKY93* sgRNA target. The reverse complementary sequence of the PAM sequence (5'-CGG-3') of the sgRNA target is green. The red T represents a one-base insertion. **(E)** Representative leaves of *Nipponbare* and *oswrky93-1* 3 and 4 days after inoculation with *M. oryzae*. Pathogen infection assays were performed on three biological replicates.

was strongly induced by dark-induced senescence and its overexpression in Arabidopsis increased tolerance to pathogen infection (Jing et al., 2009). In addition, as we knew, plant senescence is controlled by genetically materials and influenced by environmental cues. In this study our RT-qPCR profiles of a few of 11 candidate WRKYs are not matched well with RNA-seq data (**Figure 2**), an uncontrollable growth condition of different years might be one of reasons for a few OsWRKY members sensitively in response to unknown environmental factors.

Phylogenetic analyses of the WRKY domain sequences provide support for the hypothesis that gene duplication of single- and two-domain WRKY genes and loss of the WRKY domain occurred in the evolutionary history of this gene family in rice (Xie et al., 2005). Based on the number of WRKY domains and the characteristics of the zinc-finger-like motif, the WRKY family can be divided into three types. According to amino acid sequence similarity, 97 WRKY proteins in *O. sativa* were divided into three types and 13 groups, of which class II WRKYs were divided into 10 subclasses (IIa–IIj), and class III WRKYs were divided into two subclasses (IIIa and IIIb) (Qiu et al., 2004; Rushton et al., 2010). It has been reported that class II or III WRKY members are mostly involved in plant defense response (Dong et al., 2003; Cheng et al., 2019; Wang et al., 2020). Here, OsWRKY2, OsWRKY14, and OsWRKY26 belonged to class II of the WRKY family. OsWRKY69 and OsWRKY93 belonged to class III of the WRKY family. Interestingly, we

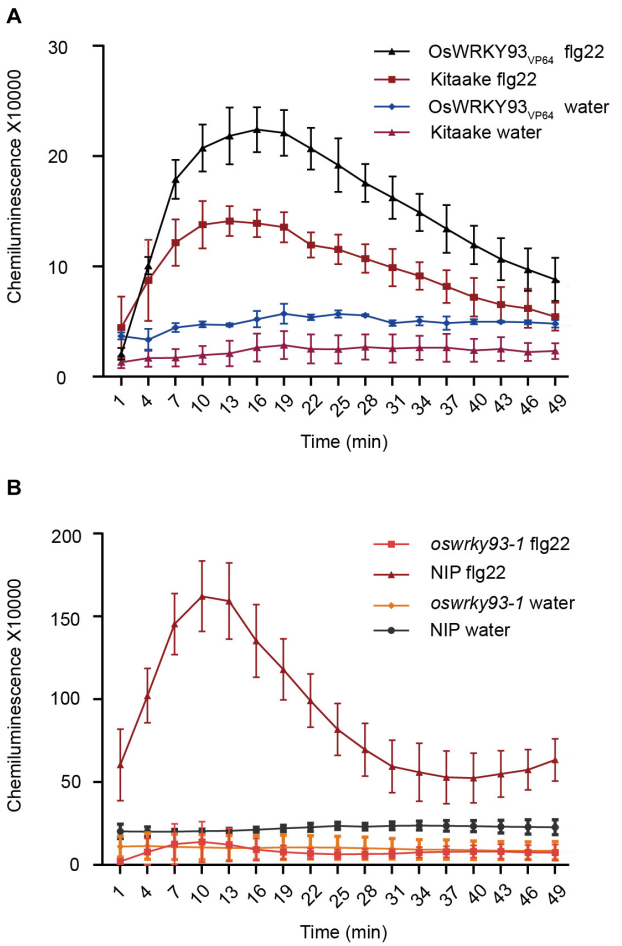

FIGURE 5 | ROS accumulation in rice leaves after flg22 treatment. **(A)** A flg22-induced ROS burst in the OsWRKY93$_{VP64}$ and Kitaake plants. **(B)** A flg22-induced ROS burst in the *oswrky93-1* and *Nipponbare* plants. Rice leaf disks were treated with 1 μM Flg22 or water. Error bars represents the SE (n = 3–5).

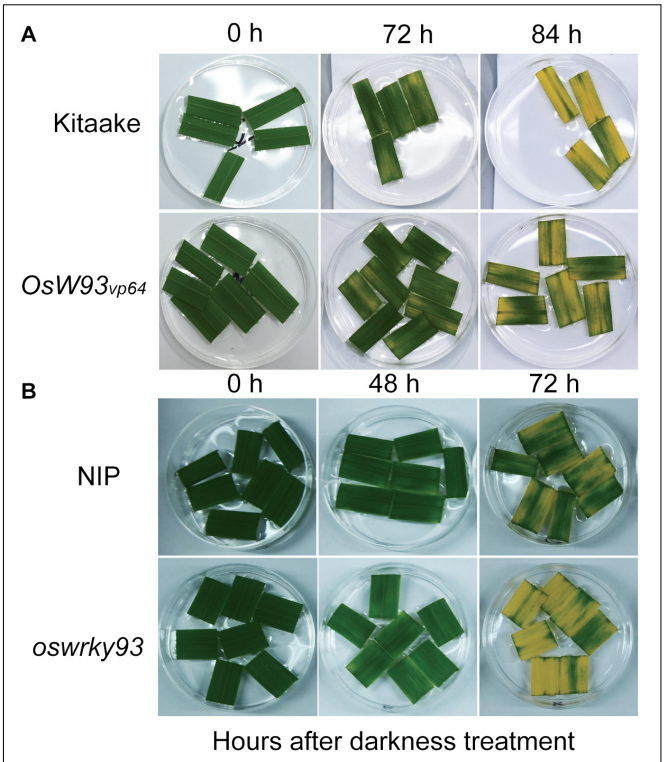

FIGURE 6 | Phenotyping of detached leaves after darkness treatment. **(A)** A delaying leaf senescence shown in the OsWRKY93$_{VP64}$ (*OsW93*$_{vp64}$) compared to Kitaake plants. **(B)** An early leaf senescence shown in the *oswrky93-1* compared to *Nipponbare* (NIP) plants. Detached leaf pieces of rice were incubated with 1 μM MES (pH8.5) buffer after darkness treatment for 0, 48, 72, and 84 h.

found that the expression profiles of five *OsWRKYs* genes were altered in both after pathogen infection and during plant aging, which showed that *OsWRKY2* was down-regulated: there was no resistance and no senescence; *OsWRKY14* was down-regulated after infection but up-regulated during plant aging: there was no resistance and senescence; *OsWRKY26* was up-regulated, with respect to both resistance and senescence; both *OsWRKY69* and *OsWRKY93* showed up-resistance after infection but were down-regulated during plant aging, with respect to resistance and no senescence (**Table 1**). Although the enhanced transgenic rice plants of *OsWRKY2*, *OsWRKY14,* and *OsWRKY26* did not show significantly changing phenotypes of infection to *M. oryzae* at seedling stage, it is possible they rely on a specific kind of pathogen or developmentally dependent. *OsWRKY69* and *OsWRKY93*, especially the latter, both are our favorite candidate genes for further in-depth understanding of their acting mechanism and the high yield and strong resistant genetically manipulation.

DATA AVAILABILITY STATEMENT

The raw data supporting the conclusions of this article will be made available by the authors, without undue reservation.

AUTHOR CONTRIBUTIONS

YL, SL, PM, YP, YZ, and XZ performed the research. YM and YL designed the research and analyzed the data. YM and YX wrote the manuscript. All authors contributed to the article and approved the submitted version.

FUNDING

This work was financially supported by the China National Science Foundation (Grant Nos. 31801266 to YX; 32001437 to YZ), the Youth Project of Fujian Provincial Education Department (JAT190135 to YL), and the Key Project of Natural Science Foundation of Fujian Province (2015 N0019 to YM).

ACKNOWLEDGMENTS

We thank Wenxiong Lin and Zhixing Zhang, Key Laboratory of Crop Ecology and Molecular Physiology, Fujian Agriculture and Forestry University, Fuzhou, China, for kindly providing us with the *OsWRKYs* $_{VP64}$ transgenic lines.

SUPPLEMENTARY MATERIAL

The Supplementary Material for this article can be found online at: https://www.frontiersin.org/articles/10.3389/fpls.2021.643011/full#supplementary-material

Supplementary Figure 1 | Chlorophyll contents of rice flag leaves at six times during aging stages (0W, 1W, 2W, 3W, 4W, and 5W).

Supplementary Figure 2 | The transcript levels of five enhanced expression OsWRKYs $_{VP64}$ transgenic lines compared to the Kitaake WT plants by RT-qPCR.

Supplementary Figure 3 | The infection phenotypes of five enhanced expression OsWRKYs $_{VP64}$ transgenic lines to *M. oryzae*.

Supplementary Table 1 | Primers used in this study.

Supplementary Table 2 | Primers for genotyping CRISPR/Cas9 mutants.

Supplementary Dataset 1 | The list of RPKM values and WRKY family DEGs.

REFERENCES

Bakshi, M., and Oelmüller, R. (2014). WRKY transcription factors: jack of many trades in plants. *Plant Signal. Behav.* 9:e27700. doi: 10.4161/psb.27700

Chen, J., Nolan, T. M., Ye, H., Zhang, M., Tong, H., Xin, P., et al. (2017). *Arabidopsis* WRKY46, WRKY54, and WRKY70 transcription factors are involved in brassinosteroid-regulated plant growth and drought responses. *Plant Cell* 29, 1425–1439.

Chen, L., Xiang, S., Chen, Y., Li, D., and Yu, D. (2017). *Arabidopsis* WRKY45 interacts with the DELLA protein RGL1 to positively regulate age-triggered leaf senescence. *Mol. Plant* 10, 1174–1189. doi: 10.1016/j.molp.2017.07.008

Cheng, H., Li, H., Deng, Y., Xiao, J., Li, X., and Wang, S. (2015). The WRKY45-2-WRKY13-WRKY42 transcriptional regulatory cascade is required for rice resistance to fungal pathogen. *Plant Physiol.* 167, 1087–1099. doi: 10.1104/pp.114.256016

Cheng, X., Zhao, Y., Jiang, Q., Yang, J., Zhao, W., Taylor, I. A., et al. (2019). Structural basis of dimerization and dual W-box DNA recognition by rice WRKY domain. *Nucleic Acids Res.* 47, 4308–4318. doi: 10.1093/nar/gkz113

Chujo, T., Miyamoto, K., Shimogawa, T., Shimizu, T., Otake, Y., Yokotani, N., et al. (2013). OsWRKY28, a PAMP-responsive transrepressor, negatively regulates innate immune responses in rice against rice blast fungus. *Plant Mol. Biol.* 82, 23–37. doi: 10.1007/s11103-013-0032-5

Chujo, T., Takai, R., Akimoto-Tomiyama, C., Ando, S., Minami, E., Nagamura, Y., et al. (2007). Involvement of the elicitor-induced gene *OsWRKY53* in the expression of defense-related genes in rice. *Biochim. Biophys. Acta* 1769, 497–505. doi: 10.1016/j.bbaexp.2007.04.006

Dong, J., Chen, C., and Chen, Z. (2003). Expression profiles of the *Arabidopsis* WRKY gene superfamily during plant defense response. *Plant Mol. Biol.* 51, 21–37.

Edwards, K., Johnstone, C., and Thompson, C. (1991). A simple and rapid method for the preparation of plant genomic DNA for PCR analysis. *Nucleic Acids Res.* 19:1349. doi: 10.1093/nar/19.6.1349

Eulgem, T., Rushton, P. J., Robatzek, S., and Somssich, I. E. (2000). The WRKY superfamily of plant transcription factors. *Trends Plant Sci.* 5, 199–206. doi: 10.1016/S1360-1385(00)01600-9

Gan, S., and Amasino, R. M. (1995). Inhibition of leaf senescence by autoregulated production of cytokinin. *Science* 270, 1986–1988. doi: 10.1126/science.270.5244.1986

Ghosh, S., Sahai, V. N., and Saran, S. (1990). Role of flag leaf on grain yield and spikelet sterility in rice cultivar. *Oryza* 27, 87–89.

Guo, P., Li, Z., Huang, P., Li, B., Fang, S., Chu, J., et al. (2017). A tripartite amplification loop involving the transcription factor WRKY75, salicylic acid, and reactive oxygen species accelerates leaf senescence. *Plant Cell* 29, 2854–2870. doi: 10.1105/tpc.17.00438

Guo, Y., and Gan, S. (2005). Leaf senescence: signals, execution, and regulation. *Curr. Top. Dev. Biol.* 71, 83–112. doi: 10.1016/S0070-2153(05)71003-6

Han, M., Kim, C.-Y., Lee, J., Lee, S.-K., and Jeon, J.-S. (2014). *OsWRKY42* represses *OsMT1d* and induces reactive oxygen species and leaf senescence in Rice. *Mol. Cells* 37, 532–539. doi: 10.14348/molcells.2014.0128

Himelblau, E., and Amasino, R. M. (2001). Nutrients mobilized from leavesof *Arabidopsis* thaliana during leaf senescence. *J. Plant Physiol.* 158, 1317–1323. doi: 10.1078/0176-1617-00608

Hinderhofer, K., and Zentgraf, U. (2001). Identification of a transcription factor specifically expressed at the onset of leaf senescence. *Planta* 213, 469–473. doi: 10.1007/s004250000512

Hu, Y., Dong, Q., and Yu, D. (2012). *Arabidopsis* WRKY46 coordinates with WRKY70 and WRKY53 in basal resistance against pathogen *Pseudomonas* syringae. *Plant Sci.* 185–186, 288–297. doi: 10.1016/j.plantsci.2011.12.003

Jing, S., Zhou, X., Song, Y., and Yu, D. (2009). Heterologous expression of *OsWRKY23* gene enhances pathogen defense and dark-induced leaf senescence in *Arabidopsis*. *Plant Growth Regul.* 58, 181–190. doi: 10.1007/s10725-009-9366-z

Kaneda, T., Taga, Y., Takai, R., Iwano, M., Matsui, H., Takayama, S., et al. (2009). The transcription factor *OsNAC4* is a key positive regulator of plant hypersensitive cell death. *EMBO J.* 28, 926–936. doi: 10.1038/emboj.2009.39

Kim, T., Kang, K., Kim, S.-H., An, G., and Paek, N.-C. (2019). *OsWRKY5* promotes rice leaf senescence via senescence-associated NAC and abscisic acid biosynthesis pathway. *Int. J. Mol. Sci.* 20:4437. doi: 10.3390/ijms20184437

Li, Z. K., Pinson, S. R. M., Stansel, J. W., and Paterson, A. H. (1998). Genetic dissection of the source-sink relationship affecting fecundity and yield in rice (*Oryza sativa L.*). *Mol. Breed.* 4, 419–426.

Lim, P. O., Kim, H. J., and Nam, H. G. (2007). Leaf senescence. *Annu. Rev. Plant Biol.* 58, 115–136.

Ma, Y. F., and Lu, D. Z. (1990). Effect of irrigation modes on the senescence and physiological activity in hybrid rice after heeding. *Chin. J. Rice Sci.* 4, 56–62.

Mersmann, S., Bourdais, G., Rietz, S., and Robatzek, S. (2010). Ethylene signaling regulates accumulation of the FLS2 receptor and is required for the oxidative burst contributing to plant immunity. *Plant Physiol.* 154, 391–400. doi: 10.1104/pp.110.154567

Miao, Y., Laun, T., Zimmermann, P., and Zentgraf, U. (2004). Targets of the WRKY53 transcription factor and its role during leaf senescence in *Arabidopsis*. *Plant Mol. Biol.* 55, 853–867. doi: 10.1007/s11103-005-2142-1

Miao, Y., and Zentgraf, U. (2007). The antagonist function of *Arabidopsis* WRKY53 and ESR/ESP in leaf senescence is modulated by the jasmonic and salicylic acid equilibrium. *Plant Cell* 19, 819–830. doi: 10.1105/tpc.106.042705

Nikolayeva, O., and Robinson, M. D. (2014). edgeR for Differential RNA-seq and ChIP-seq analysis: an application to stem cell biology. *Methods Mol. Biol.* 1150, 45–79. doi: 10.1007/978-1-4939-0512-6_3

Pic, E., de La Serve, B. T., Tardieu, F., and Turc, O. (2002). Leaf senescence induced by mild water deficit follows the same sequence of macroscopic, biochemical, and molecular events as monocarpic senescence in pea. *Plant Physiol.* 128, 236–246. doi: 10.1104/pp.128.1.236

Qiu, Y. P., Jing, S. J., Fu, J., Li, L., and Yu, D. Q. (2004). Cloning and analysis of expression profile of 13 WRKY genes in rice. *Chin. Sci. Bull.* 49, 2159–2168. doi: 10.1360/982004-183

Ramos, R. N., Martin, G. B., Pombo, M. A., and Rosli, H. G. (2021). WRKY22 and WRKY25 transcription factors are positive regulators of defense responses in *Nicotiana benthamiana*. *Plant Mol. Biol.* 105, 65–82. doi: 10.1007/s11103-020-01069-w

Riefler, M., Novak, O., Strnad, M., and Schmulling, T. (2006). *Arabidopsis* cytokinin receptor mutants reveal functions in shoot growth, leaf senescence, seed size, germination, root development, and cytokinin metabolism. *Plant Cell* 18, 40–54. doi: 10.1105/tpc.105.037796

Robatzek, S., and Somssich, I. E. (2001). A new member of the *Arabidopsis* WRKY transcription factor family, AtWRKY6, is associated with both senescence- and defence-related processes. *Plant J.* 28, 123–133. doi: 10.1046/j.1365-313X.2001.01131.x

Robatzek, S., and Somssich, I. E. (2002). Targets of *AtWRKY6* regulation during plant senescence and pathogen defense. *Genes Dev.* 16, 1139–1149. doi: 10.1101/gad.222702

Rushton, P. J., Somssich, I. E., Ringler, P., and Shen, Q. J. (2010). WRKY transcription factors. *Trends Plant Sci.* 15, 247–258.

Ryu, H. S., Han, M., Lee, S. K., Cho, J. I., Ryoo, N., Heu, S., et al. (2006). A comprehensive expression analysis of the WRKY gene superfamily in rice plants during defense response. *Plant Cell Rep.* 25, 836–847. doi: 10.1007/s00299-006-0138-1

Sadowski, I., Ma, J., Triezenberg, S., and Ptashne, M. (1988). GAL4-VP16 is an unusually potent transcriptional activator. *Nature* 335, 563–564. doi: 10.1038/335563a0

Shimono, M., Sugano, S., Nakayama, A., Jiang, C.-J., Ono, K., Takatsuji, H., et al. (2007). Rice *WRKY45* plays a crucial role in benzothiadiazole-inducible blast resistance. *Plant Cell* 19, 2064–2076. doi: 10.1105/tpc.106.046250

Vo, K. T., Kim, C. Y., Hoang, T. V., Lee, S. K., Shirsekar, G., Seo, Y. S., et al. (2018). *OsWRKY67* plays a positive role in basal and XA21-mediated resistance in rice. *Front. Plant Sci.* 8:2220. doi: 10.3389/fpls.2017.02220

Wang, D., Wang, L., Su, W., Ren, Y., You, C., Zhang, C., et al. (2020). A class III WRKY transcription factor in sugarcane was involved in biotic and abiotic stress responses. *Sci. Rep.* 10:20964. doi: 10.1038/s41598-020-78007-9

Wei, T., Ou, B., Li, J., Zhao, Y., Guo, D., Zhu, Y., et al. (2013). Transcriptional profiling of rice early response to Magnaporthe oryzae identified *OsWRKYs* as important regulators in rice blast resistance. *PLoS One* 8:e59720. doi: 10.1371/journal.pone.0059720

Xie, Z., Zhang, Z. L., Zou, X., Huang, J., Ruas, P., Thompson, D., et al. (2005). Annotations and functional analyses of the rice WRKY gene superfamily reveal positive and negative regulators of abscisic acid signaling in aleurone cells. *Plant Physiol.* 137, 176–189. doi: 10.1104/pp.104.054312

Yaghmai, R., and Cutting, G. R. (2002). Optimized regulation of gene expression using artificial transcription factors. *Mol. Ther.* 5, 685–694. doi: 10.1006/mthe.2002.0610

Yokotani, N., Sato, Y., Tanabe, S., Chujo, T., Shimizu, T., Okada, K., et al. (2013). *WRKY76* is a rice transcriptional repressor playing opposite roles in blast disease resistance and cold stress tolerance. *J. Exp. Bot.* 64, 5085–5097. doi: 10.1093/jxb/ert298

Yu, D., Chen, C., and Chen, Z. (2001). Evidence for an important role of WRKY DNA binding proteins in the regulation of *NPR1* gene expression. *Plant Cell* 13, 1527–1539. doi: 10.1105/TPC.010115

Zhang, J., Peng, Y., and Guo, Z. (2008). Constitutive expression of pathogen-inducible *OsWRKY31* enhances disease resistance and affects root growth and auxin response in transgenic rice plants. *Cell Res.* 18, 508–521. doi: 10.1038/cr.2007.104

Zhang, Y., Wang, H.-L., Li, Z., and Guo, H. (2020). Genetic network between leaf senescence and plant immunity: crucial regulatory nodes and new insights. *Plants* 9:495.

Zhou, M., Lu, Y., Bethke, G., Harrison, B. T., Hatsugai, N., Katagiri, F., et al. (2018). WRKY70 prevents axenic activation of plant immunity by direct repression of SARD1. *New Phytol.* 217, 700–712.

Zhou, X., Jiang, Y., and Yu, D. (2011). WRKY22 transcription factor mediates dark-induced leaf senescence in *Arabidopsis*. *Mol. Cells* 31, 303–313.

Conflict of Interest: The authors declare that the research was conducted in the absence of any commercial or financial relationships that could be construed as a potential conflict of interest.

frontiers in Plant Science

ORIGINAL RESEARCH
published: 23 March 2021
doi: 10.3389/fpls.2021.641300

Mutation Types of CYP71P1 Cause Different Phenotypes of Mosaic Spot Lesion and Premature Leaf Senescence in Rice

Yuhan Zheng[1†], Jiangmin Xu[1†], Fujun Wang[1,2], Yongchao Tang[1], Zheng Wei[1], Zhiyuan Ji[1], Chunlian Wang[1] and Kaijun Zhao[1*]*

[1] National Key Facility for Crop Gene Resources and Genetic Improvement, Institute of Crop Sciences, Chinese Academy of Agricultural Sciences, Beijing, China, [2] Institute of Rice Research, Guangdong Academy of Agricultural Sciences, Guangzhou, China

OPEN ACCESS

Edited by:
Nam-Chon Paek,
Seoul National University,
South Korea

Reviewed by:
Longbiao Guo,
Chinese Academy of Agricultural Sciences, China
Weibing Yang,
Shanghai Institutes for Biological Sciences (CAS), China

***Correspondence:**
Chunlian Wang
wangchunlian@caas.cn
Kaijun Zhao
zhaokaijun@caas.cn

[†] These authors have contributed equally to this work

Specialty section:
This article was submitted to Plant Physiology, a section of the journal Frontiers in Plant Science

Received: 11 January 2021
Accepted: 04 March 2021
Published: 23 March 2021

Citation:
Zheng Y, Xu J, Wang F, Tang Y, Wei Z, Ji Z, Wang C and Zhao K (2021) Mutation Types of CYP71P1 Cause Different Phenotypes of Mosaic Spot Lesion and Premature Leaf Senescence in Rice. Front. Plant Sci. 12:641300. doi: 10.3389/fpls.2021.641300

Lesion mimic mutants (LMMs) are ideal materials for studying programmed cell death and defense response in plants. Here we report investigations on two LMMs (*msl-1* and *msl-2*) from the indica rice cultivar JG30 treated by ethyl methyl sulfone. Both of the mutants showed similar mosaic spot lesions at seedling stage, but they displayed different phenotypes along with development of the plants. At tillering stage, larger orange spots appeared on leaves of *msl-2*, while only small reddish-brown spots exhibit on leaves of *msl-1*. At heading stage, the *msl-2* plants were completely dead, while the *msl-1* plants were still alive even if showed apparent premature senility. For both the mutants, the mosaic spot lesion formation was induced by light; DAB and trypan blue staining showed a large amount of hydrogen peroxide accumulated at the lesion sites, accompanied by a large number of cell death. Consequently, reactive oxygen species were enriched in leaves of the mutants; SOD and CAT activities in the scavenging enzyme system were decreased compared with the wild type. In addition, degraded chloroplasts, decreased photosynthetic pigment content, down-regulated expression of genes associated with chloroplast synthesis/photosynthesis and up-regulated expression of genes related to senescence were detected in the mutants, but the abnormality of *msl-2* was more serious than that of *msl-1* in general. Genetic analysis and map-based cloning revealed that the lesion mimic and premature senescence traits of both the mutants were controlled by recessive mutated alleles of the *SL* (Sekiguchi lesion) gene, which encodes the CYP71P1 protein belonging to cytochrome P450 monooxygenase family. The difference of mutation sites and mutation types (SNP-caused single amino acid change and SNP-caused early termination of translation) led to the different phenotypes in severity between *msl-1* and *msl-2*. Taken together, this work revealed that the CYP71P1 is involved in regulation of both premature senescence and cell death in rice, and its different mutation sites and mutation types could cause different phenotypes in terms of severity.

Keywords: lesion mimic mutants, leaf senescence, reactive oxygen species, cell death, mutation types, rice

INTRODUCTION

Plant lesion mimic mutants (LMMs) spontaneously forms necrotic spots on leaves, leaf sheaths and stems under the external conditions without damage or pathogen infection (Hu et al., 1996). LMMs have been identified in a wide range of plants, including maize (Walbot, 1991), *Arabidopsis thaliana* (Dietrich et al., 1994), wheat (Yao et al., 2009), barley (Wolter et al., 1993), rice (Takahashi et al., 1999), and peanut (Badigannavar et al., 2002).

The typic phenotype of a LMM is similar to the hypersensitive response of plant, which is a rapid response to invasion of pathogens, characterized by the rapid death of local cells at the invasion sites. The hypersensitive response can limit growth of microorganisms (Lorrain et al., 2004), usually accompanied by the characteristic of broad-spectrum disease resistance. Therefore, LMMs are ideal materials for studying programmed cell death and defense response mechanisms of plants (Gao et al., 2019).

There are various genetic pathways underlaying the lesion mimic phenotypes of rice. So far, more than 20 genes associated with rice lesion mimic have been cloned, including *spl7* (Yamanouchi et al., 2002), *spl11* (Yin et al., 2000; Zeng et al., 2004), *spl33* (Wang et al., 2017), *nls1* (Tang et al., 2011), and *sl* (Fujiwara et al., 2010). Most of the lesion mimic traits are controlled by a single recessive gene derived from mutation of cell-death negative regulators (Huang et al., 2010). For example, *SPL7* encodes a heat-stress transcription factor. The mutant allele *spl7* with a single base substitution in the coding region of a DNA binding domain, resulting in the conversion of highly conserved amino acid from tryptophan to cysteine, leads to change of the coded protein function (Yamanouchi et al., 2002). *SPL11* encodes the U-box/arm protein SPL11 with U-box domain-dependent E3 ubiquitin ligase activity. A single base substitution in the first exon of the mutant allele *spl11* results in the early termination of translation, which confers broad-spectrum resistance to rice blast and bacterial blight (Yin et al., 2000). Likewise, *SPL33* encodes a eukaryotic translation extension factor eEF1A. A single base mutation in the mutant *spl33* results in the early termination of translation, resulting in loss of protein function and activation of defense response to rice blast and bacterial blight (Wang et al., 2017). *NLS1* encodes a typical CC-NB-LRR type protein, its mutant *nls1* exhibits constitutive defense responses, including cell death, excessive accumulation of hydrogen peroxide and salicylic acid (SA), and enhanced resistance to bacterial pathogens *Xanthomonas oryzae* pv. *oryzae* (*Xoo*) (Tang et al., 2011). Furthermore, *SL* encodes the CYP71P1 protein of cytochrome P450 monooxygenase family. Mutation of *SL* causes the so called Sekiguchi lesion (Fujiwara et al., 2010). In addition to the aforementioned mutants, the *spl30* mutant also increased the resistance to rice blast (Ruan et al., 2019), the *cdr1* significantly increased rice blast resistance (Takahashi et al., 2003), and the *spl28* plants showed enhanced resistance to both blast and bacterial blight (Qiao et al., 2010). Collectively, most of the rice LMMs show improved resistance to pathogens (Xu et al., 2018; Tian et al., 2020).

Leaves are the typical photosynthetic organs of plants (Lohman et al., 1994). Normal leaf senescence is a spontaneous physiological process of plant development to a certain stage, usually accompanied by the redistribution of photosynthetic products (Buchanan-Wollaston, 1997; Lim et al., 2007). The premature senescence of plant leaves is related to changes of cell physiological and biochemical features (Breeze et al., 2011), such as degradation of macromolecular substances (proteins and nucleic acids) (Thompson et al., 1998), severe degradation of chloroplasts and decrease of chlorophyll content (Lee et al., 2009), and membrane lipid peroxidation due to the explosion of reactive oxygen species (Thompson and Lake, 1987). Premature senescence of rice shortens the functional period of leaves and seriously affects grain development during and after grouting, resulting in significant decrease of yield and quality (Gregersen et al., 2013). It has been reported that 1-day delay in leaf senescence could increase rice yield by about 1% (Liu, 1983). Therefore, analysis of the molecular regulation mechanism underlying rice leaf senescence is of great significance for development of elite rice germplasms and breeding super high yield rice varieties.

The process of premature or early senescence can be divided into three stages: the initial stage, the decline stage and the end stage (Noodén et al., 2010). Generally, the senescence-associated genes (SAGs) were classified into three types. The first type is down-regulated genes, which are characterized by significantly reduced mRNA level in senescent leaves, or their expression was inhibited during leaf senescence. The second type refers to those genes with strong senescence specificity, which are activated during senescence, but not expressed at other times. The third type SAGs are similar to the second type genes, but they have a low transcription level in early leaf development, and the transcription level elevates by leaps and bounds during senescence (Gan and Amasino, 1997). Moreover, there are some other SAGs that are specifically expressed during senescence, whose mRNAs can be detected only when the leaf is senescent. For example, three senescence-specific expression genes (*Osl20*, *Osl85*, and *Osl295*) have been cloned (Lee et al., 2001). These genes are involved in amino acid metabolism, fatty acid metabolism and protein degradation, thus affecting the senescence of rice leaves.

It has been reported that LMMs are associated with premature senescence (Qiao et al., 2010; Lee et al., 2018). For example, the growth vigor of mutant *lmm24* is obviously weaker than that of the wild type (Zhang et al., 2019). In present study, we identified two LMMs, designated as mosaic spot lesion mutants *msl-1* and *msl-2*, from indica rice cultivar JG30 treated by ethyl methyl sulfone (EMS). We also observed that *msl-1* and *msl-2* showed a characteristic pattern of premature senescence in addition to the lesion mimic phenotype, but the molecular mechanism underlaying these mutant phenotypes remains unknown. After systematic identification of the phenotypes and physiological characteristics of the two mutants, genetic analysis and map-based cloning of the genes underlying the mutant phenotypes were carried out. We found that the phenotypes of *msl-1* and *msl-2* were controlled by mutated alleles of the so-called *SL* (Sekiguchi lesion) gene (Fujiwara et al., 2010). The phenotype difference

between *msl-1* and *msl-2* is caused by the different mutation sites and types in the *SL* gene. This study demonstrated that mutation of *SL* not only mediated programmed cell death of rice, but also led to premature senescence, and mutation sites and types could cause different phenotypes in terms of severity. Based on previous publications and our present findings, a working model for *SL*-involved rice leaf senescence and cell death was proposed.

MATERIALS AND METHODS

Plant Materials

The LMMs *msl-1* and *msl-2* were isolated through EMS treatment of the indica rice cultivar JG30. After multiple generations of continuous selfing, mutant lines with stable phenotypes were selected from their progenies. The *msl-1* and *msl-2* plants were crossed with japonica rice cultivar 02428, respectively, the phenotypes of F_1 and segregation ratio of F_2 plants were surveyed for genetic analysis and gene mapping. All the rice materials were grown by conventional culture in the net room of Institute of Crop Science, Chinese Academy of Agricultural Sciences (Beijing). From seedling stage to mature stage, the phenotypic status of the mosaic spot lesions have been observed and recorded. At mature stage, 10 individual plants were randomly selected from each mutant line to investigate their traits of plant height, number of tillers, panicle length, effective panicles, seed setting rate, 1,000-grain weight, grain number per panicle, filled grain number per panicle, heading time, primary branch and secondary branch numbers per panicle. The two-tailed Student t-test was used to compare the agronomic traits of the mutants and wild-type plants.

Shading Experiment

Due to the uncertainty of the location of the lesion mimic spots, the top and fully expanded leaves of the mutant plants with non-spotted phenotype were wrapped with tinfoil at tillering stage, which were continuously shaded for 1 week, and occurrence of the mosaic spots was recorded by taking photos. After that, the tinfoil was removed and light was restored. A week later, occurrence of leaf lesions was observed and photographed.

Histochemical Analysis

Trypan Blue Staining

According to the method of Yin et al. (2000), plants of the wild-type JG30 and mutants *msl-1* and *msl-2* with the same growth vigor were selected at tillering stage. In brief, leaves at the same part of selected plants were cut off and placed in a 15cm long glass tube, then trypan blue staining solution was added and boiled for 10 min. After kept in dark for more than 12 h, the leaves were transferred to 25 mg/ml chloral hydrate to decolorize for 3 days. Blue spots on the leaves were recorded and photographed.

DAB (3,3′-Diaminobenzidine) Staining

According to Thordal Christense's method (Thordal-Christensen et al., 1997). Briefly, leaves of the mutants and WT at the same time were soaked in 1 mg/ml DAB (pH = 5.8) solution and dyed for more than 8 h under dark conditions. The leaves were taken out and decolorized in boiling water bath with 95% alcohol for 10 min, fresh anhydrous alcohol was replaced to decolorize until the leaves were transparent. Then observed whether there are reddish brown spots on the leaves of the mutants, and photographed.

H_2O_2, MDA Content and ROS-Scavenging Enzyme Assays

At peak tillering stage, leaves of JG30 and the mutants were taken to prepare tissue homogenate for determination of hydrogen peroxide (H_2O_2) and catalase (CAT), total superoxide dismutase (T-SOD), and malondialdehyde (MDA). Three biological replicates were measured for each sample. All procedures were according the manuals of reagents purchased from Nanjing Jiancheng Bioengineering Institute.

Determination of Photosynthetic Pigment Content

Leaves of wild-type JG30 and the mutant *msl-1* and *msl-2* at tillering stage were collected to measure photosynthetic pigment. The specific operation steps are as follows: weighed about 0.01 g leaves without midrib, cut leaves into pieces, then added 5 mL of 95% ethanol, placed in a 4°C refrigerator to keep out of light, soaked for 24 h and shaken every 8 h until the leaves are completely discolored. Three biological replicates were measured for each sample. The absorbance values at 470, 649, and 665 nm were measured by spectrophotometer with 95% ethanol as blank control. The photosynthetic pigment content (mg/g) were calculated according to the methods of Lichtenthaler (1987). The calculation formula of photosynthetic pigment content (mg/g) is as follows: Chla = (13.95·Abs665–6.88·Abs649) V/(1,000·m); Chlb = (24.96·Abs649–7.32·Abs665) V/(1,000·m); Car = (1,000·Abs470–2.05·Chla–114·Chlb)/245 × V/(1,000·m); Total Chl = Chla + Chlb. In the above formula: V: total volume of chlorophyll extract (ml); m: fresh weight of material (g).

Transmission Electron Microscopy (TEM) Assay

At tillering stage, leaves of the wild type and mutants were fixed in 2.5% pre-cooled glutaraldehyde for 24 h, then the samples were rinsed with 0.1 mmol/L phosphoric acid buffer (pH = 7.2) for three times, each time for 10 min. After washing, the samples were fixed with 1% osmic acid stationary solution (pH = 7.3) for 4 h; after preliminary fixation, the samples were dehydrated by gradient ethanol, and then embedded in epoxy resin after dehydration; After that, the slices were stained with uranyl acetate and lead citrate, observed and photographed under the transmission electron microscope (Hitachi, Japan).

RNA Extraction and Quantitative Real-Time PCR (qRT-PCR) Analysis

Total RNAs were extracted by Trizol method (Invitrogen, United States). The treated RNA samples were reversely transcribed into cDNA by reverse transcription Kit (TIANGEN, Beijing, China). The SYBR® Premix ExTaqTM II kit was used to configure the reaction system, and ABI 7500 Real-Time PCR

system was used as the PCR quantizer. Using rice *OsActin* as internal reference gene, the reaction volume was 20 μL, containing 10 μL 2 × SYBR Green Master Mix, 2 μL cDNA, 0.4 μL 50 × ROX Reference Dye II, 0.8 μL forward and reverse primers (10 μmol/L) and 6 μL RNase-free H_2O. The PCR procedure was pre denaturation at 95°C for 3 min, 95°C for 5 s, 60°C for 34 s, and 40 cycles. The relative expression was analyzed by $2^{-\Delta\Delta Ct}$ method (Livak and Schmittgen, 2001), and three biological replicates were measured for each sample. The primers for qRT-PCR analysis are listed in **Supplementary Table 1**. All primers were synthesized by Sangon Biotechnology Co., Shanghai, China.

Fine Mapping of *msl-1* and *msl-2*

The F_1 hybrids were obtained by crossing japonica rice cultivar 02428 as female parent and mutants *msl-1* and *msl-2* as male parents, respectively. The F_2 segregation populations were obtained by selfing of F_1 plants. Insertion/deletion (InDel) molecular markers (totally, 256) distributed evenly on 12 chromosomes of rice were used to screen the polymorphism of the parents, and then individual F_2 plants with extreme lesion mimic phenotype were selected for genetic linkage analysis. According to the results of preliminary mapping, new molecular markers were further developed, the mapping populations were expanded and 10 pairs of primers (**Supplementary Table 2**) were used for fine mapping.

Analysis of Candidate Genes, Amino Acid Sequences, and Evolutionary Relationship

Based on the RGAP[1] genome information, we downloaded the sequences of all candidate genes within the mapped location intervals, then used Primer3.0[2] to design primers to amplify the candidate genes of the wild-type JG30 and mutants. The PCR-amplified products were recovered and sent for sequencing by Sangon Biotechnology Co., Shanghai, China. Sequencing results were analyzed with the DNAMAN software.

The deduced homologous proteins of *msl-1* and *msl-2* in 17 plant species were searched and downloaded from NCBI website through blastx and saved in FASTA format. The multi-sequence alignment software ClustalX was used for the alignment analysis of amino acid sequences. Then MEGA7.0 was used to construct the phylogenetic tree, where we selected neighbor-joining method to construct the tree, and the check parameter Bootstrp was set to 1,000.

Three-Dimensional Structure Analysis of Proteins

The online protein structure prediction software Swiss-model[3] was used to conduct homologous modeling for the protein spatial structure of wild-type protein CYP71P1, mutant proteins msl-1 and msl-2, respectively. The protein sequences were saved in PDB format, and the software was used to display, then compared and analyzed the three-dimensional structure of the proteins.

[1]http://rice.plantbiology.msu.edu

[2]http://primer3.ut.ee

[3]https://swissmodel.expasy.org/

RESULTS

Phenotype Identification of *msl-1* and *msl-2*

Compared with the wild-type JG30, the mutants *msl-1* and *msl-2* showed brown necrotic spots on leaves, leaf sheaths and stems of seedlings at three-leaf stage (25 days post sowing), and the roots displayed dysplasia (**Figures 1A,C**). At tillering stage, large orange spots appeared on the leaves of *msl-2*, the number of spots increased gradually and finally the spots covered the whole leaf area; while the reddish-brown spots of mutant *msl-1* was small and the number of mosaic spots was relatively less (**Figure 1D**). At young panicle differentiation stage, the lower leaves of *msl-1* and *msl-2* plants became dying, showing significant premature senescence. In addition, the degree of premature senescence was higher and the number of dead leaves of *msl-2* was more than that of *msl-1* (**Figure 1B**). At heading stage, the spots on the leaves of *msl-2* appeared in an explosive manner, and the whole plants died, but for *msl-1*, only the lower leaves died and other functional leaves became somewhat yellow compared with the wild-type plants (**Figure 1E**).

We further investigated agronomic characters of the mutants and WT at maturity stage. Compared with the wild type, plant height, number of tillers, effective panicle number, seed setting rate, 1,000-grain weight, total grains per panicle, filled grains per panicle and secondary branch number of the mutants were all significantly decreased (**Table 1**). In addition, the wild-type plants started booting about 102 days after sowing, while the *msl-1* plants started booting about 107 days after sowing, and the mutant *msl-2* started booting about 113 days after sowing (**Table 1**). The development of both *msl-1* and *msl-2* plants were significantly delayed compared with the wild type. In general, the appearance of lesion mimic spots has a more obvious impact on the agronomic traits of mutant *msl-2* (**Table 1**).

Light-Induced Response of the Lesion Mimic Mutants

At tillering stage, shading treatment was carried out for the leaves without lesion mimic spots of *msl-1* and *msl-2*. A week later, no spots were found in the area covered by aluminum foil, while mosaic spots appeared in the same age leaves without shading treatment. Interestingly, after the tinfoil removed, and regaining normal light for 7 days, the previously tinfoil-shaded leaves displayed mosaic spots (**Figure 1F**). These results indicated that formation of the mosaic spots phenotype of *msl-1* and *msl-2* is light dependent.

Programmed Cell Death and Reactive Oxygen Species Accumulation in the Mutants

Programmed cell death is usually accompanied by accumulation of intracellular reactive oxygen species. In presence of peroxidase,

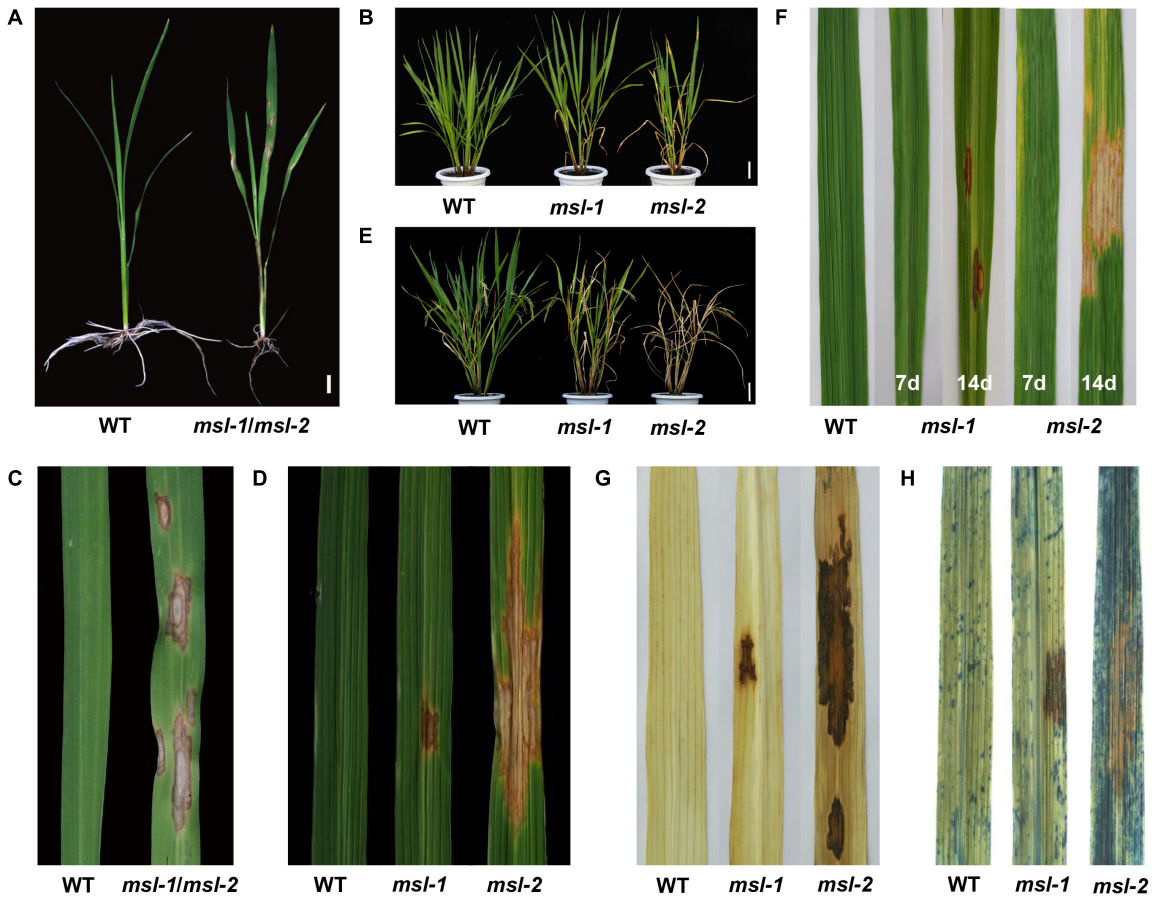

FIGURE 1 | Phenotypic characterization of wild type and mutants. **(A)** Phenotypes at seedling stage (30 days after sowing). **(B)** Phenotypes at the young panicle differentiation stage. **(C)** Leaves at seedling stage. **(D)** Leaves at tillering stage. **(E)** Plant phenotypes at heading stage. **(F)** Formation of mosaic spot lesion is light dependent. From left to right: leaf of wild type, leaf of *msl-1* covered with aluminum foil for 7 days, leaf of *msl-1* recovered to light for 7 days, leaf of *msl-2* covered with aluminum foil for 7 days, leaf of *msl-2* recovered to light for 7 days. **(G)** Diaminobenzidine (DAB) staining showing accumulation of H_2O_2 at mosaic lesions. **(H)** Trypan blue staining, showing cell death at the mosaic lesions. Bar = 1 cm **(A)**; Bar = 10 cm **(B,E)**.

diaminobenzidine (DAB) reacts with H_2O_2 to rapidly produce reddish-brown precipitation. According to this, DAB staining was performed for leaves from the mutants and wild-type JG30. Results showed that leaves from both *msl-1* and *msl-2* were stained with reddish-brown polymer deposition, while the WT had no reddish-brown spots (**Figure 1G**). These observations indicated that growth of the lesion spots was accompanied by the accumulation of a large amount of hydrogen peroxide. Trypan blue is an indicator of cell death. After trypan blue staining, the whole leaf of *msl-2* was stained with dark blue spots, while dark blue spots appeared only on and near to the spots of *msl-1*. Compared with that, the wild-type JG30 did not display obvious dark blue spots (**Figure 1H**), indicating that programmed cell death had occurred or was occurring in the mutant leaves at tillering stage.

Premature Senescence of the Mutants

In order to analyze the premature senescence of the mutants in depth, we observed the microstructure of chloroplasts, measured the content of photosynthetic pigment, and determined the expression of genes associated with senescence, chloroplast synthesis and photosynthesis.

At maximum tillering stage, leaves from the mutants with lesion mimic spots and the corresponding wild-type leaves were sampled and placed under transmission electron microscopy (TEM) to observe the chloroplast structure. TEM assays showed that the number of chloroplasts in the mesophyll cells of wild type was more, the grana lamella was more abundant; the osmiophilic plastoglobuli was less; and the chloroplast structure was complete (**Figures 2A,B**). However, in leaves of the mutants, the lamellar structure of thylakoid began to degrade gradually; the vascular structure appeared; the number of osmiophilic plastoglobuli increased significantly; the chloroplast structure was damaged and the chloroplasts began to disintegrate; and the cell wall of mutants were thinner than that of wild type, which may accelerate cell apoptosis and cell structure disintegration in the mosaic spot lesions (**Figures 2C–F**). Moreover, the damage degree of chloroplasts in *msl-2* was higher than that in *msl-1*, as indicated by more osmiophilic plastoglobuli and more serious chloroplast degradation (**Figures 2E,F**). The degree of

TABLE 1 | Agronomic traits of the wild type and mutants.

Agronomic traits	Materials		
	WT	*msl-1*	*msl-2*
Plant height (cm)	91.20 ± 6.83	83.29 ± 2.06*	75.67 ± 1.15**
Number of tillers	8.40 ± 1.34	5.29 ± 1.11**	3.33 ± 0.58**
Effective panicle	8.20 ± 1.10	3.57 ± 0.79**	3.00 ± 1.00**
Panicle length (cm)	21.40 ± 1.38	18.98 ± 1.91	19.58 ± 1.29
Grain number per panicle	137.28 ± 15.90	96.56 ± 18.14**	94.72 ± 5.04**
Filled grain number per panicle	116.13 ± 17.38	61.00 ± 11.75**	28.11 ± 2.59**
Primary branch number	11.00 ± 0.76	9.90 ± 0.98	10.28 ± 0.75
Secondary branch number	24.30 ± 5.90	13.16 ± 5.05**	10.83 ± 2.02**
Setting rate (%)	84.35 ± 3.57	63.30 ± 5.22**	29.65 ± 1.64**
1,000-grain weight (g)	26.62 ± 0.17	19.91 ± 0.17**	17.80 ± 0.18**
Heading time (day)	102.60 ± 1.14	107.14 ± 0.90**	113.33 ± 2.08**

*The data in table are the average value ± standard deviation of 10 individual plants. * and **, significant differences at $P < 0.05$ and $P < 0.01$, respectively (Student's t-test).*

chloroplast degradation was in coincidence with the severity of premature senescence.

The chlorophyll content is an important physiological index to measure the photosynthesis and premature senescence of leaves (Jiao et al., 2012). We found that the contents of chlorophyll a (Chl *a*), chlorophyll b (Chl *b*), total chlorophyll (Total Chl), and carotenoid (Car) in *msl-1* and *msl-2* were significantly decreased compared with those of the wild type at tillering stage (**Figure 2G**). Notably, the contents of Chl *a*, Chl *b,* and Total Chl in *msl-2* decreased in a larger extent than that of *msl-1* (**Figure 2G**), suggesting that *msl-2* had a higher degree of premature senescence.

We further examined expression of six chloroplast synthesis-related genes (*V1*, *V2*, *DVR*, *CHLH*, *PORA*, *PORB*), eight photosynthesis-related genes (*psaA*, *psbA*, *rbcL*, *rbcS*, *cab1R*, *cab2R*, *rpoA*, *rpoB*) and three senescence-related genes (*SGR*, *Osh36*, *Osl85*) in the mutants and wild-type by qRT-PCR analysis. Results showed that the expression of six chloroplast synthesis-related genes and all the photosynthesis-related genes in mutant leaves were dramatically down-regulated (**Figures 2H,I**). In contrast, the expression of senescence-related genes significantly increased in *msl-2* compared with the wild-type. Similarly, the expression of *Osh36* and *Osl85* exhibited elevated expression in the *msl-1* mutant (**Figure 2J**). Overall, these results suggest that premature leaf senescence occurs in *msl-1* and *msl-2*, and *msl-2* displayed premature senescence in a more serious severity.

ROS Abnormality in the Mutants

The metabolic disorder of reactive oxygen species (ROS), mainly including superoxide anion radical (O^{2-}), hydrogen peroxide (H_2O_2), hydroxyl radical (OH), and nitric oxide (NO), can accelerate leaf senescence and lead to premature senescence of plants. Cell death is usually associated with intracellular accumulation of H_2O_2. Physiological indexes of the mutants *msl-1*, *msl-2* and wild type have been measured at tillering stage, and results showed that a large amount of H_2O_2 was accumulated in *msl-1* and *msl-2* (**Figure 3A**), which are consistent with the results of DAB staining (**Figure 1G**).

The content of malondialdehyde (MDA) usually reflects the degree of lipid peroxidation in plants, and indirectly reflects the degree of cell damage. Our data showed that MDA content in *msl-1* and *msl-2* was significantly higher than that in the

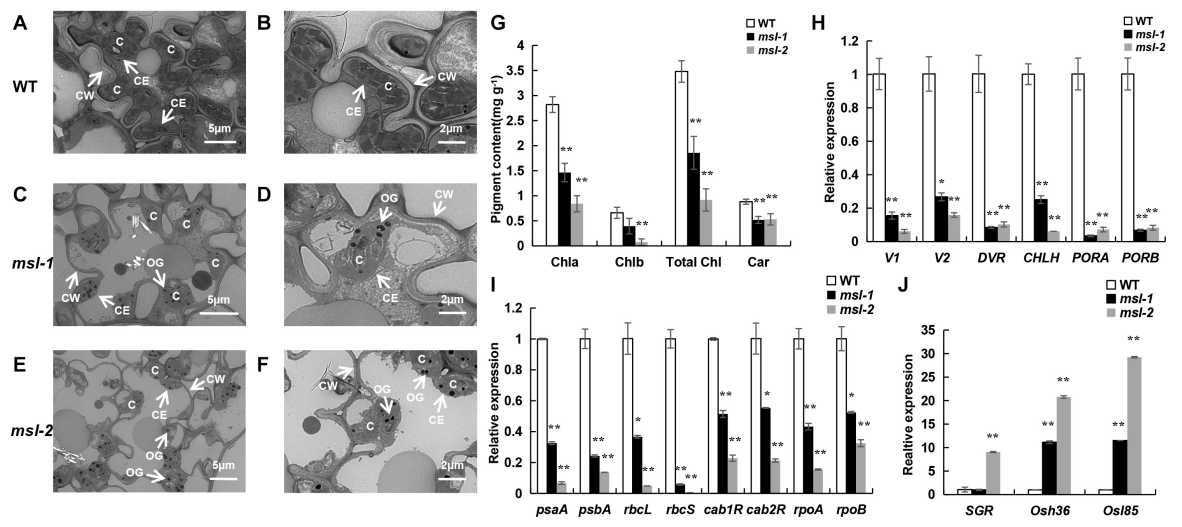

FIGURE 2 | Premature senescence identification of mutant leaves. **(A–F)** Ultrastructural analysis of chloroplasts in wild type and mutants by transmission electron microscopic. C, chloroplast; CE, chloroplast membrane; CW, cell wall; OG, osmiophilic plastoglobuli. **(G)** Determination of photosynthetic pigment content. **(H)** Expression assay of chloroplast synthesis-related genes. **(I)** Expression assay of photosynthetic-related genes. **(J)** Expression assay of senescence-related genes. Error bars represent the standard deviations of three biological replicates. * and **, significant differences at $P < 0.05$ and $P < 0.01$, respectively (Student's *t*-test).

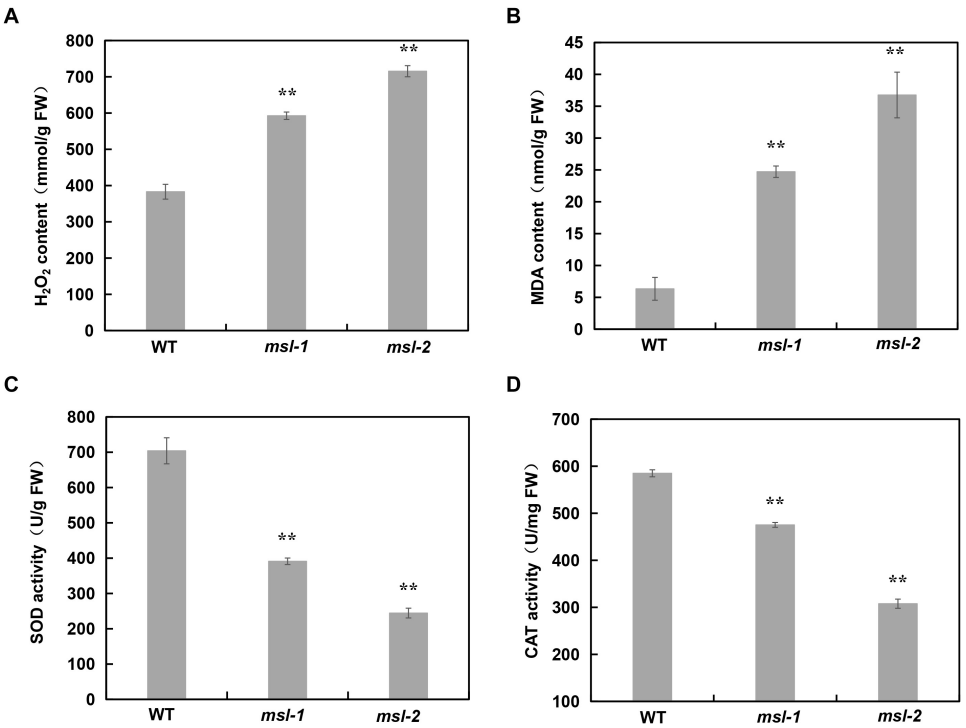

FIGURE 3 | Analysis of ROS accumulation and relative expression of antioxidant enzymes in wild type and mutants. **(A)** H_2O_2 contents. **(B)** Malondialdehyde (MDA) contents. **(C)** SOD enzyme activity. **(D)** CAT enzyme activity. Error bars represent the standard deviations of three biological replicates. **, significant differences at $P < 0.01$ (Student's *t*-test).

wild type (**Figure 3B**). Plants produce a series of antioxidant enzymes to eliminate ROS damage to cells, such as catalase (CAT), superoxide dismutase (SOD), and peroxidase (POD) (Miller et al., 2010). SOD catalyzes superoxide anion radical (O^{2-}) disproportionation to H_2O_2, and CAT catalyzes the decomposition of H_2O_2. Therefore, we also measured the activities of CAT and SOD in *msl-1*, *msl-2* and the wild type. Results showed that the activities of SOD and CAT in *msl-1* and *msl-2* significantly decreased compared with the wild type at tillering stage (**Figures 3C,D**), which caused the ROS accumulation in the mutant leaves.

Fine Mapping of *msl-1* and *msl-2*

To identify the gene(s) underlying the mosaic spot lesion and leaf senescence phenotypes of the mutants, we generated F_2 progenies from crosses between the japonica rice cultivar 02428 and the mutants *msl-1* and *msl-2*, respectively. All the F_1 individuals did not show any mosaic spot lesions and had normal phenotypes as the wild type, indicating that the mutant phenotypes were genetically recessive. In the F_2 progenies, the segregation ratios between normal plants and the plants with spot lesions statistically fitted to 3:1 (**Table 2**), following the canonical Mendelian segregation, indicating that a single recessive gene controls the mutant phenotypes of both the mutants.

The mosaic spot lesion plants in the F_2 progenies were used to map the target gene(s). A total of 256 pairs of InDel molecular markers were selected for polymorphism screening.

TABLE 2 | Genetic analysis of mutants *msl-1* and *msl-2*.

Combination	F_1	F_2			χ^2 (3:1)	*P*-value
		Wide-type	Mutant-type	Total		
02428 × *msl-1*	Normal	1,012	316	1,328	1.028	0.311
02428 × *msl-2*	Normal	1,422	458	1,880	0.408	0.523

Among them, 52 pairs showed polymorphism between mutants and 02428. The polymorphic markers differentiating *msl-1* from 02428 were identical with those between *msl-2* and 02428, implying that the mutant genes in *msl-1* and *msl-2* may be alleles of a single locus.

We then conducted genetic linkage analysis on the mutant *msl-1*. After analyzing the polymorphic markers between the two parents, we found that most of the polymorphic markers distributed on chromosome 12, indicating that the target gene might locate on chromosome 12. Therefore, F_2 individuals with obvious mosaic spot lesion phenotype were selected, and the polymorphism markers on chromosome 12 were used for the linkage analysis of *msl-1*. Results showed that there was a linkage phenomenon between the mutant phenotype and two markers designated as P3 and S11. We subsequently developed new molecular markers within the interval between P3 and S11, and the target gene was mapped between new markers S20 and S8, with a genetic distance of 1.41cM. In order to narrow

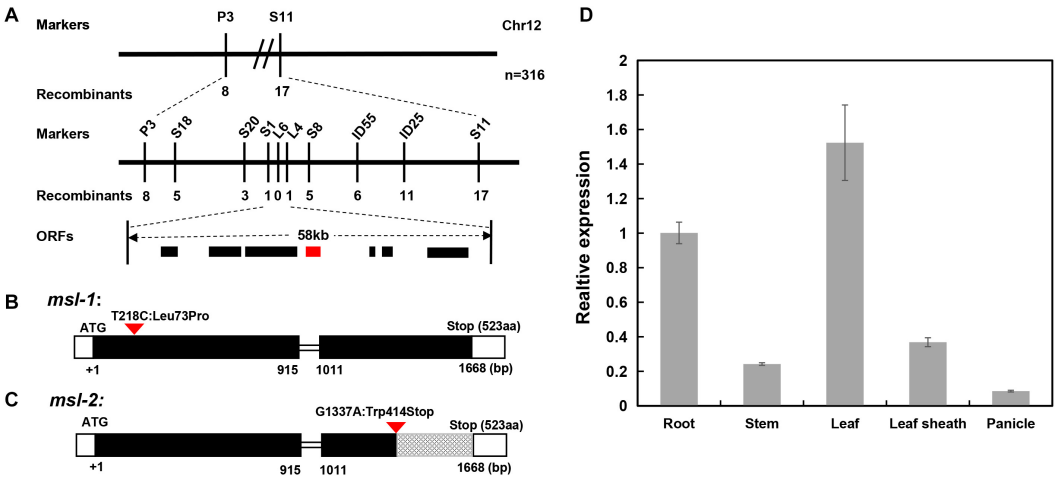

FIGURE 4 | Map-based cloning of *msl-1* and *msl-2*. **(A)** The *msl-1* and *msl-2* loci were fine-mapped to 58kb region between Indel markers S1 and L4 on chromosome 12. **(B)** Gene structure of *LOC_Os12g16720* and the mutation site in *msl-1*. **(C)** Gene structure of *LOC_Os12g16720* and the mutation site in *msl-2*. The black rectangles represent exons and the red inverted triangle represents the mutation sites. **(D)** Analysis of *SL* gene expression in different tissues of WT. Error bars represent the standard deviations of three biological replicates.

down the target interval, another 3 pairs of polymorphic InDel markers between S20 and S8 were developed, and genotyping was performed on more F_2 individuals. The target gene was finally located between InDel markers S1 and L4, with a physical distance of about 58 kb (**Figure 4A**).

Both *msl-1* and *msl-2* Are Allelic Variants of the SL Gene

According to the RGAP website of the rice genome database, there are 7 annotated genes (**Supplementary Table 3**) in the 58 kb target region flanked by molecular markers S1 and L4. By sequencing all the candidate genes in the interval, we found that only *LOC_Os12g16720* has a SNP between sequences from *msl-1* and the wild-type JG30. Compared with JG30, there is a base substitution (T to C) at 218 nucleotide position (T218C) in the first exon of *LOC_Os12g16720* locus in *msl-1*, which causes an amino acid change from isoleucine to proline at 73rd amino acid position (Leu73Pro) (**Figure 4B**). To further verify the candidate gene, we amplified and sequenced the *LOC_Os12g16720* locus in F_2 plants from the cross between 02428 and *msl-1*, and found that the T218C single-base alteration presented in all the F_2 plants with mosaic spot lesion phenotype but not in the normal F_2 plants. Based on nucleotide sequences and rice genome annotation information, *LOC_Os12g16720* is the previously reported *SL* (Sekiguchi lesion) gene, encoding a CYP71P1 protein of cytochrome P450 monooxygenase family, which has tryptamine 5-hydroxylase activity and catalyzes the conversion of tryptamine to serotonin (Fujiwara et al., 2010). Therefore, we concluded that *msl-1* is an allelic variant of the *SL* gene, with the T218C SNP conferring the mosaic spot lesion and leaf senescence phenotypes of the mutant.

Since the genetic mapping implied that the mutant genes in *msl-1* and *msl-2* may be alleles of a single locus, we then sequenced all the above-mentioned candidate genes in mutant *msl-2*, and found that there is only a single base mutation (G to A) at 1,337 nucleotide position (G1337A) in the second exon of the *LOC_Os12g16720* locus in *msl-2*, which caused a premature termination of protein translation (**Figure 4C**). Similarly, we sequenced the *LOC_Os12g16720* locus in F_2 plants from the cross between 02428 and *msl-2*, and found that the G1337A single-base substitution presented in all the F_2 plants with mosaic spot lesion phenotype but not in the normal F_2 plants. Thus, the single base substitution in the *LOC_Os12g16720* locus confers the mosaic spot lesion phenotype of both mutants *msl-1* and *msl-2*. This conclusion has been supported by the recently published research on *ell1* (early lesion leaf 1) and *sl-MH-1*, which are LMM mutants from the japonica rice variety Wuyunjing7 and indica rice line Minghui 86 (MH86), respectively, at the *LOC_Os12g16720* locus (Tian et al., 2020; Cui et al., 2021).

To check the expression pattern of the *SL* gene, qRT-PCR analysis was performed using different tissues including roots, stems, leaves, leaf sheaths and spikelets of wild-type JG30 at booting stage. Results showed that the *SL* gene was constitutively expressed in all the tissues. However, the expression levels in root, leaf and leaf sheath were higher than in other tissues, which is consistent with the fact that the occurrence of mosaic spot lesion mainly concentrated on roots, leaves and leaf sheaths (**Figure 4D**).

Bioinformatics Analysis of the Proteins Encoded by *msl-1* and *msl-2*

Since *msl-1* and *msl-2* are allelic variants of the *SL* gene that encodes the CYP71P1 protein, bioinformatics analysis on the CYP71P1-homologies was conducted. Multiple sequence alignment of target protein sequences from 17 species showed that the two amino acids (L73 and W414) are highly conserved among various species (**Figure 5A**). This should conform that the single nucleotide substitution (T218C) in *msl-1*, that causes

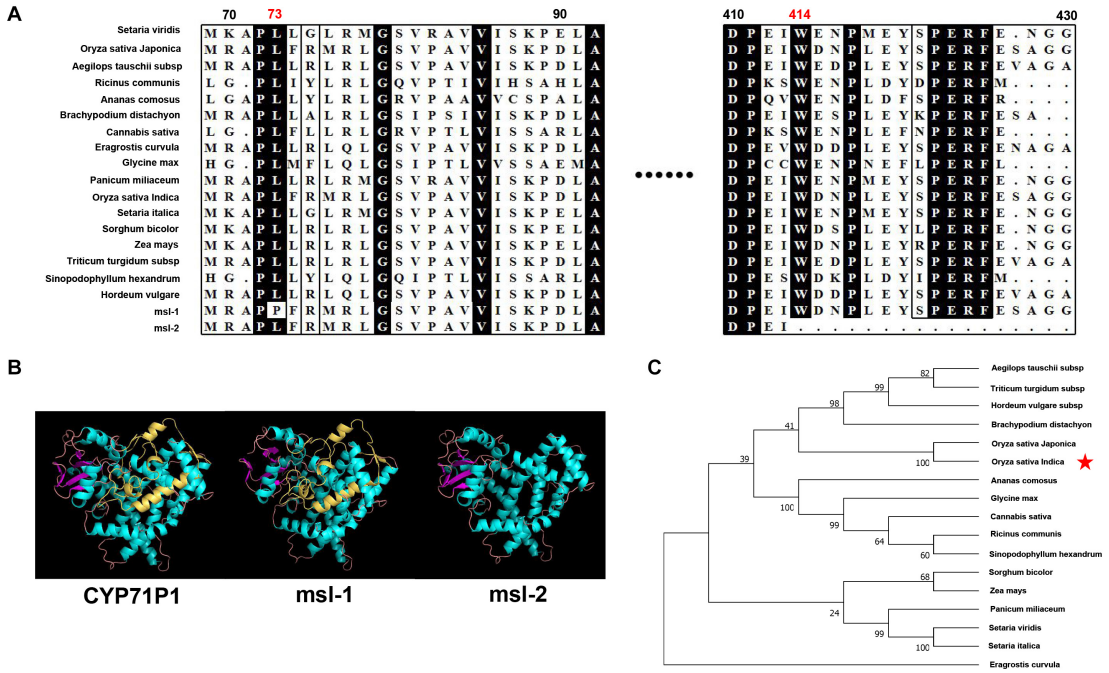

FIGURE 5 | Bioinformatics analysis of target genes. **(A)** Protein sequence alignment of the CYP71P1 protein homologies among multiple species, both the mutation sites of msl-1 (at 73nd residue) and msl-2 (at 414th residue) are highly conserved. **(B)** Protein three-dimensional structure of CYP71P1, msl-1 and msl-2. **(C)** Phylogenetic tree analysis of the CYP71P1 homologies.

the 73rd amino acid change (Leu73Pro), affects the biological function of the msl-1 protein, and resulted in the *msl-1* mutant phenotypes. Furthermore, since the G1337A SNP in *msl-2* causes premature termination of protein translation at the 414^{th} amino acid position (**Figure 5A**), the deduced msl-2 protein lacks the 109 aa-C-terminus compared with the wild type CYP71P1, this may make the *msl-2* show more serious mutant phenotypes than that of *msl-1*. The protein sequences of wild-type CYP71P1 and its mutants msl-1 and msl-2 were compared and analyzed by Swiss-model for predicting the three-dimensional structure of proteins. Deletion of the 109 aa-C-terminus in msl-2 led to the obvious conformational change of the protein (**Figure 5B**). However, the protein structures of msl-1 and WT CYP71P1 showed no significant difference (**Figure 5B**), which to some extent explained the significant difference in phenotypes of the two mutants. In addition, we used neighbor-joining method to build a phylogenetic tree, it indicated that the CYP71P1 and its homologous proteins in rice are closely related to monocots such as grasses (**Figure 5C**).

DISCUSSION

Both *msl-1* and *msl-2* Belong to the Expanding Type of Lesion Mimic Mutants but Differ Largely in Severity

In this study, we identified two LMMs (*msl-1* and *msl-2*) with stable genetic traits which were obtained from indica rice cultivar JG30 treated by EMS. Although there are no obvious differences between the two mutants at seedling stage (**Figures 1A,C**), the phenotype differences appeared along with the development of the plants. At tillering stage, not only more mosaic spots appeared on leaves of *msl-2* but also the spot size was larger than that of *msl-1* (**Figure 1D**). At maximum tillering stage, the leaves of *msl-2* appeared chlorotic, the lower leaves gradually died, and the plants showed more obvious premature senescence than *msl-1* (**Figure 1B**). At mature stage, the leaves of *msl-2* were completely yellow and the whole plant dead but not for the *msl-1* mutant (**Figure 1E**). Thus, both *msl-1* and *msl-2* displayed mosaic spot lesion and premature senescence phenotypes but differed largely in severity.

Lesion mimic mutants have been divided into two types according to the pattern of spots formation: the initial type and the expanding type (Dangl et al., 1996). In this study, the location of mosaic spots of both *msl-1* and *msl-2* are uncertain, and along with the development of the leaves, the spots enlarged and even covered the whole leaf, which ultimately led to death of a whole leaf. Therefore, the *msl-1* and *msl-2* belong to the expanding mutants. It had been reported that lesion mimic spots could also be affected by a series of external environmental factors, such as temperature (Hoisington et al., 1982), humidity (Jambunathan et al., 2001), and light (Johal et al., 1995). The formation of mosaic spots on leaves of *msl-1* and *msl-2* was induced by light, which showed that shading could inhibit the occurrence of mosaic spots, and the spots reappeared after regaining normal light (**Figure 1F**).

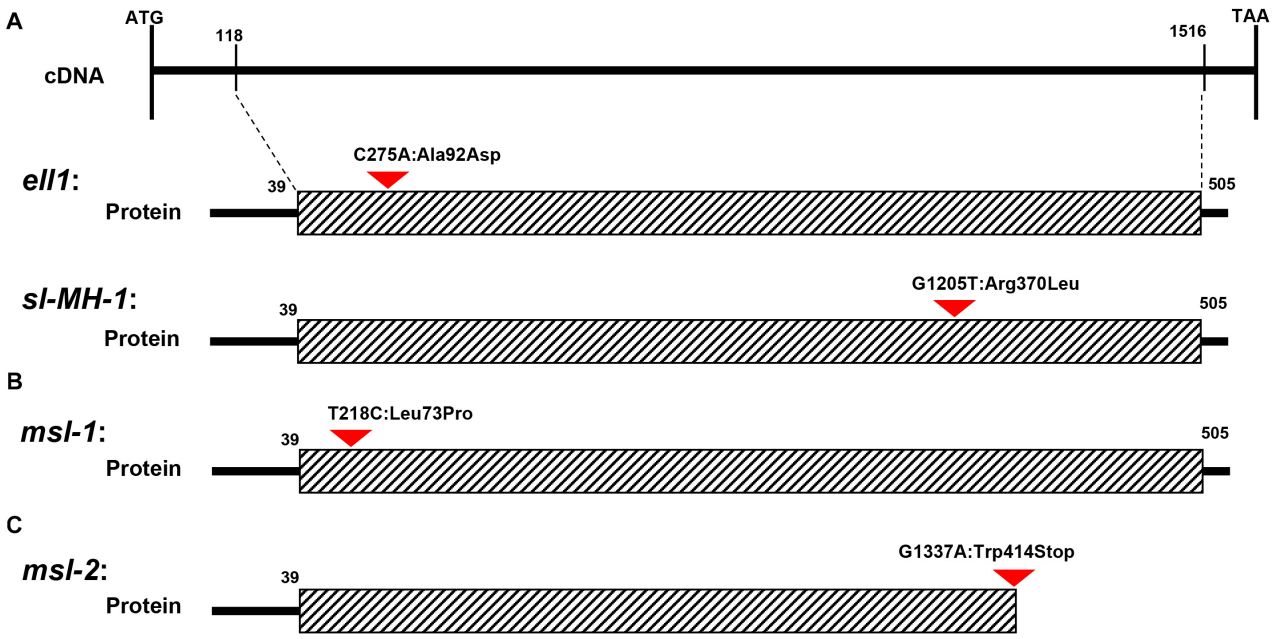

FIGURE 6 | Schematic structure of CYP71P1 protein and the mutation sites in msl-1 and msl-2. The black dotted bordered rectangle indicates CYP71P1 the highly conserved P450 superfamily domain of wild type CYP71P1. **(A)** The mutation site of *ell1* and *sl-MH-1*, *ell1* had a single base substitution at 275th nucleotide position (C275A) and *sl-MH-1* also had a single base substitution at 1,205th nucleotide position (G1205T). **(B)** The mutation site of *msl-1*, with a base change from T to C at the 218th position. **(C)** The mutation site of *msl-2*, with the G-to-A single-base alteration, leading to premature termination of the protein translation.

Different Modes of Mutation Lead to Different Mutant Phenotypes

The mutant phenotypes of *msl-1* and *msl-2* were controlled by a single recessive gene (**Table 2**). This study revealed that both the recessive genes underlying the mutant phenotypes of *msl-1* and *msl-2* are allelic variants of the *SL* gene, which encodes a CYP71P1 protein of cytochrome P450 monooxygenase family, with tryptamine 5-hydroxylase activity to catalyze the conversion of tryptamine to serotonin (Fujiwara et al., 2010). We showed that the differences of mutant phenotypes between *msl-1* and *msl-2* were due to different mutation sites and mutation types in the *SL* gene. This gene is composed of two exons and one intron, and coding a protein contained 523 amino acids. It was predicted that amino acids from positions 39–505 of this protein form a P450 domain (**Figures 6A–C**). Both mutants *msl-1* and *msl-2* had a single base mutation in this domain. The mutant *msl-2* has a G-to-A single-base alteration, leading to premature termination of the protein translation (**Figure 6C**); while *msl-1* was mutated from T to C at 218 nucleotide position (T218C) in the first exon of *SL*, which cause an amino acid change from isoleucine to proline (Leu73Pro) (**Figure 6B**). Recently, Cui et al. (2021) have cloned another allelic mutant (*ell1*) of *SL*, which has a single base mutation at 275 nucleotide position (C275A) in the first exon and changed an amino acid from alanine to aspartic acid at the 92nd position of protein sequence (**Figure 6A**). Interestingly, additional mutants at the *SL* locus have been generated from the indica rice line MH86 by tissue culture (*sl-MH-1*) and by ^{60}Co ∼ γ-ray radiation (*sl-MH-2* and *sl-MH-3*), respectively (Tian et al., 2020). These three mutants also spontaneously exhibit orange-colored lesions on leaves. A G to T mutation was found at 1,205 nucleotide of *SL* ORF, which leads to the 370 Arg mutated to Leu in *sl-MH-1*, while *sl-MH-2* and *sl-MH-3* carry C85 and A1420 deletion in the *SL* coding region, respectively, whose phenotypes have not been systematically studied (Tian et al., 2020). After comparison, we found that *ell1*, *sl-MH-1*, and *msl-1* have similar phenotypes. Based on the differences in three-dimensional structure of the proteins, we speculated that the mutation of *msl-2* which was in the key structural domain and causing pre-termination of the protein translation, resulted in the complete destruction of the protein function, while a single amino acid mutation occurred in *msl-1* or *ell1*, the protein may still retain some function. Therefore, the difference of mutation sites and mutation types (SNP-caused single amino acid change and SNP-caused early termination of translation) led to the different phenotypes in severity between *msl-1* and *msl-2*.

The Mutation of CYP71P1 Leads to Premature Senescence

Plant cytochrome P450 (CYP450) is a class of enzymes that have been classified as superfamily (Nebert et al., 1989). CYP450 is named because its reduced state can combine with CO and has the strongest absorption spectrum at 450 nm (Denisov et al., 2005). CYP450 is involved in the biosynthesis and catabolism of many substances in organisms, including various fatty acid conjugates, plant hormones, secondary metabolites and defense compounds. Because of its involvement in various physiological and biochemical reactions, CYP450 is called universal biocatalyst. It also plays an important role in plant growth and development

(Bak and Feyereisen, 2001), as well as in the response to biotic and abiotic stresses (Elzaki et al., 2019).

CYP71P1, a member of the cytochrome P450 monooxygenase family, has tryptamine 5-hydroxylase activity, and catalyzes the conversion of tryptamine to serotonin (Fujiwara et al., 2010). Serotonin is known as neurotransmitter which widely distributed in mammalian tissues, especially in cerebral cortex and synapses. In plants, serotonin is found in a range of species and plays an important role in various physiological functions (Roshchina, 2001). Serotonin synthesis involves two steps: tryptophan decarboxylase (TDC) catalyzes the conversion of tryptophan (Trp) into tryptamine, then tryptamine is further catalyzed to serotonin by tryptamine 5-hydroxylase (T5H) (Kang et al., 2007). It has been shown that serotonin is involved in slowing down leaf senescence (Kang et al., 2009), this might explain why *msl-1* and *msl-2* showed premature senescence phenotype. The mutant *msl-2* leaves aged rapidly after flowering and faded to yellow, and the leaves died at the mature stage (**Figure 1E**), indicating that the loss-of-function of CYP71P1 led to the occurrence of early senescence. Moreover, the different mutant types resulted the different expression levels of senescence-related genes, and eventually lead to different degrees of premature phenotype.

Based on our results and those findings reported previously, we proposed a working model for the role of the *SL* gene in rice leaf senescence and cell death (**Figure 7**). In rice, the conversion of tryptamine to serotonin is catalyzed by CYP71P1 encoded by *SL*. Once *SL* mutates, the catalytic process will be affected or blocked, accompanied with the accumulation of tryptamine and the low level of serotonin. It has been shown that serotonin is involved in the immune response of plants, and exogenous applied serotonin enhances resistance to *Magnaporthe grisea* (*M. grisea*) in the *sl* mutant (Fujiwara et al., 2010). In addition, the serotonin is acknowledged to be a kind of strong antioxidant compounds by scavenging ROS (Huether et al., 1997), which is in agreement with excessive ROS accumulation in the *sl* mutants (Cui et al., 2021; **Figure 3**). Excessive ROS accumulation triggers off programmed cell death (PCD)-mediated cell apoptosis, causing the lesion formation in rice (Cui et al., 2021). Moreover, ROS could also contribute to activate the pathogen-associated molecular patterns (PAMPs)-triggered immunity (PTI) responses, and thus the increased resistance to *M. oryzae* and *Xanthomonas oryzae* pv. *oryzae* (Arase et al., 2001; Tian et al., 2020). Additionally, ROS can function as signaling messengers to induce chloroplast degradation directly or by regulating the changes of senescence-associated genes (SAGs) (Gechev et al., 2006; Mao et al., 2017), and the degradation of chlorophyll further leads to decrease of chlorophyll content in the leaves of *sl* mutants, ultimately resulting in the premature leaf senescence phenotype (**Figure 7**).

In short, the novel mutants *msl-1* and *msl-2* identified in this study represent two new alleles of the *SL* gene which encodes a cytochrome P450 monooxygenase (CYP71P1), distinct from the previously reported *sl*, *sl-MH-1,* and *ell* alleles. Our results indicate that the different mutations in CYP71P1 could lead to different phenotypes in severity of both mosaic spot lesion and premature senescence. The findings might provide new insights into the regulation of chloroplast development and programmed cell death pathways during rice leaf senescence.

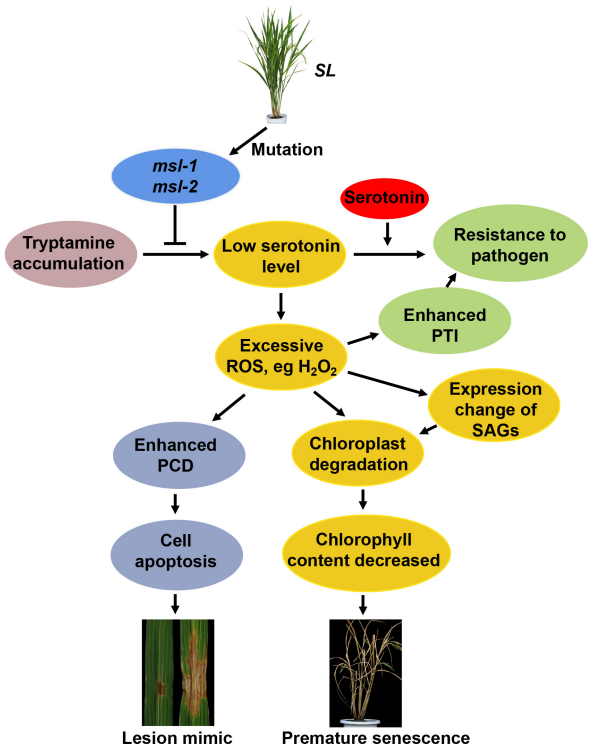

FIGURE 7 | Proposed working model for *SL*-involved rice leaf senescence and cell death. The conversion of tryptamine to serotonin is catalyzed by CYP71P1 encoded by *SL* (Sekiguchi lesion) gene. Mutations of *SL* affect or block the catalytic process, accompanied with accumulated tryptamine and the low level of serotonin. Exogenous applied serotonin enhances resistance to *Magnaporthe grisea* (*M. grisea*) in the *sl* mutant. Low level of serotonin causes excessive reactive oxygen species (ROS) accumulation in the *sl* mutants, triggering programmed cell death (PCD)-mediated cell apoptosis, resulting in lesion formation. Excessive ROS also contribute to activation of pathogen-associated molecular patterns (PAMPs)-triggered immunity (PTI) to plant pathogens like *M. oryzae* and *Xanthomonas oryzae* pv. *oryzae*. ROS can function as signaling messengers to induce chloroplast degradation directly or by regulating the changes of senescence-associated genes (SAGs), resulting in the premature leaf senescence phenotype.

DATA AVAILABILITY STATEMENT

The original contributions presented in the study are included in the article/**Supplementary Material**, further inquiries can be directed to the corresponding author/s.

AUTHOR CONTRIBUTIONS

KZ and CW conceived and designed the research. YZ, JX, FW, YT, and ZW performed the experiments. YZ, JX, and ZJ participated in data analysis. YZ and KZ wrote the manuscript. All authors contributed to the article and approved the submitted version.

FUNDING

This work was supported by grants from the National Priority Program-Breeding New Rice Varieties for Southwest China Areas (2017YFD0100202), National Science Foundation of China (U20A2035 to KZ), Beijing Municipal Natural Science Foundation (6202031 to ZJ), and the Innovation Program of Chinese Academy of Agricultural Sciences to KZ and CW.

SUPPLEMENTARY MATERIAL

The Supplementary Material for this article can be found online at: https://www.frontiersin.org/articles/10.3389/fpls.2021.641300/full#supplementary-material

Supplementary Table 1 | Primers used for real-time quantitative PCR analysis.

Supplementary Table 2 | Molecular markers for fine mapping of *msl-1* and *msl-2*.

Supplementary Table 3 | The candidate genes in the mapped 58 kb region.

REFERENCES

Arase, S., Ueno, M., Toko, M., Honda, Y., Itoh, K., and Ozoe, Y. (2001). Light-dependent accumulation of tryptamine in the rice sekiguchi lesion mutant infected with *Magnaporthe grisea*. *J. Phytopathol.* 149, 409–413. doi: 10.1046/j.1439-0434.2001.00646.x

Badigannavar, A. M., Kale, D. M., Eapen, S., and Murty, G. S. (2002). Inheritance of disease lesion mimic leaf trait in groundnut. *J. Hered.* 93, 50–52. doi: 10.1093/jhered/93.1.50

Bak, S., and Feyereisen, R. (2001). The involvement of two P450 enzymes, CYP83B1 and CYP83A1, in auxin homeostasis and glucosinolate biosynthesis. *Plant Physiol.* 127, 108–118. doi: 10.1104/pp.127.1.108

Breeze, E., Harrison, E., McHattie, S., Hughes, L., Hickman, R., Hill, C., et al. (2011). High-resolution temporal profiling of transcripts during *Arabidopsis* leaf senescence reveals a distinct chronology of processes and regulation. *Plant Cell* 23, 873–894. doi: 10.1105/tpc.111.083345

Buchanan-Wollaston, V. (1997). The molecular biology of leaf senescence. *J. Exp. Bot.* 2, 181–199.

Cui, Y. J., Peng, Y. L., Zhang, Q., Xia, S. S., Ruan, B. P., Xu, Q. K., et al. (2021). Disruption of EARLY LESION LEAF 1, encoding a cytochrome P450 monooxygenase, induces ROS accumulation and cell death in rice. *Plant J.* 105, 942–956. doi: 10.1111/tpj.15079

Dangl, J. L., Dietrich, R. A., and Richberg, M. H. (1996). Death don't have no mercy: cell death programs in plant-microbe interactions. *Plant Cell* 8, 1793–1807. doi: 10.1105/tpc.8.10.1793

Denisov, I. G., Makris, T. M., Sligar, S. G., and Schlichting, I. (2005). Structure and chemistry of cytochrome P450. *Chem. Rev.* 105, 2253–2277. doi: 10.1021/cr0307143

Dietrich, R. A., Delaney, T. P., Uknes, S. J., Ward, E. R., Ryals, J. A., and Dangl, J. L. (1994). *Arabidopsis* mutants simulating disease resistance response. *Cell* 77, 565–577. doi: 10.1016/0092-8674(94)90218-6

Elzaki, M. E. A., Xue, R. R., Hu, L., Wang, J. D., Zeng, R. S., and Song, Y. Y. (2019). Bioactivation of aflatoxin B1 by a cytochrome P450, CYP6AE19 induced by plant signaling methyl jasmonate in *Helicoverpa armigra* (Hübner). *Pestic. Biochem. Physiol.* 157, 211–218. doi: 10.1016/j.pestbp.2019.03.020

Fujiwara, T., Maisonneuve, S., Isshiki, M., Mizutani, M., Chen, L. T., Wong, H. L., et al. (2010). Sekiguchi lesion gene encodes a cytochrome P450 monooxygenase that catalyzes conversion of tryptamine to serotonin in rice. *J. Biol. Chem.* 285, 11308–11313. doi: 10.1074/jbc.M109.091371

Gan, S., and Amasino, R. M. (1997). Making sense of senescence: molecular genetic regulation and manipulation of leaf senescence. *Plant Physiol.* 113, 313–319. doi: 10.1104/pp.113.2.313

Gao, Z. Q., Liu, Q., Zhang, Y. X., Fang, H., Zhang, Y., Sinumporn, S., et al. (2019). A proteomic approach identifies novel proteins and metabolites for lesion mimic formation and disease resistance enhancement in rice. *Plant Sci.* 287:110182. doi: 10.1016/j.plantsci.2019.110182

Gechev, T. S., Breusegem, V. F., Stone, J. M., Denev, I., and Laloi, C. (2006). Reactive oxygen species as signals that modulate plant stress responses and programmed cell death. *Bioessays* 28, 1091–1101. doi: 10.1002/bies.20493

Gregersen, P. L., Culetic, A., Boschian, L., and Krupinska, K. (2013). Plant senescence and crop productivity. *Plant Mol. Biol.* 82, 603–622. doi: 10.1007/s11103-013-0013-8

Hoisington, D. A., Neuffer, M. G., and Walbot, V. (1982). Disease lesion mimics in maize. I. effect of genetic background, temperature, developmental age, and wounding on necrotic spot formation with Les1. *Dev. Biol.* 93, 381–388. doi: 10.1016/0012-1606(82)90125-7

Hu, G., Richter, T. E., Hulbert, S. H., and Pryor, T. (1996). Disease lesion mimicry caused by mutations in the rust resistance gene rp1. *Plant Cell* 8, 1367–1376. doi: 10.1105/tpc.8.8.1367

Huang, Q., Yang, Y., Shi, Y. F., Chen, J., and Wu, J. L. (2010). Spotted-Leaf mutants of rice (*Oryza sativa*). *Rice Sci.* 4, 247–256. doi: 10.1016/S1672-6308(09)60024-X

Huether, G., Fettkötter, I., Keilhoff, G., and Wolf, G. (1997). Serotonin acts as a radical scavenger and is oxidized to a dimer during the respiratory burst of activated microglia. *J. Neurochem.* 69, 2096–2101. doi: 10.1046/j.1471-4159.1997.69052096.x

Jambunathan, N., Siani, J. M., and McNellis, T. W. (2001). A humidity-sensitive *Arabidopsis* copine mutant exhibits precocious cell death and increased disease resistance. *Plant Cell* 13, 2225–2240. doi: 10.1105/tpc.010226

Jiao, B. B., Wang, J. J., Zhu, X. D., Zeng, L. J., Li, Q., and He, Z. H. (2012). A novel protein RLS1 with NB-ARM domains is involved in chloroplast degradation during leaf senescence in rice. *Mol. Plant* 5, 205–217. doi: 10.1093/mp/ssr081

Johal, G. S., Hulbert, S., and Briggs, S. P. (1995). Disease lesion mimic mutations of maize: a model for cell death in plants. *Bioessays* 17, 685–692. doi: 10.1002/bies.950170805

Kang, K., Kim, Y. S., Park, S., and Back, K. (2009). Senescence-induced serotonin biosynthesis and its role in delaying senescence in rice leaves. *Plant Physiol.* 150, 1380–1393. doi: 10.1104/pp.109.138552

Kang, S., Kang, K., Lee, K., and Back, K. (2007). Characterization of tryptamine 5-hydroxylase and serotonin synthesis in rice plants. *Plant Cell Rep.* 26, 2009–2015. doi: 10.1007/s00299-007-0405-9

Lee, D., Lee, G., Kim, B., Jang, S., Lee, Y., Yu, Y., et al. (2018). Identification of a spotted leaf sheath gene involved in early senescence and defense response in rice. *Front. Plant Sci.* 9:1274. doi: 10.3389/fpls.2018.01274

Lee, R. H., Hsu, J. H., Huang, H. J., Lo, S. F., and Chen, S. C. (2009). Alkaline alpha-galactosidase degrades thylakoid membranes in the chloroplast during leaf senescence in rice. *New Phytol.* 184, 596–606. doi: 10.1111/j.1469-8137.2009.02999.x

Lee, R. H., Wang, C. H., Huang, L. T., and Chen, S. C. (2001). Leaf senescence in rice plants: cloning and characterization of senescence up-regulated genes. *J. Exp. Bot.* 52, 1117–1121. doi: 10.1093/jexbot/52.358.1117

Lichtenthaler, H. K. (1987). Chlorophylls and carotenoids: pigments of photosynthetic biomembranes. *Methods Enzymol.* 148, 350–382. doi: 10.1016/0076-6879(87)48036-1

Lim, P. O., Kim, H. J., and Nam, H. G. (2007). Leaf senescence. *Annu. Rev. Plant Biol.* 58, 115–136. doi: 10.1146/annurev.arplant.57.032905.105316

Liu, D. H. (1983). Plant leaf senescence. *Plant Physiol. Commun.* 2, 12–19. (in Chinese)

Livak, K. J., and Schmittgen, T. D. (2001). Analysis of relative gene expression data using real-time quantitative PCR and the 2(-Delta Delta C(T)) Method. *Methods* 25, 402–408. doi: 10.1006/meth.2001

Lohman, K. N., Gan, S. S., John, M. C., and Amasino, R. M. (1994). Molecular analysis of natural senescence in *Arabidopsis*. *Physiol. Plant* 92, 322–328. doi: 10.1111/j.1399-3054.1994.tb05343.x

Lorrain, S., Lin, B., Auriac, M. C., Kroj, T., Saindrenan, P., Nicole, M., et al. (2004). Vascular associated death1, a novel GRAM domain-containing protein, is a regulator of cell death and defense responses in vascular tissues. *Plant Cell* 16, 2217–2232. doi: 10.1105/tpc.104.022038

Mao, C. J., Lu, S. C., Lv, B., Zhang, B., Shen, J. B., He, J. M., et al. (2017). A Rice NAC transcription factor promotes leaf senescence via ABA biosynthesis. *Plant Physiol.* 174, 1747–1763. doi: 10.1104/pp.17.00542

Miller, G., Suzuki, N., Ciftci-Yilmaz, S., and Mittler, R. (2010). Reactive oxygen species homeostasis and signalling during drought and salinity stresses. *Plant Cell Environ.* 33, 453–467. doi: 10.1111/j.1365-3040.2009.02041.x

Nebert, D. W., Nelson, D. R., Adesnik, M., Coon, M. J., Estabrook, R. W., Gonzalez, F. J., et al. (1989). The P450 superfamily: updated listing of all genes and recommended nomenclature for the chromosomal loci. *DNA* 8, 1–13. doi: 10.1089/dna.1.1989.8.1

Noodén, L. D., Guiamét, J. J., and John, I. (2010). Senescence mechanisms. *Physiol. Plant* 101, 746–753. doi: 10.1111/j.1399-3054.1997.tb01059.x

Qiao, Y. L., Jiang, W. Z., Lee, J. H., Park, B. S., Choi, M. S., Piao, R. H., et al. (2010). SPL28 encodes a clathrin-associated adaptor protein complex 1, medium subunit micro 1 (AP1M1) and is responsible for spotted leaf and early senescence in rice (*Oryza sativa*). *New Phytol.* 185, 258–274. doi: 10.1111/j.1469-8137.2009.03047.x

Roshchina, V. V. (2001). *Neurotransmitters in Plant Life*. Enfield: Science Publishers.

Ruan, B. P., Hua, Z. H., Zhao, J., Zhang, B., Ren, D. Y., Liu, C. L., et al. (2019). OsACL-A2 negatively regulates cell death and disease resistance in rice. *Plant Biotechnol. J.* 17, 1344–1356. doi: 10.1111/pbi.13058

Takahashi, A., Kawasaki, T., Henmi, K., ShiI, K., Kodama, O., Satoh, H., et al. (1999). Lesion mimic mutants of rice with alterations in early signaling events of defense. *Plant J.* 17, 535–545. doi: 10.1046/j.1365-313x.1999.00405.x

Takahashi, A., Kawasaki, T., Wong, H. L., Suharsono, U., Hirano, H., and Shimamoto, K. (2003). Hyperphosphorylation of a mitochondrial protein, prohibitin, is induced by calyculin A in a rice lesion-mimic mutant cdr1. *Plant Physiol.* 4, 1861–1869. doi: 10.1104/pp.103.021733

Tang, J. Y., Zhu, X. D., Wang, Y. Q., Liu, L. C., Xu, B., Li, F., et al. (2011). Semi-dominant mutations in the CC-NB-LRR-type R gene, NLS1, lead to constitutive activation of defense responses in rice. *Plant J.* 66, 996–1007. doi: 10.1111/j.1365-313X.2011.04557.x

Thompson, B. G., and Lake, B. H. (1987). The effect of radiation on the long term productivity of a plant based CELSS. *Adv. Space Res.* 7, 133–140. doi: 10.1016/0273-1177(87)90044-5

Thompson, J. E., Froese, C. D., Madey, E., Smith, M. D., and Hong, Y. (1998). Lipid metabolism during plant senescence. *Prog. Lipid Res.* 37, 119–141. doi: 10.1016/s0163-7827(98)00006-x

Thordal-Christensen, H., Zhang, Z. G., Wei, Y. D., and Collinge, D. B. (1997). Subcellular localization of H_2O_2 in plants. H_2O_2 accumulation in papillae and hypersensitive response during the barley-powdery mildew interaction. *Plant J.* 11, 1187–1194. doi: 10.1046/j.1365-313X.1997.11061187.x

Tian, D. G., Yang, F., Niu, Y. Q., Lin, Y., Chen, Z. J., Li, G., et al. (2020). Loss function of SL (sekiguchi lesion) in the rice cultivar Minghui 86 leads to enhanced resistance to (hemi) biotrophic pathogens. *BMC Plant Biol.* 20:507. doi: 10.1186/s12870-020-02724-6

Walbot, V. (1991). Maize mutants for the 21st century. *Plant Cell* 3, 851–856.

Wang, S., Lei, C. L., Wang, J. L., Ma, J., Tang, S., Wang, C. L., et al. (2017). SPL33, encoding an eEF1A-like protein, negatively regulates cell death and defense responses in rice. *J. Exp. Bot.* 68, 899–913. doi: 10.1093/jxb/erx001

Wolter, M., Hollricher, K., Salamini, F., and Schulze-Lefert, P. (1993). The mlo resistance alleles to powdery mildew infection in barley trigger a developmentally controlled defence mimic phenotype. *Mol. Gen. Genet.* 239, 122–128. doi: 10.1007/BF00281610

Xu, X., Chen, Z., Shi, Y. F., Wang, H. M., He, Y., Shi, L., et al. (2018). Functional inactivation of OsGCNT induces enhanced disease resistance to *Xanthomonas oryzae* pv. oryzae in rice. *BMC Plant Biol.* 18:264. doi: 10.1186/s12870-018-1489-9

Yamanouchi, U., Yano, M., Lin, H. X., Ashikari, M., and Yamada, K. (2002). A rice spotted leaf gene, Spl7, encodes a heat stress transcription factor protein. *Proc. Natl. Acad. Sci.U.S.A.* 99, 7530–7535. doi: 10.1073/pnas.112209199

Yao, Q., Zhou, R., Fu, T., Wu, W., Zhu, Z., Li, A., et al. (2009). Characterization and mapping of complementary lesion-mimic genes lm1 and lm2 in common wheat. *Theor. Appl. Genet.* 119, 1005–1012. doi: 10.1007/s00122-009-1104-4

Yin, Z. C., Chen, J., Zeng, L. R., Goh, M., Leung, H., Khush, G. S., et al. (2000). Characterizing rice lesion mimic mutants and identifying a mutant with broad-spectrum resistance to rice blast and bacterial blight. *Mol. Plant Microbe Interact.* 13, 869–876. doi: 10.1094/MPMI.2000.13.8.869

Zeng, L. R., Qu, S. H., Bordeos, A., Yang, C. W., Baraoidan, M., Yan, H. Y., et al. (2004). Spotted leaf11, a negative regulator of plant cell death and defense, encodes a U-box/armadillo repeat protein endowed with E3 ubiquitin ligase activity. *Plant Cell* 16, 2795–2808. doi: 10.1105/tpc.104.025171

Zhang, Y., Liu, Q. E., Zhang, Y. X., Chen, Y. Y., Yu, N., Cao, Y. R., et al. (2019). LMM24 encodes receptor-like cytoplasmic kinase 109, which regulates cell death and defense responses in rice. *Int. J. Mol. Sci.* 13:3243. doi: 10.3390/ijms20133243

Conflict of Interest: The authors declare that the research was conducted in the absence of any commercial or financial relationships that could be construed as a potential conflict of interest.

frontiers in Plant Science

MINI REVIEW
published: 12 April 2021
doi: 10.3389/fpls.2021.669170

The Role of Light and Circadian Clock in Regulation of Leaf Senescence

*Juhyeon Lee†, Myeong Hoon Kang†, Jung Yeon Kim† and Pyung Ok Lim**

Department of New Biology, DGIST, Daegu, South Korea

Leaf senescence is an integrated response of the cells to develop age information and various environmental signals. Thus, some of the genes involved in the response to environmental changes are expected to regulate leaf senescence. Light acts not only as the primary source of energy for photosynthesis but also as an essential environmental cue that directly control plant growth and development including leaf senescence. The molecular mechanisms linking light signaling to leaf senescence have recently emerged, exploring the role of Phytochrome-Interacting Factors (PIFs) as a central player leading to diverse senescence responses, senescence-promoting gene regulatory networks (GRNs) involving PIFs, and structural features of transcription modules in GRNs. The circadian clock is an endogenous time-keeping system for the adaptation of organisms to changing environmental signals and coordinates developmental events throughout the life of the plant. Circadian rhythms can be reset by environmental signals, such as light-dark or temperature cycles, to match the environmental cycle. Research advances have led to the discovery of the role of core clock components as senescence regulators and their underlying signaling pathways, as well as the age-dependent shortening of the circadian clock period. These discoveries highlight the close relationship between the circadian system and leaf senescence. Key issues remain to be elucidated, including the effect of light on leaf senescence in relation to the circadian clock, and the identification of key molecules linking aging, light, and the circadian clock, and integration mechanisms of various senescence-affecting signals at the multi-regulation levels in dynamics point of view.

Keywords: leaf senescence, light, PIFs, circadian clock, plant hormones

OPEN ACCESS

Edited by:
Yongfeng Guo,
Tobacco Research Institute (CAAS), China

Reviewed by:
Gang Li,
Shandong Agricultural University, China
Lei Wang,
Chinese Academy of Sciences, China

****Correspondence:***
Pyung Ok Lim
polim@dgist.ac.kr

†These authors have contributed equally to this work

Specialty section:
This article was submitted to Plant Physiology, a section of the journal Frontiers in Plant Science

Received: *18 February 2021*
Accepted: *23 March 2021*
Published: *12 April 2021*

Citation:
Lee J, Kang MH, Kim JY and Lim PO (2021) The Role of Light and Circadian Clock in Regulation of Leaf Senescence. Front. Plant Sci. 12:669170. doi: 10.3389/fpls.2021.669170

INTRODUCTION

Leaves are crucial to plant growth and survival. During early development, emerged leaves become photosynthetic organs that convert light energy into nutrients that are necessary for plant growth. Leaves in which photosynthesis is no longer productive begin to senesce. During leaf senescence, cellular constituents generated during the growth phase of leaves are converted into mobilizable nutrients and relocated to other developing organs. Thus, leaf senescence needs to be precisely tuned to ensure plant fitness (Woo et al., 2019).

Leaf senescence is an integral part of development despite the associated degenerative physiological changes. Under favorable conditions, this process occurs at age-dependent manner by an innate developmental program. However, unfavorable conditions, such as darkness or abiotic and biotic stresses, can induce premature leaf senescence, which shortens the lifespan of individual leaves. Sacrificing the inefficient and senescing organs would be beneficial for plants by making resources available to other organs. Besides its role in nutrient recycling, leaf senescence evolved as an adaptive strategy to respond appropriately to environmental changes (Schippers et al., 2015).

Light is a critical environmental factor affecting plant development. The importance of light for leaf senescence is becoming increasingly apparent. The regulatory networks linking light information and leaf senescence have been elucidated (Sakuraba et al., 2014; Song et al., 2014).

Plants are constantly exposed to environmental changes. To regulate development efficiently, plants have developed a circadian clock system. The circadian system is an endogenous time-keeping mechanism that measures daily and seasonal changes in the environment and allows plants to adjust physiological and developmental processes accordingly (Harmer, 2009). The circadian rhythm is entrained to cyclic environmental signals and can be reset by a variety of stimuli such as light signal. Thus, the circadian clock integrates environmental signals and coordinates developmental events throughout the life of the plant. Emerging evidence suggests that circadian clock core components are involved in leaf senescence.

Here, we review recent findings on leaf senescence, particularly the role of light and circadian clock, and how the senescence-regulatory networks are interacting with these signals. We also discuss the temporal and light-mediated regulation of plant physiology in relation to leaf senescence, which will contribute to understand the fitness and adaptive advantage of higher plants.

LIGHT AS A MODULATOR OF LEAF SENESCENCE

Light perception by photoreceptors and light signaling components are crucial for modulating leaf senescence. Light-dependent retardation of leaf senescence is a low-fluence response that shows red (R)/far-red (FR) light reversibility. The R:FR ratio also affects leaf senescence: a low R:FR ratio induces leaf senescence, whereas a high R:FR ratio can delay it. These effects are of considerable ecological significance. Light passing through the upper leaves under field conditions contains reduced R relative to FR, and this FR-enriched condition might serve as a signal to trigger senescence of the lower leaves, which permits the allocation of resources to the upper shoot.

These responses are regulated by type II phytochromes, of which phytochrome B (phyB) is the main photoreceptor mediating R-induced senescence suppression in *Arabidopsis* (Reed et al., 1994). The mutation of *phyB* induced hyposensitivity to the continuous or pulsed R in retarding leaf senescence (Sakuraba et al., 2014). Continuous FR or low light also causes a substantial delay in leaf senescence compared with the effect of darkness, and these responses are modulated by phyA (Brouwer et al., 2014).

The light signals perceived by photoreceptors are transduced to the regulatory network that drives multiple facets of plant development including leaf senescence. Phytochrome-interacting factors (PIFs) interact with light-activated phytochromes, which inhibits their activities through several mechanisms; (1) phyB-PIF interaction leads to repress the DNA-binding ability of PIFs (Park et al., 2018), (2) it also results in phosphorylation and degradation of PIFs (Pham et al., 2018), and (3) PIFs are transcriptionally controlled, allowing PIF accumulation during the day time, even when phyB is active (Sun et al., 2019; Yan et al., 2020). Multiple mechanisms might be evolved for optimal light regulation of PIFs across a wide range of light conditions.

Among PIFs, PIF4, and PIF5 (PIF4/PIF5) are critical transcription factors (TFs) that mediate the induction of leaf senescence not only under dark conditions, but also under natural senescence conditions. In *Arabidopsis*, PIF4/PIF5 are upregulated at the early stage of leaf senescence as well as in response to darkness (Song et al., 2014). PIF4/PIF5 mutants display delayed leaf senescence under prolonged darkness and in response to long-day conditions. The increase of PIF4/PIF5 under dark conditions is inhibited by intermittent pulses of R, but not when pulses of R are followed by FR, indicating that active phytochromes prevent premature senescence in the presence of light by repressing PIF4/PIF5 expression (Sakuraba et al., 2014).

In recent years, much of the research on hormone signaling has focused on understanding the interplay between hormones and environmental signals including light and temperature, highlighting the importance of signaling (Jaillais and Chory, 2010). PIFs play key roles in integrating light and hormone signals through their function as TFs targeting genes involved in hormone biosynthesis or signaling and/or by interacting with components of hormone pathways.

Comparative transcriptome analysis of dark-induced senescence in *pif4* or quadruple *pif (pifQ)* mutants identified the subset of genes responsible for the PIF-mediated leaf senescence response. These include genes involved in chloroplast maintenance/photosynthesis, degradation of chlorophyll, responses to stresses/reactive oxygen species (ROS), and those involved in ethylene and abscisic acid (ABA) senescence-promoting signals, whose expressions are altered in *pif* mutants. Chromatin immunoprecipitation assays identified ABA-INSENSITIVE5 (ABI5), ENHANCED EM LEVEL (EEL), and ETHYLENE-INSENSITIVE3 (EIN3) as the direct target genes of PIF4/PIF5 (Sakuraba et al., 2014).

ABI5 and *EEL* encode basic leucine zipper (bZIP) TFs involved in ABA signaling, and the mutations of these genes cause delayed leaf senescence, suggesting that they are positive regulators of dark-induced leaf senescence (Sakuraba et al., 2014). ABI5 is also known to suppress ABA-response protein 5, a negative regulator of dark-induced leaf senescence (Su et al., 2016). EIN3 is a key TF involved in the EIN2-mediated ethylene signaling cascade that regulates age- and dark-induced leaf senescence by inducing two NAM, AFAT, and CUC (NAC) TFs, ORESARA1 (ORE1) and NAC-LIKE, ACTIVATED BY AP3/PI (AtNAP), which are the master regulators of leaf

senescence (Kim et al., 2014). EIN3 also causes the accumulation of *ORE1* transcripts by directly repressing *microRNA (miR)-164* transcription (Kim et al., 2009). In addition to alterations of signal transduction, *pif4* mutants also show attenuated induction of ethylene biosynthesis by darkness (Song et al., 2014). Taken together, these results suggest that PIFs play an important role in transducing light information to ABA and ethylene pathways, thereby activating leaf senescence responses (**Figure 1A**).

bZIP- and EIN3-activated downstream genes are also markedly downregulated in *pifQ* mutants. Intriguingly, *ORE1* is a common direct target of PIFs, EIN3, EEL, and ABI5. Upregulation of *ORE1* activates genes involved in nucleic acid degradation, such as BIFUNCTIONAL NUCLEASE 1, as well as genes for chlorophyll catabolism, such as STAYGREEN 1 (SGR1/NYE) and NON-YELLOW COLORING 1 (NYC1; Song et al., 2014). *SGR* and *NYC1* are also direct targets of PIFs, EIN3, and ABI5 (Sakuraba et al., 2014; Song et al., 2014). ORE1 sequesters the chloroplast maintenance master regulators GOLDEN2-LIKE (GLK) 1 and GLK2 through protein-protein interactions, which decreases the transcriptional activity of GLKs during leaf aging (Rauf et al., 2013). At the transcriptional level, PIF4 acts as a repressor of *GLKs* (Song et al., 2014).

These findings suggest that the intricate gene regulatory networks (GRNs) governed by PIF4, PIF5, EIN3, EEL, ABI5, and ORE1 are linked, thereby forming multiple coherent feed-forward loops. These results also explain how the GRN modules involving PIFs coordinate various endogenous and environmental signals during leaf senescence.

Brassinosteroids (BRs) are senescence-accelerating hormones. ATBS1-INTERACTING FACTOR 2 (AIF2) was recently identified as a negative regulator of dark- and BR-induced leaf senescence in *Arabidopsis* (Kim et al., 2020). Molecular and genetic evidence led to the construction of a model describing the role of the interaction of light and BR signaling in the regulation of senescence (**Figure 1B**). BRASSINAZOLE-RESISTANT 1 family proteins (BZRs) are TFs that govern BR-regulated gene expression. Under conditions of darkness, PIF4 promotes BR synthesis and BZR1 activation, leading to a decrease of AIF2. As dark incubation proceeds, accumulated PIF4 together with BZR1 suppress senescence-retarding genes, such as C-REPEAT BINDING FACTORs (CBFs), and induces the expression of senescence-promoting genes, such as those involved in ethylene/jasmonic acid (JA) biosynthesis, and activates the corresponding signaling pathways. When leaves are exposed to light, accumulated AIF2 interacts with INDUCER OF CBF EXPRESSION 1 (ICE1). The AIF2-ICE1 complex and the subsequent upregulation of *CBFs* negatively regulate darkness-induced leaf senescence. This interaction also decreases *PIF4* transcription through the AIF2-dependent inhibition of ICE1 binding to the *PIF4* promoter, leading to the suppression of leaf senescence.

Recent evidence indicates that phytochrome-associated senescence regulation is interlinked with salicylic acid (SA) pathways (Tian et al., 2020). The *Arabidopsis* FAR-RED ELONGATED HYPOCOTYL 3 (FHY3) and its closest homolog FAR-RED IMPAIRED RESPONSE 1 (FAR1) play key roles in the phyA-mediated FR light signaling pathway (Lin et al., 2007). Disruption of *FHY3* leads to early leaf senescence in an age-dependent manner, as well as under high R:FR conditions, indicating that *FHY3* is a key negative regulator of age- and light-mediated leaf senescence. In addition, FHY3 represses the transcription of *WRKY28*, which promotes SA biosynthesis by activating SA INDUCTION DEFICIENT 2 (SID2; van Verk et al., 2011). The early senescence phenotype of the *fhy3* mutant is rescued by disruption of *WRKY28*, confirming the role of the *FHY3-WRKY28-SID2* transcriptional module in the regulation of leaf senescence. Given that FHY3 and FAR1 are important TFs involved in phyA-mediated FR light signaling (Lin et al., 2007), understanding the relationships among FHY3, phyA, and phyB may shed light on the regulatory mechanisms by which a high R:FR ratio inhibits leaf senescence (**Figure 1C**).

Further systematic studies are necessary to elucidate the detailed molecular mechanisms underlying the connections between light signaling pathways and other internal or external senescence-regulating programs. Identification of upstream regulators, downstream targets, and interaction molecules of light signal-associated TFs, such as PIFs or FHY3, at senescence conditions will help to dissect such intricate regulatory pathways of leaf senescence.

LEAF SENESCENCE AND CIRCADIAN CLOCK

The timing of developmental transitions is critical for plant fitness. Plants may possess mechanisms to measure the passage of time, although a clear understanding of these processes in plants is lacking. The circadian clock is a ubiquitous endogenous time-keeping system that generates 24 h rhythms adapted to the light–dark cycle, and it predicts daily and seasonal changes in the environment (McClung, 2006). This endogenous clock regulates many aspects of development and physiology throughout the life of a plant, and it may be critical for the temporal coordination of development.

In *Arabidopsis*, the core oscillator of the circadian clock consists of interlocking negative feedback loops. CIRCADIAN CLOCK-ASSOCIATED 1 (CCA1), LATE ELONGATED HYPOCOTYL (LHY), PSEUDO-RESPONSE REGULATOR 7 (PRR7), and PRR9 form a morning loop, whereas TIMING OF CAB EXPRESSION 1 (TOC1), EARLY FLOWERING 3 (ELF3), ELF4, and LUX ARRYTHMO (LUX) form an evening loop. ELF3, ELF4, and LUX are functionally associated and are components of the evening complex (EC). The morning and evening loops are interconnected and generate circadian outputs through transcriptional and post-transcriptional mechanisms, thereby enabling plants to express numerous genes at the proper time and phase (McClung, 2006). The relationship between senescence and the circadian clock, and the potential molecular mechanisms underlying their interaction have been explored recently (Wang et al., 2018; **Figure 2**).

The first hint comes from results showing that the circadian periods of clock-regulated genes as well as the periods of the core clock genes are shorter in older leaves than in young leaves of *Arabidopsis*. Such age-dependent period shortening is not observed in the disruption of TOC1, suggesting that TOC1 may link age to changes in the circadian clock period (Kim et al., 2016).

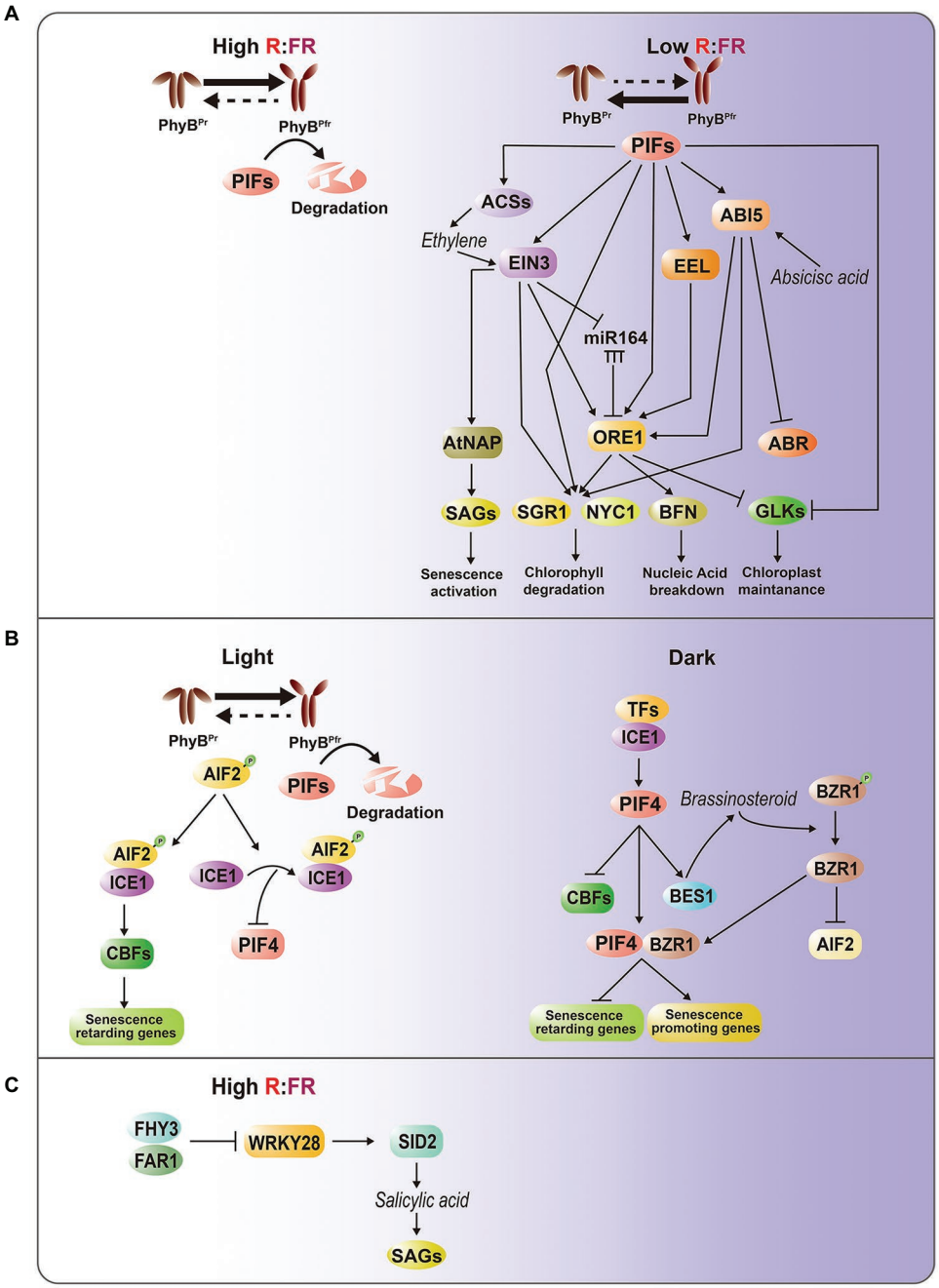

FIGURE 1 | Intricate regulatory interactions between light and hormone signaling pathways in leaf senescence. **(A)** PhyB-PIFs-mediated senescence regulatory pathways. Under light or high R/FR condition, PIFs are degraded at a phyB-dependent manner, thereby suppressing PIF-dependent senescence activation. Under darkness, shade or low R/FR condition, phyB-mediated PIF degradation is inhibited, leading to activation of senescence-promoting ABA and ethylene hormone pathways. Direct targets of PIFs include EIN3 for ethylene signaling, and ABI5 and EEL for ABA signaling. Moreover, PIFs, EIN3, ABI5, and EEL activate *ORE1*, one of master regulators in leaf senescence, through binding to its promoter. Accumulating ORE1, PIFs, ABI5, and EIN3 subsequently activate *SGR1* and *NYC1* for chlorophyll degradation, whereas ORE1 alone induces *BFN* for nucleic acid degradation and other SAGs. On the other hand, PIFs and ORE1 repress the chloroplast maintenance master regulator GOLDEN2-LIKE (GLK) by suppressing its promoter activity and sequestrating protein through protein-protein interaction, respectively. EIN3 also regulates *ORE1* through *miRNA164*, and directly activates *AtNAP*, another senescence master regulator. ABI5 suppresses *ABR*. **(B)** AIF2-ICE1-mediated retardation of dark-induced senescence. PIFs are also involved in dark- and BR-induced leaf senescence at phyB-independent manner. In light, AIF2 interacts with ICE1 to directly downregulate *PIF4* and upregulate *CBFs*, which promote self-maintenance or senescence-repressing genes. In darkness, PIF4 promotes BR synthesis and *BZR1* activation, leading to decrease of AIF2. Activated BZR and PIF4 complex suppresses senescence-retarding genes and activates senescence-promoting genes. **(C)** FHY3-WRKY28 transcription module involved in interlinking between light and salicylic acid pathways. High R/FR condition activates *FHY3* and *FAR1*, subsequently suppressing *WRKY28*, which promotes SA biosynthesis.

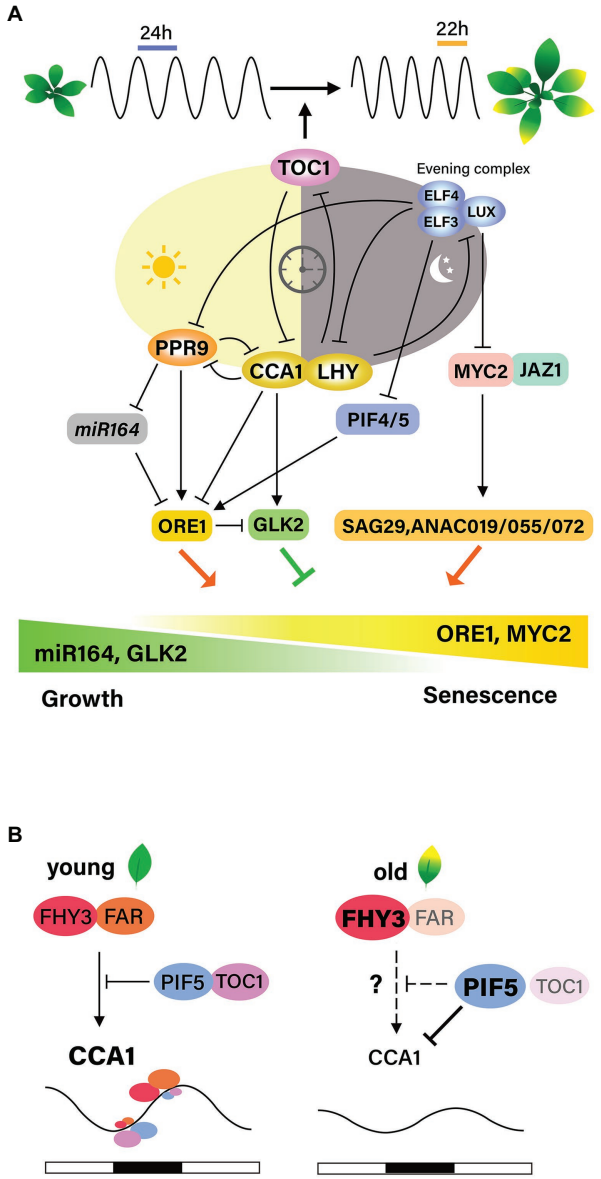

FIGURE 2 | Interactions between the circadian clock and leaf senescence. **(A)** Age information integrates with the circadian clock through TOC1, one of the core oscillators, resulting in the shortening of the circadian period with leaf senescence. Age-declined CCA1 induced the expression of *ORE1* and suppression of *GLK2* along leaf aging. PRR9 in the morning loop directly activates ORE1, and indirectly suppress miRNA164, forming the feed-forward pathway. The evening complex (EC) negatively regulates jasmonate-induced leaf senescence by repressing the expression of *MYC2*. Inactivation of EC complex causes the activation of MYC2, which induces *SAG29*, *ANAC019*, *ANAC055*, and *ANAC072*, promoting leaf senescence. ELF3, a component of EC, negatively affects *ORE1* expression by repressing PIF4/5. **(B)** FHY3/FAR1 is required for the light-induced expression of CCA1 and the role of FHY3/FAR1 in activating CCA1 expression is antagonistically regulated by TOC1 and PIF5. Under diurnal cycle conditions, the high levels of FHY3 and FAR1 and low levels of PIF5 and TOC1 at the end of the evening contribute to the peak expression of the morning gene *CCA1* before dawn. However, at aged leaves, FHY3 plays a role as a negative regulator of leaf senescence by suppressing WRKY28. Age-declined CCA1 expression might be due to PIF5, whose activity is increased at senescence conditions.

These findings suggest that age-associated information is integrated into the regulation of the circadian period, and that TOC1 is necessary for this integrative process.

The involvement of circadian components in the regulation of leaf senescence has been analyzed in detail. Song et al. (2018) proposed that CCA1 regulates leaf senescence negatively based on findings that age-declined CCA1 upregulates *ORE1* and downregulates *GLK2* by binding to their promoters, thereby promoting the onset of leaf senescence. CCA1 functions as a master regulator of ROS homeostasis by interacting with the EC in promoters of ROS-responsive genes *in vivo*, and ROS function as an input signal that affects the transcriptional output of the clock (Lai et al., 2012). Therefore, identifying proteins that interact with CCA1 during leaf senescence, as well as downstream targets of CCA1, including ROS homeostasis-related genes, may help to elucidate the relationships between aging, ROS, the circadian clock, and leaf senescence.

Recent discovery showing that FHY3 and FAR1, phytochrome signal transducers, are necessary for the light-induced CCA1 expression is particularly illuminating. FHY3 and FAR1 activate *CCA1* expression through direct binding to its promoter, but dark-activated PIF5 suppresses the transcription of *CCA1* (Liu et al., 2020). Under diurnal condition, the role of FHY3/FAR1 in activating *CCA1* transcription is antagonistically controlled through interaction with TOC1 and PIF5, leading to daily oscillation of the *CCA1* expression. Taking previous findings on the roles of these components as regulators of leaf senescence, it is plausible that the proposed mechanism might be responsible for the effect of light on leaf senescence in relation with circadian clock. However, higher level of FHY3 at aged leaves does not explain age-declined CCA1. It is likely that during senescence. Increased activity of PIF5 might cause the suppression of CCA1 transcription (**Figure 2B**).

Extensive genetic analyses using core clock component mutants have been performed to identify senescence regulators (Kim et al., 2018). The EC components ELF3, ELF4, and LUX, as well as the morning component PRR9, affect leaf senescence. Mutation of PRR9 delays age-dependent, as well as dark-induced, leaf senescence. This may be mediated by the downregulation of leaf senescence regulators, such as *NAC* and *WRKY* TFs, with a circadian expression pattern. PRR9 directly promotes rhythmic transcription of *ORE1* by binding to the *ORE1* promoter and indirectly by suppressing the clock-controlled *miR-164*, a post-transcriptional repressor of *ORE1*, thus forming a coherent feed forward regulatory loop. Importantly, ORE1 overexpression restores age-associated senescence in *prr9* mutant plants. These results suggest that the circadian clock controls leaf senescence by modulating ORE1 amplitude by PRR9, suggesting an intimate relationship between leaf senescence and the circadian clock as shown in animals.

The molecular mechanism by which the core components of the circadian clock gate JA signaling to regulate leaf senescence was elucidated in *Arabidopsis* (Zhang et al., 2018). Mutations in EC components result in accelerated age-induced senescence, as well as more pronounced JA-induced leaf senescence. Global gene expression analyses indicate that the EC is associated with JA signaling and response pathways and also controls senescence

regulators such as *WRKY53*, *WRKY70*, *ORE1*, and *AtNAP*. These results indicate that the EC may function as a negative component of the leaf senescence regulatory network by repressing senescence regulators. LUX binds directly to the promoter of *MYC2*, a JA downstream TF, and likely gates its JA-induced expression profile. Genetic analysis further demonstrated that the accelerated JA-induced leaf senescence in EC mutants is abrogated by the *myc2 myc3 myc4* triple mutation, confirming that a core component of the circadian clock gates JA signaling *via* MYC TFs to regulate leaf senescence (Zhang et al., 2018). On the other hand, ELF3 regulates dark-induced leaf senescence by repressing PIF4/PIF5 in an EC-independent manner, as ELF4 and LUX mutants do not show the accelerated senescence phenotype observed in ELF3 mutants under dark conditions (Sakuraba et al., 2014). Thus, it is plausible that intricate interactions of core components and diverse senescence responses are involved in the regulation of leaf senescence. The interaction networks between the circadian clock and leaf senescence need to be further elucidated.

PERSPECTIVES AND FUTURE CHALLENGES

Leaf senescence is a time-dependent developmental event. However, it also involves intricate interactions with various endogenous and exogenous signals. How the senescence-regulatory networks interact with these signals and how the interaction affects life and senescence in plants are long-standing questions. PIFs, which were initially recognized as components of the phytochrome signaling pathway, are currently considered as key players at the convergent points of light signals and internal hormone responses, which together modulate leaf senescence. PIFs and downstream regulators involved in senescence-promoting hormone signaling or synthesis control ORE1, a master regulator of leaf senescence. A picture is just beginning to emerge, and a comprehensive understanding of leaf senescence may require new approaches. For example, analyses to find direct targets of PIFs and their inter-players have been performed at specific developmental stages, mostly seedling, or under specific environmental conditions, which do not reflect the complete regulatory pattern of leaf senescence. Genome-wide analysis of PIF target genes or interacting molecules at leaf senescence stages is necessary.

The mechanism underlying the effect of light on plant senescence in relation to the circadian clock has also been long-term interest. PIF4/PIF5 are expressed rhythmically during the diurnal cycle, and their expression is regulated at the transcriptional and post-translational levels (Shin et al., 2013). PIFs are connected with various hormone responses, which are additionally regulated by the circadian clock as output pathways. However, whether PIFs affect the clock function in a light-dependent manner remains unclear, and, if so, the molecular mechanism by which PIFs transduce light information to the core oscillator during leaf senescence needs to be elucidated.

Analysis of PIF- or circadian core component-mediated regulation of leaf senescence has mainly focused on transcriptional regulation, which revealed the importance of multiple feed-forward loops in the regulation of leaf senescence. To better understand leaf senescence, it is necessary to perform multilayered interaction-based analyses of senescence. These should include the dynamics of PIF-interactomes (protein-protein, protein-DNA, protein-RNA, and RNA-RNA) complexes in a developmental time-dependent manner or spatial networks that involve organellar interactions.

The link between the circadian clock and leaf senescence is clear. However, the association of leaf senescence with changes in the circadian system remains unclear, particularly the potential causal relationship between them. The complex underlying regulatory network needs to be fully elucidated.

AUTHOR CONTRIBUTIONS

JL, MK, JK, and PL reviewed literature and participated in writing the manuscript. All authors contributed to the article and approved the submitted version.

FUNDING

This research was supported by Mid-career Researcher Program (2019R1A2C1089459) and Basic Research Laboratory Program (2020R1A4A1019408) through the National Research Foundation of Korea (NRF) funded by the Ministry of Science.

ACKNOWLEDGMENTS

We apologize to those authors whose excellent relevant work could not be cited due to space limitations.

REFERENCES

Brouwer, B., Gardeström, P., and Keech, O. (2014). In response to partial plant shading, the lack of phytochrome A does not directly induce leaf senescence but alters the fine-tuning of chlorophyll biosynthesis. *J. Exp. Bot.* 65, 4037–4049. doi: 10.1093/jxb/eru060

Harmer, S. L. (2009). The circadian system in higher plants. *Annu. Rev. Plant Biol.* 60, 357–377. doi: 10.1146/annurev.arplant.043008.092054

Jaillais, Y., and Chory, J. (2010). Unraveling the paradoxes of plant hormone signaling integration. *Nat. Struct. Mol. Biol.* 17, 642–645. doi: 10.1038/nsmb0610-642

Kim, H. J., Hong, S. H., Kim, Y. W., Lee, I. H., Jun, J. H., Phee, B. K., et al. (2014). Gene regulatory cascade of senescence-associated NAC transcription factors activated by ETHYLENE-INSENSITIVE2-mediated leaf senescence signalling in *Arabidopsis*. *J. Exp. Bot.* 65, 4023–4036. doi: 10.1093/jxb/eru112

Kim, H., Kim, H. J., Vu, Q. T., Jung, S., Robertson McClung, C., Hong, S., et al. (2018). Circadian control of ORE1 by PRR9 positively regulates leaf senescence in *Arabidopsis*. *Proc. Natl. Acad. Sci. U. S. A.* 115, 8448–8453. doi: 10.1073/pnas.1722407115

Kim, H., Kim, Y., Yeom, M., Lim, J., and Nam, H. G. (2016). Age-associated circadian period changes in *Arabidopsis* leaves. *J. Exp. Bot.* 67, 2665–2673. doi: 10.1093/jxb/erw097

Kim, Y., Park, S. U., Shin, D. M., Pham, G., Jeong, Y. S., and Kim, S. H. (2020). ATBS1-INTERACTING FACTOR 2 negatively regulates dark-and brassinosteroid-induced leaf senescence through interactions with INDUCER of CBF EXPRESSION 1. *J. Exp. Bot.* 71, 1475–1490. doi: 10.1093/jxb/erz533

Kim, J. H., Woo, H. R., Kim, J., Lim, P. O., Lee, I. C., Choi, S. H., et al. (2009). Trifurcate feed-forward regulation of age-dependent cell death involving miR164 in *Arabidopsis*. *Science* 323, 1053–1057. doi: 10.1126/science.1166386

Lai, A. G., Doherty, C. J., Mueller-Roeber, B., Kay, S. A., Schippers, J. H. M., and Dijkwel, P. P. (2012). Circadian clock-associated 1 regulates ROS homeostasis and oxidative stress responses. *Proc. Natl. Acad. Sci. U. S. A.* 109, 17129–17134. doi: 10.1073/pnas.1209148109

Lin, R., Ding, L., Casola, C., Ripoll, D. R., Feschotte, C., and Wang, H. (2007). Transposase-derived transcription factors regulate light signaling in *Arabidopsis*. *Science* 318, 1302–1305. doi: 10.1126/science.1146281

Liu, Y., Ma, M., Li, G., Yuan, L., Xie, Y., Wei, H., et al. (2020). Transcription factors FHY3 and FAR1 regulate light-induced circadian clock AsSOCIATED1 gene expression in *Arabidopsis*. *Plant Cell* 32, 1464–1478. doi: 10.1105/tpc.19.00981

McClung, C. R. (2006). Plant circadian rhythms. *Plant Cell* 18, 792–803. doi: 10.1105/tpc.106.040980

Park, E., Kim, Y., and Choi, G. (2018). Phytochrome B requires PIF degradation and sequestration to induce light responses across a wide range of light conditions. *Plant Cell* 30, 1277–1292. doi: 10.1105/tpc.17.00913

Pham, V. N., Kathare, P. K., and Huq, E. (2018). Phytochromes and phytochrome interacting factors. *Plant Physiol.* 176, 1025–1038. doi: 10.1104/pp.17.01384

Rauf, M., Arif, M., Dortay, H., Matallana-Ramírez, L. P., Waters, M. T., Nam, H. G., et al. (2013). ORE1 balances leaf senescence against maintenance by antagonizing G2-like-mediated transcription. *EMBO Rep.* 14, 382–388. doi: 10.1038/embor.2013.24

Reed, J. W., Nagatani, A., Elich, T. D., Fagan, M., and Chory, J. (1994). Phytochrome A and phytochrome B have overlapping but distinct functions in *Arabidopsis* development. *Plant Physiol.* 104, 1139–1149. doi: 10.1104/pp.104.4.1139

Sakuraba, Y., Jeong, J., Kang, M. Y., Kim, J. H., Paek, N. C., and Choi, G. (2014). Phytochrome-interacting transcription factors PIF4 and PIF5 induce leaf senescence in *Arabidopsis*. *Nat. Commun.* 5:4636. doi: 10.1038/ncomms5636

Schippers, J. H. M., Schmidt, R., Wagstaff, C., and Jing, H. C. (2015). Living to die and dying to live: the survival strategy behind leaf senescence. *Plant Physiol.* 169, 914–930. doi: 10.1104/pp.15.00498

Shin, J., Anwer, M. U., and Davis, S. J. (2013). Phytochrome-interacting factors (PIFs) as bridges between environmental signals and the circadian clock: diurnal regulation of growth and development. *Mol. Plant* 6, 592–595. doi: 10.1093/mp/sst060

Song, Y., Jiang, Y., Kuai, B., and Li, L. (2018). Circadian clock-associated 1 inhibits leaf senescence in *Arabidopsis*. *Front. Plant Sci.* 9:280. doi: 10.3389/fpls.2018.00280

Song, Y., Yang, C., Gao, S., Zhang, W., Li, L., and Kuai, B. (2014). Age-triggered and dark-induced leaf senescence require the bHLH transcription factors PIF3, 4, and 5. *Mol. Plant* 7, 1776–1787. doi: 10.1093/mp/ssu109

Su, M., Huang, G., Zhang, Q., Wang, X., Li, C., Tao, Y., et al. (2016). The LEA protein, ABR, is regulated by ABI5 and involved in dark-induced leaf senescence in *Arabidopsis thaliana*. *Plant Sci.* 247, 93–103. doi: 10.1016/j.plantsci.2016.03.009

Sun, Q., Wang, S., Xu, G., Kang, X., Zhang, M., and Ni, M. (2019). SHB1 and CCA1 interaction desensitizes light responses and enhances thermomorphogenesis. *Nat. Commun.* 10, 1–13. doi: 10.1038/s41467-019-11071-6

Tian, T., Ma, L., Liu, Y., Xu, D., Chen, Q., and Li, G. (2020). *Arabidopsis* FAR-RED ELONGATED HYPOCOTYL3 integrates age and liGht signals to negatively regulate leaf senescence. *Plant Cell* 32, 1574–1588. doi: 10.1105/tpc.20.00021

van Verk, M. C., Bol, J. F., and Linthorst, H. J. M. (2011). WRKY transcription factors involved in activation of SA biosynthesis genes. *BMC Plant Biol.* 11:89. doi: 10.1186/1471-2229-11-89

Wang, Y., Zhang, Y., and Wang, L. (2018). Cross regulatory network between circadian clock and leaf senescence is emerging in higher plants. *Front. Plant Sci.* 9:700. doi: 10.3389/fpls.2018.00700

Woo, H. R., Kim, H. J., Lim, P. O., and Nam, H. G. (2019). Leaf senescence: systems and dynamics aspects. *Annu. Rev. Plant Biol.* 70, 347–376. doi: 10.1146/annurev-arplant-050718-095859

Yan, Y., Li, C., Dong, X., Li, H., Zhang, D., Zhou, Y., et al. (2020). MYB30 is a key negative regulator of *Arabidopsis* photomorphogenic development that promotes PIF4 and PIF5 protein accumulation in the light. *Plant Cell* 32, 2196–2215. doi: 10.1105/tpc.19.00645

Zhang, Y., Wang, Y., Wei, H., Li, N., Tian, W., Chong, K., et al. (2018). Circadian evening complex represses Jasmonate-induced leaf senescence in *Arabidopsis*. *Mol. Plant* 11, 326–337. doi: 10.1016/j.molp.2017.12.017

Conflict of Interest: The authors declare that the research was conducted in the absence of any commercial or financial relationships that could be construed as a potential conflict of interest.

frontiers in Plant Science

ORIGINAL RESEARCH
published: 24 June 2021
doi: 10.3389/fpls.2021.685102

UDP-*N*-Acetylglucosamine Pyrophosphorylase 2 (UAP2) and 1 (UAP1) Perform Synergetic Functions for Leaf Survival in Rice

Zhaohai Wang[1,2]*, *Qiang Wang*[1,2], *Lingxia Wei*[1,2], *Yan Shi*[1,2], *Ting Li*[3], *KeKe Hu*[4], *Shuai Liu*[5], *Hua Zhong*[4], *Jianglin Liao*[1,2], *Yangsheng Li*[4]*, *Hongyu Zhang*[1]* and *Yingjin Huang*[1,2]*

[1] Key Laboratory of Crop Physiology, Ecology and Genetic Breeding, Jiangxi Agricultural University, Ministry of Education of the People's Republic of China, Nanchang, China, [2] Key Laboratory of Agriculture Responding to Climate Change, Jiangxi Agricultural University, Nanchang, China, [3] Youth League Committee, Jiangxi Agricultural University, Nanchang, China, [4] State Key Laboratory of Hybrid Rice, Key Laboratory for Research and Utilization of Heterosis in Indica Rice, Ministry of Agriculture, College of Life Sciences, Wuhan University, Wuhan, China, [5] Department of Biochemistry, Molecular Biology, Entomology and Plant Pathology, Mississippi State University, Starkville, MS, United States

OPEN ACCESS

Edited by:
Nam-Chon Paek,
Seoul National University, South Korea

Reviewed by:
Jong-Seong Jeon,
Kyung Hee University, South Korea
Timothy O. Jobe,
University of Cologne, Germany
Cheng Shihua,
China National Rice Research Institute, China

***Correspondence:**
Zhaohai Wang
zhaohai_wang@163.com
Yangsheng Li
lysh2001@whu.edu.cn
Hongyu Zhang
jn_zhanghongyu@163.com
Yingjin Huang
yjhuang_cn@126.com

Specialty section:
This article was submitted to Plant Physiology, a section of the journal Frontiers in Plant Science

Received: 29 March 2021
Accepted: 31 May 2021
Published: 24 June 2021

Citation:
Wang Z, Wang Q, Wei L, Shi Y, Li T, Hu K, Liu S, Zhong H, Liao J, Li Y, Zhang H and Huang Y (2021) UDP-N-Acetylglucosamine Pyrophosphorylase 2 (UAP2) and 1 (UAP1) Perform Synergetic Functions for Leaf Survival in Rice. Front. Plant Sci. 12:685102. doi: 10.3389/fpls.2021.685102

Functional inactivation of UDP-*N*-acetylglucosamine pyrophosphorylase 1 (UAP1) induces defense response-related lesion-mimic spots and subsequent early senescence in every newly grown leaf of the rice mutant *uap1* after a short period's normal growth. However, the molecular mechanism of these leaves sustaining the short period's survival is still unknown. Phenotypic and molecular studies show that defense response-related lesion-mimic spots and early leaf senescence appear on the normally grown *uap1* leaf and aggravate with the growth time. Bioinformatic analysis reveals that UAP proteins are evolutionarily conserved among eukaryotes, and there exists UAP2 protein except UAP1 protein in many higher organisms, including rice. Rice UAP2 and UAP1 proteins present high sequence identities and very similar predicted 3D structures. Transcriptional expression profile of the *UAP2* gene decreases with the appearance and aggravating of leaf spots and early senescence of *uap1*, implying the role of the *UAP2* gene in maintaining the initial normal growth of *uap1* leaves. Enzymatic experiments verified that the UAP2 protein performs highly similar UAP enzymatic activity with the UAP1 protein, catalyzing the biosynthesis of UDP-GlcNAc. And these two UAP proteins are found to have the same subcellular localization in the cytoplasm, where they most presumably perform their functions. Overexpression of the *UAP2* gene in *uap1* plants succeeds to rescue their leaf mutant phenotype to normal, providing direct evidence for the similar function of the *UAP2* gene as the *UAP1* gene. The *UAP2* gene is mainly expressed in the young leaf stage for functions, while the *UAP1* gene is highly expressed during the whole leaf developmental stages. Based on these findings, it is suggested that *UAP2* and *UAP1* play key roles in rice leaf survival during its development in a synergetic manner, protecting the leaf from early senescence.

Keywords: UDP-N-acetylglucosamine pyrophosphorylase 2, UDP-N-acetylglucosamine pyrophosphorylase 1, defense response, early leaf senescence, rice (*Oryza sativa*)

HIGHLIGHTS

UAP2 and *UAP1* coordinately expressed and colocalized into the cytoplasm to perform the UDP-*N*-acetylglucosamine pyrophosphorylase (UAP) enzymatic functions, maintaining rice leaf survival during its developmental process.

INTRODUCTION

N-Acetylglucosamine (GlcNAc) is the fundamental amino sugar residue for the biosynthesis of *N*-glycan, which is essential for protein glycosylation (Stanley et al., 2015). *N*-Acetylglucosamine also acts as a sugar moiety in glycolipids (Raetz and Whitfield, 2002) and glycosylphosphatidylinositol (GPI)-anchor-linked protein (Hancock, 2004). UDP-GlcNAc is the active form of GlcNAc. The biosynthesis of UDP-GlcNAc and PPi from *N*-acetylglucosamine-1-phosphate (GlcNAc-1-P) and UTP is catalyzed by the enzyme *N*-acetylglucosamine-1-phosphate uridylyltransferase (GlcNAc1pUT) (Yang et al., 2010). And this enzyme is also named UDP-*N*-acetylglucosamine pyrophosphorylase (UAP) (Mio et al., 1998; Schimmelpfeng et al., 2006; Liu et al., 2013).

Mutants of the *UAP* gene have been found in various species. In *Escherichia coli* and *Mycobacterium tuberculosis*, *glmU* encodes the UAP protein, and the *glmU* mutants showed various alterations of cell shape and the final cell lysis (Mengin-Lecreulx and van Heijenoort, 1993; Zhang et al., 2008). In *Aspergillus fumigatus*, the conditional mutant of the *UAP1* gene showed defects in cell wall integrity and morphogenesis, and influenced the cell survival (Fang et al., 2013). In *Saccharomyces cerevisiae*, the null mutation of the *UAP1* gene was lethal, and most of the mutants showed fully swelled or lysed cells (Mio et al., 1998). In *Trypanosoma brucei*, the conditional null mutant of the *UAP* gene was unable to sustain growth under the non-permissive conditions (Stokes et al., 2008). In *Drosophila melanogaster*, the *UAP* gene mutants showed many phenotypic traits ranging from defects of the central nervous system fasciculation to defects in dorsal closure and eye development (Schimmelpfeng et al., 2006). In *Tribolium castaneum*, RNAi for *UAP1* resulted in a specific arrest at the larval–larval, larval–pupal, or pupal–adult molts, depending on the time of injection of double-stranded RNAs, whereas RNAi for *UAP2* prevented larval growth or resulted in pupal paralysis. And RNAi for either *UAP* gene at the mature adult stage resulted in the cessation of oviposition in females, as well as fat body depletion and eventual death in both sexes (Arakane et al., 2011). In *Locusta migratoria*, RNAi of *UAP1* resulted in 100% mortality, whereas insects with RNAi of *UAP2* were able to develop normally (Liu et al., 2013). In *Leptinotarsa decemlineata*, RNAi of *UAP1*, *UAP2*, and both genes made the larvae not undergo larvae–pupal ecdysis and be completely wrapped in the wrinkled larval cuticle, and finally die (Shi et al., 2016). And in *Arabidopsis thaliana*, the single mutants of *UAP1* and *UAP2* (also called *GlcNAc1pUT1* and *GlcNAc1pUT2*) revealed no obvious phenotype but their homozygous double mutant was lethal (Chen et al., 2014). It seems that the *UAP* gene plays an essential role in the cell or individual death in reported species.

Moreover, our previous study identified a *UAP1* gene mutant in rice, and a point mutation of the *UAP1* gene resulted in the complete functional inactivation of the UAP1 protein, leading to the appearance of defense response-related lesion-mimic spots and subsequent early leaf senescence for the *UAP1* gene mutant from the seedling stage (Wang et al., 2015). However, in these *uap1* mutant plants, every new leaf would grow normally for a period of time before these mutant phenotypes appear, thus making *uap1* plants sustain to the mature stage. And the molecular mechanism for the short period's survival of each new leaf on *uap1* plants still needs to be studied.

In this study, we report the identification and characterization of two rice *UAP* genes, *UAP2* and *UAP1*, about their synergetic functions in leaf survival at developmental stages. The UAP2 and UAP1 proteins have the same subcellular localization and highly similar enzymatic functions, while the gene expression profiling of the *UAP2* and *UAP1* genes determines the leaf destiny.

MATERIALS AND METHODS

Plant Materials and Growth Conditions

The rice *UAP1* gene mutant *uap1*, also named *spl29* in our published paper (Wang et al., 2015), and its wild type, the rice cultivar "Zhonghua 11" (ZH11, *Oryza sativa* spp. *japonica*), were used in this study. After germination, rice seeds were grown in soil in the plant growth chamber (light cycle: 14-h light/10-h dark, 28°C) for seedling samples. For experiments at the tillering stage and on flag leaf development, rice plants were cultured under natural conditions.

Gene Expression Analysis

Samples were collected, immediately frozen in liquid nitrogen, and then stored at −80°C for use. Total RNA of samples was extracted by using the TRIzol kit (Invitrogen, the United States), digested with the RNase-free DNase, and then used for preparing the cDNA templates with M-MLV reverse transcriptase (Promega, the United States). Using the SYBR Green Master Mix reagent (Bio-Rad, the United States), qRT-PCR was performed on a Bio-Rad CFX96 real-time PCR system, with three technological replicates for each biological sample. Four rice reference genes *UBC* (LOC_Os02g42314), *Profilin-2* (LOC_Os06g05880), *Actin1* (LOC_Os03g50885), and *ARF* (LOC_Os05g41060) were selected as internal standards for leaf samples (Wang et al., 2015, 2016). All primers used for qRT-PCR analysis are listed in **Supplementary Table 1**, with good PCR efficiencies (85–105%) assessed using a 10-fold dilution series of total cDNA.

Alignment and Structure Comparison of UAP1 and UAP2 Protein Sequences

The *UAP1* and *UAP2* protein sequences were aligned with MAFFT-linsi v7.471 (Katoh and Standley, 2013). The Jalview (Waterhouse et al., 2009) was used to visualize the MSA. The standalone of I-TASSER software (Yang et al., 2015) was used to model the structure of *UAP1* and *UAP2* from rice. The top-fit models were selected based on the C-score provided by I-TASSER. Then, the best structures of two UAP proteins were

visualized by PyMOL software. The protein structure comparison was made by TM-align (Zhang and Skolnick, 2005) online server (https://zhanglab.ccmb.med.umich.edu/TM-align/), and the TM-score value was used to scale the structural similarity with 1 indicating the excellent match.

Recombinant Protein Construction, Expression, and Purification

To generate the glutathione S-transferase (GST) gene fusion constructs GST-UAP1 and GST-UAP2, the full-length coding sequence of *UAP1* and *UAP2* were amplified from the cDNA of ZH11 leaf, separately (primers GST-UAP1/UAP2 in **Supplementary Table 2**). PCR products were inserted into pGEX-6P-1 using the restriction enzyme sites *Bam*H I and *Eco*R I. Expression and purification of the recombinant protein were conducted according to the published method (Wang et al., 2015).

^{1}H-Nuclear Magnetic Resonance Analysis of UAP1 and UAP2 Enzymatic Activities *in situ*

The enzymatic reactive experiments were performed according to the procedure as described previously (Wang et al., 2015). The forward reactions were carried out in the 540-μl mixture consisting of $^2H_2O/H_2O$ (8:1, v/v), Na^+/K^+ phosphate buffer (80 mM K_2HPO_4, 20 mM NaH_2PO_4, pH 7.4), 5 mM $MgCl_2$, 0.2 mM UTP, 0.2 mM GlcNAc-1-P, 1.5 units of yeast inorganic pyrophosphatase, and recombinant enzyme (0.5 μg of GST, GST-UAP1, or GST-UAP2). The reverse reactions were performed in a 540 μl solution containing $^2H_2O/H_2O$ (8:1, v/v), Na^+/K^+ phosphate buffer, 5 mM $MgCl_2$, 0.2 mM PPi, 0.2 mM UDP-GlcNAc (or UDP-GalNAc), and recombinant enzyme (0.5 μg of GST, GST-UAP1, or GST-UAP2). Examination of GlcNAc-1-P/GalNAc-1-P and UDPGlcNAc/UDP-GalNAc was performed by ^{1}H-nuclear magnetic resonance (^{1}H-NMR) as described previously (Zhang et al., 2011). Data acquisition started at 1 h after the addition of enzyme to the reaction mixture.

Subcellular Localization of UAP1 and UAP2

The subcellular localization of the UAP1 and UAP2 proteins was predicted by using the online SignalP 4.1 Server (http://www.cbs.dtu.dk/services/SignalP-4.1/), ChloroP 1.1 Server (http://www.cbs.dtu.dk/services/ChloroP/), and TargetP 2.0 Server (http://www.cbs.dtu.dk/services/TargetP/).

To get the fusion construction of UAP1 and UAP2 with the yellow fluorescent protein (YFP), the coding sequences of UAP1 and UAP2 were amplified by using the primer pair UAP1-YFP and UAP2-YFP (**Supplementary Table 2**), and then cloned into the vector pBWD(LB)-p35SYFP using Bsa I restriction site. The fusion constructs (p35S::UAP1-YFP and p35S::UAP2-YFP) and the control (p35S::YFP) were transformed into the rice protoplasts for transient expression (Yu et al., 2014). And the subcellular localization results were examined using an FV1000 confocal system (OLYMPUS FLUOVIEW).

Transgenic Plants

The *uap1* transgenic lines with the *UAP1* gene complementary vector (also named p*SPL29*C) were obtained from our previous research (Wang et al., 2015). For overexpressing the *UAP2* gene in *uap1*, the full-length coding sequence of the *UAP2* was amplified using primers "*UAP2*-OE" (**Supplementary Table 2**). PCR products were inserted into the binary vector pBWA(V)BU (reconstructed from pCAMBIA3300) using *Bsa* I sites for the digesting-link one-step reaction. The recombinant vectors were transferred into *Escherichia coli* DH5α and then sequenced to check whether the constructions were correct. The correct construction vector with *UAP2* and the empty vector were separately introduced into *Agrobacterium tumefaciens* EHA105 and then transformed into the *uap1* calli. Positive transgenic plants were confirmed by PCR amplifying the phosphinothricin gene with primer "*Bar178*" (**Supplementary Table 2**) and survival screening with the phosphinothricin solution (20 mg/L).

RESULTS

Lesion-Mimic Spots and Early Leaf Senescence Appear on the Newly Developed Leaves of the *uap1* Mutant After a Short Period's Normal Growth

The *uap1* mutant appears to have the phenotype of lesion-mimic leaf spots and early leaf senescence after a period of normal growth. When the wild-type and *uap1* plants were grown in the plant growth chamber (14-h light/10-h dark, 28 °C), there was no visible mutant phenotype in leaves of the 18-day-old *uap1* plants (**Figure 1A**). However, small, dark-brown lesion-mimic leaf spots started to appear on the 23-day-old *uap1* plant leaves (**Figure 1A**). Soon, amounts of leaf spots spread over the 28-day-old *uap1* plant leaves; meanwhile, the leaves started to wither from the tip (**Figure 1A**).

The appearance of lesion-mimic leaf spots usually implies induced defense responses for plant resistance, and defense response genes will be activated in this process (Lorrain et al., 2003). In order to identify the defense response state of *uap1* leaves, gene expression analysis of two defense response genes (*PR1a* and *PBZ1*) was performed by qRT-PCR. Results showed that the expression levels of these two genes were equal in 18-day-old *uap1* and wild-type plant leaves, but gradually and significantly increased in leaves of 23- and 28-day-old *uap1* plants compared with the wild type (**Figures 1B,C**). These results showed that the defense response state in *uap1* leaves is originally normal, but is activated along with the appearance of leaf spots and aggravated with spots spreading.

Since early leaf senescence followed after the appearance of leaf spots in *uap1* mutant, this phenotype was additionally verified at the physiological and molecular level. The decline of chlorophyll content is an important physiological index of leaf senescence. Compared with the wild type, the chlorophyll content did not change in leaves of 18-day-old *uap1* plants, but it decreased in leaves of 23-day-old *uap1* plants, and continuously reduced in leaves of 28-day-old *uap1* plants (**Figure 1D**). Transcription factor genes and senescence-associated genes

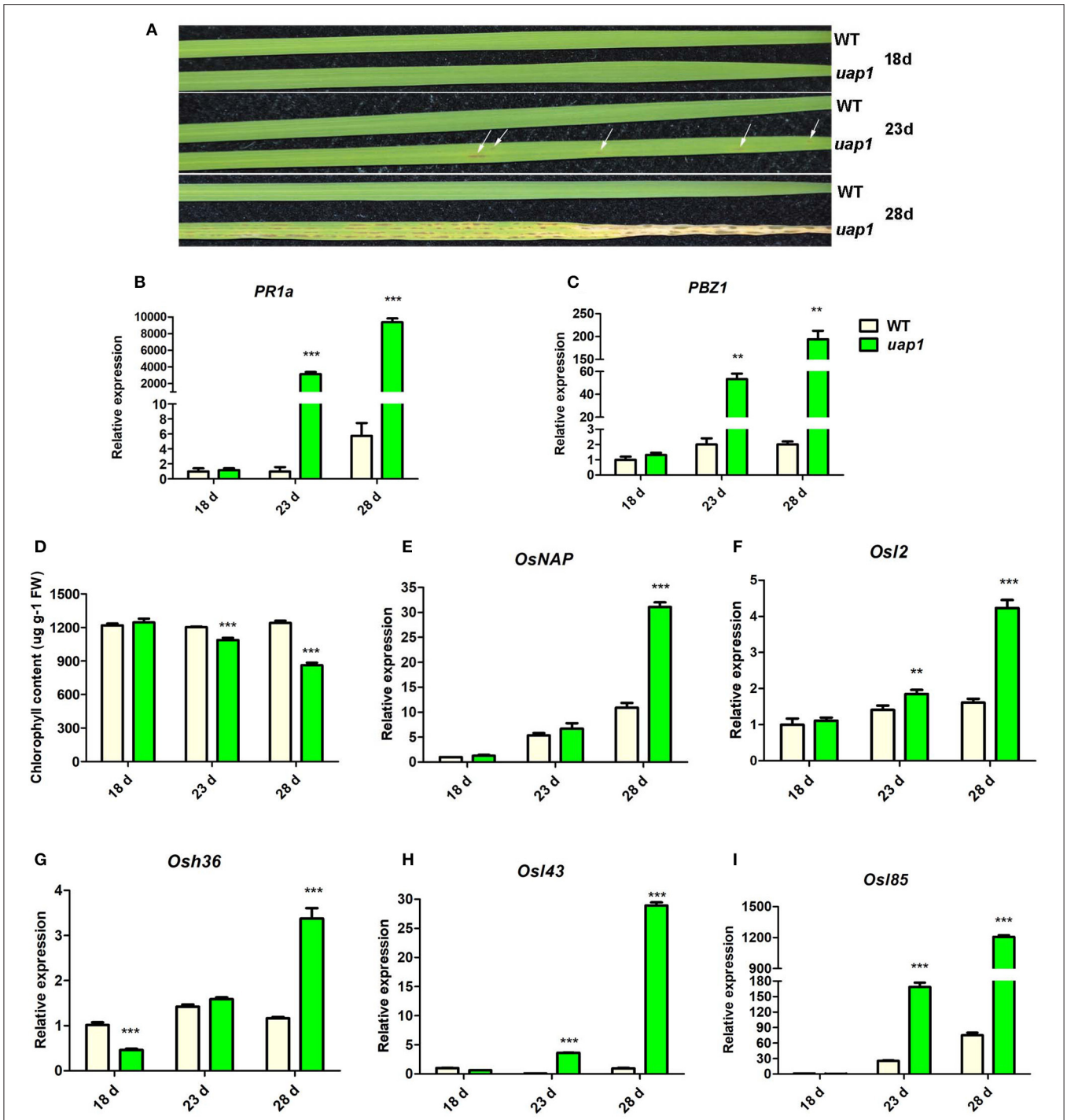

FIGURE 1 | Characteristics of phenotype and molecular markers of wild-type and *uap1* mutant leaves. **(A)** Leaf phenotype of plants at the seedling stage (18, 23, and 28 days after germination). The white arrows indicate the leaf spots. **(B,C)** Relative expression of two defense signaling-related genes *PR1a* and *PBZ1*. **(D)** Chlorophyll contents. FW, fresh weight. **(E)** Relative expression of senescence-associated transcriptional factor *OsNAP*. **(F–I)** Relative expression of four senescence-associated genes (SAGs) *Osl2*, *Osh36*, *Osl43,* and *Osl85*. Relative expression of genes by qRT-PCR is normalized with reference genes *UBC*, *Profilin-2,* and *Actin1*. All data represent the mean ± *SD* of three biological replicates, and the asterisk indicates the statistically significant difference between *uap1* and WT (**$P < 0.005$, ***$P <$ 0.0005, Student's *t*-test).

(SAGs) are usually up-regulated during leaf senescence to trigger or control the process (Lee et al., 2001; Liang et al., 2014). To further confirm that senescence occurred at the early stage of leaf developmental process of *uap1* plants, gene expression analysis of the senescence-associated transcription factor *OsNAP* and four SAGs (*Osl2*, *Osh36*, *Osl43,* and *Osl85*)

was performed by qRT-PCR. Compared with the wild type, the mRNA levels of these genes were not raised in leaves of the 18-day-old *uap1* plants, but showed the upward trend in leaves of the 23-day-old *uap1* plants, and were all significantly up-regulated in leaves of the 28-day-old *uap1* plants (**Figures 1E–I**). The up-regulated expression patterns of senescence-associated transcription factor and SAGs further support the notion that early leaf senescence of *uap1* plants appeared from nothing during the process of young leaf development to mature.

Analysis on Evolutionary Relationship and Expression Profile Implies That the *UAP2* Gene Is Responsible for the Short Time's Normal Growth of the *uap1* Young Leaves

Previous study has verified that the mutation of *UAP1* to *uap1* makes its encoded protein eliminate the UAP enzymatic function, responsible for the early leaf senescence, and defense response phenotype of the mutant (Wang et al., 2015). However, it is still not clear why the leaves of *uap1* mutant can grow normally for a period of time, despite the lost function of the UAP1 protein.

To solve this problem, the evolutionary relationship of UAP1 protein was investigated. UAP proteins from diverse species, including plants, animals, fungi, and bacterium, were used to construct the NJ tree (**Figure 2A**). The results showed that UAP proteins were widely found in various organisms. However, the EcGlmU performing UAP functions in prokaryotes was significantly different from UAPs in eukaryotes. Besides, the UAP proteins were mainly divided into two clusters (plants and animals), indicating the different origins of UAPs from plants and animals. Interestingly, there exist two UAPs in some animals and most investigated plants, including rice. Through NCBI searching in the rice genome, a gene LOC_Os04g52370 is also annotated as UAP, thus named *UAP2*. The rice *UAP2* gene is highly homologous with the *UAP1* gene, separately sharing 82% identities for the coding sequence (**Supplementary Figure 1**) and 88% identities for the protein sequence (**Figure 2B**). The three-dimensional models of rice UAP2 and UAP1 proteins were generated using I-TASSER software. These two rice UAPs were predicted to have very similar 3D structures (**Figure 2C**) with some changes mainly at the N-terminal site (**Figures 2C,D**). In detail, for the first 20 amino acids of the two proteins, the UAP1 showed a β-sheet, while the UAP2 exhibited an α-helix (**Figure 2D**). Besides, the TM-score value of these two proteins was 0.97, which also indicated the high similarity on protein structures of UAP2 and UAP1. The analogous protein structures of UAP2 and UAP1 implied that these two proteins might have similar enzymatic functions. Presumably, the function of the *UAP2* gene would rescue the mutation of *uap1*, ensuring the normal growth of the young leaves of *uap1*.

To validate this hypothesis, the expression patterns of the *UAP2* gene and the *UAP1* gene were checked in wild-type and *uap1* plant leaves by qRT-PCR. The expression levels of the *UAP1* gene were constantly high and showed a rising trend separately in the 18-, 23-, 28-day-old wild-type and *uap1* leaves (**Figure 3A**). Meanwhile, the expression level of the *UAP2* gene was high in the 18-day-old wild-type and *uap1* leaves, but showed a declining trend in the 23- and 28-day-old wild-type and *uap1* leaves (**Figure 3B**). And the declining trend of the *UAP2* gene expression was more in *uap1* leaves than in wild-type leaves (**Figure 3B**). The fact that the reduction of expression of the *UAP2* gene in 23- and 28-day-old leaves of wild-type and *uap1* plants is perfectly synchronous with the appearance of defense response-related lesion-mimic spots and early senescence in the *uap1* mutant leaves. These results implied that the *UAP2* gene is highly possible to be responsible for the normal growth of the *uap1* young leaves.

The Enzymatic Function of the UAP2 Protein Is Consistent With That of the UAP1 Protein

In order to identify the UAP2 protein performing the function of UAP, in common with the UAP1 protein, recombinant proteins of GST-UAP2 and GST-UAP1 were produced. The molecular weights of GST, UAP1, and UAP2 are theoretically 26, 54.071, and 54.447 kDa, respectively. GST, GST-UAP1 (about 80 kDa), and GST-UAP2 (about 80 kDa) were highly expressed after induction (**Supplementary Figure 2**, lanes 2–4). These three proteins were column-purified to detect the UAP enzymatic activity (**Supplementary Figure 2**, lanes 5–7).

The enzymatic reaction of UAP2 and UAP1 proteins was monitored by ^{1}H-NMR spectroscopy *in situ*. After 1-h enzymatic progression, forward conversion of GlcNAc-1-P (5.36 ppm) to UDP-GlcNAc (5.52 ppm) was observed both with GST-UAP2 and with GST-UAP1, but not with the GST control (**Figure 4A**). Similarly, the reverse conversion of UDP-GlcNAc (5.52 ppm) to GlcNAc-1-P (5.36 ppm) was both observed with GST-UAP2 and GST-UAP1, but not with GST (**Figure 4B**). GST-UAP2 and GST-UAP1 could also catalyze the reverse conversion of UDP-*N*-acetylgalactosamine (UDP-GalNAc) (5.55 ppm) to *N*-acetylgalactosamine-1-phosphate (GalNAc-1-P) (5.39 ppm) with the catalytic ability of GST-UAP2 weaker than GST-UAP1, whereas GST could not (**Figure 4C**). The forward reaction for the synthesis of UDP-GalNAc from GalNAc-1-P could not be tested since GalNAc-1-P was commercially unavailable.

These NMR-based assays provide unambiguous evidence that the UAP2 protein performs very similar UAP enzymatic activity with the UAP1 protein. It is speculated that UAP2 can compensate for the lost function of UAP1 in *uap1* plant leaves to maintain leaf survival from early senescence.

The UAP2 Protein and the UAP1 Protein Located at the Same Subcellular Position to Perform Functions

To reveal where the UAP2 and UAP1 proteins perform their functions in the cells, the online SignalP, ChloroP, and TargetP servers were used to predict the subcellular localization of these two proteins. The SignalP found that the UAP1 and UAP2 proteins had no signal peptide. The ChloroP found that the UAP1 and UAP2 proteins didn't contain N-terminal chloroplast transit peptides. And the TargetP predicted that the UAP1 and UAP2 proteins were not localized in the chloroplast and mitochondria,

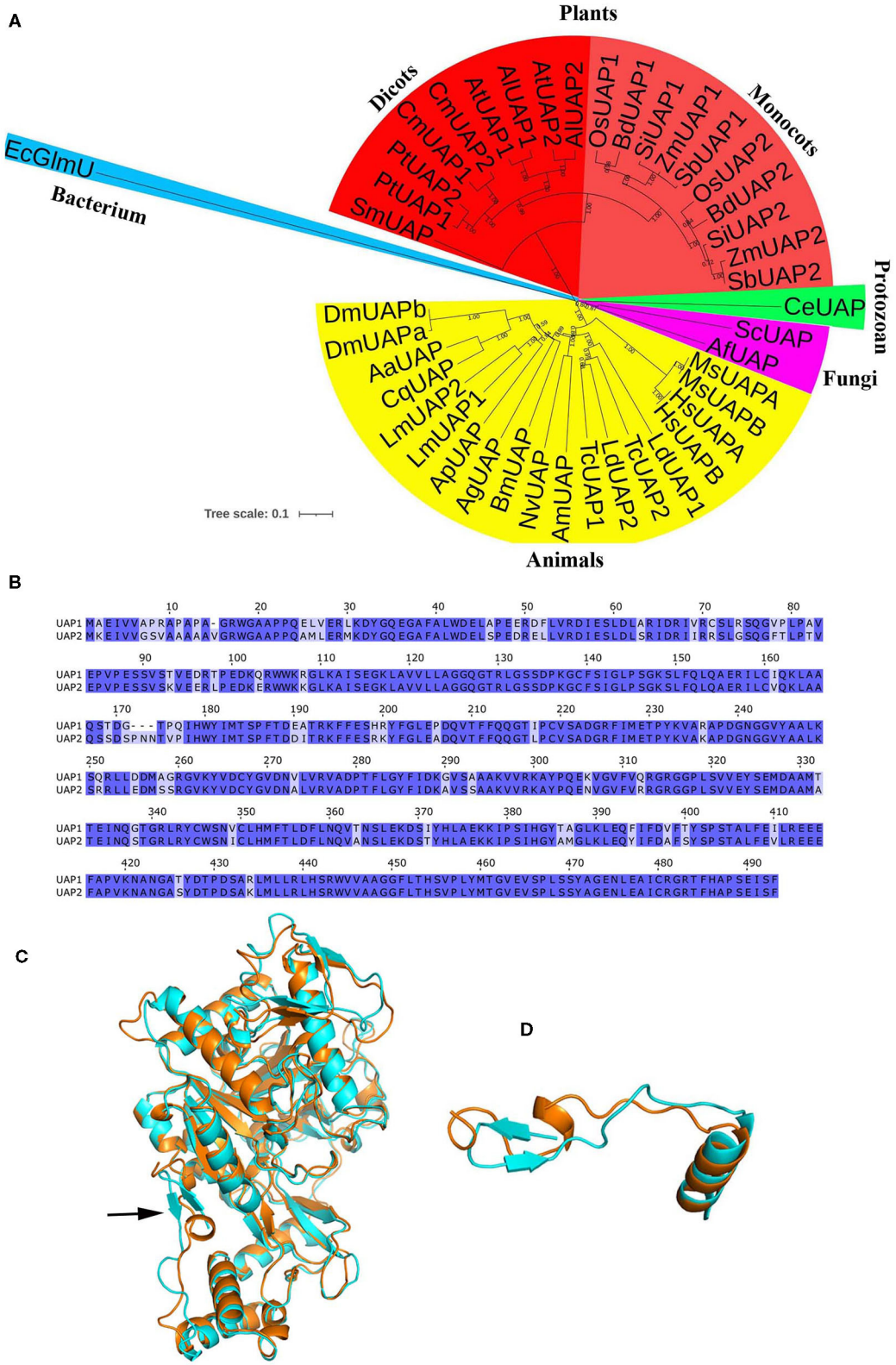

FIGURE 2 | Bioinformatic analysis of UAP proteins. **(A)** Phylogenetic analysis of UAPs in different organisms. The tree was constructed based on the full-length amino acid sequences of UAPs. The tree scale indicates the units of amino acid substitutions per site. GenBank accession numbers are as follows: SmUAP, *Selaginella moellendorffii* (XP_024532253.1); PtUAP1, *Populus trichocarpa* (XP_006369047.1); PtUAP2, *Populus trichocarpa* (XP_002303345.3); CmUAP1, *Cucurbita moschata*

(Continued)

FIGURE 2 | (XP_022925908.1); CmUAP2, *Cucurbita moschata* (XP_022926514.1); AtUAP1, *Arabidopsis thaliana* (NP_564372.3); AlUAP1 *Arabidopsis lyrate* (XP_020870296.1); AtUAP2, *Arabidopsis thaliana* (NP_181047.1); AlUAP2, *Arabidopsis lyrate* (XP_002879530.1); OsUAP1, *Oryza sativa* (XP_015650402.1); BdUAP1, *Brachypodium distachyon* (XP_010234461.1); SiUAP1, *Setaria italica* (XP_004972591.1); ZmUAP1, *Zea mays* (PWZ43849.1); SbUAP1, *Sorghum bicolor* (XP_002444024.1); OsUAP2, *Oryza sativa* (XP_015633457.1); BdUAP2, *Brachypodium distachyon* (XP_003580539.1); SiUAP2, *Setaria italica* (XP_004976790.1); ZmUAP2, *Zea mays* (ONM14001.1); SbUAP2, *Sorghum bicolor* (XP_021317962.1); CeUAP, *Caenorhabditis elegans* (NP_497777.1); ScUAP, *Saccharomyces cerevisiae* (NP_010180.1); AfUAP, *Aspergillus fumigatus*, (XP_746714.1); MsUAPA, *Mus musculus* (NP_001291975.1, isoform A); MsUAPB, *Mus musculus* (NP_001291974.1, isoform B); HsUAPA, *Homo sapiens* (NP_001311044.1, isoform A); HsUAPB, *Homo sapiens* (NP_001311045.1, isoform B); LdUAP1, *Leptinotarsa decemlineata* (XP_023024179.1); LdUAP2, *Leptinotarsa decemlineata* (XP_023022882.1); TcUAP1, *Tribolium castaneum* (NP_001164533.1); TcUAP2, *Tribolium castaneum* (NP_001164534.1); AmUAP, *Apis mellifera* (XP_624349.1); NvUAP, *Nasonia vitripennis* (XP_001602623.1); BmUAP, *Bombyx mori* (AIQ85099.1); AgUAP, *Anopheles gambiae* (XP_317600.4); ApUAP, *Acyrthosiphon pisum* (XP_001944680.1); LmUAP1, *Locusta migratoria* (AGN56418.1); LmUAP2, *Locusta migratoria* (AGN56419.1); CqUAP, *Culex quinquefasciatus* (EDS38218.1); AaUAP, *Aedes aegypti* (EAT47260.1); DmUAPA, *Drosophila melanogaster* (NP_609032.1, isoform A); DmUAPB, *Drosophila melanogaster* (NP_723183.1, isoform B); EcGlmU, *Escherichia coli* (P0ACC7.1). **(B)** Alignment of the UAP1 and UAP2 protein sequences. **(C)** The 3D structure of the UAP1 and UAP2 proteins. Cyan, UAP1. Orange, UAP2. The arrow indicates the main difference between UAP1 and UAP2. **(D)** The structure of the first 20 amino acids of the two UAP proteins: The UAP1 has a β-sheet, while the UAP2 exhibits an α-helix.

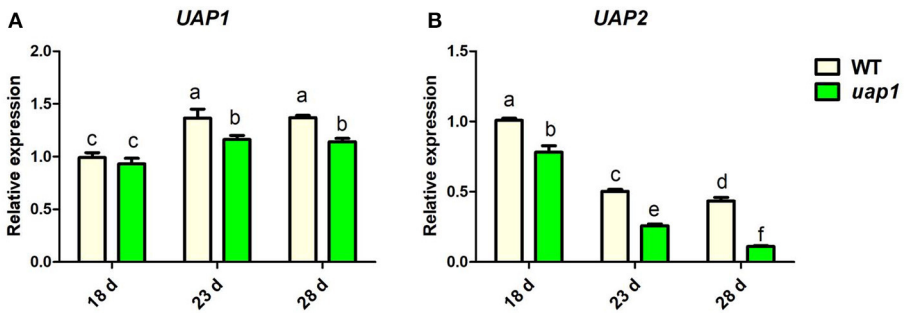

FIGURE 3 | Relative expression of *UAP* genes in wild-type and *uap1* mutant leaves. **(A)** The *UAP1* gene. **(B)** The *UAP2* gene. Leaf samples in 18-, 23-, and 28-day-old plants at the seedling stage were detected (corresponding to **Figure 1A**). Relative expression of genes by qRT-PCR is normalized with reference genes *UBC*, *Profilin-2,* and *Actin1*. All data represent the mean ± *SD* of three biological replicates, and lowercase letters above columns indicate the statistically significant difference among all samples (one-way ANOVA).

but might be in any other subcellular place. According to these prediction results, it is speculated that the UAP1 and UAP2 proteins are most possibly localized in the cytoplasm.

To find their real subcellular localization, the coding sequences of *UAP2* and *UAP1* were separately fused with *YFP*. Then the 35S::*UAP2-YFP*, 35S::*UAP1-YFP*, and 35S::*YFP* constructs were introduced into the rice protoplasts, respectively. Results showed that the YFP fluorescence signaling mechanisms indeed appeared throughout the cytoplasm in those protoplasts transformed with 35S::*UAP1-YFP* and 35S::*UAP2-YFP* (**Figures 5C–F**), like in protoplasts that were transformed with the control 35S::*YFP* (**Figures 5A,B**). These results indicated that the UAP2 and UAP1 proteins are both localized in the cytoplasm where they most presumably perform their functions.

Overexpression of the *UAP2* Gene in *uap1* Plants Rescues Their Leaf Mutant Phenotype

In order to identify the role of the *UAP2* gene in compensating for the lost function of the *UAP1* gene in *uap1* mutant plants, a transgenic experiment to overexpress the *UAP2* gene in the *uap1* plants was performed. The full-length CDS fragment (1,482 bp) of *UAP2* was constructed into the overexpression vector p*UAP2*-OE using the ubiquitin promoter. The p*UAP2*-OE vector and the empty control vector were transferred into the *uap1* calli by *A. tumefaciens*-mediated transformation. Eight independent transgenic lines overexpressing the *UAP2* gene were obtained, showing a complete rescue of the mutant phenotype; meanwhile, six independent transgenic lines with the empty vector were obtained, failing to compensate the *uap1* mutant (**Figures 6A,B**). The expression changes of the *UAP2* gene in three representative transgenic lines with *UAP2* overexpression were additionally detected. The result showed that the *UAP2* gene was overexpressed significantly in these three transgenic lines (**Figure 6C**), which were thus used for subsequent analysis.

The defense response for plant resistance was tested in leaves of wild-type plants, *uap1* plants, *uap1* transgenic plants with the empty vector, *uap1* transgenic lines with the *UAP1* gene complementary vector, and *uap1* transgenic lines with the *UAP2* gene overexpression vector. To test their resistance to the pathogen, these plants were inoculated with the bacterial blight strain PXO99 at the tillering stage. The *uap1* plants and *uap1* transgenic plants with the empty vector exhibited significantly enhanced resistance, while three *uap1* transgenic lines overexpressing the *UAP2* gene showed the typical response to bacterial blight diseases, like as the wild-type plants and three *uap1* transgenic lines with *UAP1* gene complementation (**Figures 6D,E**). Correspondingly, expression levels of two

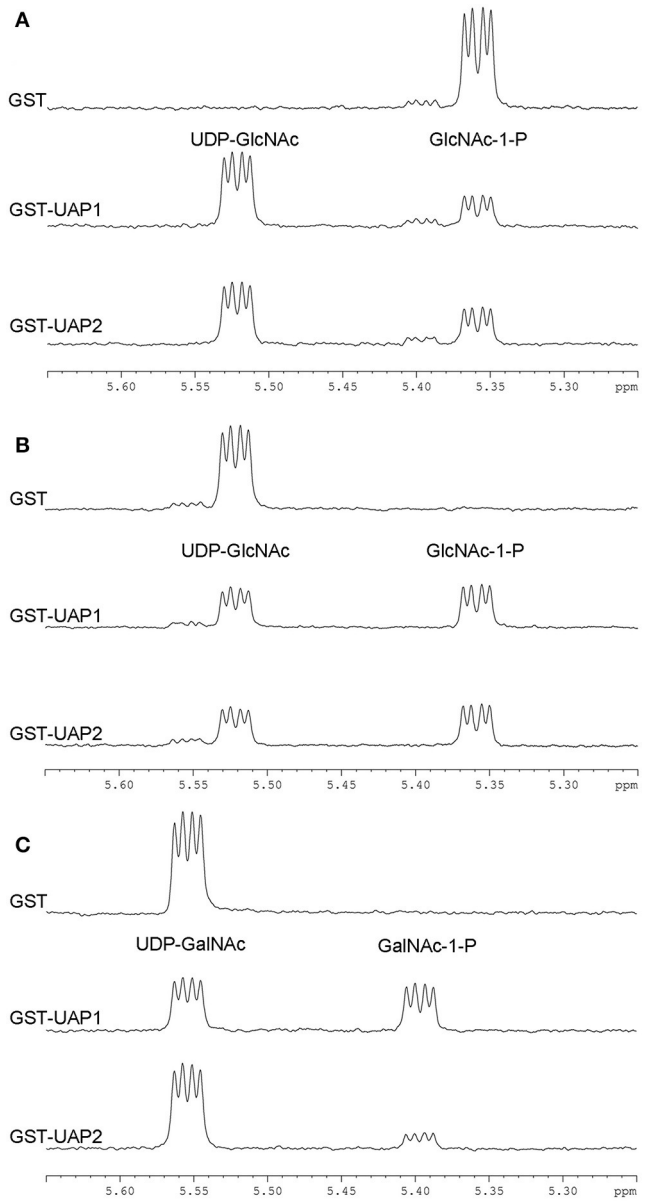

FIGURE 4 | Enzymatic activities of UAP2 and UAP1 proteins based on ^{1}H-NMR. **(A)** Forward UAP activity: UTP + GlcNAc-1-P → UDP-GlcNAc + PPi. The chemical shift (indicated by the "peak" shape) of 5.36 p.p.m is for the substrate GlcNAc-1-P and 5.52 p.p.m for the product UDP-GlcNAc. **(B)** Reverse UAP activity: UDP-GlcNAc + PPi → GlcNAc-1-P + UTP. The chemical shift of 5.52 p.p.m is for the substrate UDP-GlcNAc and 5.36 p.p.m for the product GlcNAc-1-P. **(C)** Reverse UAP activity: UDP-GalNAc + PPi → GalNAc-1-P + UTP. The chemical shift of 5.55 p.p.m is for the substrate UDP-GalNAc and 5.39 p.p.m for the product GalNAc-1-P. Data acquisition was performed at 1 h after the addition of the purified protein (GST, GST-UAP1, or GSP-UAP2) in the reaction mixture, with each line indicating each measurement. Results are representative of two independent experiments.

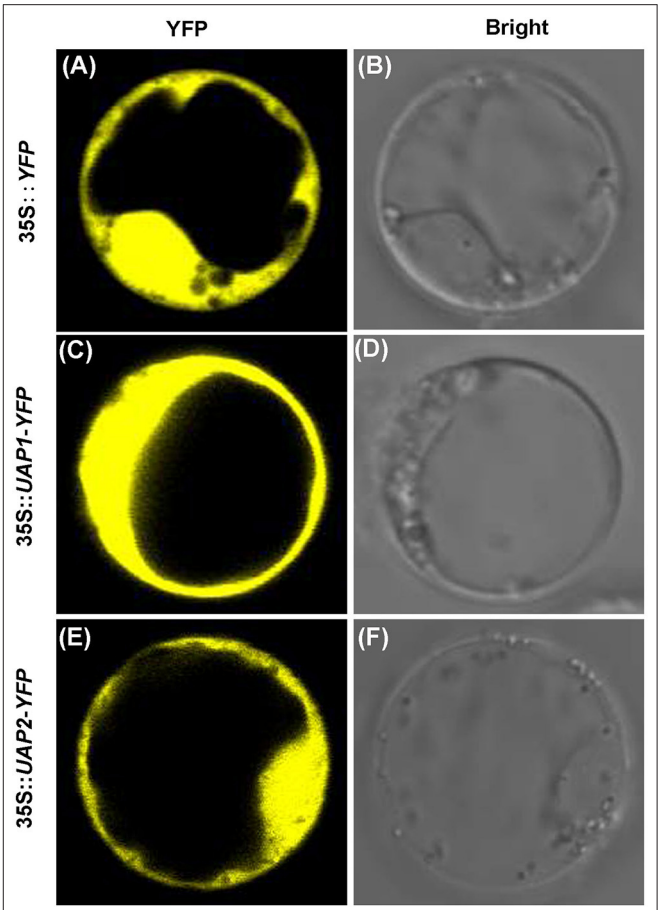

FIGURE 5 | Subcellular localization of UAP1 and UAP2 proteins. Rice protoplast transformed with **(A,B)** empty vector 35S::*YFP* as control, **(C,D)** 35S::*UAP1-YFP*, and **(E,F)** 35S::*UAP2-YFP*. **(A,C,E)** YFP fluorescence images. **(B,D,F)** Bright field.

defense response genes (*PR1a* and *PBZ1*) were analyzed by qRT-PCR. Results showed that expression levels of *PR1a* and *PBZ1* were all up-regulated in leaves of *uap1* plants and *uap1* transgenic plants with the empty vector compared with the wild type, but recovered to the normal level in three *uap1* transgenic lines overexpressing the *UAP2* gene, as these three *uap1* transgenic lines with *UAP1* gene complementation (**Figures 6F,G**). These phenotypic and molecular studies all supported the fact that overexpression of the *UAP2* gene in *uap1* can rescue its defense response phenotype, just the same as the *UAP1* gene, implying the similar gene function of these two *UAP* genes on plant defense.

Chlorophyll contents were measured in leaves of wild-type plants, *uap1* plants, *uap1* transgenic plants with the empty vector, *uap1* transgenic lines with the *UAP1* gene complementary vector, and *uap1* transgenic lines with the *UAP2* gene overexpression vector. Results showed that the chlorophyll contents in leaves of three *uap1* transgenic lines overexpressing the *UAP2* gene were restored to the normal level, as in leaves of wild-type plants and three *uap1* transgenic lines with *UAP1* gene complementation, while those in leaves of *uap1* plants and *uap1* transgenic plants with the empty vector were significantly decreased (**Figure 6H**). Expression levels of the senescence-associated transcription factor *OsNAP* and four SAGs (*Osl2*, *Osh36*, *Osl43*,

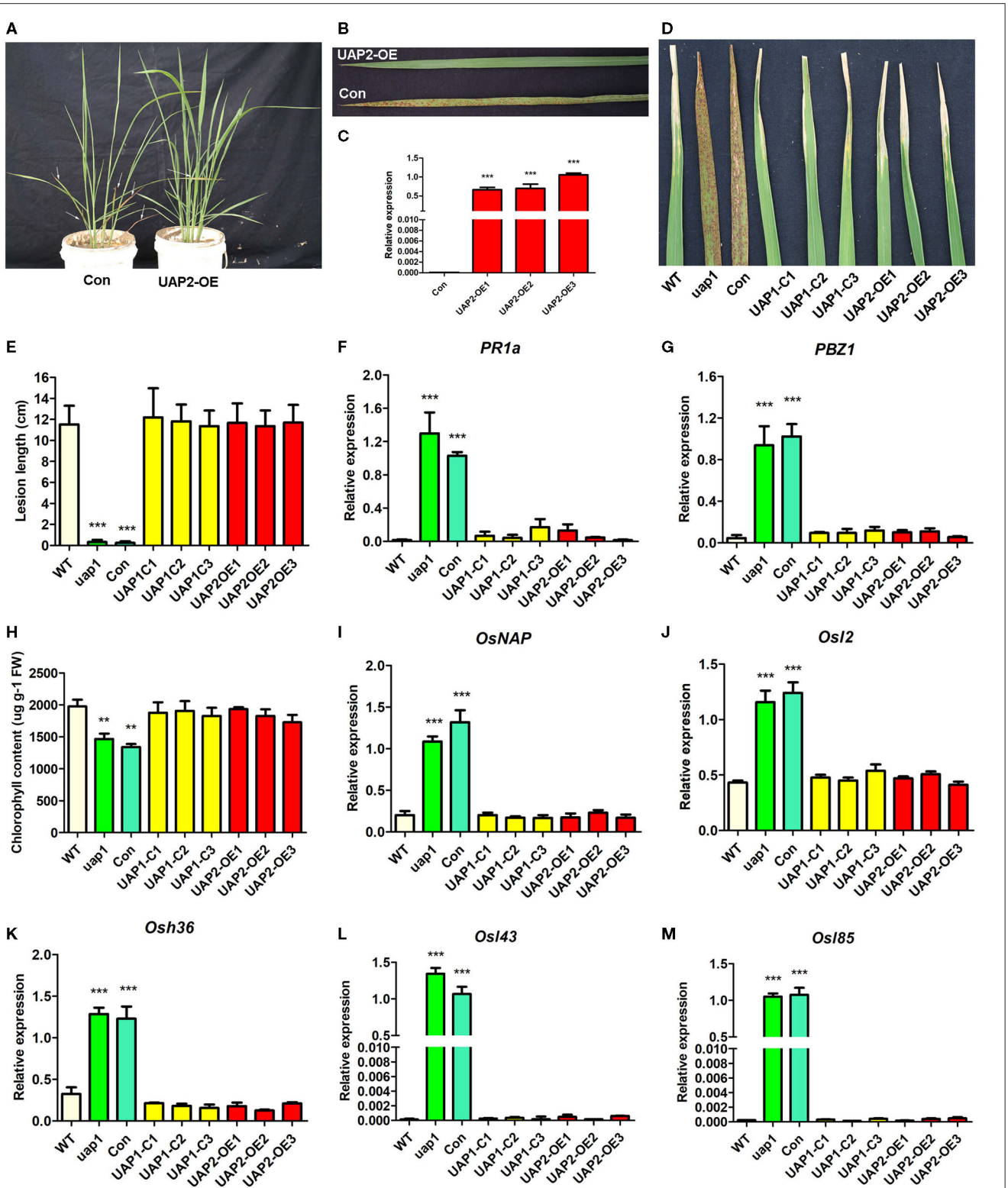

FIGURE 6 | Phenotypic and molecular characteristics for transgenic plants with the *UAP2* gene rescuing the mutant phenotype of *uap1*. **(A)** Representative transgenic plants overexpressing *UAP2* (UAP2-OE) and with empty vector control (Con) at the tillering stage. Arrows indicate the leaves with the mutant phenotype. **(B)** Clear leaf phenotype in representative transgenic plants shown in **(A)**. **(C)** Relative expression of the *UAP2* gene in three representative transgenic plants overexpressing *UAP2* (UAP2-OE1, UAP2-OE2, and UAP2-OE3) and control transgenic plant with empty vector (Con). Data represent the mean ± *SD* of three biological replicates, and the asterisk indicates the statistically significant difference of overexpression samples compared with Con (***$P < 0.0005$, Student's *t*-test).

(Continued)

FIGURE 6 | (D) Infection phenotype after inoculation of plant leaves with bacterial blight pathogen PXO99. **(E)** Mean lesion length after inoculation of plant leaves with bacterial blight pathogen PXO99. Data represent the mean ± *SD* from three to five independent plants at tillering stage, and the asterisk indicates the statistically significant difference of samples compared with WT (***$P < 0.0005$, Student's *t*-test). **(F,G)** Relative expression of two defense signaling-related genes in plant leaves at tillering stage by qRT-PCR. **(H)** Chlorophyll contents in plant leaves at the tillering stage. FW: fresh weight. **(I–M)** Relative expression of senescence-associated transcription factors (*OsNAP*) and four *SAGs* (*Osl2*, *Osh36*, *Osl43,* and *Osl85*) in plant leaves at tillering stage. In **(F–M)**, data represent the mean ± *SD* of three biological replicates, and the asterisk indicates the statistically significant difference of samples compared with WT (**$P < 0.005$, ***$P < 0.0005$, Student's *t*-test). Relative expression of genes by qRT-PCR is normalized with reference genes *UBC*, *Profilin-2,* and *ARF*. WT, wild type. *uap1*, mutant of the *UAP1* gene. Con, transgenic plant with empty vector control. *UAP1*-C1, *UAP1*-C2, and *UAP1*-C3, three *uap1* transgenic lines with *UAP1* gene complementation. *UAP2*-OE1, *UAP2*-OE2, and *UAP2*-OE3, three *uap1* transgenic lines overexpressing the *UAP2* gene.

and *Osl85*) were additionally detected by qRT-PCR in these materials. Results suggested that these five genes were equally expressed in the leaves of wild-type plants, *uap1* transgenic lines overexpressing the *UAP2* gene, and *uap1* transgenic lines with *UAP1* gene complementation, but they were up-regulated in leaves of *uap1* plants and *uap1* transgenic plants with the empty vector (**Figures 6I–M**). These physiological and molecular studies all supported the fact that overexpression of the *UAP2* gene in *uap1* can rescue its early leaf senescence phenotype, just as the *UAP1* gene, indicating the similar function of these two *UAP* genes on leaf senescence.

Taken together, phenotypes of defense response-related leaf spots and subsequent early leaf senescence of the *uap1* mutant can also be rescued by the *UAP2* gene, in addition to the *UAP1* gene, providing effective results for the synergetic role of *UAP2* and *UAP1* genes on protecting leaf from early senescence.

The *UAP2* Gene Is Mainly Expressed in Young Leaves, While the *UAP1* Gene Maintains Continuous High Expression During the Whole Leaf Development

The expression profile of the *UAP2* and *UAP1* genes was identified in rice flag leaves during their whole developmental periods, including unexpanded young leaf stage, booting stage, flowering stage, filling stage, and maturation stage (**Figure 7A**). Results showed that the expression level of the *UAP1* gene slightly increased in flag leaf from the unexpanded young leaf stage to flowering stage, and then showed a minor decrease at filling stage and maturation stage (**Figure 7B**). As a whole, the *UAP1* gene is expressed at a continuously high level in flag leaves during all these developmental stages. Meanwhile, the expression level of the *UAP2* gene was the highest at the unexpanded young leaf stage, but soon exhibited a sharp and continuous decline at the next four stages (**Figure 7C**). These results implied the fact that the *UAP2* gene mainly plays a role at the young leaf stage, while the *UAP1* gene performs its role during the whole leaf developmental stages.

DISCUSSION

UAP Genes Are Essential for Survival Among Organisms

UDP-*N*-acetylglucosamine pyrophosphorylase catalyzes the final step of the hexosamine biosynthetic pathway, producing UDP-GlcNAc, an essential sugar moiety involved in protein glycosylation, glycolipids, and GPI-anchor-linked protein (Raetz and Whitfield, 2002; Hancock, 2004; Stanley et al., 2015). UDP-*N*-acetylglucosamine pyrophosphorylases are conserved and widely distributed among organisms (**Figure 2A**). Their functions have been partially studied from prokaryotes to eukaryotes, such as bacteria, fungi, animals, and plants. As reported, the copy number of the *UAP* gene varies depending on the species. In fungi like yeast and *A. fumigatus*, *UAP* is a single gene, showing the essential roles in cell morphogenesis and survival (Mio et al., 1998; Fang et al., 2013). In *T. brucei*, the single *UAP* gene is also absolutely necessary for cell growth, and its null mutant will cause the happening of cell lysis (Stokes et al., 2008). For the insects, there were two *UAP* genes reported in *T. castaneum*, *Locusta migratoria*, and *Leptinotarsa decemlineata*, but only a single *UAP* gene in most other investigated insects, such as *Aedes aegypti*, *Culex quinquefasciatus*, *D. melanogaster*, *Bombyx mori*, *Anopheles gambiae*, *Acyrthosiphon pisum*, *Apis mellifera*, and *Nasonia vitripennis* (Arakane et al., 2011; Liu et al., 2013; Shi et al., 2016). Both *UAP1* and *UAP2* were found to be critical for individual development and survival in *T. castaneum* and *Leptinotarsa decemlineata*, while only *UAP1* was identified as essential for the development and survival of *Locusta migratoria* at least in nymphal stage (Arakane et al., 2011; Liu et al., 2013; Shi et al., 2016). The humans only have a single *UAP* gene, but two isoforms, *HsUAPA* and *HsUAPB* (also called *AGX1* and *AGX2*), which can use GlcNAc-1-P or *N*-acetylgalactosamine-1-phosphate (GalNAc-1-P) as substrates to synthesize UDP-GlcNAc or UDP-GalNAc, with the preferred substrate of GlcNAc-1-P for UAPA and the preferred substrate of GalNAc-1-P for UAPB (Wang-Gillam et al., 1998; Peneff et al., 2001). The same situation of one *UAP* gene with two isoforms is found in the mammal *Mus musculus* (**Figure 2A**). No *UAP* mutant was reported in these two higher model animals; however, *UAP1* was found to be overexpressed in prostate cancer and protect against inhibitors of *N*-linked glycosylation, conferring a growth advantage (Itkonen et al., 2015). It is interesting to find that two *UAP* genes are found in the analyzed monocotyledons and dicotyledons (**Figure 2A**). The single gene mutants of *UAP1* and *UAP2* both showed no obvious phenotype in *Arabidopsis*, but their homozygous double mutant was lethal, reflecting the functional redundancy of these two genes in survival of *Arabidopsis* plants (Chen et al., 2014). In summary, the *UAP* genes play an essential role in the survival of cells or individuals for different organisms.

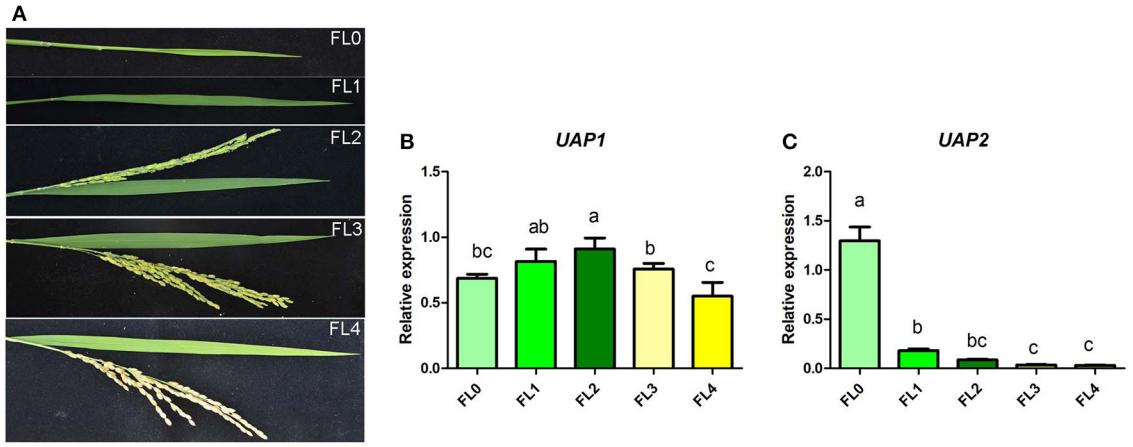

FIGURE 7 | Relative expression of the *UAP1* and *UAP2* genes during flag leaf development. **(A)** Flag leaf phenotype at unexpanded young leaf stage (FL0), booting stage (FL1), flowering stage (FL2), filling stage (FL3), and maturation stage (FL4). **(B,C)** Relative expression levels of the *UAP1* and *UAP2* genes. Data represent the mean ± *SD* of three biological replicates, and lowercase letters above columns indicate the statistically significant difference among all samples (one-way ANOVA). Relative expression of genes by qRT-PCR is normalized with reference genes *UBC*, *Profilin-2*, and *ARF*.

Possible Mechanisms by Which *UAP2* Cooperates With *UAP1* on Protecting Leaves From Lesion-Mimic Spots and Subsequent Early Senescence

The mutation of the *UAP1* gene in rice has lost its protein enzymatic function, leading to the appearance of phenotypes of lesion-mimic spots and early senescence in *uap1* (also called *spl29*) mutant leaves (Wang et al., 2015). However, it is interesting that every newly grown leaf of *uap1* could normally grow for a period of time, and then the defense response-related lesion-mimic spots and early leaf senescence appeared and became aggravated with the increase in growth time (**Figure 1A**). The UAP enzymatic function of the uap1 protein was found lost due to the substitution of a key single amino acid (Wang et al., 2015). This meant that the *uap1* mutant leaves lack the UAP1 enzymatic activity and there probably exists another enzyme compensating it.

A bioinformatic search on the rice genome database identified the *UAP2* gene, the homologous gene of *UAP1*. The two rice *UAP* genes are located on different chromosomes and controlled by different promoters. The *UAP2* and *UAP1* genes showed high homology for the nucleotide and protein sequences (**Supplementary Figure 1** and **Figure 2B**), implying that these two genes must have derived from a recent gene duplication event in rice. Transcriptional expression of the *UAP2* gene was high when the newly grown leaves of *uap1* were normal, but decreased a lot accompanying with the appearance and exacerbation of lesion-mimic sports and early leaf senescence (**Figure 3B**). It is seemed that the dosage effect and time specificity of the *UAP2* gene expression can influence the leaf cell death of the *uap1* mutant. Thus, we speculated that the high expression of the *UAP2* gene can compensate the lost function of the *UAP1* gene in *uap1* young leaves and that during the process of the leaf development to mature, the *UAP2* gene expression decreases and the function of total UAPs in the *uap1* leaf cells is not enough to maintain the normal growth, producing defense response-related lesion-mimic spots and early leaf senescence. In this study, the enzymatic assay verified that the UAP2 protein performed a very similar or overlapping UAP enzymatic activity with the UAP1 protein (**Figure 4**). And the UAP2 protein showed the same subcellular localization as the UAP1 protein (**Figure 5**), meaning that the UAP2 and UAP1 proteins perform their enzymatic reactions in the same cellular location. These molecular studies predominantly suggested that the *UAP2* gene was able to compensate for the lost function of the *UAP1* gene in *uap1* mutant. Eventually, the transgene of *UAP2* into *uap1* mutant recovered its leaf mutant phenotypes (**Figure 6**), providing direct evidence that the *UAP2* gene can perform similar biological functions as the *UAP1* gene, protecting the *uap1* mutant from lesion-mimic sports and subsequent early leaf senescence. In addition, transcriptional expression of the *UAP2* gene was high in young flag leaf, but decreased with the leaf becoming mature, while expression levels of the *UAP1* gene were continuously high during all analyzed leaf developmental stages (**Figure 7**), suggesting that the *UAP2* gene mainly functioned in young leaves, and the *UAP1* gene functioned in all leaf stages.

The Possible Role of Protein Glycosylation on Cell Death or Senescence

Protein glycosylation is essential for the proper folding, targeting, and functioning of proteins. So far, several studies have also been reported to reveal the glycosylation being involved in plant defense, senescence, and cell death. The *Arabidopsis* glucosyltransferase UGT76B1 conjugates isoleucic acid and modulates plant defense and senescence by small-molecule glucosylation (von Saint Paul et al., 2011). The rice OsDGL1, a homolog of an oligosaccharyltransferase complex subunit, is involved in *N*-glycosylation and cell death in the

root (Qin et al., 2013). The *N*-acetylglucosaminyltrasferase I (GnT1) mutant exhibited complete inhibition of *N*-glycan maturation, resulting in early lethality without transition to the reproductive stage in rice (Fanata et al., 2013). The rice *PLS2*, encoding a glycosyltransferase, its mutation makes premature leaf senescence begin at the tillering stage (Wang et al., 2018). Interestingly, a qualitative analysis of *N*-linked glycoproteome in the senescent flag leaf of rice has identified 183 *N*-glycoproteins involved in various and famous senescence-related biological processes (Huang et al., 2019).

N-Linked glycans are the components of most membrane-associated and secreted proteins in eukaryotic cells. And UDP-GlcNAc is an initial and key sugar donor of *N*-glycan synthesis for glycosylation. The *GNA1* encodes the glucosamine-6-phosphate acetyltransferase in the pathway for the biosynthesis of UDP-GlcNAc. And the *gna1* mutants in *Arabidopsis* and rice showed temperature-sensitive growth defects of the root, accompanying with insufficient biosynthesis of endogenous UDP-GlcNAc and impairment of protein *N*-glycosylation (Jiang et al., 2005; Nozaki et al., 2012). In rice, UAP1 is the very enzyme for the catalytic synthesis of UDP-GlcNAc, and functional inactivation of UAP1 induces early leaf senescence and defense responses (Wang et al., 2015). In *Arabidopsis*, GlcNAc1pUT-1 and GlcNAc1pUT-2 catalyze the biosynthesis of UDP-GlcNAc (Yang et al., 2010). The single mutants *glcna.ut1* and *glcna.ut2* revealed no obvious phenotype but their homozygous double mutant was lethal, revealing the GlcNAc1pUTs' indispensable role in the unique mediation of gametogenesis and embryogenesis, despite the overlapping functions (Chen et al., 2014). Taking together, the synthesis defect for UDP-GlcNAc leads to cell death in different plant tissues, probably attributing to the divergent demand for UDP-GlcNAc contents in these tissues to sustain normal cell survival. In this study, the UAP2 protein is found to be able to synthesize UDP-GlcNAc, just as the UAP1 protein does (**Figure 4A**). Meanwhile, the UAP1 and UAP2 proteins are both localized in the cytoplasm in rice (**Figure 5**), where they can function to synthesize UDP-GlcNAc, and this is coincident with the fact that GlcNAc is used for the *N*-glycan biosynthesis on the cytosolic side of the endoplasmic reticulum (ER) (Stanley et al., 2015). It is speculated that the dosage defect of UDP-GlcNAc and subsequently induced abnormal of protein glycosylation are responsible for the mutant phenotypes of *uap1*. Although there is no direct evidence linking UDP-GlcNAc with the lesion-mimic spots and early leaf senescence phenotypes found in *uap1* mutants, it will be interesting to study the UDP-GlcNAc levels, protein glycosylation status, and the downstream molecular pathways in the future, to better reveal the biological roles of the *UAP* proteins in leaf survival.

CONCLUSION

Our data demonstrate that *UAP2*, the homologous gene of *UAP1*, could maintain the short period's normal growth of the *uap1* mutant leaves. The expression level of the *UAP2* gene was high in the initial normal growth stage, but decreased accompanying with the appearance of defense response-related lesion-mimic spots and early senescence of the *uap1* mutant leaves. The UAP2 protein performed a very similar UAP enzymatic activity with the UAP1 protein. And these two UAP proteins were both localized in the cytoplasm to perform their function. Overexpression of the *UAP2* gene in the *uap1* mutant could rescue its mutant phenotype, confirming the similar molecular and biological function of the *UAP2* gene with the *UAP1* gene. The *UAP2* gene was mainly expressed in the young leaves, while the *UAP1* gene maintains continuous high expression during the whole leaf development. Taking together, rice UAP2 cooperates with UAP1 to perform a synergetic function for leaf survival during its developmental process, protecting the leaf from early senescence. However, further investigation is required to elucidate the downstream pathways underlying rice *UAPs*.

DATA AVAILABILITY STATEMENT

The original contributions presented in the study are included in the article/**Supplementary Materials**, further inquiries can be directed to the corresponding author/s.

AUTHOR CONTRIBUTIONS

ZW conceptualized this study research and wrote the manuscript. QW and LW did experiments for transgenic plants. YS helped in the data analysis. TL helped in language revision. KH performed qRT-PCR for *UAP* genes in flag leaves. SL and HZho performed bioinformatic analysis. HZha and JL helped in bioinformatic analysis and manuscript revision. YL helped in molecular experiments. YH helped in data consolidation and manuscript revision. All authors contributed to the article and approved the submitted version.

FUNDING

This work was supported by the National Natural Science Foundation of China (Grant Numbers 31760380 and 32060071), the National Key Research and Development Project (2016YFD0100400), and the Science and Technology Projects of Jiangxi Province (20181BAB214011).

SUPPLEMENTARY MATERIAL

The Supplementary Material for this article can be found online at: https://www.frontiersin.org/articles/10.3389/fpls.2021.685102/full#supplementary-material

Supplementary Figure 1 | Alignment of the coding sequences of the *UAP1* and *UAP2* genes.

Supplementary Figure 2 | SDS/PAGE of proteins. Lane 1, prestained protein ladder. Total soluble proteins from *E.coli* cells expressing control empty vector (lane 2), recombinant *UAP1* (lane 3), and recombinant *UAP2* (lane 4). Purified GST (lane 5), GST-UAP1 (lane 6), and GST-UAP2 (lane 7) proteins. Bands of GST, GST-UAP1, and GST-UAP2 are indicated by *arrows*.

Supplementary Table 1 | All primers used for qRT-PCR analysis.

Supplementary Table 2 | Primers for vector construction and confirmation of positive transgenic plants.

REFERENCES

Arakane, Y., Baguinon, M. C., Jasrapuria, S., Chaudhari, S., Doyungan, A., Kramer, K. J., et al. (2011). Both UDP N-acetylglucosamine pyrophosphorylases of *Tribolium castaneum* are critical for molting, survival and fecundity. *Insect Biochem. Mol. Biol.* 41, 42–50. doi: 10.1016/j.ibmb.2010.09.011

Chen, Y. H., Shen, H. L., Hsu, P. J., Hwang, S. G., and Cheng, W. H. (2014). N-acetylglucosamine-1-P uridylyltransferase 1 and 2 are required for gametogenesis and embryo development in *Arabidopsis thaliana*. *Plant Cell Physiol.* 55, 1977–1993. doi: 10.1093/pcp/pcu127

Fanata, W. I., Lee, K. H., Son, B. H., Yoo, J. Y., Harmoko, R., Ko, K. S., et al. (2013). N-glycan maturation is crucial for cytokinin-mediated development and cellulose synthesis in *Oryza sativa*. *Plant J.* 73, 966–979. doi: 10.1111/tpj.12087

Fang, W., Du, T., Raimi, O. G., Hurtado-Guerrero, R., Urbaniak, M. D., Ibrahim, A. F., et al. (2013). Genetic and structural validation of *Aspergillus fumigatus* UDP-N-acetylglucosamine pyrophosphorylase as an antifungal target. *Mol. Microbiol.* 89, 479–493. doi: 10.1111/mmi.12290

Hancock, J. F. (2004). GPI-anchor synthesis: Ras takes charge. *Dev Cell* 6, 743–745. doi: 10.1016/j.devcel.2004.05.011

Huang, X., Zhang, H., Liao, J., Wei, L., Guo, R., Xiao, W., et al. (2019). Qualitative analysis of N-linked glycoproteome in senescent flag leaf of rice. *Plant Growth Regul.* 88, 309–326. doi: 10.1007/s10725-019-00509-y

Itkonen, H. M., Engedal, N., Babaie, E., Luhr, M., Guldvik, I. J., Minner, S., et al. (2015). UAP1 is overexpressed in prostate cancer and is protective against inhibitors of N-linked glycosylation. *Oncogene* 34, 3744–3750. doi: 10.1038/onc.2014.307

Jiang, H., Wang, S., Dang, L., Wang, S., Chen, H., Wu, Y., et al. (2005). A novel short-root gene encodes a glucosamine-6-phosphate acetyltransferase required for maintaining normal root cell shape in rice. *Plant Physiol.* 138, 232–242. doi: 10.1104/pp.104.058248

Katoh, K., and Standley, D. M. (2013). MAFFT multiple sequence alignment software version 7: improvements in performance and usability. *Mol. Biol. Evol.* 30, 772–780. doi: 10.1093/molbev/mst010

Lee, R. H., Wang, C. H., Huang, L. T., and Chen, S. C. (2001). Leaf senescence in rice plants: cloning and characterization of senescence up-regulated genes. *J. Exp. Bot.* 52, 1117–1121. doi: 10.1093/jexbot/52.358.1117

Liang, C., Wang, Y., Zhu, Y., Tang, J., Hu, B., Liu, L., et al. (2014). OsNAP connects abscisic acid and leaf senescence by fine-tuning abscisic acid biosynthesis and directly targeting senescence-associated genes in rice. *Proc. Natl. Acad. Sci. U.S.A.* 111, 10013–10018. doi: 10.1073/pnas.1321568111

Liu, X., Li, F., Li, D., Ma, E., Zhang, W., Zhu, K. Y., et al. (2013). Molecular and functional analysis of UDP-N-acetylglucosamine pyrophosphorylases from the migratory locust, *Locusta migratoria*. *PLoS ONE* 8:e71970. doi: 10.1371/journal.pone.0071970

Lorrain, S., Vailleau, F., Balague, C., and Roby, D. (2003). Lesion mimic mutants: keys for deciphering cell death and defense pathways in plants? *Trends Plant Sci.* 8, 263–271. doi: 10.1016/S1360-1385(03)00108-0

Mengin-Lecreulx, D., and van Heijenoort, J. (1993). Identification of the glmU gene encoding N-acetylglucosamine-1-phosphate uridyltransferase in *Escherichia coli*. *J. Bacteriol.* 175, 6150–6157. doi: 10.1128/jb.175.19.6150-6157.1993

Mio, T., Yabe, T., Arisawa, M., and Yamada-Okabe, H. (1998). The eukaryotic UDP-N-acetylglucosamine pyrophosphorylases. Gene cloning, protein expression, and catalytic mechanism. *J. Biol. Chem.* 273, 14392–14397. doi: 10.1074/jbc.273.23.14392

Nozaki, M., Sugiyama, M., Duan, J., Uematsu, H., Genda, T., and Sato, Y. (2012). A missense mutation in the glucosamine-6-phosphate N-acetyltransferase-encoding gene causes temperature-dependent growth defects and ectopic lignin deposition in Arabidopsis. *Plant Cell* 24, 3366–3379. doi: 10.1105/tpc.112.102806

Peneff, C., Ferrari, P., Charrier, V., Taburet, Y., Monnier, C., Zamboni, V., et al. (2001). Crystal structures of two human pyrophosphorylase isoforms in complexes with UDPGlc(Gal)NAc: role of the alternatively spliced insert in the enzyme oligomeric assembly and active site architecture. *EMBO J.* 20, 6191–6202. doi: 10.1093/emboj/20.22.pbr6191

Qin, C., Li, Y., Gan, J., Wang, W., Zhang, H., Liu, Y., et al. (2013). OsDGL1, a homolog of an oligosaccharyltransferase complex subunit, is involved in N-glycosylation and root development in rice. *Plant Cell Physiol.* 54, 129–137. doi: 10.1093/pcp/pcs159

Raetz, C. R., and Whitfield, C. (2002). Lipopolysaccharide endotoxins. *Annu. Rev. Biochem.* 71, 635–700. doi: 10.1146/annurev.biochem.71.110601.135414

Schimmelpfeng, K., Strunk, M., Stork, T., and Klambt, C. (2006). Mummy encodes an UDP-N-acetylglucosamine-dipohosphorylase and is required during Drosophila dorsal closure and nervous system development. *Mech. Dev.* 123, 487–499. doi: 10.1016/j.mod.2006.03.004

Shi, J. F., Fu, J., Mu, L. L., Guo, W. C., and Li, G. Q. (2016). Two *Leptinotarsa uridine* diphosphate N-acetylglucosamine pyrophosphorylases are specialized for chitin synthesis in larval epidermal cuticle and midgut peritrophic matrix. *Insect Biochem. Mol. Biol.* 68, 1–12. doi: 10.1016/j.ibmb.2015.11.005

Stanley, P., Taniguchi, N., and Aebi, M. (2015). "N-Glycans," in *Essentials of Glycobiology*, eds A. Varki, R. D. Cummings, J. D. Esko, P. Stanley, G. W. Hart, M. Aebi, A. G. Darvill, T. Kinoshita, N. H. Packer, J. H. Prestegard, R. L. Schnaar and P. H. Seeberger (Cold Spring Harbor, NY: Cold Spring Harbor Laboratory Press), 99–111.

Stokes, M. J., Guther, M. L., Turnock, D. C., Prescott, A. R., Martin, K. L., Alphey, M. S., et al. (2008). The synthesis of UDP-N-acetylglucosamine is essential for bloodstream form *Trypanosoma brucei in vitro* and *in vivo* and UDP-N-acetylglucosamine starvation reveals a hierarchy in parasite protein glycosylation. *J. Biol. Chem.* 283, 16147–16161. doi: 10.1074/jbc.M709581200

von Saint Paul, V., Zhang, W., Kanawati, B., Geist, B., Faus-Kessler, T., Schmitt-Kopplin, P., et al. (2011). The Arabidopsis glucosyltransferase UGT76B1 conjugates isoleucic acid and modulates plant defense and senescence. *Plant Cell* 23, 4124–4145. doi: 10.1105/tpc.111.088443

Wang, M., Zhang, T., Peng, H., Luo, S., Tan, J., Jiang, K., et al. (2018). Rice premature leaf senescence 2, encoding a Glycosyltransferase (GT), is involved in leaf senescence. *Front. Plant Sci.* 9:560. doi: 10.3389/fpls.2018.00560

Wang, Z., Wang, Y., Hong, X., Hu, D., Liu, C., Yang, J., et al. (2015). Functional inactivation of UDP-N-acetylglucosamine pyrophosphorylase 1 (UAP1) induces early leaf senescence and defense responses in rice. *J. Exp. Bot.* 66, 973–987. doi: 10.1093/jxb/eru456

Wang, Z., Wang, Y., Yang, J., Hu, K., An, B., Deng, X., et al. (2016). Reliable selection and holistic stability evaluation of reference genes for rice under 22 different experimental conditions. *Appl. Biochem. Biotechnol.* 179, 753–775. doi: 10.1007/s12010-016-2029-4

Wang-Gillam, A., Pastuszak, I., and Elbein, A. D. (1998). A 17-amino acid insert changes UDP-N-acetylhexosamine pyrophosphorylase specificity from UDP-GalNAc to UDP-GlcNAc. *J. Biol. Chem.* 273, 27055–27057.

Waterhouse, A. M., Procter, J. B., Martin, D. M., Clamp, M., and Barton, G. J. (2009). Jalview Version 2–a multiple sequence alignment editor and analysis workbench. *Bioinformatics* 25, 1189–1191. doi: 10.1093/bioinformatics/btp033

Yang, J., Yan, R., Roy, A., Xu, D., Poisson, J., and Zhang, Y. (2015). The I-TASSER Suite: protein structure and function prediction. *Nat Methods* 12, 7–8. doi: 10.1038/nmeth.3213

Yang, T., Echols, M., Martin, A., and Bar-Peled, M. (2010). Identification and characterization of a strict and a promiscuous N-acetylglucosamine-1-P uridylyltransferase in Arabidopsis. *Biochem. J.* 430, 275–284. doi: 10.1042/BJ20100315

Yu, C., Wang, L., Chen, C., He, C., Hu, J., Zhu, Y., et al. (2014). Protoplast: a more efficient system to study nucleo-cytoplasmic interactions. *Biochem. Biophys. Res. Commun.* 450, 1575–1580. doi: 10.1016/j.bbrc.2014.07.043

Zhang, J., Zhang, Y., Du, Y., Chen, S., and Tang, H. (2011). Dynamic metabonomic responses of tobacco (*Nicotiana tabacum*) plants to salt stress. *J. Proteome Res.* 10, 1904–1914. doi: 10.1021/pr101140n

Zhang, W., Jones, V. C., Scherman, M. S., Mahapatra, S., Crick, D., Bhamidi, S., et al. (2008). Expression, essentiality, and a microtiter plate assay for mycobacterial GlmU, the bifunctional glucosamine-1-phosphate acetyltransferase and N-acetylglucosamine-1-phosphate uridyltransferase. *Int. J. Biochem. Cell Biol.* 40, 2560–2571. doi: 10.1016/j.biocel.2008.05.003

Zhang, Y., and Skolnick, J. (2005). TM-align: a protein structure alignment algorithm based on the TM-score. *Nucleic Acids Res.* 33, 2302–2309. doi: 10.1093/nar/gki524

Conflict of Interest: The authors declare that the research was conducted in the absence of any commercial or financial relationships that could be construed as a potential conflict of interest.

frontiers in Plant Science

ORIGINAL RESEARCH
published: 28 June 2021
doi: 10.3389/fpls.2021.679852

Dynamics of Foliar Responses to O_3 Stress as a Function of Phytotoxic O_3 Dose in Hybrid Poplar

Benjamin Turc[1,2], Pierre Vollenweider[2], Didier Le Thiec[1], Anthony Gandin[1], Marcus Schaub[2], Mireille Cabané[1] and Yves Jolivet[1]*

[1]University of Lorraine, AgroParisTech, INRAE, SILVA, Nancy, France, [2]Section Forest Dynamics, Swiss Federal Institute for Forest, Snow and Landscape Research WSL, Birmensdorf, Switzerland

With background concentrations having reached phytotoxic levels during the last century, tropospheric ozone (O_3) has become a key climate change agent, counteracting carbon sequestration by forest ecosystems. One of the main knowledge gaps for implementing the recent O_3 flux-based critical levels (CLs) concerns the assessment of effective O_3 dose leading to adverse effects in plants. In this study, we investigate the dynamics of physiological, structural, and morphological responses induced by two levels of O_3 exposure (80 and 100 ppb) in the foliage of hybrid poplar, as a function of phytotoxic O_3 dose (POD_0) and foliar developmental stage. After a latency period driven by foliar ontological development, the gas exchanges and chlorophyll content decreased with higher POD_0 monotonically. Hypersensitive response-like lesions appeared early during exposure and showed sigmoidal-like dynamics, varying according to leaf age. At current POD_{1_SPEC} CL, notwithstanding the aforementioned reactions and initial visible injury to foliage, the treated poplars had still not shown any growth or biomass reduction. Hence, this study demonstrates the development of a complex syndrome of early reactions below the flux-based CL, with response dynamics closely determined by the foliar ontological stage and environmental conditions. General agreement with patterns observed in the field appears indicative of early O_3 impacts on processes relevant, e.g., biodiversity ecosystem services before those of economic significance – i.e., wood production, as targeted by flux-based CL.

Keywords: ozone, poplar, hypersensitive response-like, accelerated cell senescence, foliar response

OPEN ACCESS

Edited by:
Nam-Chon Paek, Seoul National University, South Korea

Reviewed by:
Neil J. Willey, University of the West of England, United Kingdom
Ling Li, Mississippi State University, United States

****Correspondence:***
Benjamin Turc
benjamin.turc@univ-lorraine.fr

Specialty section:
This article was submitted to Plant Physiology, a section of the journal Frontiers in Plant Science

Received: *25 March 2021*
Accepted: *03 June 2021*
Published: *28 June 2021*

Citation:
Turc B, Vollenweider P, Le Thiec D, Gandin A, Schaub M, Cabané M and Jolivet Y (2021) Dynamics of Foliar Responses to O_3 Stress as a Function of Phytotoxic O_3 Dose in Hybrid Poplar. Front. Plant Sci. 12:679852. doi: 10.3389/fpls.2021.679852

INTRODUCTION

The ground-level concentrations of ozone (O_3) have increased during the past century (Maas and Grennfelt, 2016), and are predicted to remain stable or increase during the 21st century (Revell et al., 2015; Fu and Tian, 2019). They have already reached levels negatively affecting crop plants and the natural vegetation (Wittig et al., 2009; Jolivet et al., 2016; Proietti et al., 2016; Li et al., 2017), and steady or increasing impacts are expected over the course of next decades (Karlsson et al., 2017).

Once entering the leaf through stomata, O_3 degradation causes the formation of reactive oxygen species (ROS), the accumulation of which triggers rapid oxidative bursts (Schraudner et al., 1998; Pasqualini et al., 2003; Moura et al., 2018). ROS can also act as elicitors of programed cell death (PCD) reminiscent of plant responses during defensive plant/pathogen interactions which are subsequently designated as hypersensitive response-like (HR-like; Vollenweider et al., 2002; Bhattacharjee, 2005; Günthardt-Goerg and Vollenweider, 2007; Moura et al., 2018). In parallel, an acceleration of cell senescence (ACS), with distinct apparent mechanisms, can be observed (Pell et al., 1999; Günthardt-Goerg and Vollenweider, 2007; Vollenweider et al., 2019). The characteristic symptoms thus include marked degenerative injuries in chloroplasts, in apparent relation to an increase in the constitutive ROS load resulting from the daily photosynthetic activity. As a consequence, these latter organelles are particularly sensitive to O_3 stress (Joo et al., 2005; Kangasjarvi et al., 2005). However, the sequence of plant reactions in response to O_3 stress remains unclear, especially given the driving – but still partially understood – effects of interacting environmental conditions and ontological development. In field vs. climate chamber conditions, for example, the high vs. low-intensity illumination can lead to contrasted symptom expression, with clear synergies between photooxidative and O_3 stress in the former case only (Günthardt-Goerg and Vollenweider, 2007; Paoletti et al., 2009; Moura et al., 2018; Vollenweider et al., 2019). Hence, the dynamics of responses to O_3 stress as a function of environmental conditions needs further research.

Although the effects of O_3 stress have been observed in both mature and developing foliage, their intensity is strongly related to the leaf ontology, the mature leaves being more sensitive than those still in expansion. However, the younger vs. older leaves can show higher rates of stomatal conductance and O_3 uptake (Reich, 1983; Strohm et al., 1999; Bagard et al., 2008; Zhang et al., 2010; Guerrero et al., 2013), suggesting an enhanced detoxification capacity (Bellini and De Tullio, 2019). Still, the mechanisms underlying the higher O_3 tolerance in developing foliage remain largely obscure (Strohm et al., 2002) and the differences in response dynamics as a function of leaf ontogenetic development require further investigations.

To assess and prevent O_3 injury on vegetation and forest trees, a concentration-based index, namely, the accumulated O_3 exposure threshold over 40 ppb (AOT40), was initially proposed (Fuhrer et al., 1997). Given the dependency of O_3 phytotoxicity on stomatal conductance, the biologically (Karlsson et al., 2007; Mills et al., 2011) and environmentally (Musselman et al., 2006; Dizengremel et al., 2013; Büker et al., 2015) more relevant flux-based approach has been increasingly implemented. Nowadays, the O_3 critical level (CL) is defined for given vegetation types or plant species and calculated as the Phytotoxic O_3 Dose over a Y threshold for a specific species or group of species (POD_{Y_SPEC} (Mills et al., 2017). Based on empirical evidence from risk assessment studies – linking POD_{Y_SPEC} values to tree biomass loss or foliar injury – the current CL typically targets 4% maximum, i.e., growth reductions by oxidative stress. However, such markers represent some late O_3 stress effects, at least partly resulting from earlier processes in foliage (i.e., reduced physiological activity/extensive cellular injury) which dynamics primarily depends on detoxification processes (Dghim et al., 2013; Dumont et al., 2014; Dusart et al., 2019a). With a view to the larger implementation and acceptance of flux-based approach, there is then an important knowledge gap regarding the dynamics and effective POD_x of first effective O_3 stress effects, prior to the appearance of current risk assessment markers.

In this study, our main objective was to characterize the dynamics of early physiological and structural responses to O_3 stress in poplar trees as a function of flux-based O_3 dose and before, e.g., growth reduction and extensive foliar injury, the primary markers of O_3 stress for defining O_3 CL (Sanz and Catalayud, 2011; Mills et al., 2017). The tested hypotheses (H) included: (H1) the development of injury and growth response to O_3 stress, as well as physiological and structural changes, proceeds in sequential order, with each response showing specific dynamics; (H2a) O_3 elicits different injury responses within the foliage of trees (H2b) with ACS occurring before the development of HR-like lesions (Vollenweider et al., 2019); (H3a) at comparable O_3 dose and irrespective of the applied O_3 concentration, leaves show similar responses and (H3b) response dynamics; (H4) the dynamics of responses depends on the leaf developmental stage (Moura et al., 2018). Therefore, rooted cuttings of hybrid poplar (*Populus tremula x alba*) were exposed to three O_3 concentrations in fully controlled conditions for a month. The leaf physiology, development of ACS and HR-like lesions, and appearance of visible injuries were monitored over the course of 29 days. The interaction between foliar response dynamics and leaf ontological development was evaluated by assessing the responses to treatments at two distinct leaf positions.

MATERIALS AND METHODS

Plant Material and Controlled O_3 Exposure

Young trees from a hybrid *Populus tremula x alba* clone (INRAE 717-1b4) were cultivated similarly to Cabane et al. (2004). Before the experimental exposure, micro propagated cuttings were grown for 2 weeks in 0.5 L pots containing compost (Gramoflor Universel) and perlite [1:1 (v/v)], and placed in containers covered with transparent acrylic hoods inside a growth chamber. The environmental conditions were set at 22°C/18°C day/night temperature, 350 μmol m^{-2} s^{-1} photosynthetic active radiation (PAR, 1 m below lamps) during a 14-h photoperiod (Philips Son-T Agro 400 W lamps), 75%/85% relative humidity (day/night). The young trees were then transplanted into 10 L pots filled with compost (Gramoflor Universel) and fertilized with 3 g l^{-1} of slow-release Nutricot T 100 granules (13:13:13:2 N:P:K:MgO, Fertil, Boulogne-Billancourt, France). They were further cultivated for 1 month in the same growth chamber and watered to field capacity every day. The trees retained (n = 48), with a view to the forthcoming O_3 exposure experiments, were 29.5 ± 0.2 cm high, with 13.1 ± 0.1 leaves. During experiments, all foliar assessments were repeated at the third and tenth leaf position

from the tree base, thus selecting the youngest fully expanded leaf and that still in expansion at treetop by the start of exposure.

Before exposure, the selected trees were randomly distributed among six ventilated phytotron chambers (1 air change min^{-1}; 120 cm × 117 cm and 204 cm high) within the O_3-exposure facility of the PEPLor platform (Faculty of Sciences and Technologies, University of Lorraine). Within each chamber ($N = 8$ trees), the plant position was randomized by each assessment. The transferred poplars were then left to acclimate for 1 week, with environmental conditions similar to those in the growth chamber. The O_3 exposure experiment included three treatments [charcoal-filtered (CF) air; CF + 80 ppb O_3; CF + 100 ppb O_3] replicated in two chambers each and performed for 30 days ($N = 16$ trees per treatment). O_3 was generated from pure oxygen using an O_3 generator (Innovatec II, Rheinbach, Germany), and provided to the chambers during the daytime period in the form of a 13 h square wave, starting 1 h after the light was switched on. The O_3 concentrations within each phytotron chamber were monitored twice an hour using a computer-assisted automatic O_3 analyzer (O341M, Environment SA, Paris).

Dynamics of Leaf Physiology Responses and Estimation of Phytotoxic O_3 Dose

The effect of treatments on the dynamics of leaf gas exchanges was assessed by measuring the net CO_2 assimilation rates (A_{net}) and stomatal conductance to water vapor (g_w) every 2 days, 3 h after starting the O_3 exposure. Selecting six trees per treatment, the measurements were performed using a Li-6400XT portable photosynthesis system (LiCor, Inc., Lincoln, NE, United States), with cuvette temperature set at 22°C, light intensity (PAR) at 300 and 320 µmol m^{-2} s^{-1} for measurements at the third and tenth leaf position, respectively, airflow at 300 µmol s^{-1}, CO_2 concentration at 400 ppm, and leaf vapor pressure deficit (VPD_{leaf}) < 1 kPa. The values were recorded once g_w and A_{net} remained stable for 30 s.

The g_w estimates (mol H_2O m^{-2} s^{-1}) were used to calculate the instantaneous O_3 uptake into the leaf under environmental stable conditions (F_{O_3}), according to Bagard et al. (2015):

$$F_{O_3} = [O_3]_{atm} * g_{O_3}$$

with F_{O_3} as the O_3 flux (nmol O_3 m^{-2} s^{-1}), $[O_3]_{atm}$ as the O_3 concentration (ppb) in the phytotron chamber, and g_{O_3} (O_3 m^{-2} s^{-1}) as the stomatal conductance to O_3, according to (Lamaud et al., 2009):

$$g_{O_3} = \frac{D_{O_3}}{D_{H_2O}} * g_w$$

with D_{O_3} and D_{H_2O} as the O_3 and water molecular diffusivity (cm^{-2} s^{-1}) respectively (Massman, 1998). The hourly O_3 uptake (mmol O_3 m^{-2} h^{-1}) was calculated by integrating F_{O_3} over an hour and the POD_0 (mmol O_3 m^{-2}), by cumulating the hourly O_3 uptake since the beginning of experiment. Missing g_w measurements were estimated based on values from flanking days (Bagard et al., 2008).

The effect of treatments on the dynamics of leaf chlorophyll content was assessed by measuring estimates of surface-based concentrations of chlorophylls (total chlorophyll index) every day, 1 h after switching the light on and before the start of O_3 treatment. Selecting six trees per treatment, the estimates were obtained averaging 10 measurements per leaf performed with a leaf clamp sensor device (Dualex Force-A, Orsay, France).

Dynamics of Microscopic and Visible Leaf Injury

The development of HR-like lesions within the mesophyll and that of O_3 symptoms throughout foliage was monitored using completing microscopic assessments and visible injury observations. For microscopic assessments, two discs (diameter = 6 mm) per leaf position in two trees per chamber were sampled every 2 days, until HR-like lesions were detected in the 100 ppb O_3 treatment at both leaf positions; the sampling interval was then extended (3–6 days). The harvested discs were processed immediately after sampling.

Necrotic cells within mesophyll as a consequence of HR-like lesions were evidenced using the Trypan blue assay (Pasqualini et al., 2003; Joo et al., 2005; Faoro and Iriti, 2009). Briefly, the leaf discs were stained for 3 min in a hot lactophenol Trypan blue mixture (60 ml staining solution: 10 g phenol, 10 mg Trypan blue, 30 ml ethanol, 10 ml glycerol, 10 ml lactic acid, and 10 ml distilled water) and the necrotic cells contrasted for 20 min against a clear background using 2.5 g ml^{-1} hot chloral hydrate, before mounting in 60% glycerol (Pasqualini et al., 2003). The preparations were then transferred to WSL where all microscopy assessments were performed. The disk's central part, free of staining artifacts, was observed using the 5× objective of a Leica microscope (Leitz DM/RB). Given the disk thickness (>200 µm) and to create high contrast pictures, the preparations were imaged after inserting the 10x condenser and removing most filters and diaphragms, using the INFINITY 2-1R camera and Lumenera Infinity Analyze (release 6.4) software (Lumenera Corp., Ottawa, ON, Canada). The center of each disk preparation was photographed, creating composite images made of nine tiles each. The percentage area, particle size, and shape properties of HR-like lesions inside of stitched images were quantified using computer-assisted color image analysis (software WinCELL™ 2004, Regent Instruments Inc., Québec, QC, Canada). Briefly, the software attributed the whole lesion or part of it to one of two color classes (non-oxidized: violet hue; oxidized: dark blue hue) made of 10 shades each, defined based on a representative batch of images and contrasting with the background color class (grayish hue, based on 10 white to gray shades). The quantified parameters characterized the size and shape properties of total and individual lesion particles.

The HR-like lesions and oxidation diagnosis were verified based on hand, and semi-thin sections from samples collected in all treatments at the two leaf positions during the whole study and subsequently processed and observed as described previously (Moura et al., 2018). Briefly, supplementary leaf discs were infiltrated upon sampling with EM-grade 2.5%

glutaraldehyde buffered at pH 7.0 with 0.067 M Soerensen phosphate buffer, renewed after vacuum infiltration. Sections (60 µm) obtained using a custom-made hand microtome and kept unstained were used for visualizing chlorophylls and the oxidation of HR-like lesions. Technovit-embedded 1.5 µm sections, obtained using a Supercut Reichert 2050 microtome and stained with Toluidine blue (Vollenweider et al., 2016), were used to identify HR-like markers within necrotic mesophyll cells, after observation with phase contrast illumination in bright field microscopy using the 5–100× objectives of the Leica microscope and imaged using the Infinity camera, as mentioned above.

The development of O_3 injury in response to treatments was surveyed in the morning, before the start of O_3 exposure, daily. Upon appearance, the development of visible injury was monitored with pictures of symptomatic leaves. The percentage area of necrosis per leaf within the latter material was quantified using color image analysis, using the Color Segmentation plugin in Fiji freeware (ver. 2.0.0; Schindelin et al., 2012).

Morphological Assessments

After 30 days of exposure, all trees were harvested and biometric assessments were conducted. Tree height was recorded and stem diameter 1.5 cm above root collar was measured, using a hand caliper. The number of leaves per tree, shed or still attached, was recorded before harvest. Leaf and stem material was oven-dried to constant weight, before determining the dry mass of each fraction.

Statistical Analysis

The dynamics of physiological and structural responses to treatments in foliage and the differences in whole-tree morphology and biomass between groups by the end of the experiment were analyzed using linear mixed-effects models (lmem). The fixed-effect factors included the O_3 treatment, leaf position, time or POD_0 and interactions, whereas the tree nested in the chamber (leaf data; with the leaf position as the statistical unit) or the chamber (morphology/biomass data; with the tree as the statistical unit) were introduced in models as random terms. Homoscedasticity and normality of residuals were verified graphically, and the dependent variables were log- or square-transformed to meet the model assumptions, as needed. The differences between treatments at given assessment dates were tested using *post-hoc* tests (Tukey's honest significant difference). All statistical analyses were performed using R statistical software, version 3.5.0 (R Development Core Team, 2017), with the packages lme4 (Bates et al., 2015) for linear mixed-effects models, and emmeans (Lenth, 2016) for *post-hoc* testing.

RESULTS

Morphological Responses

After 30 days of exposure, no change in tree height, stem diameter, or foliar dry mass in response to O_3 exposure was observed (**Table 1**). However, the stem biomass ($p = 0.014$), amount of leaves ($p = 0.003$), and leaf shedding ($p = 1.2 \times 10^{-6}$) were increased, with significant differences between the 80 and 100 ppb O_3 treatments in the case of leaf shedding.

Dynamics of Stomatal Responses and Changes in the Phytotoxic O_3 Dose

At both leaf positions, the 100 and 80 ppb O_3 treatments significantly reduced g_w (**Figure 1A**; O_3 treatment: $p < 0.001$) and accelerated its leaf ontology-driven decrease (O_3 treatment*Time: $p < 0.001$). This reduction was delayed at the tenth vs. third leaf position (O_3 treatment*leaf position, O_3 treatment*time*leaf position: $p < 0.001$), with a 50% decrease in g_w reached in 15 vs. 6 days, respectively, in the 100 ppb treatment. As indicated by increasing g_w in maturing leaves (tenth leaf position) during the first 10 days of exposure irrespective of O_3 exposure (leaf position: $p < 0.001$), the O_3 treatment affected g_w only once the ontological development had been achieved (latency phase, **Figure 1A**). By the end of the experiment and only at the tenth leaf position, the differences in g_w between the 100 and 80 ppb treatments were significant.

By the end of the experiment, trees in the 100 vs. 80 ppb O_3 treatment showed a larger POD_0, as a consequence of their higher O_3 concentrations and mostly similar g_w (**Figure 1B**; O_3 treatment, O_3 treatment*time: $p < 0.001$). After 30 days of exposure, the POD_0 at the third and tenth leaf positions was thus 1.4 and 1.2 times higher in the 100 vs., 80 ppb O_3 treatments. The POD_0 was also higher in leaves at the tenth vs. third leaf position (leaf position: $p < 0.001$), as a consequence of the delayed leaf ontogeny and higher g_w (O_3 treatment*leaf position: $p < 0.001$). After 10 days of exposure, the POD_0 levels in younger foliage thus exceeded those in older material by approximately 25% and outpaced them by 40% by the end of exposure (O_3 treatment*time*leaf position: $p < 0.001$).

TABLE 1 | Morphological responses to O_3 treatments in hybrid poplar (*Populus tremula x alba*) at the end of the experiment.

Treatment	Tree height (cm)	Stem diameter (mm)	Foliage biomass (g)	Stem dry mass (g)	Leaf shedding (%)	Leaf number
Charcoal-filtered	100.31 ± 0.95	9.93 ± 0.18	30.09 ± 0.86	15.72 ± 0.53a	1.59 ± 0.81a	33.31 ± 0.54a
80 ppb ozone	104.38 ± 1.66	10.16 ± 0.33	31.54 ± 1.50	17.51 ± 0.91b	7.41 ± 1.99b	35.00 ± 0.61b
100 ppb ozone	101.75 ± 0.81	10.23 ± 0.12	28.83 ± 0.61	16.50 ± 0.39ab	16.94 ± 2.21c	35.44 ± 0.39b
Treatment	ns	ns	ns	*	***	**

*model: lmer(variable) ~ O_3 treatment + (1 | chamber); ***$p \leq 0.001$; **$p \leq 0.01$; *$p \leq 0.05$; ns, not significantly different. Values represent means ± SE, n = 16. Different letters indicate significant differences between treatments by the end of experiment (post-hoc Tukey's honest significant difference, $p \leq 0.05$).*

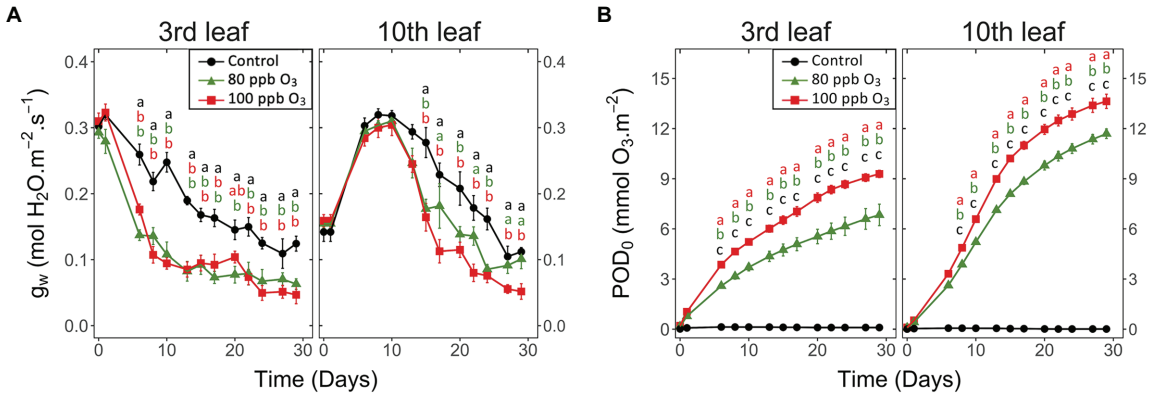

	g_w
O_3 treatment	***
Leaf Position	***
Time	***
O_3 treatment:Time	***
O_3 treatment:Leaf Position	***
Leaf Position:Time	***
O_3 treatment:Time:Leaf Position	***

	POD_0
O_3 treatment	***
Leaf Position	***
Time	***
O_3 treatment:Time	***
O_3 treatment:Leaf Position	***
Leaf Position:Time	***
O_3 treatment:Time:Leaf Position	***

FIGURE 1 | Dynamics of changes in the **(A)** stomatal conductance to water (g_w) and **(B)** phytotoxic O_3 dose (POD_0) of hybrid poplar leaves (*Populus tremula x alba*), as a function of O_3 treatment (charcoal-filtered air ●, 80 ppb O_3 ▲, 100 ppb O_3 ■), leaf position, time of assessment and interactions {model: lmer[sqrt(variable)] ~ O_3 treatment * leaf position * time + (1 | tree / chamber); *** $p \leq 0.001$}. Values represent means ± SE, $n = 6$. Different letters indicate significant differences between treatments for a given assessment date (*post-hoc* Tukey's Honest significant difference, $p \leq 0.05$).

Dynamics of Leaf Physiology Responses

Irrespective of the leaf position, A_{net} showed responses to treatments and response dynamics similar to g_w (**Figure 2A** vs. **Figure 1A**). After 30 days of exposure, A_{net} in the 100 ppb O_3 vs. CF treatment was decreased by 70 and 35% at the third and tenth leaf position, respectively. Once the leaf ontogenetic differentiation achieved, A_{net} decreased with POD_0 in a constant and monotonic manner (**Figure 2B**; POD: $p < 0.001$), regardless of the treatment or leaf position. The significant effects of O_3 treatment and O_3 treatment*POD factors ($p < 0.001$) could then be related to the less affected A_{net} values in the 80 vs. 100 ppb treatment at the highest POD_0 reached by the end of the exposure. The observed reduction in A_{net} as a function of POD_0 was stronger at the third vs. tenth leaf position (**Figure 2B**; leaf position $p < 0.001$) but the dynamics at both leaf positions was similar (leaf position*POD: ns). Hence, at POD_0 of 5 mmol O_3 m^{-2}, A_{net} at the tenth leaf position did not show any reduction relative to CF treatment yet, vs. 50% A_{net} loss in older leaves, irrespective of the O_3 treatment. The response differences between the two leaf positions were further observed at higher POD_0. With POD_0 above 9 mmol O_3 m^{-2}, as recorded in younger leaves only, and also as a consequence of the aforementioned latency effect (**Figure 1B**), A_{net} never dropped to levels observed at the third leaf position for lower POD_0. Consequently, the photosynthetic activity in younger vs. older foliage appeared less sensitive to the absorbed O_3 dose.

An O_3 impact on the chlorophyll content index of leaves was detected after 24 days of the experiment. The impact was restricted to the third leaf position (**Figure 3A**; O_3 treatment: ns; O_3 treatment*time, O_3 treatment*leaf position: $p < 0.001$), showing a decrease of 30% for the total chlorophyll index in the 100 ppb O_3 vs. CF treatment. These findings primarily related to latency effects due to leaf ontological maturation, which were observed at the third as well as the tenth leaf position in the case of this parameter, lasting 7 and 17 days, respectively. Accordingly, a larger latency peak was observed in younger than older foliage. The total chlorophyll index decreased with higher POD_0 (**Figure 3B**; POD: $p < 0.05$), irrespective of the O_3 treatment (O_3 treatment: ns, O_3 treatment*POD: ns). At low POD_0, the decline was rather monotonic, but accelerated with values exceeding 8 mmol m^{-2} at the third leaf position, thus contrasting with the nearly linear drop observed in younger leaves. Confirming a higher O_3 tolerance leaves at the tenth leaf position showed smaller (leaf position: $p < 0.05$) and slower (leaf position*POD_0 $p < 0.001$) drops with higher POD_0.

Dynamics of HR-Like Lesion Spread and Development

The microscopic necrosis observed in mesophyll using the Trypan blue assay was diagnosed as being caused by HR-like processes (**Figures 4A–D**), based on several typical O_3-stress markers (Paoletti et al., 2009; Vollenweider et al., 2019). They included (1) the characteristic intercostal distribution of lesions (**Figure 4E**), (2) the development of injury first in older leaves (**Figure 5A**), or (3) the multiple HR-like events restricted to cells or small groups of cells within mesophyll (**Figures 4E–G,I** vs. **Figure 4H**). Collapsed dead cells were mainly observed in

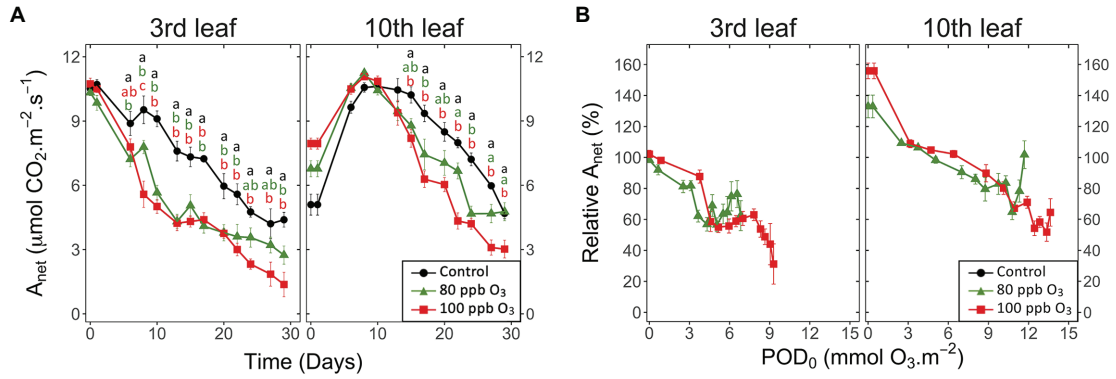

	A_{net}
O_3 treatment	***
Leaf Position	***
Time	***
O_3 treatment:Time	***
O_3 treatment:Leaf Position	***
Leaf Position:Time	***
O_3 treatment:Time:Leaf Position	***

	A_{net}
O_3 treatment	***
Leaf Position	***
POD_0	***
O_3 treatment:POD_0	***
O_3 treatment:Leaf Position	ns
Leaf Position:POD_0	ns
O_3 treatment:POD_0:Leaf Position	ns

FIGURE 2 | Dynamics of changes in the net CO_2 assimilation (A_{net}) of hybrid poplar leaves (*Populus tremula x alba*), as a function of assessment time **(A)**, phytotoxic O_3 dose (POD_0; **B**), O_3 treatment (charcoal-filtered air ●, 80 ppb O_3 ▲, 100 ppb O_3 ■), leaf position and interactions [model: lmer(variable) ~ O_3 treatment * leaf position * time + (1 | tree / chamber); *** $p \leq 0.001$; ns, not significantly different]. Values represent means ± SE, $n = 6$. Different letters indicate significant differences between treatments at a given assessment date (*post-hoc* Tukey's Honest significant difference, $p \leq 0.05$).

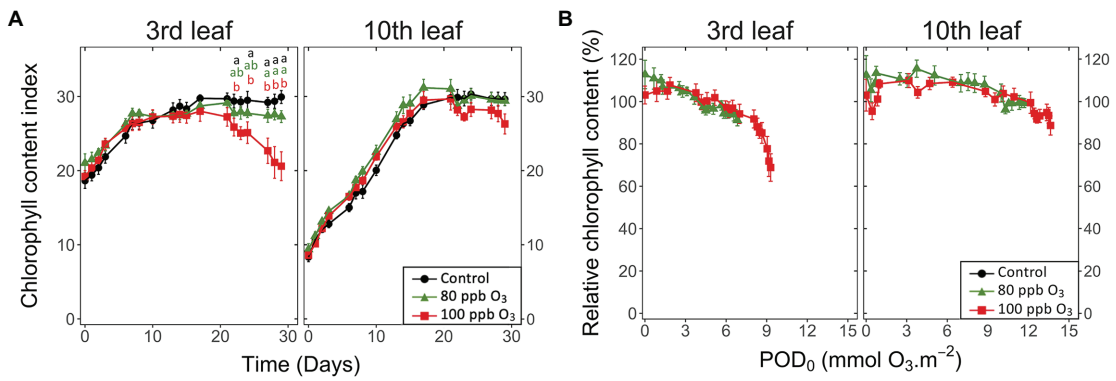

	Chlorophyll Content Index
O_3 treatment	ns
Leaf Position	***
Time	***
O_3 treatment:Time	***
O_3 treatment:Leaf Position	***
Leaf Position:Time	***
O_3 treatment:Time:Leaf Position	***

	Chlorophyll Content Index
O_3 treatment	ns
Leaf Position	*
POD_0	***
O_3 treatment:POD_0	ns
O_3 treatment:Leaf Position	*
Leaf Position:POD_0	***
O_3 treatment:POD_0:Leaf Position	ns

FIGURE 3 | Dynamics of changes in the surface-based concentration of chlorophylls (total chlorophyll content index of Dualex) within hybrid poplar leaves (*Populus tremula x alba*), as a function of assessment time **(A)**, phytotoxic O_3 dose (POD_0; **B**), O_3 treatment (charcoal-filtered air ●, 80 ppb O_3 ▲, 100 ppb O_3 ■), leaf position and interactions [model: lmer(variable) ~ O_3 treatment * leaf position * time + (1 | tree / chamber); *** $p \leq 0.001$; * $p \leq 0.05$; ns, not significantly different]. Values represent means ± SE, $n = 6$. Different letters indicate significant differences between treatments at a given assessment date (*post-hoc* Tukey's Honest significant difference, $p \leq 0.05$).

the lower palisade parenchyma (**Figures 4I–L**). Non-oxidized lesions (**Figure 4G**) showed up first (**Figures 5A,C, 6C**), with, for instance, still green chloroplasts visible within collapsed dead cells (**Figures 4I,J**). The dark hues of oxidized lesions (**Figure 4L**) were enhanced by staining with Trypan blue (**Figures 4E,G**). Oxidized cells showed sharp wall angles indicative

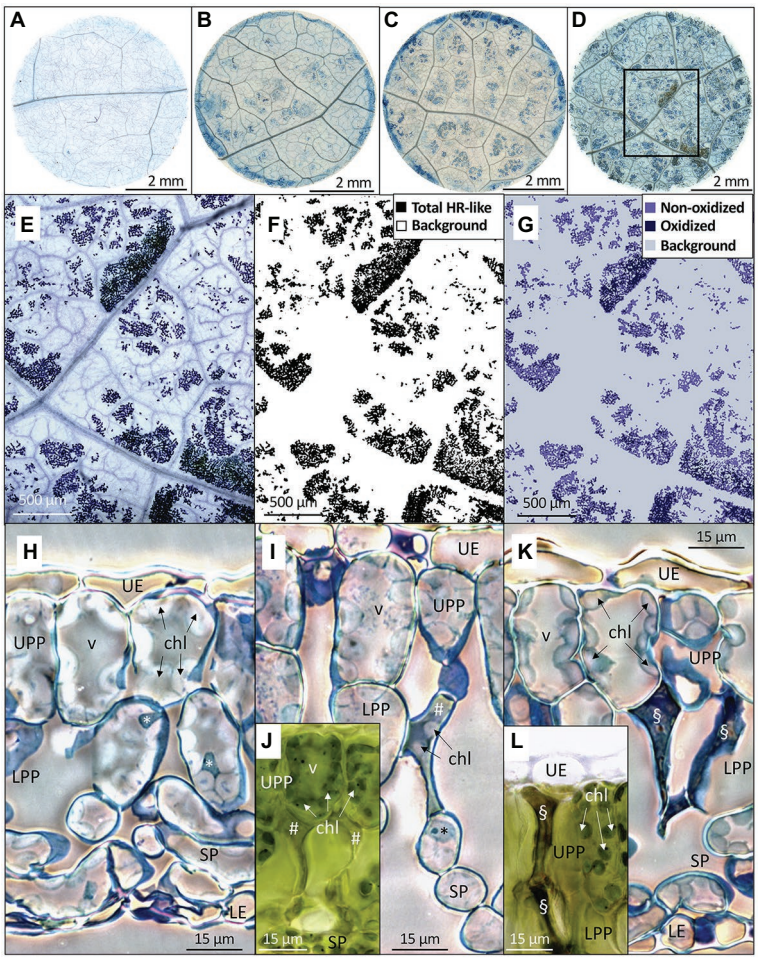

FIGURE 4 | Distribution, morphology, and structural properties of HR-like lesions within hybrid poplar leaves (*Populus tremula x alba*). **(A–D)** Foliar discs excised at low leaf position (third) from leaves exposed to 100 ppb O_3 during 2 **(A)**, 8 **(B)**, 13 **(C)**, and 27 **(D)** days. **(A)** Central area within each disk was photographed each time (frame in **D**). **(E–G)** Image analysis of HR-like lesion after 27 days of treatment, as framed in **(D)**. **(E)** Synthetic digital image, made of 9 stitched micrographs (5x magnification). The lesions are separated by veinlets and non-symptomatic tissues. **(F)** The binary image of total HR-like lesion vs. background (white). **(G)** Classification of HR-like injuries into oxidized and non-oxidized lesion groups, based on color classes. **(H–L)** Changes in the mesophyll tissue and cell structure underlying the HR-like lesions. **(H)** Asymptomatic leaf tissues in a leaf sample from the filtered air treatment. I–L: necrotic cells within the upper (UPP) and lower (LPP) palisade parenchyma underlying the HR-like lesions. **(I,J)** Within mesophyll cells having recently undergone HR-like necrosis (#), the chloroplasts (chl) were still visible and had retained their green color **(J)**. **(K,L)** at a later stage, the HR-like lesions (§) showed cell-content disruption and oxidation **(L)**. Other structures: UE, upper epidermis; SP, spongy parenchyma; LE, lower epidermis; v, vacuole; *, nucleus. Technical specifications: staining with Trypan blue **(A–E)** and Toluidine blue **(H,I,K)**; observations in bright field microscopy **(A–E,H–L)** using phase-contrast **(H,I,K)**; **(J,L)** fresh, unfixed and unstained leaf sample preparations.

of breaks and disrupted cell content (**Figures 4K,L**). All these typical HR-like traits showed little variation, regardless of the O_3 treatment or leaf position.

The first HR-like lesions at the third and tenth leaf position were observed after 6 and 13 days of exposure, respectively. This was much earlier than reductions in the chlorophyll content index (**Figure 5A**). Despite large response variability among trees, the effect of O_3 treatment was significant (**Figure 5A**; O_3 treatment: $p < 0.05$; O_3 treatment*time: $p < 0.001$). A larger leaf percentage area showing HR-like lesions was observed for the 100 vs. 80 ppb O_3 treatment, with differences between the two treatments at the third leaf position becoming significant after 20 days of exposure (O_3*time; $p < 0.001$). After 27 days of treatment, the percentage area of lesions in the 100 vs. 80 ppb O_3 treatment was two and five times higher at the third and tenth leaf positions, respectively. However, each leaf position showed specific response dynamics (O_3 treatment*leaf position: $p < 0.01$, O_3 treatment*time*leaf position: $p < 0.05$), rather sigmoidal-like vs. linear – once lesions appeared – in older vs. younger foliage (**Figure 5A**). Moreover, the HR-like lesions in response to the two O_3 concentrations showed up simultaneously at the third leaf position whereas a 7-day delay was observed at the tenth leaf position (**Figure 5A**).

When expressed as a function of POD_0, the differences between the two O_3 treatments in the leaf percentage area showing HR-like lesions were leveled out, especially at the third leaf position (**Figure 5B**; O_3 treatment: ns). However, the dependency on POD_0 was lessened at the tenth vs. third

leaf position (leaf position*POD: $p < 0.001$), and distinctly higher lesion percentage areas in response to similar POD_0 were observed in the 100 vs. 80 ppb O_3 treatment in younger leaves (O_3 treatment*POD*leaf position: $p < 0.05$). Hence, not only the O_3 dose but also the O_3 absorption rate then determined the lesion severity. The oxidized HR-like lesions, expressed as a function of time or POD_0, showed responses and response dynamics similar to HR-like lesions taken globally (**Figures 5C,D** vs. **Figures 5A,B**). The main differences included a smaller percentage of the injured area and a weaker symptom dynamics. At the tenth leaf position, oxidized HR-like lesions in the 80 ppb O_3 treatment were observed only occasionally.

Analyzing single HR-like injuries, the shape (data not shown) and size of lesions remained stable over time or with increasing POD_0. Furthermore, they did not respond to the O_3 treatment, leaf position, or interaction factors (**Figures 6A,B**; all factors: ns). The only change observed was increasing oxidation with longer exposures and at higher POD_0 (**Figures 6C,D**; Time, POD: $p < 0.05$). Hence, the observed increases in the percentage area of HR-like lesions with time, or higher POD_0 and in response to the O_3 treatment (**Figures 5A,B**) resulted as a consequence of the multiplication of single HR-like reactions and higher lesion density, rather than from increased growth of already developed injuries. However, both the higher lesion density and the growing oxidation of individual HR-like lesions could contribute to the observed increase in the leaf percentage area showing oxidation (**Figures 5C,D**).

Emergence of Visible Symptoms

The first visible symptoms in leaves exposed to the O_3 treatments appeared by the end of the experiment, that is, 23 days after the start of exposure. The first HR-like lesions had been detected more than 2 weeks earlier, whereas the observed drops in foliar chlorophyll content index were rather synchronous (**Figure 7A** vs. **Figures 3A, 5A**). These visible symptoms consisted of intercostal necrotic dark spots spread in the leaf

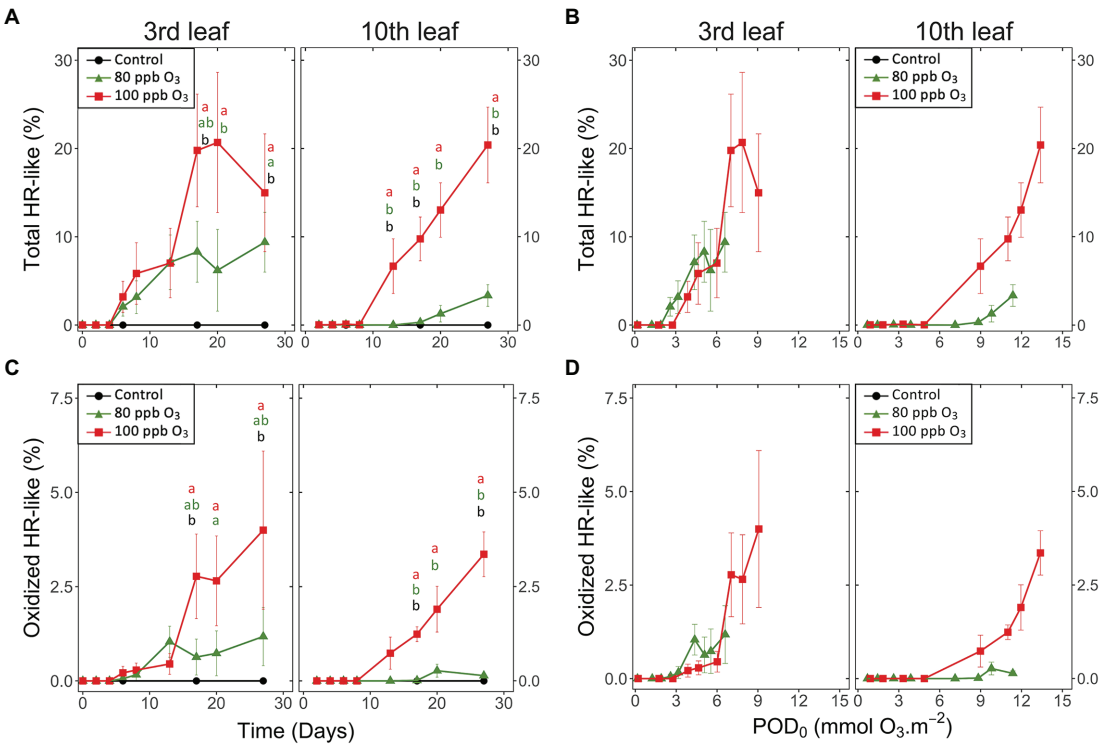

	Total HR-like	Oxidized HR-like
O_3 treatment	*	ns
Leaf Position	ns	ns
Time	***	***
O_3 treatment:Time	***	***
O_3 treatment:Leaf Position	**	ns
Leaf Position:Time	*	ns
O_3 treatment:Time:Leaf Position	*	ns

	Total HR-like	Oxidized HR-like
O_3 treatment	ns	ns
Leaf Position	ns	ns
POD_0	***	***
O_3 treatment:POD_0	**	***
O_3 treatment:Leaf Position	ns	ns
Leaf Position:POD_0	***	***
O_3 treatment:POD_0:Leaf Position	*	ns

FIGURE 5 | Development dynamics of HR-like lesions **(A,B)** and lesion oxidation **(C,D)** in hybrid poplar leaves (*Populus tremula x alba*), as a function of the assessment time **(A,C)**, phytotoxic O_3 dose (POD_0; **B,D**), O_3 treatment (charcoal-filtered air ●, 80 ppb O_3 ▲, 100 ppb O_3 ■), leaf position and interactions {model: lmer[sqrt(variable)] ~ O_3 treatment * leaf position * time + (1 | tree / chamber); ***$p \leq 0.001$; **$p \leq 0.01$; *$p \leq 0.05$; ns, not significantly different}. Values represent means ± SE of percentage area of leaf discs showing microscopic injury, $n = 4$. Different letters indicate significant differences between treatments at a given assessment date (*post-hoc* Tukey's honest significant difference, $p \leq 0.05$).

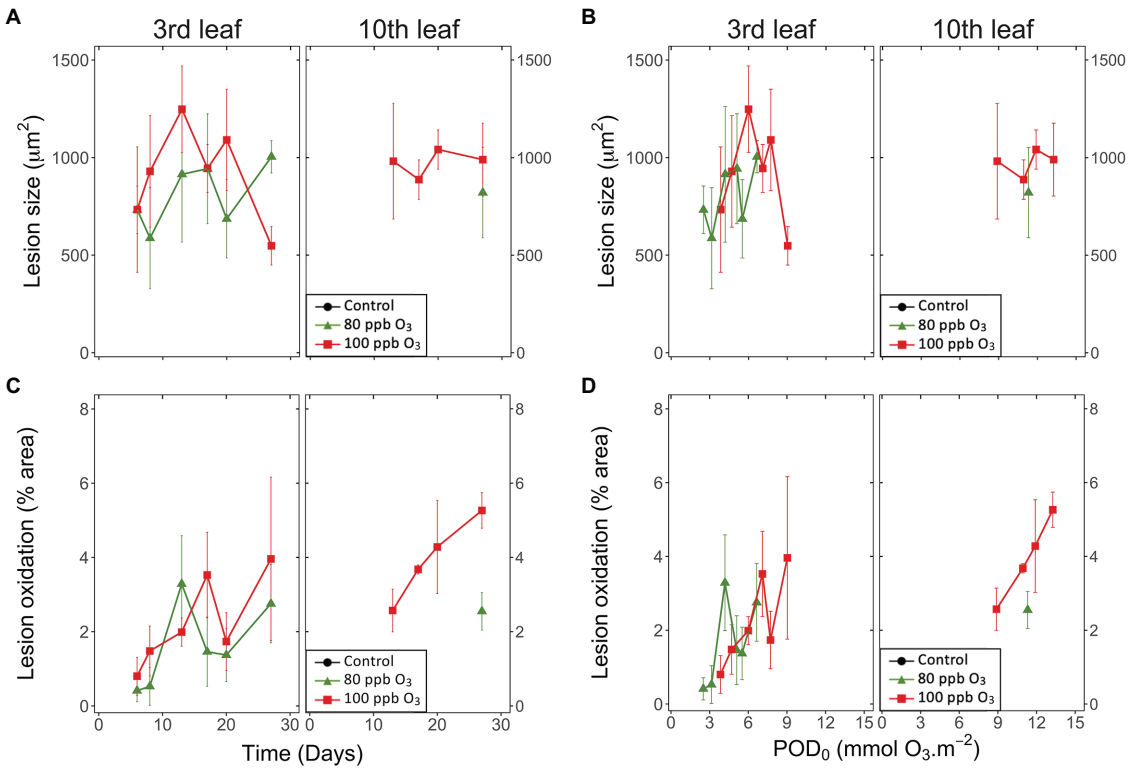

	Lesion size	Lesion oxidation
O_3 treatment	ns	ns
Leaf Position	ns	ns
Time	ns	*
O_3 treatment:Time	ns	ns
O_3 treatment:Leaf Position	ns	ns
Leaf Position:Time	ns	ns
O_3 treatment:Time:Leaf Position	ns	ns

	Lesion size	Lesion oxidation
O_3 treatment	ns	ns
Leaf Position	ns	ns
POD_0	ns	*
O_3 treatment:POD_0	ns	ns
O_3 treatment:Leaf Position	ns	ns
Leaf Position:POD_0	ns	ns
O_3 treatment:POD_0:Leaf Position	ns	ns

FIGURE 6 | Dynamics of changes in the size **(A,B)** and degree of oxidation **(C,D)** of single HR-like lesions in hybrid poplar leaves (*Populus tremula x alba*), as a function of the assessment time **(A,C)**, phytotoxic O_3 dose (POD_0; **B,D**), O_3 treatment (charcoal-filtered air ●, 80 ppb O_3 ▲, 100 ppb O_3 ■), leaf position and interactions [model: lmer(variable) ~ O_3 treatment * leaf position * time + (1 | tree/chamber); * $p \leq 0.05$; ns, not significantly different, na not tested]. **(A,B)** The size of HR-like lesions did not respond to the experimental factors and interactions. Values represent means ± SE of distinct lesion size **(A,B)** and percentage area showing oxidation **(C,D)**, $n = 4$.

blade, as previously observed in poplar (**Figure 7A**; Cabane et al., 2004; Giacomo et al., 2010; Dghim et al., 2013). By the end of exposure, only low levels of injury could develop (O_3 treatment: ns; O_3 treatment*Time $p < 0.001$), with significantly higher percentages in the 100 vs. 80 ppb O_3 treatment at the third leaf position only. In younger leaves, the visible injury appeared 4 days later than at the third leaf position, and differences between treatments throughout the experiment remained non-significant (leaf position, O_3 treatment*time*leaf position: $p < 0.05$; O_3 treatment*leaf position: $p < 0.01$).

When expressed as a function of POD_0, the visible injuries appeared at a lower O_3 threshold at the third than tenth leaf position (9 and 12 mmol O_3 m^{-2} in the case of 100 ppb treatment; **Figure 7B**). With only the beginning of injury development assessed in a 30-day experiment, the O_3 treatment effects could not reach any significance, and only preliminary information on the dynamics of visible symptom development was thus obtained. The simultaneous detection of early injury in the two O_3 treatments (**Figure 7A**) thereby resulted in higher injury values for similar POD_0 in the 80 vs. 100 ppb O_3 treatment (**Figure 7B**; O_3 treatment*POD: $p < 0.05$). Similarly, differences between younger and older leaves were detected as a trend only, with still very low injury values recorded at the tenth leaf position and for the higher POD_0 values only (leaf position: ns; leaf position*POD: $p < 0.001$).

DISCUSSION

Dynamics of Physiological and Structural Responses to O_3 Stress

The physiological and structural responses detected during 30 days of O_3 exposure developed mostly before and in some cases at the same time as the initial visible injury and first

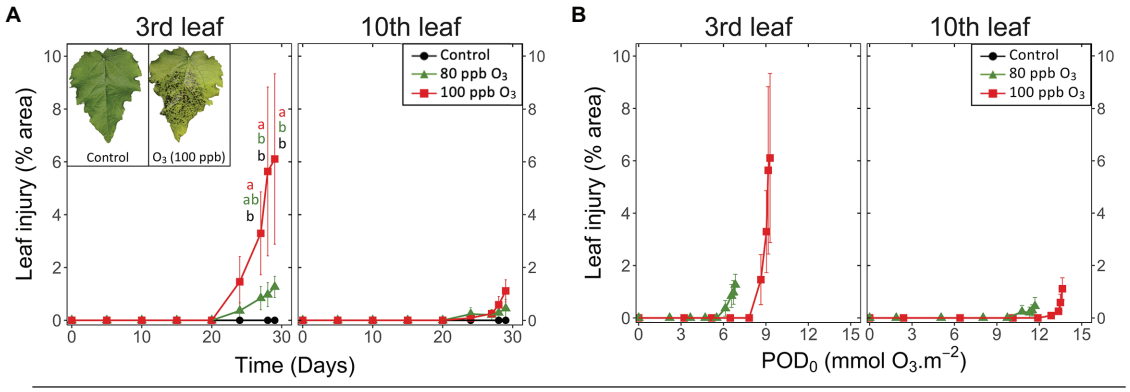

	Leaf injury
O_3 treatment	ns
Leaf Position	*
Time	***
O_3 treatment:Time	***
O_3 treatment:Leaf Position	**
Leaf Position:Time	**
O_3 treatment:Time:Leaf Position	*

	Leaf injury
O_3 treatment	ns
Leaf Position	ns
POD_0	***
O_3 treatment:POD_0	*
O_3 treatment:Leaf Position	ns
Leaf Position:POD_0	***
O_3 treatment:POD_0:Leaf Position	*

FIGURE 7 | Development dynamics of visible O_3 injury in hybrid poplar leaves (*Populus tremula x alba*), as a function of the assessment time **(A)**, phytotoxic O_3 dose (POD_0; **B**), O_3 treatment (charcoal-filtered air ●, 80 ppb O_3 ▲, 100 ppb O_3 ■), leaf position and interactions {lmer[log(variable)] ~ O_3 treatment * leaf position * time + (1 | tree / chamber); $^{***}p \leq 0.001$; $^{**}p \leq 0.01$; $^{*}p \leq 0.05$; ns, not significantly different}. The insert in **(A)** shows typical O_3 symptoms, in the form of intercostal necrotic dark spots, within a leaf at third leaf position exposed for 30 days (POD_0 = 9.3 mmol O_3 m^{-2}, 100 ppb O_3 treatment) vs. an asymptomatic leaf from the CF treatment, sampled at the same leaf position and the end of treatment. Values represent means ± SE of leaf percentage area showing visible injury, n = 6. Letters indicate significant differences between treatments at a given assessment date (*post-hoc* Tukey's Honest significant difference, $p \leq 0.05$).

leaf shedding, whereas no O_3 effect on the gross morphology of trees was observed. The two O_3 treatments accelerated the ontological decline of leaf gas exchange at the two-leaf positions, once leaf physiology had reached maturity. O_3-induced reductions in the stomatal conductance and net CO_2 assimilation are well-documented in the case of various species, including poplars (Pell et al., 1992; Bagard et al., 2015; Dusart et al., 2019a) but more rarely with a leaf ontogenetic perspective. The decrease in net CO_2 assimilation could result from a smaller stomatal aperture, limiting CO_2 availability. Indeed, the O_3 effects on stomata are well-established (Kangasjarvi et al., 2005), including slower movements of cell guard cells upon exposure referred to as stomatal sluggishness, as observed in different species but with higher measurement frequency than in our case (Paoletti and Grulke, 2010; Dumont et al., 2013; Dusart et al., 2019b). Lower mesophyll conductance could also contribute to the observed acceleration of A_{net} reduction, as compared with the ontogenetic decrease observed in CF trees (Xu et al., 2019). Although not significant in older foliage, the drop in A_{net} tended to be more expressed in the 100 vs. 80 ppb treatment after 20 days, suggesting an additional reduction in carboxylation efficiency and rate of electron transport (Bagard et al., 2008; Shang et al., 2017). A possible cause could be the starting degradation of the photosynthetic machinery, as suggested by the concomitant reduction in the chlorophyll content index.

The reduction in leaf chlorophyll content is another well-documented leaf physiological response to elevated O_3 (Reich, 1983; Bagard et al., 2015; Dusart et al., 2019b), indicative of ACS, together with other markers of chloroplast degeneration (Mikkelsen and HeideJorgensen, 1996; Günthardt-Goerg and Vollenweider, 2007; Moura et al., 2018). Also typical of ACS and degenerative processes was the progressive and mostly monotonic reductions observed in the case of all physiology parameters (g_w, A_{net}, and chlorophyll index). This contrasted with abrupt responses upon exceedance of a threshold, as observed in the case of HR-like reactions. In the field, the ontogeny-driven ACS latency observed in both younger and older foliage (total chlorophyll index) may also contribute to delaying the onset of degenerative events in response to O_3-stress, as suggested by the development of ACS traits and visible injury rarely occurring before summer, once the foliage has fully matured (Vollenweider et al., 2019).

The new cell necrosis assay, using computer-assisted color image analysis, allowed us to monitor the emergence and development of validated HR-like reactions for the first time. It provided unprecedented capacity for quantitative assessments of cell death reactions in experimental conditions, overcoming limitations and uncertainties regarding the observation of visible injury only. Typical HR-like markers were detected in the lesions (Paoletti et al., 2009; Vollenweider et al., 2013, 2019; Feng et al., 2016). However, there were marked differences in classical traits as well, including the mid- rather than the upper-mesophyll location of HR-like lesions or a missing intra- and intercellular gradient of injury. Such features indicated low levels of photo-oxidative stress (Foyer et al., 1994; Günthardt-Goerg and Vollenweider, 2007;

Guerrero et al., 2013). Given maximum PAR above 2000 vs. 350 μmol m−2 s^{-1} with high (Ritchie, 2010; Poorter et al., 2019) vs. low light conditions, HR-like reaction peculiarities – together with the late onset of ACS – can be attributed to specifics in the environmental conditions, especially regarding PAR supply. This finding thus provides further confirmation of the close dependency relating the O_3 symptom expression in foliage and precise experimental and exposure conditions of tested material (Paoletti et al., 2009; Moura et al., 2018; Vollenweider et al., 2019).

The rather sigmoidal-like injury dynamics observed in older foliage was in good agreement with already existing molecular and trait evidence on HR-like processes. The 6 days/3 mmol O_3 m^{-2} s^{-1} delay between the start of exposure and occurrence of first lesions was thus indicative of the O_3 dose-dependent onset of genetically controlled PCD (Rao et al., 2000; Overmyer et al., 2005). The steep increase in injury percentage area reflected the rapid cell death completion once PCD started (Overmyer et al., 2005; Günthardt-Goerg and Vollenweider, 2007). Finally, the plateau reached was indicative of lesion containment, blocking its further spread (Overmyer et al., 2003; Kangasjarvi et al., 2005; Marchica et al., 2019). In younger foliage, the experiment was terminated before a plateau could be reached, with values of lesion percentage area which would probably have been sizably higher than at the third leaf position. Further suggesting the genetic control of PCD, in older foliage, the first HR-like reactions occurred 17 days/at 5.3 mmol O_3 m^{-2} s^{-1} before any evidence of biochemical limitation and chloroplast injury, as indicated by low levels of chlorophyll content indexes. The early HR-like responses, and their antecedence concerning ACS and first visible injury, contrasted with field evidence (Vollenweider et al., 2019), further outlining how important the environmental conditions can be regarding response order and dynamics.

Image analysis in WinCELL based on three color classes allowed us to quantify the structurally contrasted non-oxidized and oxidized lesions, based on constitutive and stained-color characteristics. REDOX changes during oxidative stress and cell death form an important cell physiology process (Foyer and Noctor, 2005) that is well-documented in the case of O_3 stress (Ranieri et al., 2000; Baier et al., 2005; Chen and Gallie, 2005; Bellini and De Tullio, 2019), detectable with different structural and ultrastructural markers (Moura et al., 2018; Vollenweider et al., 2019) and underlying changes in visible symptom expression. Expressed as leaf area percentages, the oxidized and total HR-like lesions showed similar dynamics and responses to increasing POD_0 (same results for non-oxidized lesions, data not shown). The main differences in oxidized vs. non-oxidized lesions included their (1) lower percentage area, (2) delay in development, and (3) higher severity (i.e., cell wall breaks, cell content disruption). Non-oxidized and oxidized lesions may thus correspond to two types or two stages of HR-like reactions. However, the first hypothesis appears unlikely, given lacking molecular evidence for alleged PCD severity variation. In favor of the second, oxidized vs. non-oxidized lesions appeared later, and the oxidation degree of a lesion increased with time. However, it implies the further evolution of HR-like lesions after cell collapse and death, which needs further structural and ultrastructural confirmation.

The visible injury was detected only once 2–5% of the leaf percentage area showed oxidized lesions, thus with a detection delay and a POD_0 gap compared to the onset of HR-like reactions amounting to 18 days and 4.9 mmol O_3 m^{-2} s^{-1}. Similarly, risk assessment studies using visible injury markers rather target the late and final structural evolution of responses to O_3 stress in foliage, with possible interspecific variation, instead of the injury appearance in foliage.

Leaf Position Dependency of Responses to O_3 Stress

Reductions in leaf gas exchanges or the development of HR-like lesions and visible symptoms at the tenth vs. third leaf position occurred later and for larger POD_0. Given the higher stomatal conductance and POD_0 in younger leaves, their greater physiological activity and lower levels of injury suggest higher O_3 tolerance, while a contribution by enhanced stomatal closure can be excluded. This finding is confirmed by similar reports on enhanced O_3 tolerance in maturing leaves (Reich, 1983; Paakkonen et al., 1996; Strohm et al., 2002; Bagard et al., 2008; Zhang et al., 2010; Guerrero et al., 2013). This may be related to sink functional properties and larger resource availability for defense and repair (Coleman, 1986). Resource availability in young leaves could be increased by the supply of nutrients (such as nitrogen, potassium, and phosphorus) coming from senescent leaves (Maillard et al., 2015; Have et al., 2017). Hence, the concentration of phenolics with antioxidant properties and other antioxidative capacities decline during the sink-to-source transition in maturing foliage, thus increasing leaf susceptibility to oxidative stress (Coleman, 1986; Strohm et al., 2002; Blokhina and Fagerstedt, 2006; Bellini and De Tullio, 2019). However, and in contrast to older foliage, the development of HR-like lesions as a function of POD_0 at the tenth leaf position depended on the O_3 treatment, with a higher O_3 tolerance in the 80 ppb O_3 treatment. Given the high O_3 dose in maturing leaves, this finding highlights the importance of the O_3 absorption rate given the saturation of the antioxidative system. The higher O_3 tolerance in younger vs. older foliage was further confirmed by their still comparable leaf percentage areas showing HR-like lesions in the 100 ppb O_3 treatment despite 1.8 times higher POD_0 at the tenth leaf position.

Reaction Gradient in Foliage Concerning Critical O_3 Levels

In our experiment, the current CL (POD_{Y_SPEC} for beech and birch = 5.2 mmol O_3 m^{-2}; Mills et al., 2017) was equivalent to a POD_0 of 5.7 mmol O_3 m^{-2}. By the end of exposure, this CL had thus been exceeded by 1.54 and 2.35 times at the third and tenth leaf positions, respectively. If any impairment of tree morphology and biomass was still lacking, reductions in leaf gas exchange, development of structural injury, and the emergence of visible symptoms at the third leaf position had already been observed for O_3 dose, amounting to 0.82, 0.69, and 1.46 times the current CL, respectively. At the tenth

leaf position, these responses were detected for POD_{Y_SPEC} 1.83, 1.18, and 2.32 times above CL. These findings highlight the high dependency of sensitivity evaluations on the selected parameters and scale of observation. They also outline the within-tree gradient of sensitivity to O_3 stress, given the large size of such organisms, which, as a result, complicates O_3 risk assessment. They finally indicate that below CL, significant effects in the foliage of trees, such as in the impairment of leaf physiology and development of microscopic necrosis in extended parts of mesophyll, can be expected. These responses may already contribute to reduced carbon uptake and storage in foliage and other tree organs before reaching CL thresholds.

CONCLUSION

In this study, we characterized the dynamics of physiological, structural, and morphological responses to two levels of O_3 exposure and as a function of time, POD_0 and leaf position, in fully controlled conditions. We observed contrasting dynamics, monotonic or sigmoidal-like, as a function of plant responses but irrespective of leaf position, before any visible symptoms and effects on the gross morphology of trees. The first microscopic necrosis developed weeks before the appearance of visible symptoms and at half the O_3 dose. Concerning experimental hypotheses (H), the sequential development and distinct dynamics of physiological, structural, and morphological responses to O_3 stress was confirmed (confirmation of H1); both HR-like and ACS responses were elicited, the former occurring first (confirmation of H2a, rejection of H2b). When expressed as a function of POD_0, leaf responses did not depend on the O_3 treatment (confirmation of H3a), except for the development of structural injury that depended on the O_3 absorption rates in younger foliage (partial rejection of H3b). Finally, response dynamics were strongly related to leaf age as a function of time or POD_0, showing delay in younger foliage (confirmation of H4). This study thus sheds light on the syndrome of early reactions to O_3 stress and disentangles the specific dynamics of distinct but co-occurring plant responses, before CL exceedance. The resulting variety of symptoms, as observed by the end of the experiment, provides an exemplary experimental demonstration for integrative injury display, as found in the field late in summer. Given ACS and HR-like timing inversion, compared to field conditions, the ontogenetical and environmental drivers also appear to have a prevailing effect over the sensitivity of affected markers, regarding the timing and dynamics of each cellular response. Whatever the exact sequence order of early reactions to O_3 stress below CL – in the field or controlled conditions, they will modify key foliage properties. Such impacts can be relevant for some, e.g., biodiversity ecosystem services before those of economic significance – i.e., wood production, as targeted by flux-based CL.

DATA AVAILABILITY STATEMENT

The raw data supporting the conclusions of this article will be made available by the authors, without undue reservation.

AUTHOR CONTRIBUTIONS

BT, YJ, MC, and PV: conception or design of the work and final approval of the version to be published. BT: data collection. BT, PV, AG, DT, YJ, and MC: data analysis and interpretation. BT and PV: drafting the article. BT, PV, AG, DT, YJ, MC, and MS: critical revision of the article. All authors contributed to the article and approved the submitted version.

FUNDING

The research was funded by grants from the French National Research Agency (ANR, "*Investissements d'Avenir*" from the program Lab of Excellence ARBRE: ANR-11-LABX-0002-01), Grand-Est region, France, and WSL (201701N1428).

ACKNOWLEDGMENTS

Technical support by Terry Menard (microscopy), Christophe Robin (leaf physiology), and Jean-Charles Olry and Stéphane Martin (members of the experimental phytotrons platform of Lorraine PEPLor, University of Lorraine, France) was gratefully acknowledged.

REFERENCES

Bagard, M., Jolivet, Y., Hasenfratz-Sauder, M. P., Gerard, J., Dizengremel, P., and Le Thiec, D. (2015). Ozone exposure and flux-based response functions for photosynthetic traits in wheat, maize and poplar. *Environ. Pollut.* 206, 411–420. doi: 10.1016/j.envpol.2015.07.046

Bagard, M., Le Thiec, D., Delacote, E., Hasenfratz-Sauder, M. P., Banvoy, J., Gerard, J., et al. (2008). Ozone-induced changes in photosynthesis and photorespiration of hybrid poplar in relation to the developmental stage of the leaves. *Physiol. Plant.* 134, 559–574. doi: 10.1111/j.1399-3054.2008.01160.x

Baier, M., Kandlbinder, A., Golldack, D., and Dietz, K. J. (2005). Oxidative stress and ozone: perception, signaling and response. *Plant Cell Environ.* 28, 1012–1020. doi: 10.1111/j.1365-3040.2005.01326.x

Bates, D., Machler, M., Bolker, B. M., and Walker, S. C. (2015). Fitting linear mixed-effects models using lme4. *J. Stat. Softw.* 67, 1–48. doi: 10.18637/jss.v067.i01

Bellini, E., and De Tullio, M. C. (2019). Ascorbic acid and ozone: novel perspectives to explain an elusive relationship. *Plants* 8:122. doi: 10.3390/plants8050122

Bhattacharjee, S. (2005). Reactive oxygen species and oxidative burst: roles in stress, senescence and signal transduction in plants. *Curr. Sci.* 89, 1113–1121.

Blokhina, O., and Fagerstedt, K. (2006). *Oxidative Stress and Antioxidant Defenses in Plants*. Covent Garden: Imperial College Press.

Büker, P., Feng, Z., Uddling, J., Briolat, A., Alonso, R., Braun, S., et al. (2015). New flux based dose-response relationships for ozone for European forest tree species. *Environ. Pollut.* 206, 163–174. doi: 10.1016/j.envpol.2015.06.033

Cabane, M., Pireaux, J. C., Leger, E., Weber, E., Dizengremel, P., Pollet, B., et al. (2004). Condensed lignins are synthesized in poplar leaves exposed to ozone. *Plant Physiol.* 134, 586–594. doi: 10.1104/pp.103.031765

Chen, Z., and Gallie, D. R. (2005). Increasing tolerance to ozone by elevating foliar ascorbic acid confers greater protection against ozone than increasing avoidance. *Plant Physiol.* 138, 1673–1689. doi: 10.1104/pp.105.062000

Coleman, J. S. (1986). Leaf development and leaf stress: increased susceptibility associated with sink-source transition. *Tree Physiol.* 2, 289–299. doi: 10.1093/treephys/2.1-2-3.289

Dghim, A. A., Dumont, J., Hasenfratz-Sauder, M. P., Dizengremel, P., Le Thiec, D., and Jolivet, Y. (2013). Capacity for NADPH regeneration in the leaves of two poplar genotypes differing in ozone sensitivity. *Physiol. Plant.* 148, 36–50. doi: 10.1111/j.1399-3054.2012.01686.x

Dizengremel, P., Jolivet, Y., Tuzet, A., Ranieri, A., and Le Thiec, D. (2013). "Integrative leaf-level phytotoxic ozone dose assessment for forest risk modelling," in *Climate Change, Air Pollution and Global Challenges: Understanding and Perspectives from Forest Research*. eds. R. Matyssek, N. Clarke, P. Cudlin, T. N. Mikkelsen, J. P. Tuovinen, G. Wieser et al (Netherlands: Elsevier), 267–288.

Dumont, J., Keski-Saari, S., Keinanen, M., Cohen, D., Ningre, N., Kontunen-Soppela, S., et al. (2014). Ozone affects ascorbate and glutathione biosynthesis as well as amino acid contents in three Euramerican poplar genotypes. *Tree Physiol.* 34, 253–266. doi: 10.1093/treephys/tpu004

Dumont, J., Spicher, F., Montpied, P., Dizengremel, P., Jolivet, Y., and Le Thiec, D. (2013). Effects of ozone on stomatal responses to environmental parameters (blue light, red light, CO2 and vapour pressure deficit) in three *Populus deltoides* x *Populus nigra* genotypes. *Environ. Pollut.* 173, 85–96. doi: 10.1016/j.envpol.2012.09.026

Dusart, N., Gerard, J., Le Thiec, D., Collignon, C., Jolivet, Y., and Vaultier, M. N. (2019a). Integrated analysis of the detoxification responses of two Euramerican poplar genotypes exposed to ozone and water deficit: focus on the ascorbate-glutathione cycle. *Sci. Total Environ.* 651, 2365–2379. doi: 10.1016/j.scitotenv.2018.09.367

Dusart, N., Vaultier, M. N., Olry, J. C., Bure, C., Gerard, J., Jolivet, Y., et al. (2019b). Altered stomatal dynamics of two Euramerican poplar genotypes submitted to successive ozone exposure and water deficit. *Environ. Pollut.* 252, 1687–1697. doi: 10.1016/j.envpol.2019.06.110

Faoro, F., and Iriti, M. (2009). Plant cell death and cellular alterations induced by ozone: key studies in Mediterranean conditions. *Environ. Pollut.* 157, 1470–1477. doi: 10.1016/j.envpol.2008.09.026

Feng, G., Calatayud, V., García-Breijo, F., Reig-Armiñana, J., and Feng, Z. (2016). Effects of elevated ozone on physiological, anatomical and ultrastructural characteristics of four common urban tree species in China. *Ecol. Indic.* 67, 367–379. doi: 10.1016/j.ecolind.2016.03.012

Foyer, C. H., Lelandais, M., and Kunert, K. J. (1994). Photooxidative stress in plants. *Physiol. Plant.* 92, 696–717. doi: 10.1111/j.1399-3054.1994.tb03042.x

Foyer, C. H., and Noctor, G. (2005). Redox homeostasis and antioxidant signaling: a metabolic interface between stress perception and physiological responses. *Plant Cell* 17, 1866–1875. doi: 10.1105/tpc.105.033589

Fu, T. M., and Tian, H. (2019). Climate change penalty to ozone air quality: review of current understandings and knowledge gaps. *Curr. Pollut. Rep.* 5, 159–171. doi: 10.1007/s40726-019-00115-6

Fuhrer, J., Skarby, L., and Ashmore, M. R. (1997). Critical levels for ozone effects on vegetation in Europe. *Environ. Pollut.* 97, 91–106. doi: 10.1016/S0269-7491(97)00067-5

Giacomo, B., Forino, L. M. C., Tagliasacchi, A. M., Bernardi, R., and Durante, M. (2010). Ozone damage and tolerance in leaves of two poplar genotypes. *Caryologia* 63, 422–434. doi: 10.1080/00087114.2010.10589755

Guerrero, C. C., Gunthardt-Goerg, M. S., and Vollenweider, P. (2013). Foliar symptoms triggered by ozone stress in irrigated holm oaks from the city of Madrid, Spain. *PLoS One* 8:e69171. doi: 10.1371/journal.pone.0069171

Günthardt-Goerg, M. S., and Vollenweider, P. (2007). Linking stress with macroscopic and microscopic leaf response in trees: new diagnostic perspectives. *Environ. Pollut.* 147, 467–488. doi: 10.1016/j.envpol.2006.08.033

Have, M., Marmagne, A., Chardon, F., and Masclaux-Daubresse, C. (2017). Nitrogen remobilization during leaf senescence: lessons from *Arabidopsis* to crops. *J. Exp. Bot.* 68, 2513–2529. doi: 10.1093/jxb/erw365

Jolivet, Y., Bagard, M., Cabane, M., Vaultier, M. N., Gandin, A., Afif, D., et al. (2016). Deciphering the ozone-induced changes in cellular processes: a prerequisite for ozone risk assessment at the tree and forest levels. *Ann. For. Sci.* 73, 923–943. doi: 10.1007/s13595-016-0580-3

Joo, J. H., Wang, S. Y., Chen, J. G., Jones, A. M., and Fedoroff, N. V. (2005). Different signaling and cell death roles of heterotrimeric G protein alpha and beta subunits in the *Arabidopsis* oxidative stress response to ozone. *Plant Cell* 17, 957–970. doi: 10.1105/tpc.104.029603

Kangasjarvi, J., Jaspers, P., and Kollist, H. (2005). Signaling and cell death in ozone-exposed plants. *Plant Cell Environ.* 28, 1021–1036. doi: 10.1111/j.1365-3040.2005.01325.x

Karlsson, P., Braun, S., Broadmeadow, M., Elvira, S., Emberson, L., Gimeno, B. S., et al. (2007). Risk assessments for forest trees: the performance of the ozone flux versus the AOT concepts. *Environ. Pollut.* 146, 608–616. doi: 10.1016/j.envpol.2006.06.012

Karlsson, P. E., Klingberg, J., Engardt, M., Andersson, C., Langner, J., Karlsson, G. P., et al. (2017). Past, present and future concentrations of ground-level ozone and potential impacts on ecosystems and human health in northern Europe. *Sci. Total Environ.* 576, 22–35. doi: 10.1016/j.scitotenv.2016.10.061

Lamaud, E., Loubet, B., Irvine, M., Stella, P., Personne, E., and Cellier, P. (2009). Partitioning of ozone deposition over a developed maize crop between stomatal and non-stomatal uptakes, using eddy-covariance flux measurements and modelling. *Agric. For. Meteorol.* 149, 1385–1396. doi: 10.1016/j.agrformet.2009.03.017

Lenth, R. V. (2016). Least-squares means: the R package lsmeans. *J. Stat. Softw.* 69, 1–33. doi: 10.18637/jss.v069.i01

Li, P., Feng, Z. Z., Catalayud, V., Yuan, X. Y., Xu, Y. S., and Paoletti, E. (2017). A meta-analysis on growth, physiological, and biochemical responses of woody species to ground-level ozone highlights the role of plant functional types. *Plant Cell Environ.* 40, 2369–2380. doi: 10.1111/pce.13043

Maas, R., and Grennfelt, P. (2016). Towards cleaner air. Scientific assessment report. Emep steering body and working group on effects of the convention on long-range transboundary air pollution, Oslo. 12–16.

Maillard, A., Diquelou, S., Billard, V., Laine, P., Garnica, M., Prudent, M., et al. (2015). Leaf mineral nutrient remobilization during leaf senescence and modulation by nutrient deficiency. *Front. Plant Sci.* 6:317. doi: 10.3389/fpls.2015.00317

Marchica, A., Lorenzini, G., Papini, R., Bernardi, R., Nali, C., and Pellegrini, E. (2019). Signaling molecules responsive to ozone-induced oxidative stress in *Salvia officinalis*. *Sci. Total Environ.* 657, 568–576. doi: 10.1016/j.scitotenv.2018.11.472

Massman, W. J. (1998). A review of the molecular diffusivities of H_2O, CO_2, CH_4, CO, O_3, SO_2, NH_3, N_2O, NO, and NO_2 in air, O_2 and N_2 near STP. *Atmos. Environ.* 32, 1111–1127. doi: 10.1016/S1352-2310(97)00391-9

Mikkelsen, T. N., and Heidejorgensen, H. S. (1996). Acceleration of leaf senescence in *Fagus sylvatica* L by low levels of tropospheric ozone demonstrated by leaf colour, chlorophyll fluorescence and chloroplast ultrastructure. *Trees-Struct. Funct.* 10, 145–156. doi: 10.1007/BF02340766

Mills, G., Harmens, H., Hayes, F., Pleijel, H., Buker, P., and González, I. (2017). "Mapping critical levels for vegetation," in *Manual on Methodologies and Criteria for Modelling and Mapping Critical Loads and Levels and Air Pollution Effects, Risks and Trends*. International Cooperative Programme on Effects of Air Pollution on Natural Vegetation and Crops, 1–66.

Mills, G., Pleijel, H., Braun, S., Buker, P., Bermejo, V., Calvo, E., et al. (2011). New stomatal flux-based critical levels for ozone effects on vegetation. *Atmos. Environ.* 45, 5064–5068. doi: 10.1016/j.atmosenv.2011.06.009

Moura, B. B., Alves, E. S., Marabesi, M. A., De Souza, S. R., Schaub, M., and Vollenweider, P. (2018). Ozone affects leaf physiology and causes injury to foliage of native tree species from the tropical Atlantic Forest of southern Brazil. *Sci. Total Environ.* 610, 912–925. doi: 10.1016/j.scitotenv.2017.08.130

Musselman, R. C., Lefohn, A. S., Massman, W. J., and Heath, R. L. (2006). A critical review and analysis of the use of exposure- and flux-based ozone indices for predicting vegetation effects. *Atmos. Environ.* 40, 1869–1888. doi: 10.1016/j.atmosenv.2005.10.064

Overmyer, K., Brosche, M., and Kangasjarvi, J. (2003). Reactive oxygen species and hormonal control of cell death. *Trends Plant Sci.* 8, 335–342. doi: 10.1016/S1360-1385(03)00135-3

Overmyer, K., Brosche, M., Pellinen, R., Kuittinen, T., Tuominen, H., Ahlfors, R., et al. (2005). Ozone-induced programmed cell death in the *Arabidopsis* radical-induced cell death1 mutant. *Plant Physiol.* 137, 1092–1104. doi: 10.1104/pp.104.055681

Paakkonen, E., Metsarinne, S., Holopainen, T., and Karenlampi, L. (1996). The ozone sensitivity of birch (*Betula pendula*) in relation to the developmental stage of leaves. *New Phytol.* 132, 145–154. doi: 10.1111/j.1469-8137.1996.tb04520.x

Paoletti, E., Contran, N., Bernasconi, P., Gunthardt-Goerg, M. S., and Vollenweider, P. (2009). Structural and physiological responses to ozone in

manna ash (*Fraxinus ornus* L.) leaves of seedlings and mature trees under controlled and ambient conditions. *Sci. Total Environ.* 407, 1631–1643. doi: 10.1016/j.scitotenv.2008.11.061

Paoletti, E., and Grulke, N. E. (2010). Ozone exposure and stomatal sluggishness in different plant physiognomic classes. *Environ. Pollut.* 158, 2664–2671. doi: 10.1016/j.envpol.2010.04.024

Pasqualini, S., Piccioni, C., Reale, L., Ederli, L., Della Torre, G., and Ferranti, F. (2003). Ozone-induced cell death in tobacco cultivar Bel W3 plants. The role of programmed cell death in lesion formation. *Plant Physiol.* 133, 1122–1134. doi: 10.1104/pp.103.026591

Pell, E. J., Eckardt, N., and Enyedi, A. J. (1992). Timing of ozone stress and resulting status of ribulose bisphosphate carboxylase oxygenase and associated net photosynthesis. *New Phytol.* 120, 397–405. doi: 10.1111/j.1469-8137.1992.tb01080.x

Pell, E. J., Sinn, J. P., Brendley, B. W., Samuelson, L., Vinten-Johansen, C., Tien, M., et al. (1999). Differential response of four tree species to ozone-induced acceleration of foliar senescence. *Plant Cell Environ.* 22, 779–790. doi: 10.1046/j.1365-3040.1999.00449.x

Poorter, H., Niinemets, U., Ntagkas, N., Siebenkas, A., Maenpaa, M., Matsubara, S., et al. (2019). A meta-analysis of plant responses to light intensity for 70 traits ranging from molecules to whole plant performance. *New Phytol.* 223, 1073–1105. doi: 10.1111/nph.15754

Proietti, C., Anav, A., De Marco, A., Sicard, P., and Vitale, M. (2016). A multi-sites analysis on the ozone effects on gross primary production of european forests. *Sci. Total Environ.* 556, 1–11. doi: 10.1016/j.scitotenv.2016.02.187

Ranieri, A., Petacco, F., Castagna, A., and Soldatini, G. F. (2000). Redox state and peroxidase system in sunflower plants exposed to ozone. *Plant Sci.* 159, 159–167. doi: 10.1016/S0168-9452(00)00352-6

Rao, M. V., Lee, H., Creelman, R. A., Mullet, J. E., and Davis, K. R. (2000). Jasmonic acid signaling modulates ozone-induced hypersensitive cell death. *Plant Cell* 12, 1633–1646. doi: 10.1105/tpc.12.9.1633

R Development Core Team (2017). "R: A language and environment for statistical computing." Vienna, Austria: R Foundation for Statistical Computing.

Reich, P. B. (1983). Effects of low concentrations of O3 on net photosynthesis, dark respiration, and chlorophyll contents in aging hybrid poplar leaves. *Plant Physiol.* 73, 291–296. doi: 10.1104/pp.73.2.291

Revell, L. E., Tummon, F., Stenke, A., Sukhodolov, T., Coulon, A., Rozanov, E., et al. (2015). Drivers of the tropospheric ozone budget throughout the 21st century under the medium-high climate scenario RCP 6.0. *Atmospheric Chem. Phys.* 15, 5887–5902. doi: 10.5194/acp-15-5887-2015

Ritchie, R. J. (2010). Modelling photosynthetic photon flux density and maximum potential gross photosynthesis. *Photosynthetica* 48, 596–609. doi: 10.1007/s11099-010-0077-5

Sanz, M., and Catalayud, V. (2011). *Ozone Injury in European Forest Species*. Available at: http://www.ozoneinjury.org/ (Accessed December 12, 2020).

Schindelin, J., Arganda-Carreras, I., Frise, E., Kaynig, V., Longair, M., Pietzsch, T., et al. (2012). Fiji: an open-source platform for biological-image analysis. *Nat. Methods* 9, 676–682. doi: 10.1038/nmeth.2019

Schraudner, M., Moeder, W., Wiese, C., Van Camp, W., Inze, D., Langebartels, C., et al. (1998). Ozone-induced oxidative burst in the ozone biomonitor plant, tobacco Bel W3. *Plant J.* 16, 235–245. doi: 10.1046/j.1365-313x.1998.00294.x

Shang, B., Feng, Z. Z., Li, P., Yuan, X. Y., Xu, Y. S., and Calatayud, V. (2017). Ozone exposure- and flux-based response relationships with photosynthesis, leaf morphology and biomass in two poplar clones. *Sci. Total Environ.* 603, 185–195. doi: 10.1016/j.scitotenv.2017.06.083

Strohm, M., Eiblmeier, M., Langebartels, C., Jouanin, L., Polle, A., Sandermann, H., et al. (1999). Responses of transgenic poplar (*Populus tremula* x *P-alba*) overexpressing glutathione synthetase or glutathione reductase to acute ozone stress: visible injury and leaf gas exchange. *J. Exp. Bot.* 50, 365–374. doi: 10.1093/jxb/50.332.365

Strohm, M., Eiblmeier, M., Langebartels, C., Jouanin, L., Polle, A., Sandermann, H., et al. (2002). Responses of antioxidative systems to acute ozone stress in transgenic poplar (*Populus tremula* x *P-alba*) over-expressing glutathione synthetase or glutathione reductase. *Trees-Struct. Funct.* 16, 262–273. doi: 10.1007/s00468-001-0157-z

Vollenweider, P., Fenn, M. E., Menard, T., Günthardt-Goerg, M., and Bytnerowicz, A. (2013). Structural injury underlying mottling in ponderosa pine needles exposed to ambient ozone concentrations in the San Bernardino Mountains near Los Angeles, California. *Trees* 27, 895–911. doi: 10.1007/s00468-013-0843-7

Vollenweider, P., Günthardt-Goerg, M. S., Menard, T., Baumgarten, M., Matyssek, R., and Schaub, M. (2019). Macro- and microscopic leaf injury triggered by ozone stress in beech foliage (*Fagus sylvatica* L.). *Ann. For. Sci.* 76:71. doi: 10.1007/s13595-019-0856-5

Vollenweider, P., Menard, T., Arend, M., Kuster, T. M., and Gunthardt-Goerg, M. S. (2016). Structural changes associated with drought stress symptoms in foliage of central European oaks. *Trees-Struct. Funct.* 30, 883–900. doi: 10.1007/s00468-015-1329-6

Vollenweider, P., Ottiger, M., and Günthardt-Goerg, M. S. (2002). Validation of leaf ozone symptoms in natural vegetation using microscopical methods. *Environ. Pollut.* 124, 101–118. doi: 10.1016/s0269-7491(02)00412-8

Wittig, V. E., Ainsworth, E. A., Naidu, S. L., Karnosky, D. F., and Long, S. P. (2009). Quantifying the impact of current and future tropospheric ozone on tree biomass, growth, physiology and biochemistry: a quantitative meta-analysis. *Glob. Change Biol.* 15, 396–424. doi: 10.1111/j.1365-2486.2008.01774.x

Xu, Y. S., Feng, Z. Z., Shang, B., Dai, L. L., Uddling, J., and Tarvainen, L. (2019). Mesophyll conductance limitation of photosynthesis in poplar under elevated ozone. *Sci. Total Environ.* 657, 136–145. doi: 10.1016/j.scitotenv.2018.11.466

Zhang, J., Schaub, M., Ferdinand, J. A., Skelly, J. M., Steiner, K. C., and Savage, J. E. (2010). Leaf age affects the responses of foliar injury and gas exchange to tropospheric ozone in *Prunus serotina* seedlings. *Environ. Pollut.* 158, 2627–2634. doi: 10.1016/j.envpol.2010.05.003

Conflict of Interest: The authors declare that the research was conducted in the absence of any commercial or financial relationships that could be construed as a potential conflict of interest.

frontiers in Plant Science

ORIGINAL RESEARCH
published: 01 September 2021
doi: 10.3389/fpls.2021.717233

TaWRKY13-A Serves as a Mediator of Jasmonic Acid-Related Leaf Senescence by Modulating Jasmonic Acid Biosynthesis

Hualiang Qiao[1,2†], Yongwei Liu[2†], Lingling Cheng[1], Xuelin Gu[1], Pengcheng Yin[1], Ke Li[1], Shuo Zhou[2], Geng Wang[1] and Chunjiang Zhou[1*]*

[1] Ministry of Education Key Laboratory of Molecular and Cell Biology, Hebei Innovation Center for Cell Signaling, College of Life Sciences, Hebei Normal University, Shijiazhuang, China, [2] Institute of Genetics and Physiology, Hebei Academy of Agriculture and Forestry Sciences/Plant Genetic Engineering Center of Hebei Province, Shijiazhuang, China

OPEN ACCESS

Edited by:
Judy Brusslan,
California State University,
United States

Reviewed by:
Zenglin Zhang,
Tobacco Research Institute (CAAS), China
Yanjuan Jiang,
Xishuangbanna Tropical Botanical Garden (CAS), China

***Correspondence:**
Geng Wang
gengwang@hebtu.edu.cn
Chunjiang Zhou
cjzhou@hebtu.edu.cn

[†] These authors have contributed equally to this work and share first authorship

Specialty section:
This article was submitted to Plant Physiology, a section of the journal Frontiers in Plant Science

Received: 30 May 2021
Accepted: 19 July 2021
Published: 01 September 2021

Citation:
Qiao H, Liu Y, Cheng L, Gu X, Yin P, Li K, Zhou S, Wang G and Zhou C (2021) TaWRKY13-A Serves as a Mediator of Jasmonic Acid-Related Leaf Senescence by Modulating Jasmonic Acid Biosynthesis. Front. Plant Sci. 12:717233. doi: 10.3389/fpls.2021.717233

Leaf senescence is crucial for crop yield and quality. Transcriptional regulation is a key step for integrating various senescence-related signals into the nucleus. However, few regulators of senescence implicating transcriptional events have been functionally characterized in wheat. Based on our RNA-seq data, we identified a WRKY transcription factor, TaWRKY13-A, that predominately expresses at senescent stages. By using the virus-induced gene silencing (VIGS) method, we manifested impaired transcription of *TaWRKY13-A* leading to a delayed leaf senescence phenotype in wheat. Moreover, the overexpression (*OE*) of *TaWRKY13-A* accelerated the onset of leaf senescence under both natural growth condition and darkness in *Brachypodium distachyon* and *Arabidopsis thaliana*. Furthermore, by physiological and molecular investigations, we verified that TaWRKY13-A participates in the regulation of leaf senescence *via* jasmonic acid (JA) pathway. The expression of JA biosynthetic genes, including *AtLOX6*, was altered in *TaWRKY13-A*-overexpressing *Arabidopsis*. We also demonstrated that TaWRKY13-A can interact with the promoter of *AtLOX6* and *TaLOX6* by using the electrophoretic mobility shift assay (EMSA) and luciferase reporter system. Consistently, we detected a higher JA level in *TaWRKY13-A*-overexpressing lines than that in Col-0. Moreover, our data suggested that TaWRKY13-A is partially functional conserved with AtWRKY53 in age-dependent leaf senescence. Collectively, this study manifests TaWRKY13-A as a positive regulator of JA-related leaf senescence, which could be a new clue for molecular breeding in wheat.

Keywords: wheat, leaf senescence, jasmonic acid, WRKYs, transcriptional regulation

INTRODUCTION

Leaf senescence is a highly regulated developmental process and triggered by diverse environmental factors (Woo et al., 2019). As a sophisticated biological event, leaf senescence comprises multidimensional alterations in cell structure, metabolism, and expression of genes (Mayta et al., 2019). Organelles and macromolecular substances gradually degraded in an ordered manner. Then, nutrients transfer from senescent parts to developing and storage organs (Thomas and Ougham, 2014; Kim et al., 2018; Koyama, 2018; Zhang et al., 2018b; Woo et al., 2019). Meanwhile,

the initiation and progression of leaf senescence are also governed by numerous senescence-related genes that function in phytohormone pathways, transcriptional regulation, epigenetic modification, autophagy, circadian clock, DNA damage repair, and chlorophyll metabolism and light (Jia et al., 2019; Li et al., 2020; Xie et al., 2020; Xu et al., 2020; Yuan et al., 2020).

To date, more and more mechanistic details about how phytohormones regulate leaf senescence have been clarified. Phytohormones directly or indirectly regulate the onset and progression of leaf senescence by fine-tuning developmental programs or responses to stress (Jibran et al., 2013; Smith et al., 2017; Zhang et al., 2020). Different hormones participate in the regulation of leaf senescence with a distinct mechanism. Hormones, such as ethylene, abscisic acid, jasmonic acid (JA), salicylic acid (SA), brassinosteroids, and strigolactones, promote the initiation of leaf senescence, whereas cytokinins (CKs), gibberellins, and auxins delay leaf senescence (Arrom and Munne-Bosch, 2012; Khan et al., 2014; Tan et al., 2019; Wojciechowska et al., 2020; Zhang et al., 2021).

Jasmonic acid as a lipid-derived hormone has been long known for its crucial role in plant development and stress responses. JA is generally considered to be synthesized from alpha-linolenic acid that is further catalyzed by 13-lipoxygenase (LOX), allene oxide synthase, and allene oxide cyclase and then converted to (9S,13S)-12-oxo-phytodienoic acid (OPDA). After undergoing a series of reduction and oxidation reactions, OPDA is changed into JA in peroxisomes. Then, JA is transferred to the cytoplasm and conjugated with isoleucine to form (+)-7-*iso*-JA-Ile (JA-Ile). Meanwhile, JA-Ile can be inactivated by CYP94B3 (Khan et al., 2014; Wasternack and Song, 2016; Huang et al., 2017). To date, many studies have demonstrated that the JA pathway is involved in the regulation of leaf senescence (He et al., 2002b; Fonseca et al., 2009; Wasternack and Hause, 2013; Ahmad et al., 2016; Chini et al., 2016; Wojciechowska et al., 2018; Ruan et al., 2019; Aubry et al., 2020). For instance, some genes related to JA biosynthesis are upregulated during leaf senescence to varying degrees, such as *AtLOX1*, *AtLOX2*, *AtLOX3*, *AtLOX4*, and *AtAOC1* (He et al., 2002b; Kim et al., 2015; Hu et al., 2017). Moreover, TCP4 affects JA biosynthesis by interacting with *LOX2* and thus participates in the regulation of leaf senescence in *Arabidopsis* (Schommer et al., 2008; Koyama et al., 2017). Meanwhile, as positive regulators of the JA signaling pathway, MYC2, MYC3, and MYC4 can directly regulate the expression of *senescence-associated genes* (*SAG*s) by binding their G-box/G-box-like motifs (Qi et al., 2015; Liu et al., 2016; Song et al., 2017; Uji et al., 2017). However, leaf senescence is nearly unaffected by missing some key components of JA signaling transduction and biosynthesis (He et al., 2002a; Seltmann et al., 2010). Thus, more details about JA-related leaf senescence need to be carefully inspected and discussed. Importantly, although the roles of some genes in integrating the JA pathway with leaf senescence have been functionally studied in *Arabidopsis*, the mechanism underlying JA-related leaf senescence in wheat is still obscure.

WRKY transcription factors (TFs) are one of the largest TFs in plants, which play vital roles in many biological processes, including leaf senescence (Lin and Wu, 2004; Li et al., 2018). WRKY TFs contain the WRKY domain (a conserved amino acid sequence of WRKYGQK) at the N-terminus and an atypical zinc finger domain at the C-terminus. WRKY proteins are initially divided into three groups as follows: the first group contains a C_2H_2 ($CX_{4-5}CX_{22-23}HX_1H$) zinc finger motif and a WRKY domain, the second group contains a C_2H_2 zinc finger motif and two WRKY domains, and the third group contains a C_2-HC ($CX_7Cx_{23}HX_1C$) zinc finger motif. Recently, the phylogenetic analysis among different plant species suggested that WRKY protein should be divided into groups I, IIa + IIb, IIc, IId + IIe, and III. WRKYs generally bind to the W-box (TTGACC/T) in diverse target genes and hence mediate various signals (Eulgem et al., 2000; Rushton et al., 2010; Jiang et al., 2017; Song et al., 2018). To date, the functional role of some WRKYs in the regulation of leaf senescence has been predominately demonstrated in *Arabidopsis* (Hinderhofer and Zentgraf, 2001; Schippers, 2015). Among the senescence-related WRKYs, AtWRKY53 functions as a central regulator and integrates many senescence-related signals at the transcriptional level (Miao and Zentgraf, 2007; Zheng et al., 2020). AtWRKY45, AtWRKY57, and AtWRKY75 regulate the initiation of leaf senescence *via* phytohormone pathways (Jiang et al., 2014; Chen et al., 2017; Guo et al., 2017). AtWRKY54 and AtWRKY70 cooperatively suppress the onset of leaf senescence (Besseau et al., 2012). AtWRKY6 promotes leaf senescence but it is repressed by DELLA proteins (Robatzek and Somssich, 2001; Lim et al., 2018; Zhang et al., 2018c). AtWRKY55 positively regulates leaf senescence by affecting reactive oxygen species and SA level (Wang et al., 2020). Although many senescence-related WRKYs have been functionally characterized in *Arabidopsis*, WRKYs implicated in the regulation of leaf senescence are extremely elusive in wheat.

Common wheat (*Triticum aestivum* L.) is one of the most widely cultivated food crops. However, due to the allohexaploid genome of wheat, studies on candidate genes of various biological processes are difficult to carry out. Hence, some functional studies on wheat genes are also conducted with the help of some analysis in other monocots. For instance, as a model plant of monocot grass, *Brachypodium distachyon* possesses a much smaller genome than wheat and is more easily to be transformed (Scholthof et al., 2018). Thus, the experimental data from *B. distachyon* are also significantly helpful to understand the mechanistic framework of leaf senescence in wheat. To date, as more and more detailed information on the wheat genome is available, researchers have identified some key components of different regulatory networks in wheat (Borrill et al., 2019; Sultana et al., 2021). *NAM-B1* is reported to accelerate leaf senescence onset and promote nutrients redistribution (Uauy et al., 2006). The wheat copper-binding protein (WCBP1) is tightly related to the regulation of leaf senescence when wheat plants undergo the infection of stripe rust (Li et al., 2015). Our data reveal TaWRKY42-B and TaWRKY40-D as positive regulators in phytohormone-related wheat leaf senescence (Zhao et al., 2020a,b). Moreover, cisZOGT1, a *cis*-zeatin *O*-glucosyltransferase, is involved in wheat leaf senescence by regulating CK and N metabolism (Wang et al., 2019). By the high-throughput analysis, researchers have also identified some candidate genes in drought-induced leaf senescence in wheat

(Luo et al., 2019). Meanwhile, TaSCL14 is a member of the GRAS protein family in wheat and plays multiple roles in development, photosynthesis, stress response, and dark-induced senescence (Chen et al., 2015).

In this study, we identified a WRKY type TF, *TaWRKY13-A*, as a positive regulator of leaf senescence under both natural condition and darkness. *TaWRKY13-A*-silenced wheat plants showed the delayed leaf senescence phenotype. Consistently, the overexpression of *TaWRKY13-A* promoted leaf senescence in *B. distachyon* and *Arabidopsis*. Furthermore, we manifested that *TaWRKY13-A* regulates leaf senescence by targeting JA biosynthetic genes. By affecting the expression of *LOXs*, TaWRKY13-A can enhance the JA content, which finally contributes to the initiation and progression of leaf senescence. Our data also suggested that TaWRKY13-A is partially conserved with AtWRKY53.

MATERIALS AND METHODS

Plant Materials and Growth Conditions

The *Arabidopsis* seeds were sterilized with ethanol and sprinkled on 1/2MS solid medium. The above seeds were placed at 4°C under darkness for 2 days and then continued to grow in a growth chamber for the next 5 days. Seven-day-old seedlings were transferred to a greenhouse at 22°C (16-h light/8-h dark) for the subsequent cultivation. *Arabidopsis thaliana* Col-0 and *atwrky53* (SALK_034157) seeds used in this study were obtained from Arabidopsis Biological Resource Center and provided by Prof. Ying Miao (Fujian Agriculture and Forestry University). The background of *atwrky53* mutants was confirmed with PCR assay by following the published data (Miao and Zentgraf, 2007).

Bread wheat seeds germinated and were grown to the two-leaf stage in water, and then they were transferred into the greenhouse at 25°C, with the humidity at 70% and in the period of 16/8 h light/dark. Bread wheat varieties "ShiLuan 02-1" were provided by Prof. Zhanjing Huang (Hebei Normal University), and "cv. Chinese spring," "KeNong199" was preserved and obtained from the seed bank of the Institute of Genetics and Physiology, Hebei Academy of Agriculture and Forestry Sciences. Wheat plants of "ShiLuan02-1" were used for the expression mode analysis of *TaWRKY13-A*. The 10-day-old etiolated seedlings of "KeNong199" were used to generate wheat protoplasts.

Plasmid Construction and Plant Transformation

The full-length coding sequences (CDS) of *TaWRKY13-A* was constructed into the pCAMBIA1300-MYC-HIS vector and driven by using the 35S promoter (**Supplementary Figure 3C**). Vectors were transformed into Col-0 and *atwrky53* mutants by *Agrobacterium* stain GV3101 by using the floral dip transformation method (Clough and Bent, 1998).

For the transcription activation assay, the CDS of *TaWRKY13-A* was fused with the GAL4 DNA binding domain in pSAT-GAL4DB.

For the subcellular localization analysis, the full-length *TaWRKY13-A* CDS was constructed into the pUC19 vector and transformed into wheat protoplasts to observe the subcellular localization of TaWRKY13-A.

To express and purify the MBP-TaWRKY13-A fusion protein for the electrophoretic mobility shift assay (EMSA), the open reading frame sequence of *TaWRKY13-A* was cloned into the pMAL-C2X expression vector and transformed into *Escherichia coli* (strain *Rosetta*) competent cells for the prokaryotic expression.

Ion Leakage and Chlorophyll Content

The chlorophyll content was measured by using a chlorophyll meter (SPAD 502 Plus Chlorophyll Meter, Minolta Corporation, Tokyo, Japan). First, leaves were placed in 10 ml of deionized water and vacuumed for 1 h, and then the conductivity was measured. Then, leaves were boiled for 10 min and the conductivity was measured again after the water cooled down. Ion leakage rate was indicated by the ratio of conductivity of leaves before boiled/after boiled in deionized water.

Quantitative Real-Time-PCR

By using Trizol (Takara, 9109), the total RNA was extracted from *Arabidopsis*, wheat, and *Brachypodium*. A total of 500 ng of RNA was used to generate cDNA by using 5 × HiScriptII qRT SuperMixII (R223-01). The real-time PCR analysis was performed on a CFX96 real-time fluorescent quantitative PCR instrument by using 2 × ChamQ Universal STBR Master Mix (Q711-02/0).

All the primers used in this study are listed in **Supplementary Table 1**. In the quantitative real-time (qRT)-PCR analysis, each sample was tested in three technical and three biological repeats. In wheat, the expression of the *TaACTIN* gene is used as an internal control, while in *Arabidopsis*, it is *AtUBC30*.

Quantification of JA Content

To analyze the JA content in *TaWRKY13-A-OE* and Col-0 *Arabidopsis* plants, fifth and sixth leaves of 4-week-old and 5-week-old *Arabidopsis* were selected for liquid chromatography-tandem mass spectrometry (LC-MS/MS) assay. A total amount of 200 mg leaves of the above plants were grounded and incubated with methanol for 24 h. By using the Oasis Max solid-phase extraction cartridge, all samples were purified. The JA content was measured using the ultra-performance liquid chromatography (UPLC) system (Waters) (Agilent Technologies Inc, California, USA) and QTRAP 6500 system (AB SCIEX, Framingham, MA, USA). The measurement of each sample was repeated in three biological replicates, and $^{2}H_{5}$-JA was used as the internal reference. The JA content of each sample was finally examined by ultra-performance liquid chromatography-mass spectrometry/mass spectrometry (UPLC-MS/MS) (Waters) and QTRAP 6500 system (AB SCIEX).

Barley Stripe Mosaic Virus-Virus-Induced Gene Silencing

The vectors for Barley stripe mosaic virus (BSMV)–virus-induced gene silencing (VIGS) were provided by Prof. Dawei Li. A 326 bp fragment amplified from TaWRKY13-A cDNA was introduced into the pCaBS-γbLIC vector. *Agrobacterium*

containing each pCaBS-α, β, and γ vector was cultured on a shaker overnight and collected. Each of the above bacterial solutions [10 mM MES, 10 mM $MgCl_2$, pH 5.2, and 0.1 mM Acetosyringone (AS)] was adjusted to Optical Density (OD) = 0.7, mixed with the others, and incubated at 30°C for 5 h. The mixed solution was further injected into 2-week-old tobacco leaves. Two weeks later, we grounded the infected tobacco leaves with PBS buffer and then injected it into the two-leaf wheat seedlings. The wheat plants harboring the empty vectors (i.e., pCaBS-α, pCaBS-β, and pCaBS-γbLIC) were used as negative controls.

Electrophoretic Mobility Shift Assay

The protein used in the EMSA experiment was purified using the Amylose Resin (0812S, New England Biolabs, Beverly, MA, USA). The CDS of *TaWRKY13-A* was subcloned into the pMal-c2X vector and transformed into *Rosetta* strain. After the addition of Isopropyl-beta-D-thiogalactopyranoside (IPTG) (final concentration of 1 mM), MBP-TaWRKY13-A was expressed at 18°C for 5 h and purified. The probes used in the EMSA experiment (**Supplementary Table 1**) were all labeled with biotin at the 5′end. We performed the EMSA by using the Chemiluminescent Nucleic Acid Detection Module (Thermo Scientific, 89,880) to detect the interaction between protein and DNA. The total reaction system is 10 μl, including 1 μl of binding buffer, 0.5 μl of poly-dIdC, 0.5 μl of glycerol, 0.5 μl of 1 M KCl, 1 μl of biotin-probe, and 400 ng of the target protein. Unlabeled probes were added at 100- and 200-fold of labeled probes as competitors. The mixture was placed at 4°C for 20 min and subjected to the electrophoresis analysis. Biotin-labeled probes are listed in **Supplementary Table 1**.

RESULTS

Identification and Sequence Analysis of *TaWRKY13-A*

To identify WRKY TFs related to leaf senescence in wheat, we analyzed our RNA-seq data at four developmental stages of flag leaves (i.e., YL, young leaves with half size of mature leaves; ML, mature leaves, fully expanded leaves; ES, early senescence leaves with <25% leaf area yellowing; and LS, late senescence leaves with >50% leaf area yellowing) in wheat (cv. Chinese Spring) (Zhao et al., 2020b) and selected a WRKY TF (TraesCS4A02G193600.1) that shows a more significantly increasing expression trend during leaf senescence than its paralogs on chromosomes B and D (**Supplementary Figures 1B,C**). Hence, in this study, we mainly focused on this gene. According to the corresponding sequence obtained from the WheatOmics (http://202.194.139.32/), we confirmed that the candidate gene is *TaWRKY13-A* that encodes a 24.49-kDa protein of 222 amino acids and with an isoelectric point of 8.33. The presence of a WRKY domain and a C_2HC zinc finger motif indicated that TaWRKY13-A is a member of the group III WRKYs (**Supplementary Figure 3A**). Then, we performed a phylogenetic analysis among the amino sequence of TaWRKY13-A and some published senescence-related WRKYs, and we found that TaWRKY13-A is relatively close to AtWRKY55, AtWRKY70, AtWRKY54, and AtWRKY53 (**Supplementary Figure 1A**).

Spatiotemporal Expression Pattern of TaWRKY13-A

To investigate the role of TaWRKY13-A, we first checked the expression profiling of *TaWRKY13-A* in wheat flag leaves at four different developmental stages (i.e., YL, ML, ES, and LS) (**Figure 1A**). Parameters related to leaf senescence, including chlorophyll content, ion leakage rate (**Figures 1B,C**), and the transcription level of a senescence marker gene *TaSAG3*, were measured to verify the accuracy of harvesting different leaves (**Figure 1E**). Consistent with the information on WheatOmics (http://202.194.139.32/) and our RNA-seq data (**Supplementary Figures 1B,C**), we confirmed that *TaWRKY13-A* predominantly expressed at ES and LS stages by the qRT-PCR assay (**Figure 1D**). In general, the onset of senescence is from the tip of a leaf and gradually proceeds to the leaf base (**Figure 1F**). Consistently, we measured the most chlorophyll content and the least ion leakage rate in the leaf tip (**Figures 1G,H**). We also detected more *TaWRKY13-A* transcripts in the leaf tip than in the middle and base (**Figure 1I**), which is in line with the expression of *TaSAG3* (**Figure 1J**). Then, we analyzed the transcription level of *TaWRKY13-A* in different tissues, including spike, seed, root, internode, flag leaf, and mature leaf (**Figure 2A**). We detected a ubiquitous expression pattern of *TaWRKY13-A*, while transcripts of *TaWRKY13-A* were predominantly concentrated in flag leaves (**Figure 2B**). The above results indicated that *TaWRKY13-A* may play a role in wheat leaf senescence.

TaWRKY13-A Localizes in the Nucleus and Possesses Transcriptional Activity

It is widely acknowledged that WRKYs are responsible for mediating diverse signals at the transcriptional level. To investigate whether TaWRKY13-A has the potential to regulate transcriptional events, we generated a *35S:TaWRK13-A-GFP* construct, which was transformed and transiently expressed in wheat protoplasts. Fluorescent signals of TaWRKY13-A-GFP fusion appeared only in the nucleus, while the single GFP protein was detectable among plasma membrane, cytoplasm, and nucleus (**Figure 2C**). To further verify whether TaWRKY13-A functions as a TF, we used the dual-luciferase reporter system to test the transcriptional activity of TaWRKY13-A in wheat protoplasts. We fused the TaWRKY13-A with Gal4-DNA binding domain (GDBD) and then transformed GDBD-TaWRKY13-A with the *firefly luciferase* (*LUC*) gene driven by a fusion of CaMV 35S promoter and upstream activation sequence. The 35S:*Renilla luciferase* (*REN*) construct served as an internal control (**Figure 2D**). We found that the activity ratio of LUC/REN was specifically elevated by GDBD-TaWRKY13-A (**Figure 2E**). These results suggested that TaWRKY13-A may function as a TF.

Silencing of *TaWRKY13-A* Causes the Delayed Leaf Senescence Phenotype in Wheat

To further evaluate the function of TaWRKY13-A, we silenced TaWRKY13-A in wheat by using the BSMV–VIGS method. Bleached leaves induced by the impairment of the *TaPDS* gene indicated that the BSMV–VIGS method used in this study

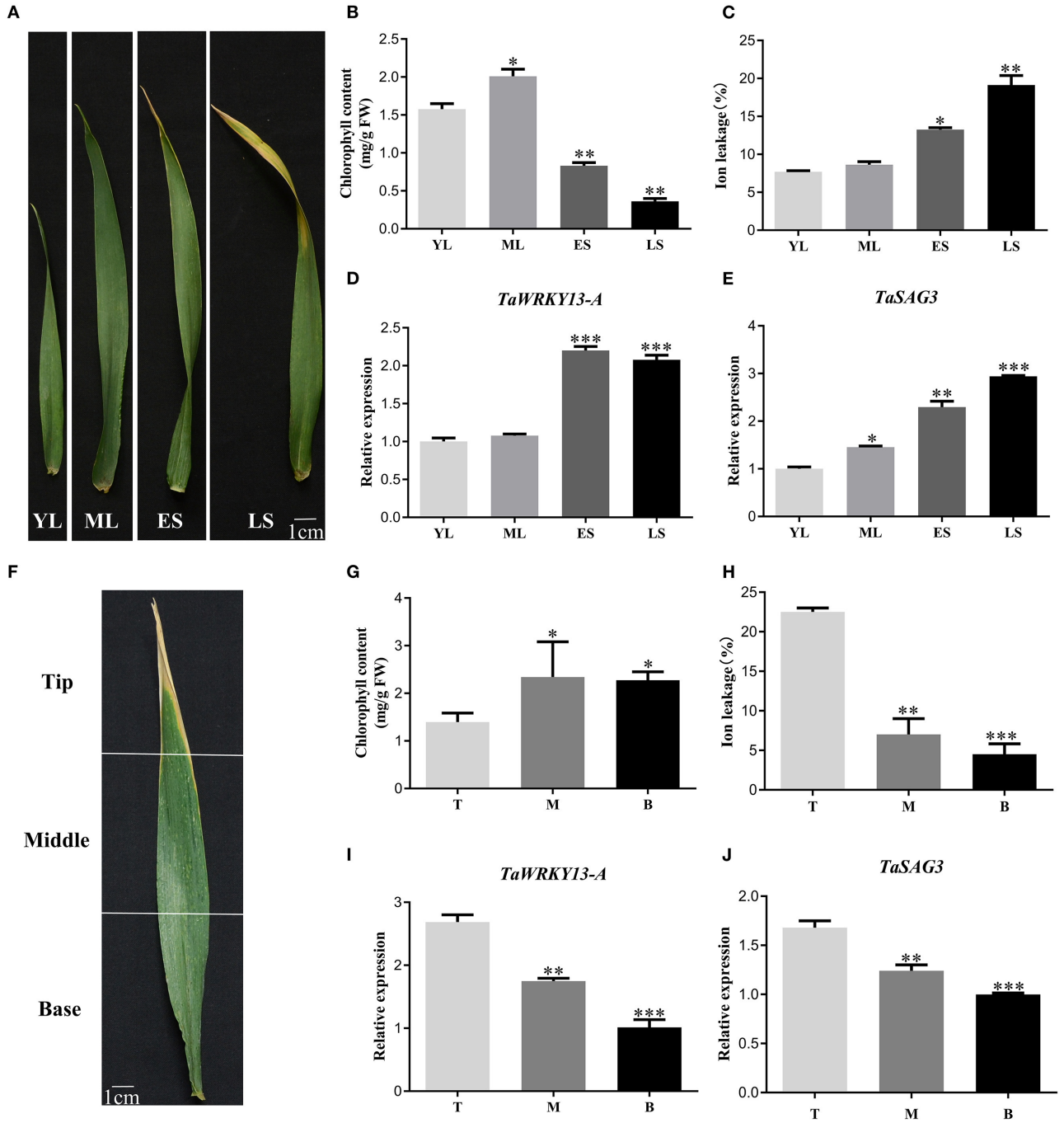

FIGURE 1 | Expression pattern of *TaWRKY13-A* in wheat. **(A)** Four different development stages of flag leaf (i.e., YL, young leaves with half size of mature leaves; ML, mature leaves, fully expanded leaves; ES, early senescence leaves with <25% leaf area yellowing; and LS, late senescence leaves with >50% leaf area yellowing) in cv. Chinese spring. **(B,C)** Chlorophyll content and ion leakage rate of **(A)**. **(D)** Transcription level detection of *TaWRKY13-A* in **(A)** by using the quantitative real-time (qRT)-PCR. **(E)** Transcription level detection of a *senescence-associated gene, TaSAG3*, in **(A)** by using the qRT-PCR. **(F)** The tip, middle, and base of a senescent wheat flag leaf. **(G,H)** Chlorophyll content and ion leakage rate of **(F)**. **(I)** Transcription level detection of *TaWRKY13-A* expression in **(F)** by qRT-PCR. **(J)** Transcription level detection of *TaSAG3* in **(F)** by using the qRT-PCR. (Error bars indicate SD. Asterisks indicate significant differences. Student's *t*-test, $^{*}P < 0.05$, $^{**}P < 0.01$, $^{***}P < 0.001$, and $n \geq 30$. Above experiments were repeated at least in three biological replicates).

is feasible (**Supplementary Figures 4A,B**). Hence, we selected a 326 bp target sequence from 342 bp downstream of the translation initiation codon of TaWRKY13-A for BSMV–VIGS. However, due to the high similarity between *TaWRKY13-A* and *TaWRKY13-B*, we were not able to select a unique target sequence only in *TaWRKY13-A* cDNA. One-week-old

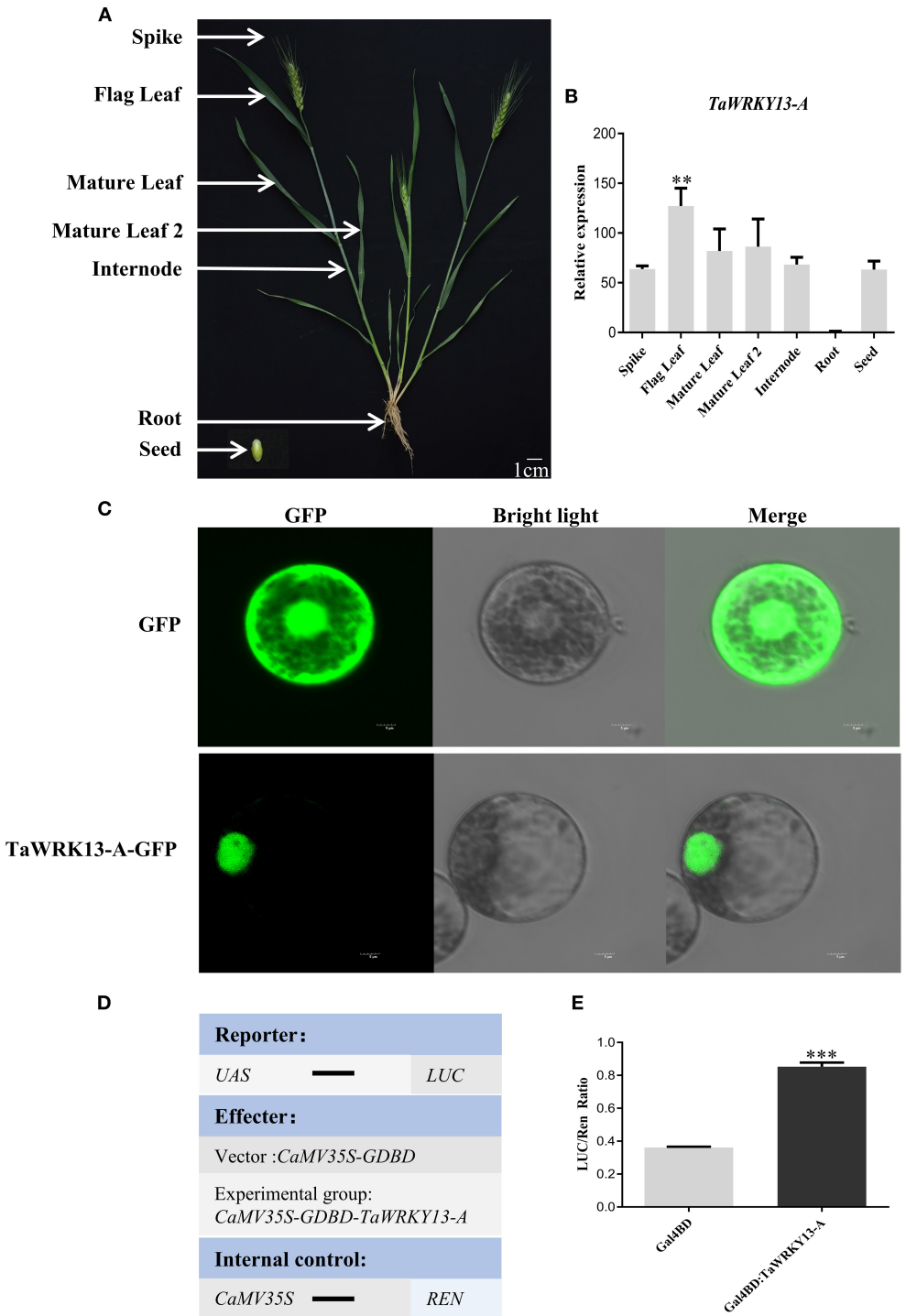

FIGURE 2 | Expression pattern and subcellular localization analysis of TaWRKY13-A. **(A)** Different tissues of 6-month-old mature wheat. **(B)** The tissue expression pattern of *TaWRKY13-A* in **(A)** by using the qRT-PCR (Flag leaf, Spike, 1st mature leaf from the top, Mature leaf 1; 2nd mature leaf from the top, Mature leaf 2; stem, root, and seed). **(C)** Subcellular localization of TaWRKY13-A in wheat protoplasts (scale bar = 5 μm). **(D,E)** Transcriptional activity assay of TaWRKY13-A in wheat protoplasts. Schematic diagrams indicate the vector constructs. Measurement of relative activity LUC after transient expression of fusion vector in wheat protoplasts. (Error bars indicate SD. Asterisks indicate significant differences. Student's *t*-test, $^{**}P < 0.01$, $^{***}P < 0.001$, and $n \geq 30$. The above experiments were repeated at least in three biological replicates).

wild-type (WT) wheat plants and wheat seedlings that were infected by BSMV that contains *TaWRKY13-A*$_{326}$ (pCaBS-α, pCaBS-β, and pCaBS-γbTaWRKY13-A$_{326}$) or empty vector (pCaBS-γbLIC) were used in this research. By using the qRT-PCR assay, we selected all the wheat plants with the decreased transcription level of *TaWRKY13-A* among those infected plants for subsequent analysis. After 25 days of growth, the eighth leaf from the top of *TaWRKY13-A*-silenced plants and control groups were used to compare the dark-induced leaf senescence phenotype. After 6 days under darkness, leaf senescence was remarkably accelerated in *TaWRKY13-A*-silenced leaves when compared with that in vector control (VC) and WT (**Supplementary Figure 4C**). Meanwhile, chlorophyll degradation and ion leakage rate were in line with the phenotypic changes (**Supplementary Figures 4D,E**). Moreover, we counted the number of senescent and non-senescent leaves among 9-week-old *TaWRKY13-A*-silenced plants and control groups (**Figure 3C**). The statistical data showed a significantly lower ratio of yellow/green leaves in *TaWRKY13-A*-silenced plants than that in control groups (**Figure 3B**). These results suggested that TaWRKY13-A is involved in the regulation of leaf senescence in wheat.

Overexpression of *TaWRKY13-A* Promotes Age-Dependent and Dark-Induced Leaf Senescence in *B. distachyon* and *Arabidopsis*

To further assess the role of TaWRKY13-A in leaf senescence, we produced *TaWRKY13-A*-overexpressing (*OE*) lines in *B. distachyon* and *Arabidopsis*. First, we generated a construct where the fusion of full-length *TaWRKY13-A* CDS and Flag tag is under the control of the ubiquitin (Ubi) promoter. The constructs of P_{Ubi}:TaWRKY13-A-Flag were further transformed into *Brachypodium* callus. The expression of *TaWRKY13-A* was confirmed by semi-quantitative reverse transcript PCR (RT-PCR) (**Figure 3G**). Two *TaWRKY13-A*-overexpression *Brachypodium* lines (i.e., Line 10 and Line 32) and WT both exhibited normal growth at the seedling stage. While 7 weeks after sowing, Line 10 and Line 32 showed the obviously precocious leaf senescence phenotype when compared with WT (**Figure 3D**). The chlorophyll content and cell membrane integrity were significantly lower than those in WT at the senescent stage (**Figures 3E,F**). Dark-induced leaf senescence was also assessed among detached leaves of Line 10, Line 32, and WT. After treatment, leaf senescence triggered by darkness appeared earlier in Line 10 and Line 32 than that in WT (**Supplementary Figure 5A**). Consistently, chlorophyll degradation and ion leakage were more severe in Line 10 and Line 32 than those in WT (**Supplementary Figures 5B,C**).

Moreover, the full-length 669 bp CDS of *TaWRKY13-A* was cloned into pCAMBIA1300 and fused with the 7Myc-6His tag. This *TaWRKY13-A-7Myc6His* fusion was driven by using the CaMV 35S promoter. Two independent homozygous transgenic *Arabidopsis* lines (*OE-2* and *OE-5*) were selected for phenotypic and physiological analysis. We confirmed the increased expression level of *TaWRKY13-A*-overexpressing lines by using the RT-PCR and Western blot (**Figure 4B**). Then, we observed that 5-week-old *OE-2* and *OE-5* plants exhibited obviously early leaf senescence when compared with Col-0 (**Figure 4A**). Consistently, the chlorophyll content in *TaWRKY13-A*-overexpressing lines was lower than that in Col-0 (**Figure 4C**), and the overexpression of *TaWRKY13-A* also accelerated ion leakage (**Figure 4D**). Additionally, the expression level of two *SAGs*, namely, *AtSAG12* and *AtSAG113*, in *TaWRKY13-A*-overexpressing lines were higher than those in Col-0 (**Figures 4E,F**), while two senescence downregulated genes, namely, *AtRBCS* and *AtCAB1*, were decreased in *OE-2* and *OE-5* when compared with those in Col-0 (**Figures 4G,H**). To investigate whether TaWRKY13-A is also involved in dark-induced leaf senescence in *Arabidopsis*, we covered the fifth and sixth leaves on 4-week-old *OE-2*, *OE-5*, and Col-0 by using the aluminum foil for 6 days. Meanwhile, we also harvested the fifth and sixth rosette leaves of 4-week-old *TaWRKY13-A*-overexpressing lines and Col-0 for treatment under darkness. Then, these phenotypically indistinguishable leaves were incubated under darkness for 6 days (**Supplementary Figures 6A,D**). After treatment, leaves of *OE-2* and *OE-5* showed a significantly precious leaf senescence compared with WT leaves. Chlorophyll degradation (**Supplementary Figures 6B,E**) and ion leakage rate altered more dramatically than those in Col-0 (**Supplementary Figures 6C,F**). All above data proved that TaWRKY13-A can promote leaf senescence under both natural growth conditions and darkness. Moreover, the functional role of TaWRKY13-A in leaf senescence seemed to be conserved in *B. distachyon* and *Arabidopsis*, which helps us to screen the target genes of TaWRKY13-A in leaf senescence with the help of some more convenient strategies than only in wheat.

Inducible Overexpression of *TaWRKY13-A* Promotes Leaf Senescence

To rule out the effect of constitutive expression of *TaWRKY13-A* by CaMV 35S promoter, we generated two inducible *TaWRKY13-A*-overexpressing lines (i.e., *iOE-1* and *iOE-5*). The CDS of *TaWRKY13-A* was under the control of the dexamethasone (DEX)-inducible promoter, thus the expression of *TaWRKY13-A* was rapidly induced by exogenous application of 30 μM DEX (**Supplementary Figure 7E**). Transgenic plants harboring empty vectors were used as VC. We sprayed dexamethasone on 28-day-old *iOE-1*, *iOE-5*, VC, and Col-0 *Arabidopsis* plants. Compared with VC and Col-0, *iOE-1* and *iOE-5* showed the significantly premature phenotype at 4 days after the application of DEX (**Supplementary Figure 7A**). We detected the significantly reduced chlorophyll level (**Supplementary Figure 7C**) and the higher membrane ion leakage rate (**Supplementary Figure 7D**) in *iOE-1* and *iOE-5* when compared with control groups. Generally, the H_2O_2 level is increasing with the progression of leaf senescence. Thus, we performed the 3,3-diaminobenzidine staining among *iOE-1*, *iOE-5*, VC, and Col-0 to indicate the H_2O_2 level *in vivo*. Compared with VC and Col-0,

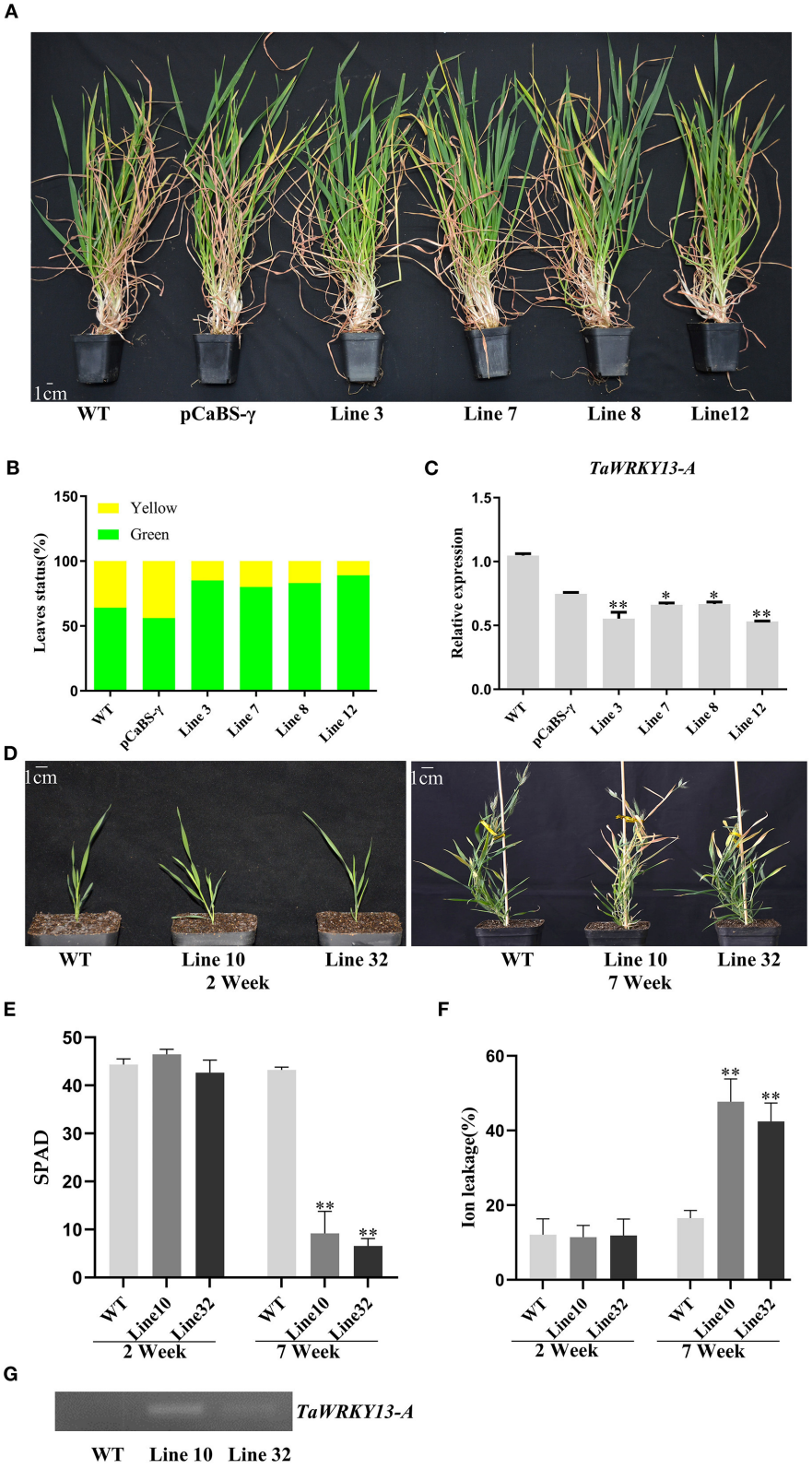

FIGURE 3 | Phenotypic observation in *TaWRKY13-A*-silenced wheat and *TaWRKY13-A*-overexpressing *Brachypodium distachyon*. **(A)** Observation of the leaf senescence phenotype in *TaWRKY13*-A-silenced (VIGS technology) wheat leaves under natural conditions. **(B)** Statistics of green leaves and senescent leaves (yellow

(Continued)

FIGURE 3 | of 9-week-old wheat plants in **(A)**. **(C)** Expression of *TaWRKY13-A* in *TaWRKY13-A*-silenced wheat by using the qRT-PCR. **(D)** Observation of the leaf senescence phenotype in *TaWRKY13-A*-overexpressing *B. distachyon.* **(E,F)** Physiological data measurements in **(D)** including chlorophyll content **(E)** and ion leakage rate **(F)**. **(G)** Detections of the overexpression of *TaWRKY13-A* at transcription levels in *B. distachyon.* (Error bars indicate SD. Asterisks indicate significant differences. Student's *t*-test, $^{*}P < 0.05$, $^{**}P < 0.01$, and $n \geq 30$. The above experiments were repeated at least in three biological replicates).

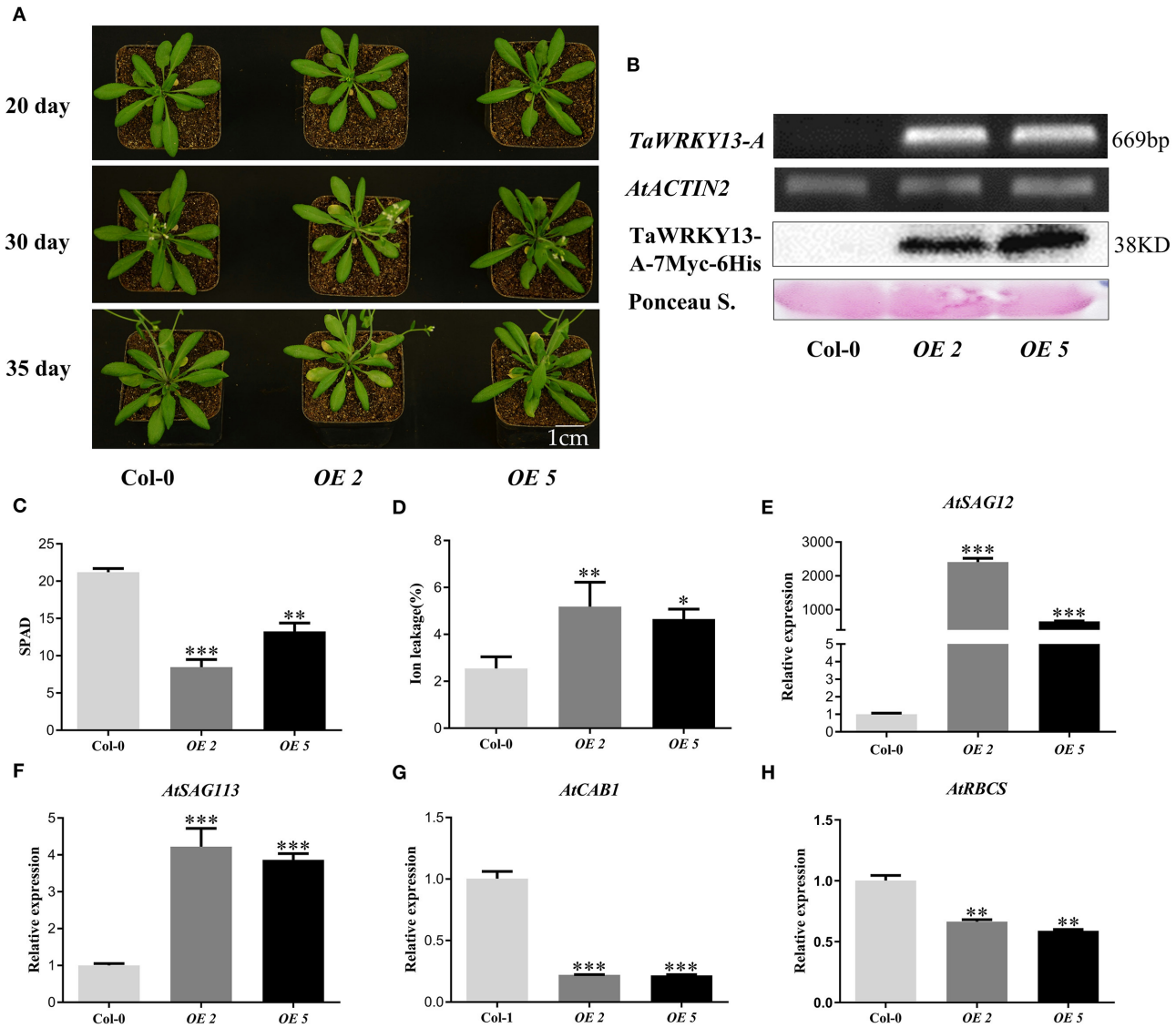

FIGURE 4 | Phenotypic observation in *TaWRKY13-A*-overexpressing *Arabidopsis*. **(A)** Observation of leaf senescence phenotype of *TaWRKY13-A*-overexpressing *Arabidopsis* and Col-0 under the natural growth condition. **(B)** Detections of the overexpression of *TaWRKY13-A* at transcription and protein levels in *Arabidopsis*. **(C,D)** Physiological data measurement in **(A)** including chlorophyll content **(C)** and ion leakage rate **(D)**. **(E,H)** Detection of senescence-associated genes including up-regulated genes *AtSAG12* **(E)**, *AtSAG113* **(F)** and downregulated genes *AtCAB1* **(G)**, *AtRBCS* **(H)**. (Error bars indicate SD. Asterisks indicate significant differences. Student's *t*-test, $^{*}P < 0.05$, $^{**}P < 0.01$, $^{***}P < 0.001$, and $n \geq 30$. The above experiments were repeated at least in three biological replicates).

more dark brown spots were detected in *iOE-1* and *iOE-5* (**Supplementary Figure 7B**). Furthermore, the expression level of senescence-specific marker genes including *AtSAG12*, *AtSAG13*, *AtSAG113*, *AtCAB1,* and *AtRBCS* in leaves of *iOE-1*, *iOE-5*, VC, and Col-0 was analyzed. We confirmed that *AtSAG12*, *AtSAG13*, and *AtSAG113* in *iOE-1* and *iOE-5* were enhanced compared with VC and Col-0 (**Supplementary Figures 7F–H**). Transcriptions of two senescence downregulated genes, namely, *AtCAB1* and *AtRBCS*, were strongly reduced by overexpression of *TaWRKY13-A* (**Supplementary Figures 7I,J**). The above results further illustrated that TaWRKY13-A can specifically function in leaf senescence.

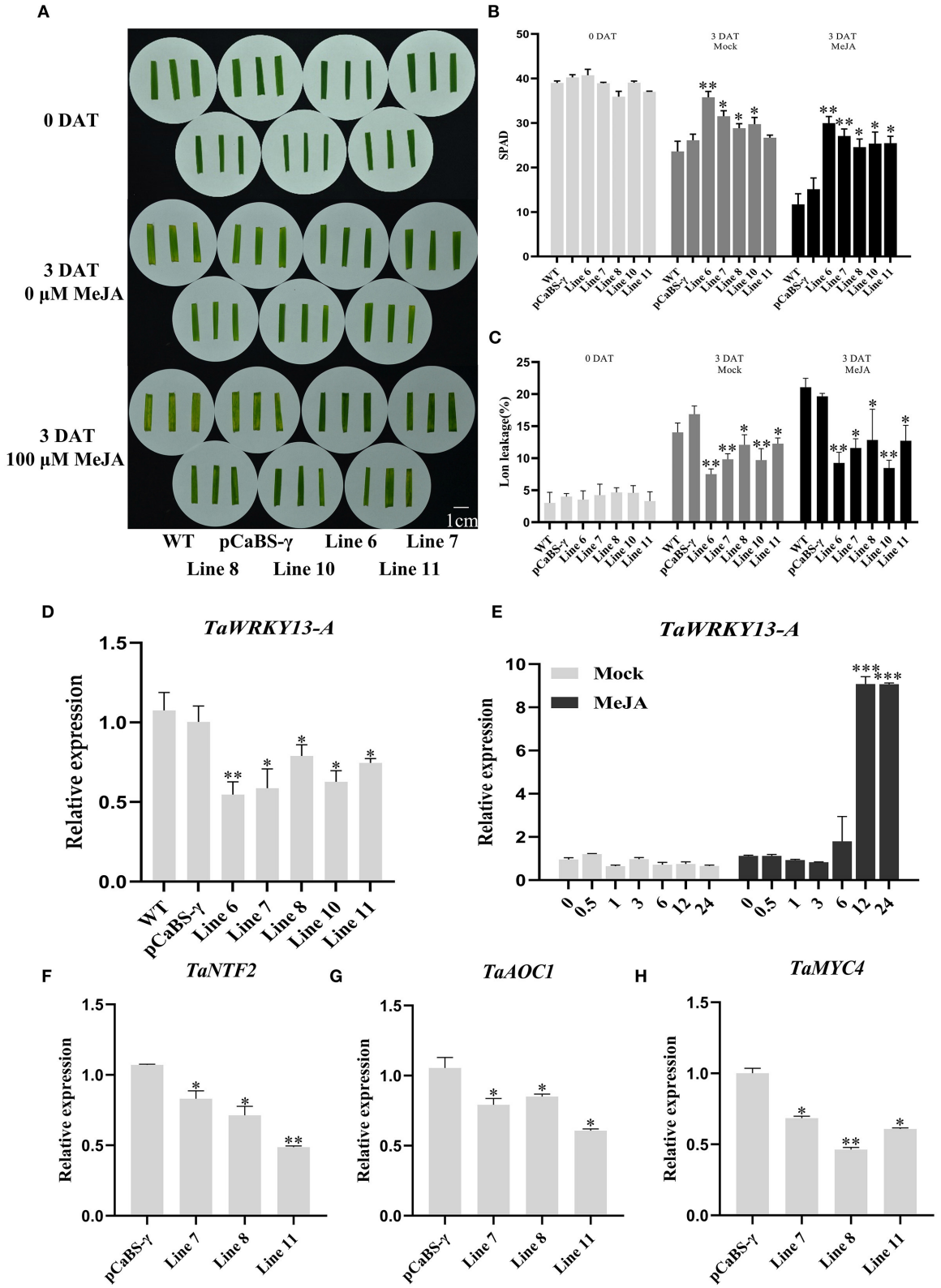

FIGURE 5 | *TaWRKY13-A*-silenced wheat is insensitive to MeJA treatment. **(A)** Observation of the leaf senescence phenotype of *TaWRKY13-A*-silenced wheat and control groups under 100 μM of MeJA treatment. **(B,C)** Physiological data measurement in **(A)** including chlorophyll content **(B)** and ion leakage rate **(C)**.

(Continued)

FIGURE 5 | (D) Detection of *TaWRKY13-A* transcription in **(A)**. **(E)** Expression pattern of *TaWRKY13-A* under MeJA treatment. **(F–H)** Expression of the JA-responsive gene, *TaNTF2* **(F)**, *TaAOC1* **(G)**, and *TaMYC4* **(H)** in *TaWRKY13-A*-silenced and VC wheat plants. (Error bars indicate SD. Asterisks indicate significant differences. Student's *t*-test, $^{*}P < 0.05$, $^{**}P < 0.01$, $^{***}P < 0.001$, and $n \geq 30$. The above experiments were repeated at least in three biological replicates).

TaWRKY13-A Promotes Leaf Senescence by Upregulating JA Pathway Genes

To reveal the mechanism underlying TaWRKY13-A-promoted leaf senescence, we inspected the *cis*-acting elements in the *TaWRKY13-A* promoter region for clues. Notably, eight CGTCA motifs related to JA responsiveness are located at −990 bp, −972 bp, −853 bp, −766 bp, −754 bp, −734 bp, −550 bp, −502 bp, and −454 bp of the TaWRKY13-A promoter (**Supplementary Figure 3B**). Therefore, we speculated that TaWRKY13-A regulates leaf senescence *via* the JA pathway. First, we examined the expression pattern of *TaWRKY13-A* under 100 μM of MeJA. Transcripts of *TaWRKY13-A* increased from 6 h and reached the peak at 12 h after treatment when compared with the mock (**Figure 5E**). Then, we analyzed the JA-induced leaf senescence among *TaWRKY13-A*-silenced wheat plants and controls. Leaf senescence was remarkably induced in all plants, while the premature phenotype was most accelerated in controls than *TaWRKY13-A*-silenced wheat (**Figures 5A–D**). Meanwhile, we examined the expression of three JA-responsive genes, including *TaNTF2*, *TaAOC1*, and *TaMYC4* between VC and *TaWRKY13-A*-silenced wheat plants (Zhao et al., 2014; Zhang et al., 2018a; Jing et al., 2019). By using the qRT-PCR assay, we detected the significantly lower levels of *TaNTF2*, *TaAOC1*, and *TaMYC4* in *TaWRKY13-A*-silenced wheat plants when compared with VC plants (**Figures 5F–H**).

In addition, we treated the non-senescent fifth or sixth rosette leaves of 4-week-old *TaWRKY13-A*-overexpressing *Arabidopsis* lines and Col-0 with 100 μM of MeJA for 2 days under darkness (**Figure 6A**). Leaf senescence was also accelerated by MeJA treatment in all leaves, but chlorophyll degradation and ion leakage in *TaWRKY13-A*-overexpressing plants were more severe than control plants after MeJA treatment (**Figures 6B,C**).

To further analyze the interaction between the TaWRKY13-A and JA pathways, we detected the expression levels of different genes related to JA signaling transduction and biosynthesis in *TaWRKY13-A*-overexpressing *Arabidopsis* and Col-0. JA biosynthetic genes, including *AtLOX1*, *AtLOX2*, *AtLOX5*, and *AtLOX6* in *OE-2* and *OE-5* were enhanced when compared with those in Col-0 (**Figures 6D–I**). Moreover, signaling components, such as *AtMYC2*, *AtMYC3*, *AtMYC4*, *AtVSP1*, and *AtVSP2*, were also affected by *TaWRKY13-A* overexpression (**Supplementary Figures 10A–F**). These results indicated that TaWRKY13-A promotes leaf senescence tightly related to the JA pathway.

TaWRKY13-A Promotes JA Biosynthesis by Binding to Promoters of *LOXs*

As TaWRKY13-A affected the expression of some JA pathway genes, we further investigated whether TaWRKY13-A binds to the promoters of those genes. First, we scanned the 1-kb promoters of *AtLOX1*, *AtLOX2*, *AtLOX5*, and *AtLOX6* for the W-box motif (TTGACC/T), which is the main target site of WRKYs. We found that one and two W-box motifs lay in the promoter of *AtLOX1* and *AtLOX6*, respectively (**Figure 7A**, **Supplementary Figure 9A**). However, no W-box motif was identified in the *AtLOX5* promoter. Hence, we performed the EMSA to test the interaction between TaWRKY13-A and promoter of *AtLOX6* and *AtLOX1*. We fused the TaWRKY13-A to maltose-binding protein (MBP), and this MBP-TaWRKY13-A fusion as well as single MBP were expressed in *E. coli* (strain *Rosseta*). Then, we designed probe 1 (P1) against the promoter of *AtLOX6* and which specifically hybridizes with MBP-TaWRKY13-A but not MBP only, and this interaction could be completed by unlabeled probes (**Figure 7B**), whereas we found that the interaction between TaWRKY13-A and *AtLOX1* was not specific and competitive (**Supplementary Figure 9B**). This result suggested that TaWRKY13-A has the potential to bind *LOXs* and subsequently affects their expression.

However, we aimed to clarify the mechanistic details of TaWRKY13-A-related leaf senescence in wheat. Thus, we searched the homologs of *AtLOX6* on WheatOmics (http://202.194.139.32/). We performed the sequence blast with the Pfam (PF00305) number of lipoxygenase family and conducted a phylogenetic analysis based on our RNA-seq data at four developmental stages (i.e., YL, ML, ES, and LS) of wheat leaf (**Supplementary Figure 8A**). We found a gene (TraesCS2B02G333600.1) showing the highest similarity with *AtLOX6* and hence named *TaLOX6,* which is increasing during leaf senescence and has not been functionally characterized before (**Supplementary Figure 8B**). We identified two W-box elements in the promoter region of *TaLOX6* (**Figure 7C**). Thus, we planned to analyze the interaction between TaWRKY13-A and *TaLOX6* by using the EMSA and luciferase reporter system. First, we synthesized probe 2 (P2) and probe 3 (P3) both harboring one W-box motif on the promoter of *TaLOX6* (**Figure 7C**). Both P2 and P3 showed the specific and competitive interaction with MBP-TaWRKY13-A protein but not MBP only (**Figure 7D**). Furthermore, we confirmed the interaction between MBP-TaWRKY13-A and *TaLOX6* by using the luciferase reporter system. *LUC* gene driven by the promoter of *TaLOX6* was co-transformed with *35S:TaWRKY13-A-GFP* into wheat protoplasts (**Figure 8A**). The reaction catalyzed by LUC was quantification, indicating the bond strength between TaWRKY13-A and *TaLOX6* promoter. TaWRKY13-A-GFP but not GFP alone was able to elevate the ratio of LUC activity to REN activity (internal reference) (**Figure 8B**). These data further manifested TaWRKY13-A can bind to *LOXs* in wheat. Meanwhile, we also proved that the expression of *TaLOX6* was suppressed in *TaWRKY13-A*-silenced wheat plants compared with VC plants (**Figure 8C**). This result

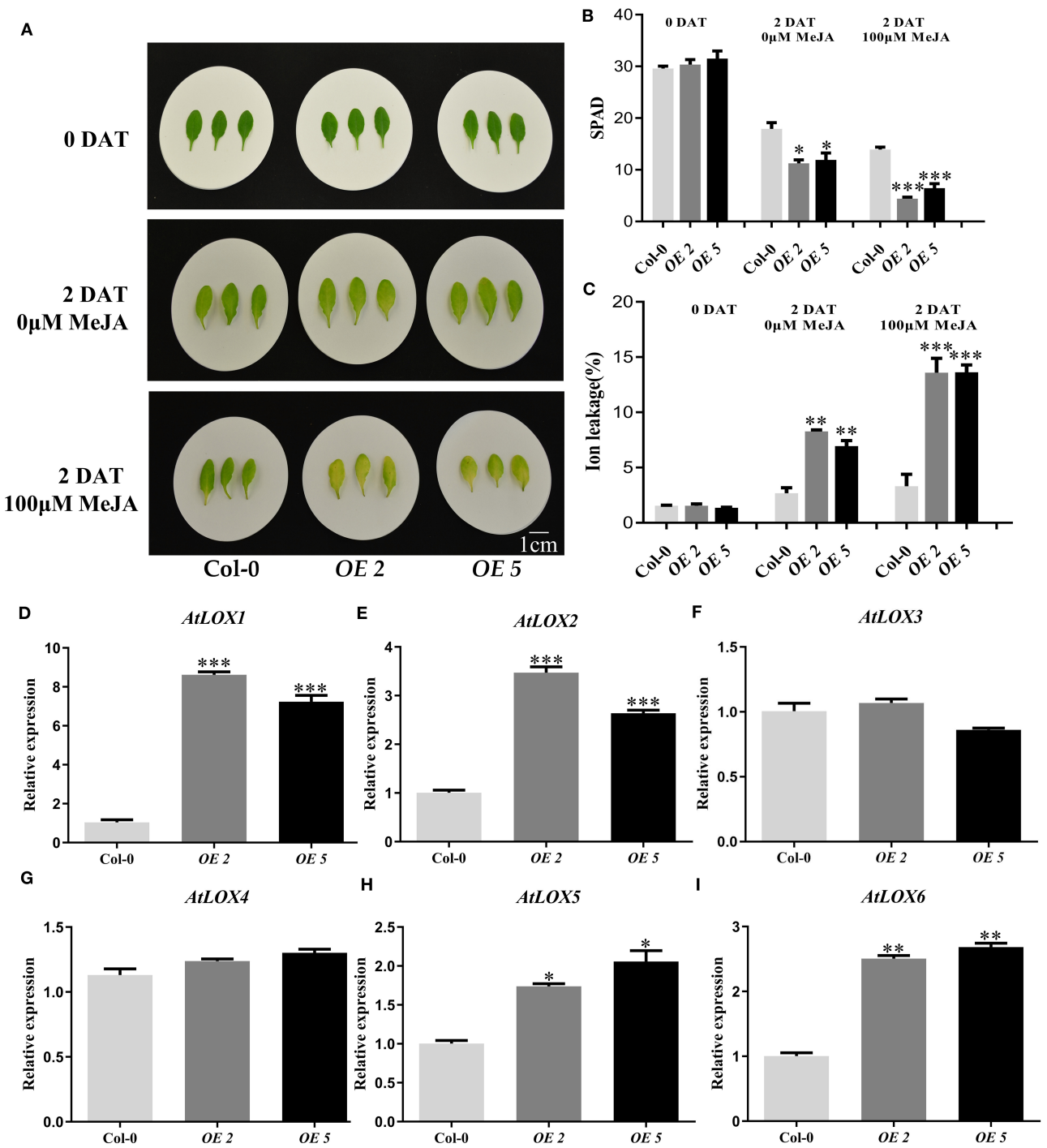

FIGURE 6 | TaWRKY13-A participates in JA-induced leaf senescence in *Arabidopsis*. **(A)** Phenotypic observation of 4-week-old *TaWRKY13-A*-overexpressing *Arabidopsis* and Col-0 under MeJA treatment. **(B,C)** Chlorophyll content **(B)** and ion leakage rate **(C)** before and after MeJA treatment **(A)**. **(D–I)** The transcription level of some JA biosynthetic genes, including *AtLOX1*, *AtLOX2*, *AtLOX3*, *AtLOX4*, *AtLOX5*, and *AtLOX6*, in the fourth and fifth rosette leaves of 4-week-old T*aWRKY13-A*-overexpressing and Col-0 *Arabidopsis* by qRT-PCR. (Error bars indicate SD. Asterisks indicate significant differences. Student's *t*-test, $^{*}P < 0.05$, $^{**}P < 0.01$, $^{***}P < 0.001$, and $n \geq 30$. The above experiments were repeated at least in three biological replicates).

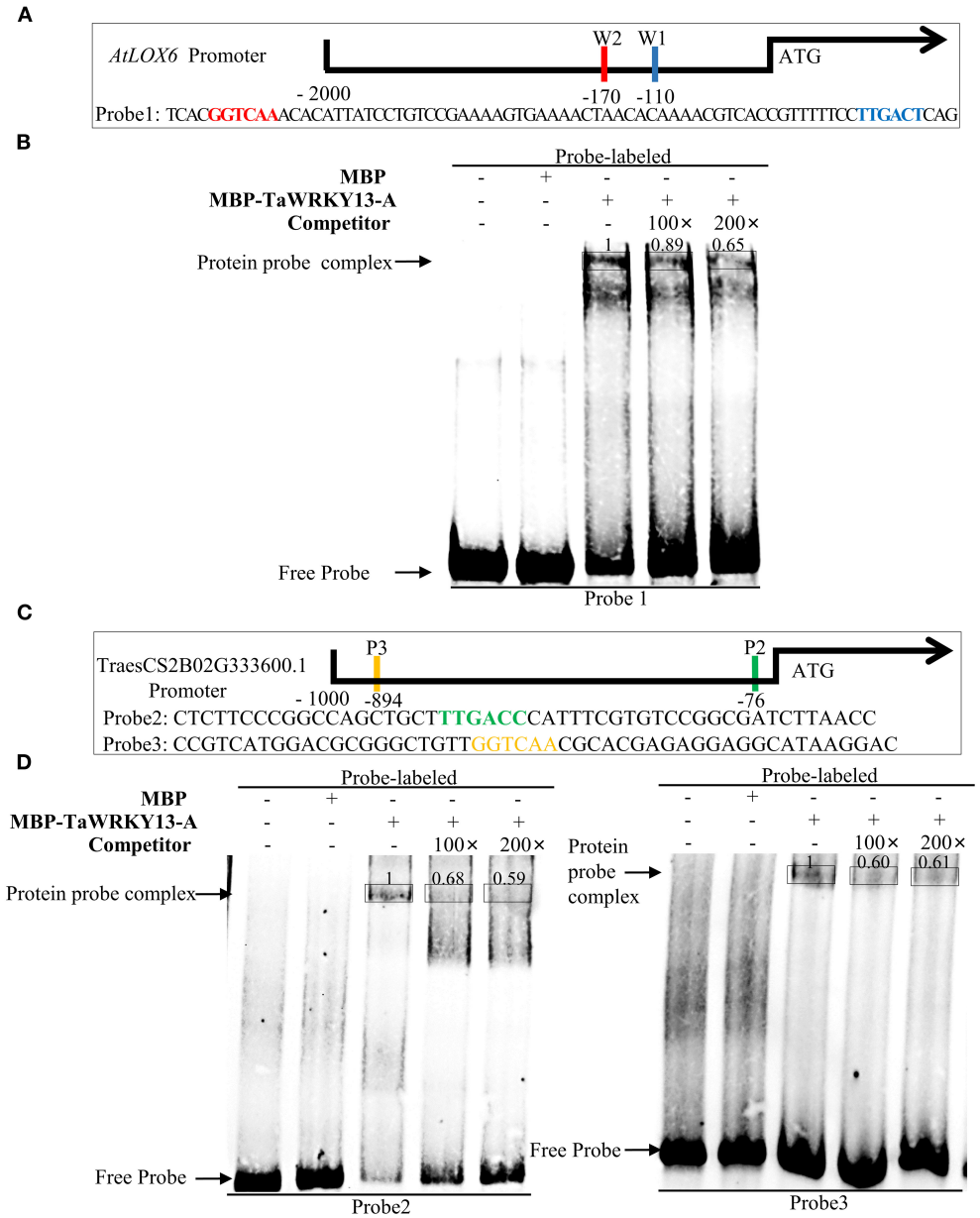

FIGURE 7 | TaWRKY13-A can directly bind to the promoter region of *AtLOX6* and *TaLOX6*. **(A,C)** Positions of the W-box sites (with red, blue, yellow, and green colors) on promoters of *AtLOX6* and *TaLOX6* and probes (i.e., Probe1, Probe2, and Probe3) against W-box sites for EMSA. **(B,D)** Interactions of TaWRKY13-A protein and probes against *AtLOX6* and *TaLOX6* for EMSA experiment. The symbols of (+) and (–) indicated the presence and absence of specific probes, respectively. Numbers on the bands indicated the relative binding strength between MBP-TaWRKY13-A and labeled probes (The above experiments were repeated at least in three biological replicates).

suggested that TaWRKY13-A is the potential to regulate *TaLOX6 in vivo*.

Less was known about the functional role of *TaLOX6*. In this study, we preliminarily analyzed the responses of *TaLOX6* to MeJA treatment. We verified that the expression level of *TaLOX6* was induced by MeJA treatment (**Supplementary Figure 8C**). Despite this, more studies are needed to verify that TaLOX6 is involved in the regulation of leaf senescence by cooperating with TaWRKY13-A. To further validate TaWRKY13-A regulating leaf senescence *via* the JA pathway, we measured the content of JA and JA-Ile between *TaWRKY13-A*-silenced and VC wheat plants in **Supplementary Figure 4** by using the LC-MS/MS method. In line with the phenotypic differences among the above plants after dark treatment, we detected the significantly lower levels of JA and JA-Ile in *TaWRKY13-A*-silenced wheat plants than that in VC plants (**Figures 8D,E**). Meanwhile, we also measured the JA content in *TaWRKY13-A*-overexpressing *Arabidopsis* plants and Col-0 at juvenile and senescent stages

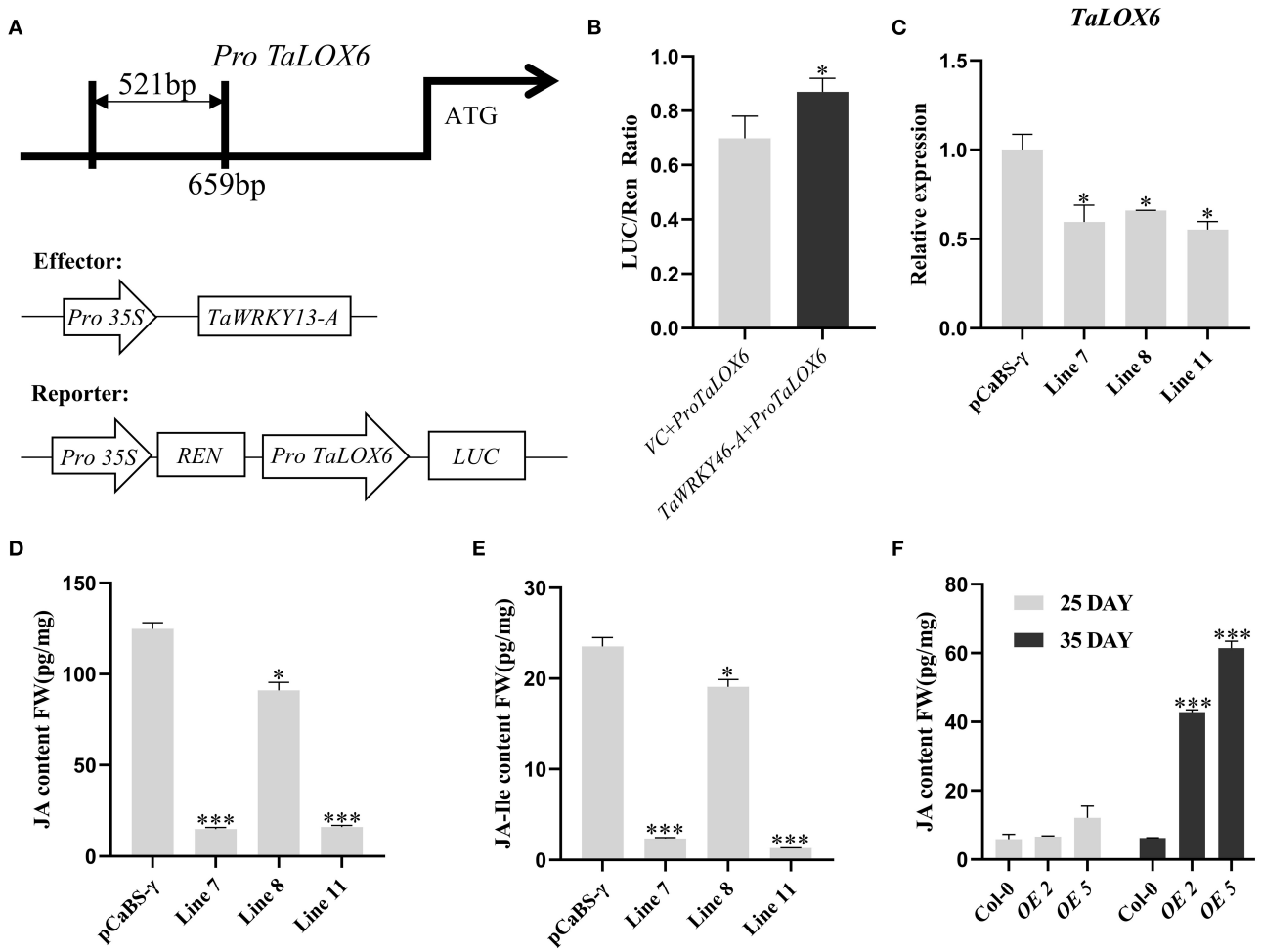

FIGURE 8 | TaWRKY13-A can bind to the promoter region of *TaLOX6* in wheat protoplasts. **(A)** Diagram of fragment selected on *TaLOX6* and transient expression vectors. **(B)** The dual-luciferase reporter system shows that TaWRKY13-A can activate the *luciferase* gene linked to the *TaLOX6* promoter fragment, *Renilla* luciferase was used for normalization. The 35S:GFP acts as a negative control. **(C)** Expression of *TaLOX6* in *TaWRKY13-A*-silenced and VC wheat plants. **(D)** Measurement of endogenous JA content in 2-month-old *TaWRKY13-A*-silenced and VC wheat plants. **(E)** Measurement of endogenous JA-Ile content in 2-month-old *TaWRKY13-A*-silenced and VC wheat plants. **(F)** Measurement of endogenous JA content in 25-day-old and 35-day-old *TaWRKY13-A*-overexpressing *Arabidopsis*. (Error bars indicate SD. Asterisks indicate significant differences. Student's *t*-test, $^{*}P < 0.05$, $^{***}P < 0.001$. The above experiments were repeated at least in three biological replicates).

(**Figure 8F**). Notably, we detected a slightly higher JA level in *TaWRKY13-A*-overexpressing young leaves than Col-0, while the JA level elevated in senescent leaves of *TaWRKY13-A*-overexpressing plants more dramatically than that in Col-0 (**Figure 8F**). This result demonstrated that leaf senescence onset promoted by TaWRKY13-A involves the activation of JA biosynthesis. Nevertheless, relevant experimental studies in wheat will be much more helpful for assessing the regulatory network of TaWRKY13-A in future.

TaWRKY13-A Is Possibly Partially Functional Conserved With AtWRKY53

Based on the phylogenetic analysis among those published senescence-related WRKYs, we identified that TaWRKY13-A shares a relatively high similarity with AtWRKY53, and they both belong to the group III WRKYs (**Supplementary Figure 1A**). Besides, many studies have revealed the crucial role of AtWRKY53 in the regulation of leaf senescence and the connection between AtWRKY53 and JA pathway (Miao and Zentgraf, 2007). Thus, we investigated the functional conservation between TaWRKY13-A and AtWRKY53. Subsequently, we generated a construct where the CDS of TaWRKY13-A was driven by CaMV 35S promoter, and it was introduced into the *atwrky53* mutant. After confirming the expression of TaWRKY13-A-7Myc6His by Western blot, the process of leaf senescence was compared among Col-0, *atwrky53* mutant, and *atwrky53* mutant harboring 35S:*TaWRKY13-A-7Myc6His* construct (**Figure 9B**). Three-week-old above plants showed parallel growth phenotypes, while after growing for 5 weeks, *atwrky53* exhibited a delayed leaf senescence phenotype compared with Col-0 and *35S:TaWRKY13-A-7Myc6His*/*atwrky53* (**Figure 9A**). Chlorophyll content, ion

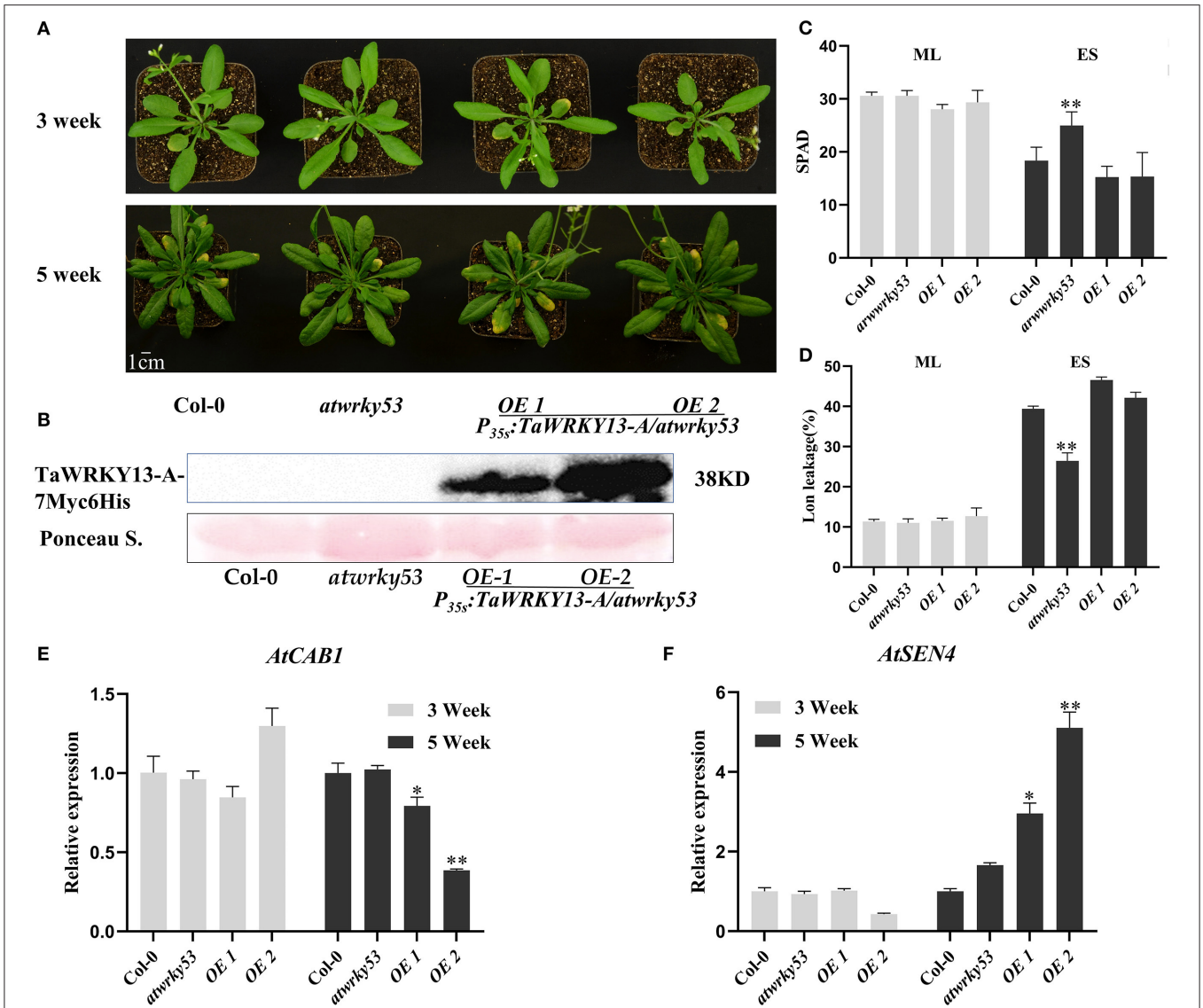

FIGURE 9 | Overexpression of *TaWRKY13-A* rescues delayed leaf senescence in *atwrky53* mutant. **(A)** Phenotypic observation of P_{35s}*:TaWRKY13-A-7Myc6His/atwrky53,* Col-0, and *atwrky53 Arabidopsis* plants. **(B)** Identification of TaWRKY13-A-7Myc6His in P_{35s}*:TaWRKY13-A-7Myc6His/atwrky53*, Col-0, and *atwrky53 Arabidopsis* by using the Western blot. **(C,D)** Measurement of chlorophyll content **(C)** and ion leakage rate **(D)** in **(A)**. **(E,F)** Detection of senescence-associated genes including an upregulated gene *AtSEN4* **(F)** and a downregulated gene *AtCAB1* **(E)** in the above plants. (Error bars indicate SD. Asterisks indicate significant differences. Student's *t*-test, $^{*}P < 0.05$, $^{**}P < 0.01$, and $n \geq 30$. The above experiments were repeated at least in three biological replicates).

leakage rate, and expression of two senescence-related genes, namely, *AtCAB1* and *AtSEN4*, were detected before and after leaf senescence onset, which were in line with the senescence-related phenotypic alterations among the above plants (**Figures 9C–F**). This result suggested that TaWRKY13-A may be partially conserved with AtWRKY53 under the natural growth condition.

DISCUSSION

Although numerous studies have identified multidimensional regulators of senescence, the regulatory network of lifespan remains a mystery. Plant senescence is obviously distinguished from the aging in animals, which is mainly reflected in the decline of assimilation and the nutrients redistribution. Moreover, the telomere length has been recently demonstrated to be positively related to early flowering time, while longer telomere in animals usually means longevity (Choi et al., 2021). Therefore, appropriate timing of leaf senescence is of immense importance for plant growth and especially for crop yield and quality.

To date, researchers have addressed the roles of various genes related to leaf senescence in phytohormone pathways, transcriptional regulation, epigenetic modification, autophagy, circadian clock, DNA damage repair, and chlorophyll metabolism (Woo et al., 2019). Among these regulators of leaf senescence,

TFs are one of the most intensively studied gene families (Schippers, 2015). TFs function as a key step for integrating senescence-related signals and further executing the precise transcriptional modulation of diverse senescence-related genes. WRKYs are one of the largest TF families in higher plants and play important roles mainly in the responses to biotic and abiotic stresses, carbohydrate synthesis, leaf senescence, development, and secondary metabolism (Rushton et al., 2010; Viana et al., 2018). Some studies have revealed the connection between WRKYs and phytohormones in the regulation of leaf senescence. Moreover, some experimental data suggested that there is a feedback loop among leaf senescence, phytohormones, and WRKYs, which makes the regulation of WRKYs in leaf senescence more sophisticate (Miao and Zentgraf, 2007; Jiang et al., 2014; Guo et al., 2017; Kim et al., 2019; Zhao et al., 2020b). This fine-tuning also suggests that the progression of leaf senescence is a highly ordered process. In this study, TaWRKY13-A promotes the accumulation of JA mainly by activating the transcription of *LOXs*. Notably, the transcription of *TaWRKY13-A* is also activated by MeJA treatment and leaf senescence onset, which implies that *TaWRKY13-A* may be under the control of a feedback loop. Nevertheless, more data are needed for verifying this hypothesis.

WRKYs show their multiple roles in various biological events, which partially results from their potentials to interact with numerous target genes. Meanwhile, the single WRKY protein could also bind to diverse promoters to mediate different signals. In this study, we focused on the regulation of TaWRKY13-A on the expression of *LOXs* during leaf senescence. It has been known that *LOXs* encode lipoxygenases and participate in JA biosynthesis (Wasternack and Song, 2016). In *Arabidopsis*, *LOX2* is responsible for JA biosynthesis and under the regulation of TCP4 in JA-induced leaf senescence, which is simultaneously repressed by miRNA319 (Schommer et al., 2008; Koyama et al., 2017). Our data showed that TaWRKY13-A prefers *AtLOX6* and its ortholog in wheat as target genes during leaf senescence. Previously, AtLOX6 has been reported to function in the responses to long-distance wound signaling and stress resistance (Chauvin et al., 2013; Grebner et al., 2013). However, *TaLOX6* has never been functionally characterized in wheat. In this study, we proved that the expression of *TaLOX6* is affected by MeJA treatment and senescence process, which suggests that *TaLOX6* is possibly related to JA-induced leaf senescence, whereas the overexpression and impairment of *TaLOX6* in wheat will be extremely helpful for identifying the function of *TaLOX6* in future.

The JA pathway has long been acknowledged for its role in leaf senescence onset. However, some studies also reveal the complexity of JA-related senescence. For instance, mutants of some JA signaling components, such as *coi1-1*, show indistinguishable senescence phenotypes compared with WT *Arabidopsis* plants (He et al., 2002a; Seltmann et al., 2010). In this study, we predominately focused on the connection between TaWRKY13-A and JA biosynthesis. Notably, the expression level of some JA signaling components, including *MYC2*, *MYC3*, and *MYC4*, were altered in *TaWRKY13-A*-overexpressing *Arabidopsis* plants. To further assess whether this affection is directly carried out by TaWRKY13-A, the analysis of the interaction between TaWRKY13-A and *MYCs* in *Arabidopsis* and wheat is essential. Moreover, since *TaWRKY13-A* itself is regulated by MeJA, the potential of TaWRKY13-A as a target gene of JA-related TFs is also considerable.

Studies on functional genes in wheat are lagging behind those in other crops, mainly due to their allohexaploid genome and the high similarity among the paralogs. By using the BSMV–VIGS method, we planned to specifically silence the transcription of *TaWRKY13-A*. In fact, there is just a single nucleotide difference in CDS between TaWRKY13-A and TaWRKY13-D and which even does not alter the amino acid sequence. Thus, we conducted the phenotypic analysis to investigate the role of TaWRKY13-A by choosing the wheat plants with significantly decreased *TaWRKY13-A* and irregularly changed *TaWRKY13-B* and *TaWRKY13-D* among those infected seedlings. It is conceivable that the delayed leaf senescence phenotype in VIGS plants may be an eventual outcome caused by decreased *TaWRKY13s*. More importantly, although the overexpression of *TaWRKY13-A* led precious leaf senescence in *B. distachyon* and *Arabidopsis*, it is hard to demonstrate whether TaWRKY13-A and TaWRKY13-B are completely redundant. Moreover, as there is an extremely high similarity between *TaWRKY13-A* and *TaWRKY13-B*, specific studies on each gene by CRSIPR-Cas technology are difficult. Even so, we found that the upstream regulatory sequences of *TaWRKY13-A* and *TaWRKY13-B* are distinct, and their expression profiles and abundance of transcripts during leaf senescence are also very different (**Supplementary Figure 2**). These data implied that TaWRKY13-A and TaWRKY13-B may play diverse roles in wheat. However, details about how TaWRKY13-B and TaWRKY13-D participating in the regulation of leaf senescence will help us to comprehensively understand the roles of TaWRKY13s in wheat leaf senescence and whether they are functionally redundant.

To data, WRKYs are divided into seven groups based on the number of WRKY domains and the type of zinc finger structures. According to this classification, TaWRKY13-A belongs to group III WRKYs, which also contains a key regulator of leaf senescence, AtWRKY53. Our results indicated that TaWRKY13-A has the potential to rescue the delayed leaf senescence phenotype in *atwrky53* mutants. These data suggested that TaWRKY13-A is partially functional conserved with AtWRKY53 in age-dependent leaf senescence. Previously, AtWRKY53 has been demonstrated to relate with the JA pathway by interacting with a JA-inducible protein ESR/ESP in leaf senescence (Miao and Zentgraf, 2007). Here, we concluded that TaWRKY13-A also regulates leaf senescence by modulating JA biosynthesis, whereas whether TaWRKY13-A regulates leaf senescence in a comparable way with AtWRKY53 is needed to be determined in future. To data, as few regulators of leaf senescence have been characterized in wheat, whether the underlying mechanisms of phytohormones-related leaf senescence are similar to those in other model plants, such as *Arabidopsis* and rice, remain to be proved (Sultana et al., 2021). Collectively, we identified a novel activator of wheat leaf senescence, TaWRKY13-A, which accelerates leaf senescence by promoting JA biosynthesis,

and is partially functional conserved with AtWRKY53 in age-dependent leaf senescence. Moreover, TaWRKY13-A could be a new clue for molecular breeding in wheat.

DATA AVAILABILITY STATEMENT

The datasets presented in this study can be found in online repositories. The names of the repository/repositories and accession number(s) can be found in the article/**Supplementary Material**.

AUTHOR CONTRIBUTIONS

CZ and GW conceived and designed the experiments. HQ, LC, and XG generated the constructs and transgenic lines. LC, YL, and SZ tested the transcriptional activity and performed the phenotypic and physiological analyses. KL conducted the bioinformatics analysis. HQ performed the EMSA experiment. HQ, PY, CZ, and GW wrote the manuscript. All authors read and approved the final manuscript.

FUNDING

This study was supported by grants from the National Natural Science Foundation of China (Grant No. 31671694 and 31871616 to CZ, Grant No. 31600227 and 31970199 to GW), the Central Government Guides Local Science and Technology Development Project (Grant No. 216Z2901G to CZ), the S&T Program of Hebei (Grant No. 20322912D to YL), the S&T Program of Hebei (Grant No. 21322915D to GW), the Hebei Natural Science Foundation (C2021205013), the HAAFS Agriculture Science and Technology Innovation Project (Grant No. 2019-4-8-1 to GW), and the China Postdoctoral Science Foundation (Grant No. 2017 M621096 to GW). The funders had no role in the design of the study and collection, analysis, and interpretation of data and in writing the manuscript.

ACKNOWLEDGMENTS

We thank Prof. Dawei Li (China Agricultural University) for sharing BSMV vectors and Prof. Ying Miao (Fujian Agriculture and Forestry University) for sharing the *atwrky53* mutant.

SUPPLEMENTARY MATERIAL

The Supplementary Material for this article can be found online at: https://www.frontiersin.org/articles/10.3389/fpls.2021.717233/full#supplementary-material

REFERENCES

Ahmad, P., Rasool, S., Gul, A., Sheikh, S. A., Akram, N. A., Ashraf, M., et al. (2016). Jasmonates: multifunctional roles in stress tolerance. *Front. Plant Sci.* 7:813. doi: 10.3389/fpls.2016.00813

Arrom, L., and Munne-Bosch, S. (2012). Hormonal regulation of leaf senescence in Lilium. *J. Plant Physiol.* 169, 1542–1550. doi: 10.1016/j.jplph.2012.06.012

Aubry, S., Fankhauser, N., Ovinnikov, S., Pruzinska, A., Stirnemann, M., Zienkiewicz, K., et al. (2020). Pheophorbide a may regulate jasmonate signaling during dark-induced senescence. *Plant Physiol.* 182, 776–791. doi: 10.1104/pp.19.01115

Besseau, S., Li, J., and Palva, E. T. (2012). WRKY54 and WRKY70 co-operate as negative regulators of leaf senescence in *Arabidopsis thaliana*. *J. Exp. Bot.* 63, 2667–2679. doi: 10.1093/jxb/err450

Borrill, P., Harrington, S. A., Simmonds, J., and Uauy, C. (2019). Identification of transcription factors regulating senescence in wheat through gene regulatory network modelling. *Plant Physiol.* 180, 1740–1755. doi: 10.1104/pp.19.00380

Chauvin, A., Caldelari, D., Wolfender, J. L., and Farmer, E. E. (2013). Four 13-lipoxygenases contribute to rapid jasmonate synthesis in wounded *Arabidopsis thaliana* leaves: a role for lipoxygenase 6 in responses to long-distance wound signals. *N. Phytol.* 197, 566–575. doi: 10.1111/nph.12029

Chen, K., Li, H., Chen, Y., Zheng, Q., Li, B., and Li, Z. (2015). TaSCL14, a novel wheat (*Triticum aestivum* L.) GRAS gene, regulates plant growth, photosynthesis, tolerance to photooxidative stress, and senescence. *J. Genet. Genom.* 42, 21–32. doi: 10.1016/j.jgg.2014.11.002

Chen, L., Xiang, S., Chen, Y., Li, D., and Yu, D. (2017). Arabidopsis WRKY45 interacts with the DELLA protein RGL1 to positively regulate age-triggered leaf senescence. *Mol. Plant* 10, 1174–1189. doi: 10.1016/j.molp.2017.07.008

Chini, A., Gimenez-Ibanez, S., Goossens, A., and Solano, R. (2016). Redundancy and specificity in jasmonate signalling. *Curr. Opin. Plant Biol* 33, 147–156. doi: 10.1016/j.pbi.2016.07.005

Choi, J. Y., Abdulkina, L. R., Yin, J., Chastukhina, I. B., Lovell, J. T., Agabekian, I. A., et al. (2021). Natural variation in plant telomere length is associated with flowering time. *Plant Cell* 33:1118–34. doi: 10.1093/plcell/koab022

Clough, S. J., and Bent, A. F. (1998). Floral dip: a simplified method for Agrobacterium-mediated transformation of *Arabidopsis thaliana*. *Plant J.* 16, 735–743. doi: 10.1046/j.1365-313x.1998.00343.x

Eulgem, T., Rushton, P. J., Robatzek, S., and Somssich, I. E. (2000). The WRKY superfamily of plant transcription factors. *Trends Plant Sci.* 5, 199–206. doi: 10.1016/S1360-1385(00)01600-9

Fonseca, S., Chico, J. M., and Solano, R. (2009). The jasmonate pathway: the ligand, the receptor and the core signalling module. *Curr. Opin. Plant Biol.* 12, 539–547. doi: 10.1016/j.pbi.2009.07.013

Grebner, W., Stingl, N. E., Oenel, A., Mueller, M. J., and Berger, S. (2013). Lipoxygenase6-dependent oxylipin synthesis in roots is required for abiotic and biotic stress resistance of Arabidopsis. *Plant Physiol.* 161, 2159–2170. doi: 10.1104/pp.113.214544

Guo, P., Li, Z., Huang, P., Li, B., Fang, S., Chu, J., et al. (2017). A tripartite amplification loop involving the transcription factor WRKY75, salicylic acid, and reactive oxygen species accelerates leaf senescence. *Plant Cell* 29, 2854–2870. doi: 10.1105/tpc.17.00438

He, Y., Fukushige, H., Hildebrand, D. F., and Gan, S. (2002a). Evidence supporting a role of jasmonic acid in Arabidopsis leaf senescence. *Plant Physiol.* 128, 876–884.

He, Y., Fukushige, H., Hildebrand, D. F., and Gan, S. (2002b). Evidence supporting a role of jasmonic acid in arabidopsis leaf senescence. *Plant Physiol.* 128, 876–884. doi: 10.1104/pp.010843

Hinderhofer, K., and Zentgraf, U. (2001). Identification of a transcription factor specifically expressed at the onset of leaf senescence. *Planta* 213, 469–473. doi: 10.1007/s004250000512

Hu, Y., Jiang, Y., Han, X., Wang, H., Pan, J., and Yu, D. (2017). Jasmonate regulates leaf senescence and tolerance to cold stress: crosstalk with other phytohormones. *J. Exp. Bot.* 68, 1361–1369. doi: 10.1093/jxb/erx004

Huang, H., Liu, B., Liu, L., and Song, S. (2017). Jasmonate action in plant growth and development. *J. Exp. Bot.* 68, 1349–1359. doi: 10.1093/jxb/erw495

Jia, M., Liu, X., Xue, H., Wu, Y., Shi, L., Wang, R., et al. (2019). Noncanonical ATG8-ABS3 interaction controls senescence in plants. *Nat. Plants* 5, 212–224. doi: 10.1038/s41477-018-0348-x

Jiang, J., Ma, S., Ye, N., Jiang, M., Cao, J., and Zhang, J. (2017). WRKY transcription factors in plant responses to stresses. *J. Integr. Plant Biol.* 59, 86–101. doi: 10.1111/jipb.12513

Jiang, Y., Liang, G., Yang, S., and Yu, D. (2014). Arabidopsis WRKY57 functions as a node of convergence for jasmonic acid- and auxin-mediated signaling in jasmonic acid-induced leaf senescence. *Plant Cell* 26, 230–245. doi: 10.1105/tpc.113.117838

Jibran, R., A., and Hunter, D., and, P., Dijkwel, P. (2013). Hormonal regulation of leaf senescence through integration of developmental and stress signals. *Plant Mol. Biol.* 82, 547–561. doi: 10.1007/s11103-013-0043-2

Jing, Y., Liu, J., Liu, P., Ming, D., and Sun, J. (2019). Overexpression of TaJAZ1 increases powdery mildew resistance through promoting reactive oxygen species accumulation in bread wheat. *Sci. Rep.* 9:5691. doi: 10.1038/s41598-019-42177-y

Khan, M., Rozhon, W., and Poppenberger, B. (2014). The role of hormones in the aging of plants - a mini-review. *Gerontology* 60, 49–55. doi: 10.1159/000354334

Kim, J., Chang, C., and Tucker, M. L. (2015). To grow old: regulatory role of ethylene and jasmonic acid in senescence. *Front. Plant Sci.* 6:20. doi: 10.3389/fpls.2015.00020

Kim, J., Kim, J. H., Lyu, J. I., Woo, H. R., and Lim, P. O. (2018). New insights into the regulation of leaf senescence in Arabidopsis. *J. Exp. Bot.* 69, 787–799. doi: 10.1093/jxb/erx287

Kim, T., Kang, K., Kim, S. H., An, G., and Paek, N. C. (2019). OsWRKY5 promotes rice leaf senescence via senescence-associated NAC and abscisic acid biosynthesis pathway. *Int. J. Mol. Sci.* 20:4437. doi: 10.3390/ijms20184437

Koyama, T. (2018). A hidden link between leaf development and senescence. *Plant Sci.* 276, 105–110. doi: 10.1016/j.plantsci.2018.08.006

Koyama, T., Sato, F., and Ohme-Takagi, M. (2017). Roles of miR319 and TCP transcription factors in leaf development. *Plant Physiol.* 175, 874–885. doi: 10.1104/pp.17.00732

Li, X., Liu, T., Chen, W., Zhong, S., Zhang, H., Tang, Z., et al. (2015). Wheat WCBP1 encodes a putative copper-binding protein involved in stripe rust resistance and inhibition of leaf senescence. *BMC Plant Biol.* 15:239. doi: 10.1186/s12870-015-0612-4

Li, Z., Kim, J. H., Kim, J., Lyu, J. I., Zhang, Y., Guo, H., et al. (2020). ATM suppresses leaf senescence triggered by DNA double-strand break through epigenetic control of senescence-associated genes in Arabidopsis. *N. Phytol.* 227, 473–484. doi: 10.1111/nph.16535

Li, Z., Woo, H. R., and Guo, H. (2018). Genetic redundancy of senescence-associated transcription factors in Arabidopsis. *J. Exp. Bot.* 69, 811–823. doi: 10.1093/jxb/erx345

Lim, J., Park, J. H., Jung, S., Hwang, D., Nam, H. G., and Hong, S. (2018). Antagonistic roles of PhyA and PhyB in Far-red light-dependent leaf senescence in *Arabidopsis thaliana*. *Plant Cell Physiol* 59, 1753–1764. doi: 10.1093/pcp/pcy153

Lin, J.-F., and Wu, S.-H. (2004). Molecular events in senescing Arabidopsisleaves. *Plant J.* 39, 612–628. doi: 10.1111/j.1365-313X.2004.02160.x

Liu, L., Xu, W., Hu, X., Liu, H., and Lin, Y. (2016). W-box and G-box elements play important roles in early senescence of rice flag leaf. *Sci. Rep.* 6:20881. doi: 10.1038/srep20881

Luo, Y., Pang, D., Jin, M., Chen, J., Kong, X., Li, W., et al. (2019). Identification of plant hormones and candidate hub genes regulating flag leaf senescence in wheat response to water deficit stress at the grain-filling stage. *Plant Direct.* 3:e00152. doi: 10.1002/pld3.152

Mayta, M. L., Hajirezaei, M. R., Carrillo, N., and Lodeyro, A. F. (2019). Leaf senescence: the chloroplast connection comes of age. *Plants* 8:495. doi: 10.3390/plants8110495

Miao, Y., and Zentgraf, U. (2007). The antagonist function of Arabidopsis WRKY53 and ESR/ESP in leaf senescence is modulated by the jasmonic and salicylic acid equilibrium. *Plant Cell* 19, 819–830. doi: 10.1105/tpc.106.042705

Qi, T., Wang, J., Huang, H., Liu, B., Gao, H., Liu, Y., et al. (2015). Regulation of jasmonate-induced leaf senescence by antagonism between bHLH subgroup IIIe and IIId factors in arabidopsis. *Plant Cell* 27, 1634–1649. doi: 10.1105/tpc.15.00110

Robatzek, S., and Somssich, I. E. (2001). A new member of the Arabidopsis WRKY transcription factor family, AtWRKY6, is associated with both senescence- and defence-related processes. *Plant J.* 28, 123–133. doi: 10.1046/j.1365-313X.2001.01131.x

Ruan, J., Zhou, Y., Zhou, M., Yan, J., Khurshid, M., Weng, W., et al. (2019). Jasmonic acid signaling pathway in plants. *Int. J. Mol. Sci.* 20:2479. doi: 10.3390/ijms20102479

Rushton, P. J., Somssich, I. E., Ringler, P., and Shen, Q. J. (2010). WRKY transcription factors. *Trends Plant Sci.* 15, 247–258. doi: 10.1016/j.tplants.2010.02.006

Schippers, J. H. (2015). Transcriptional networks in leaf senescence. *Curr. Opin. Plant Biol.* 27, 77–83. doi: 10.1016/j.pbi.2015.06.018

Scholthof, K. B. G., Irigoyen, S., Catalan, P., and Mandadi, K. K. (2018). Brachypodium: a monocot grass model genus for plant biology. *Plant Cell* 30, 1673–1694. doi: 10.1105/tpc.18.00083

Schommer, C., Palatnik, J. F., Aggarwal, P., Chetelat, A., Cubas, P., Farmer, E. E., et al. (2008). Control of jasmonate biosynthesis and senescence by miR319 targets. *PLoS Biol* 6:e230. doi: 10.1371/journal.pbio.0060230

Seltmann, M. A., Stingl, N. E., Lautenschlaeger, J. K., Krischke, M., Mueller, M. J., and Berger, S. (2010). Differential impact of lipoxygenase 2 and jasmonates on natural and stress-induced senescence in Arabidopsis. *Plant Physiol.* 152, 1940–1950. doi: 10.1104/pp.110.153114

Smith, S. M., Li, C., and Li, J. (2017). "Hormone function in plants," in *Hormone Metabolism and Signaling in Plants*, eds J. Li, C. Li, and S. M. Smith (London: ELSEVIER Academic Press), 1–38. doi: 10.1016/B978-0-12-811562-6.00001-3

Song, H., Sun, W., Yang, G., and Sun, J. (2018). WRKY transcription factors in legumes. *BMC Plant Biol.* 18:243. doi: 10.1186/s12870-018-1467-2

Song, S., Huang, H., Wang, J., Liu, B., Qi, T., and Xie, D. (2017). MYC5 is involved in jasmonate-regulated plant growth, leaf senescence and defense responses. *Plant Cell Physiol.* 58, 1752–1763. doi: 10.1093/pcp/pcx112

Sultana, N., Islam, S., Juhasz, A., and Ma, W. (2021). Wheat leaf senescence and its regulatory gene network. *Crop J.* 184:775–91.e14. doi: 10.1016/j.cj.2021.01.004

Tan, X. L., Fan, Z. Q., Kuang, J. F., Lu, W. J., Reiter, R. J., Lakshmanan, P., et al. (2019). Melatonin delays leaf senescence of Chinese flowering cabbage by suppressing ABFs-mediated abscisic acid biosynthesis and chlorophyll degradation. *J. Pineal Res.* 67:e12570. doi: 10.1111/jpi.12570

Thomas, H., and Ougham, H. (2014). The stay-green trait. *J. Exp. Bot.* 65, 3889–3900. doi: 10.1093/jxb/eru037

Uauy, C., Distelfeld, A., Fahima, T., Blechl, A., and Dubcovsky, J. (2006). A NAC gene regulating senescence improves grain protein, zinc, and iron content in wheat. *Science* 314, 1298–1301. doi: 10.1126/science.1133649

Uji, Y., Akimitsu, K., and Gomi, K. (2017). Identification of OsMYC2-regulated senescence-associated genes in rice. *Planta* 245, 1241–1246. doi: 10.1007/s00425-017-2697-5

Viana, V. E., Busanello, C., da Maia, L. C., Pegoraro, C., and Costa de Oliveira, A. (2018). Activation of rice WRKY transcription factors: an army of stress fighting soldiers? *Curr. Opin. Plant. Biol.* 45(Pt B), 268–275. doi: 10.1016/j.pbi.2018.07.007

Wang, W., Hao, Q., Wang, W., Li, Q., Chen, F., Ni, F., et al. (2019). The involvement of cytokinin and nitrogen metabolism in delayed flag leaf senescence in a wheat stay-green mutant, tasg1. *Plant Sci.* 278, 70–79. doi: 10.1016/j.plantsci.2018.10.024

Wang, Y., Cui, X., Yang, B., Xu, S., Wei, X., Zhao, P., et al. (2020). WRKY55 transcription factor positively regulates leaf senescence and the defense response by modulating the transcription of genes implicated in the biosynthesis of reactive oxygen species and salicylic acid in Arabidopsis. *Development* 147:dev189647. doi: 10.1242/dev.189647

Wasternack, C., and Hause, B. (2013). Jasmonates: biosynthesis, perception, signal transduction and action in plant stress response, growth and development. An update to the 2007 review in Annals of Botany. *Annals Botany* 111, 1021–1058. doi: 10.1093/aob/mct067

Wasternack, C., and Song, S. (2016). Jasmonates: biosynthesis, metabolism, and signaling by proteins activating and repressing transciption. *J. Exp. Bot.* 68, 1303–1321. doi: 10.1093/jxb/erw443

Wojciechowska, N., Sobieszczuk-Nowicka, E., and Bagniewska-Zadworna, A. (2018). Plant organ senescence - regulation by manifold pathways. *Plant Biol.* 20, 167–181. doi: 10.1111/plb.12672

Wojciechowska, N., Wilmowicz, E., Marzec-Schmidt, K., Ludwikow, A., and Bagniewska-Zadworna, A. (2020). Abscisic acid and jasmonate metabolisms are jointly regulated during senescence in roots and leaves of populus trichocarpa. *Int. J. Mol. Sci.* 21:2042. doi: 10.3390/ijms21062042

Woo, H. R., Kim, H. J., Lim, P. O., and Nam, H. G. (2019). Leaf senescence: systems and dynamics aspects. *Annu. Rev. Plant Biol.* 70, 347–376. doi: 10.1146/annurev-arplant-050718-095859

Xie, Y., Zhou, Q., Zhao, Y., Li, Q., Liu, Y., Ma, M., et al. (2020). FHY3 and FAR1 integrate light signals with the miR156-SPL module-mediated aging pathway to regulate arabidopsis flowering. *Mol. Plant* 13, 483–498. doi: 10.1016/j.molp.2020.01.013

Xu, P., Chen, H., and Cai, W. (2020). Transcription factor CDF4 promotes leaf senescence and floral organ abscission by regulating abscisic acid and reactive oxygen species pathways in Arabidopsis. *EMBO Rep*. 21:e48967. doi: 10.15252/embr.201948967

Yuan, L., Wang, D., Cao, L., Yu, N., Liu, K., Guo, Y., et al. (2020). Regulation of leaf longevity by DML3-mediated DNA demethylation. *Mol. Plant* 13, 1149–1161. doi: 10.1016/j.molp.2020.06.006

Zhang, D., Zhu, Z., Gao, J., Zhou, X., Zhu, S., Wang, X., et al. (2021). The NPR1-WRKY46-WRKY6 signaling cascade mediates probenazole/salicylic acid-elicited leaf senescence in *Arabidopsis thaliana*. *J. Integr. Plant Biol*. 63, 924–936. doi: 10.1111/jipb.13044

Zhang, Q., Wang, B., Wei, J., Wang, X., Han, Q., and Kang, Z. (2018a). TaNTF2, a contributor for wheat resistance to the stripe rust pathogen. *Plant Physiol. Biochem*. 123, 260–267. doi: 10.1016/j.plaphy.2017.12.020

Zhang, Q., Xia, C., Zhang, L., Dong, C., Liu, X., and Kong, X. (2018b). Transcriptome analysis of a premature leaf senescence mutant of common wheat (*Triticum aestivum* L.). *Int. J. Mol. Sci* 19:782. doi: 10.3390/ijms19030782

Zhang, Y., Li, Y., Hassan, M. J., Li, Z., and Peng, Y. (2020). Indole-3-acetic acid improves drought tolerance of white clover via activating auxin, abscisic acid and jasmonic acid related genes and inhibiting senescence genes. *BMC Plant Biol*. 20:150. doi: 10.1186/s12870-020-02354-y

Zhang, Y., Liu, Z., Wang, X., Wang, J., Fan, K., Li, Z., et al. (2018c). DELLA proteins negatively regulate dark-induced senescence and chlorophyll degradation in Arabidopsis through interaction with the transcription factor WRKY6. *Plant Cell Rep*. 37, 981–992. doi: 10.1007/s00299-018-2282-9

Zhao, L., Zhang, W., Song, Q., Xuan, Y., Li, K., Cheng, L., et al. (2020a). A WRKY transcription factor, TaWRKY40-D, promotes leaf senescence associated with jasmonic acid and abscisic acid pathways in wheat. *Plant Biol.* 22, 1072–1085. doi: 10.1111/plb.13155

Zhao, M. M., Zhang, X. W., Liu, Y. W., Li, K., Tan, Q., Zhou, S., et al. (2020b). A wrky transcription factor, Tawrky42-B, facilitates initiation of leaf senescence by promoting jasmonic acid biosynthesis. *BMC Plant Biol*. 20:444. doi: 10.1186/s12870-020-02650-7

Zhao, Y., Dong, W., Zhang, N., Ai, X., Wang, M., Huang, Z., et al. (2014). A wheat allene oxide cyclase gene enhances salinity tolerance via jasmonate signaling. *Plant Physiol*. 164, 1068–1076. doi: 10.1104/pp.113.227595

Zheng, Y., Ge, J., Bao, C., Chang, W., Liu, J., Shao, J., et al. (2020). Histone deacetylase HDA9 and WRKY53 transcription factor are mutual antagonists in regulation of plant stress response. *Mol. Plant* 13, 598–611. doi: 10.1016/j.molp.2019.12.011

Conflict of Interest: The authors declare that the research was conducted in the absence of any commercial or financial relationships that could be construed as a potential conflict of interest.

Publisher's Note: All claims expressed in this article are solely those of the authors and do not necessarily represent those of their affiliated organizations, or those of the publisher, the editors and the reviewers. Any product that may be evaluated in this article, or claim that may be made by its manufacturer, is not guaranteed or endorsed by the publisher.

frontiers in Plant Science

ORIGINAL RESEARCH
published: 07 December 2021
doi: 10.3389/fpls.2021.722525

A Dual Role for Abscisic Acid Integrating the Cold Stress Response at the Whole-Plant Level in *Iris pseudacorus* L. Growing in a Natural Wetland

Vicent Caselles[1], *Andrea Casadesús*[1] *and Sergi Munné-Bosch*[1,2]*

[1]*Department of Evolutionary Biology, Ecology and Environmental Sciences, Faculty of Biology, University of Barcelona, Barcelona, Spain,* [2]*Research Biodiversity Institute, Faculty of Biology, University of Barcelona, Barcelona, Spain*

Leaf senescence, the last stage of the developmental program of leaves, can be induced by both internal and external signals. Cold stress-induced leaf senescence is an efficient strategy to overcome winter temperatures. In this work, we studied leaf senescence in yellow flag (*Iris pseudacorus* L.) individuals growing in a natural wetland, not only considering its relationship with external and internal cues, but also the plant developmental program, and the biological significance of rhizomes, storage organs that remain viable through winter. Total chlorophyll contents and the maximum efficiency of PSII (*Fv/Fm* ratio) decreased in senescing leaves, which was associated with a sharp increase in abscisic acid (ABA) contents. Furthermore, total cytokinin and 2-isopentenyladenine contents decreased in December compared to November, as plants became more stressed due to a decline in air temperatures. ABA increases in senescing leaves increased in parallel to reductions in violaxanthin. Rhizomes also accumulated large amounts of ABA during winter, while roots did not, and neither roots nor rhizomes accumulated 9-*cis*-epoxycarotenoids, thus suggesting ABA, which might play a role in conferring cold tolerance to this subterranean organ, may result from phloem transport from senescing leaves. It is concluded that (i) leaf senescence is a highly regulated physiological process in yellow flag playing a key role in the modulation of the entire plant developmental program, and (ii) ABA plays a major role not only in the regulation of leaf senescence but also in the establishment of cold tolerance in rhizomes, two processes that appear to be intimately interconnected.

Keywords: ABA, cold stress, *Iris pseudacorus* L., leaf senescence, perennial, rhizome, winter

OPEN ACCESS

Edited by:
Salma Balazadeh,
Leiden University, Netherlands

Reviewed by:
Szabolcs Rudnóy,
Eötvös Loránd University, Hungary
Vicent Arbona,
University of Jaume I, Spain

***Correspondence:**
Sergi Munné-Bosch
smunne@ub.edu

Specialty section:
This article was submitted to Plant Physiology, a section of the journal Frontiers in Plant Science

Received: *08 June 2021*
Accepted: *03 November 2021*
Published: *07 December 2021*

Citation:
Caselles V, Casadesús A and Munné-Bosch S (2021) A Dual Role for Abscisic Acid Integrating the Cold Stress Response at the Whole-Plant Level in Iris pseudacorus L. Growing in a Natural Wetland. Front. Plant Sci. 12:722525. doi: 10.3389/fpls.2021.722525

INTRODUCTION

Plants, being sessile organisms in their post-embryonic development, have developed several strategies to cope with environmental stresses. Among them, leaf senescence, which allows a progressive dismantling of the photosynthetic apparatus and a recycling of its components, includes not only photoassimilates but also amino acids, amides, glutathione, and other nutrient-rich compounds, thus helping promote survival at the organism level (Munné-Bosch and

Alegre, 2004; Fischer, 2012). This process is a key phase in a plant's development program as it represents the last stage of leaf development and is therefore tightly regulated by internal and external cues (Gan and Amasino, 1997).

Cold stress is characterized by an alteration of the physicochemical properties of key cellular components such as membrane lipids and enzymes, leading to changes in membrane fluidity and eventual damage to membranes, solute leakage, and a dysregulation of metabolic reactions due to alterations to enzymatic properties, which in turn lead to the production of reactive oxygen species (Welti et al., 2002). Being the last stage of leaf development, cold-induced leaf senescence is tightly regulated at several levels and can serve a role in acclimation (Masclaux-Daubresse et al., 2007). Indeed, depending on the influence of other environmental factors, such as photoperiod, light intensity, and quality, the impact of low temperature stress on plants largely varies (Novák et al., 2021). Therefore, carrying out experiments in plants growing in their natural habitat, although complex due to changing environmental conditions, is essential to understand better the mechanisms underlying cold stress tolerance in nature.

Plant hormones act as signaling molecules and exert the function of stress response and senescence regulation. ABA has been reported to act as the main phytohormone involved in stress signaling, since it induces stomatal closure and osmolyte accumulation in plants under environmental stresses such as drought and chilling stress (Daszkowska-Golec and Szarejko, 2013). Furthermore, it plays a pivotal role in leaf senescence induction and it has been reported that ABA contents increase during this process in several species (Gepstein and Thimann, 1980). ABA is synthesized from epoxycarotenoids such as neoxanthin and violaxanthin (Gepstein and Thimann, 1980), which are metabolized to obtain xanthoxin by the 9-*cis*-epoxycarotenoid dioxygenase (NCED) enzyme (Schwartz et al., 1997). Xanthophylls, besides being the precursors of ABA, are involved in the protection of the photosynthetic apparatus carrying out the process known as the xanthophyll cycle, which helps dissipate excess energy in the chloroplast through thermal dissipation (Thiele and Krause, 1994). On the other hand, cytokinins (CKs) play an antagonistic role to ABA in regulating leaf senescence. They have been reported to inhibit chloroplast degradation in senescent leaves, as they promote plant vigor and cellular division therefore delaying leaf senescence (Joshi et al., 2019). Furthermore, cytokinins regulate nutrient recycling during leaf senescence by participating in the establishment of source–sink relations; the contents of this phytohormone decrease as senescence progresses in leaves, while they are present at high concentrations in sink tissues during nutrient mobilization from sources (senescing leaves) to sinks (roots, storage organs, or reproductive tissues; Roitsch and Ehneß, 2000).

Iris pseudacorus L. is an angiosperm that grows in habitats with high soil water content. Its roots are usually submerged in water, and leaves emerge from the surface. Due to its low prevalence in high-altitude regions, *I. pseudacorus* is believed to be sensitive to low temperatures (Sutherland, 1990). When temperatures start to decline, *I. pseudacorus* starts a process of leaf senescence which culminates in December–January. At the beginning of spring, leaves regrow from the rhizome, which is a very desiccation-tolerant tissue (Washington State Noxious Weed Control Board, 2013). Given that, to the best of our knowledge, the literature describing leaf senescence processes at a whole-plant level in wetland plants is very scarce, we aimed to elucidate how *I. pseudacorus* regulates the senescence process that its leaves undergo during the last months of the year, while describing the intertwined physiological response of non-photosynthetic underground tissues. Particular attention was put on rhizomes, which specifically are those organs staying viable through winter and, when spring arrives, start the process of leaf regrowth, thus allowing perenniality and most importantly plant survival during winter.

MATERIALS AND METHODS

Study Species and Experimental Design

Iris pseudacorus L., or yellow flag, is an angiosperm with stiff and erect leaves that emerge from the water. It mainly inhabits water communities, and it can be found both with its leaves partially submerged in the water or growing in the banks of water masses. It is considered as a plant with great invasive potential, since it spreads with ease both through its seeds and *via* vegetative propagation through its rhizomes, which can range from 1 cm to 4 cm in diameter and form thickets that hinder the growth of other species' seedlings (Sutherland and Walton, 1990). *Iris pseudacorus* leaves undergo a senescence process that culminates during the winter and, later, in the early spring, new leaves re-grow from the rhizome, which remains as a perennial subterranean organ. Flowering occurs in May–June, resulting in bright yellow flowers.

An experiment with *I. pseudacorus* L. growing under natural conditions in the wetlands located in the lake *Estany de Vilaüt* (42.283 N, 3.117E; **Figure 1A**), in the province of Girona, Catalonia, Spain, was conducted during later autumn and the beginning of winter 2020, a period of the year characterized by marked phenological changes associated with cold-induced leaf senescence. This location is characterized by mild winters, with minimum registered temperatures of 0 and −1°C in November and December (and minimum average monthly temperatures were of 7 and 3°C in November and December, respectively, **Figure 1B**). Climatic data for 2020 were provided by the *Servei Meteorològic de Catalunya*, recorded at the closest meteorological station to the study site, located near *Castelló d'Empúries* (42.260 N, 3.074E). To study the processes regulating leaf senescence in response to cold stress at a whole-plant level, two samplings were conducted during November and December 2020. The first sampling was conducted on November 30, 2020, and the temperature recorded at the time of sampling was 16.9°C, with a photosynthetic photon flux density (PPFD) of 1,283 µmol/m^2s, a relative humidity (RH) of 70.1%, and water temperature of 14.3°C. The second sampling was conducted on December 22, 2020, and at the time of sampling the temperature was 14.6°C, with a PPFD of 1,200 µmol/m^2 s, a RH of 63.6, and 12.9°C water temperature (**Figure 1C**). Both samplings were conducted at solar midday to ensure comparable responses.

A

B

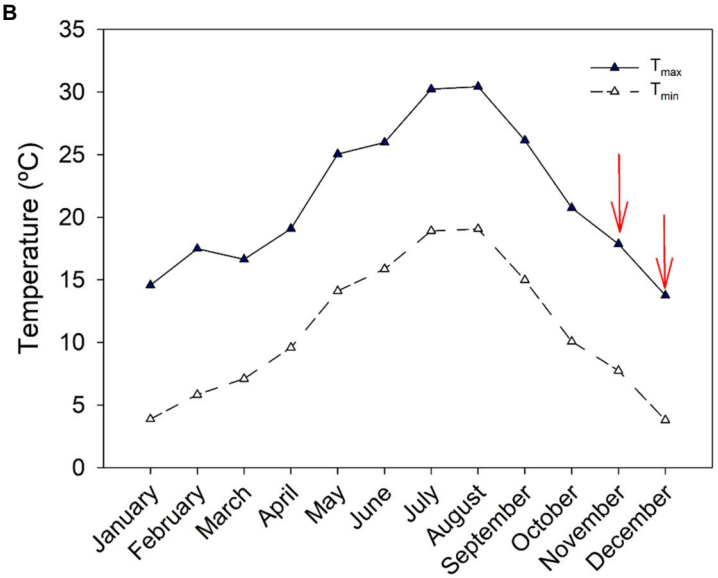

C

Sampling day	Temperature (ºC)	Relative Humidity (%)	PPFD (µmol/m²*s)	Water temperature (ºC)
t_1 (30/11/2020)	16,9	70,1	1283	14,03
t_2 (22/12/2020)	14,6	63,6	1200	12,85

FIGURE 1 | Ecosystem description and climatological data from the study site. **(A)** Image taken from the study site at *Estany de Vilaüt* (42.283 N, 3.117E) located in the northeast of Catalonia, Spain. *Iris pseudacorus* mats can be seen in the water. **(B)** Maximum and minimum average monthly temperatures during 2020 recorded by the *Servei Meteorològic de Catalunya* meteorological station located closest to the study site, in *Castelló d'Empúries* (42.260 N, 3.074E). **(C)** Temperature, relative humidity (RH), photosynthetic photon flux density (PPFD), and water temperature at midday during the two sampling days (November 30 and December 22, 2020) recorded at the site of study.

In each sampling, 12 homogenous *I. pseudacorus* L. mature individuals were randomly selected and sampled. Two leaves were selected for each individual based on their phenotype: a senescent leaf (SL) and a non-senescent one (NSL; **Figure 2**). For each leaf type, a sample was immediately frozen in liquid nitrogen and then stored at −80°C until the biochemical analysis, and another one was used to assess physiological parameters such as F_v/F_m and relative leaf water content (RWC). Additionally, samples from subterranean organs were collected, including both the rhizome, henceforth called "rhizome," and the root system, from now on called "root" (see **Figure 2**). A sample from each organ was

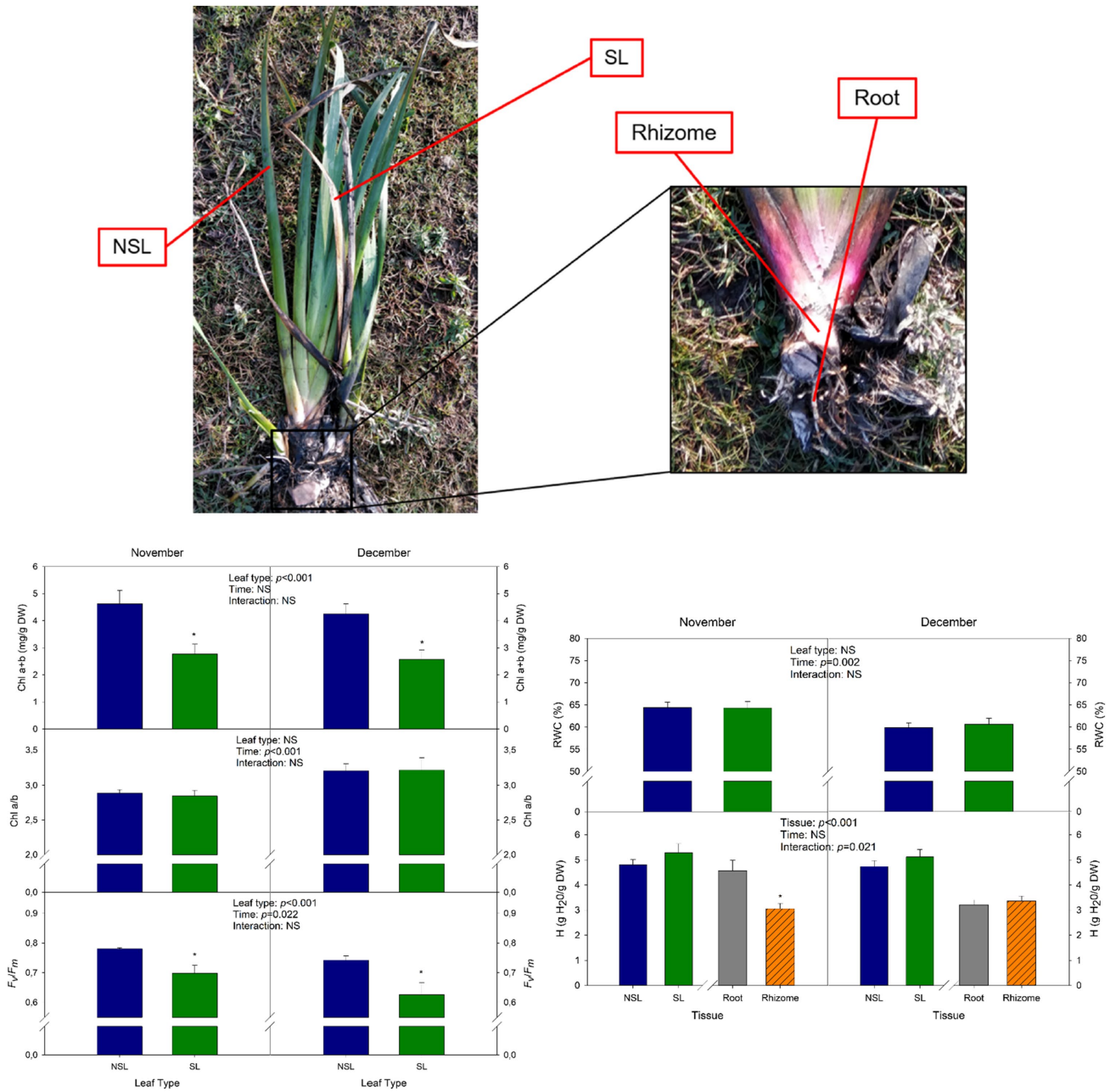

FIGURE 2 | Cold stress-induced leaf senescence in *Iris pseudacorus* individuals at the start of winter. Phenotype of senescent leaves (SLs) and non-senescent leaves (NSLs) sampled in this study, with a close-up of a rhizome and the root system of *I. pseudacorus*. Total chlorophyll contents (Chl a + b), chlorophyll a-to-b ratio (Chl a/b), and maximum efficiency of PSII (*Fv/Fm*) of SL and NSL leaves sampled in November and December. The relative water content (RWC) of SLs and NSLs, and the hydration (H) of SLs, NSLs, roots, and rhizomes are also shown. Values of *p* from the two-way mixed factorial analysis are shown in the inlets, including the factor *Time*, *Leaf type/Tissue*, and their interaction. An asterisk indicates differences between leaf types or root tissue types. Data show the mean ± SE of $n = 12$ individuals. NSL, non-senescent leaf; SL, senescent leaf.

frozen in liquid nitrogen as described before, and another one was used for the determination of physiological parameters such as the water content.

The physiological parameters assessed for each leaf were RWC, hydration (H), and maximum efficiency of PSII (F_v/F_m); and for the non-photosynthetically active organs (rhizome and root), hydration (H) was determined. The biochemical parameters analyzed were the chlorophyll, carotenoid, and hormone contents.

Water Contents and F_v/F_m Ratio

Relative water content was determined as (FW−DW)/(TW−DW) × 100, where FW means fresh weight, TW means turgid

weight and was measured after 24 h submerged in water at 4°C, and DW means dry weight and was obtained by oven-drying at 70°C until constant weight. Hydration was calculated as (FW−DW)/DW. The maximum efficiency of PSII (F_v/F_m) was measured in dark-adapted leaves using a portable chlorophyll fluorimeter (Mini-PAM II Photosynthesis Yield Analyser, Walz, Germany).

Chlorophyll Contents

Fifty micrograms of leaf sample were ground in liquid nitrogen and extracted with 0.5 ml of cold methanol with 0.01% butylated hydroxytoluene (BHT), using ultrasonication for 30 min (Bransonic ultrasonic bath 2800, Emerson Industrial, Danbury, CT, United States) and vortexing before and after ultrasonication. Afterward, extracts were centrifuged for 10 min at 13,000 rpm and 4°C (centrifuge MR18-22, Jouan, Saint-Herblain, France), and the supernatant was collected. The pellet was re-extracted twice with 0.5 ml of methanol as described before, and the supernatants were pooled, equating to a final extract volume of 1.5 ml. Then, samples were filtered using 0.22-μm PTFE filters (Phenomenex, Torrance, CA, United States). Before spectrophotometric analysis, samples were diluted 1:10 (v/v) with pure methanol and absorbances were then read at 470, 653, 666, and 750 nm using an UV/visible spectrophotometer (Shimadzu UV-160A, Shimadzu, Kyoto, Japan), and chlorophyll contents were calculated using the equations described in Lichtenthaler and Wellburn (1983).

Carotenoid Contents Determination

The quantification of carotenoids was carried out by HPLC as described in Munné-Bosch and Alegre (2000). Briefly, the extraction was carried out as described in the previous section, using methanol with 0.01 BHT as solvent. Samples were injected into reverse-phase HPLC, separated using a binary-solvent gradient (A: acetonitrile/methanol, 85:15, v/v; B: methanol/ethyl acetate, 68:32, v/v) and quantified with a diode array detector at 445 nm. The de-epoxidation state (DPS) of the xanthophyll cycle was calculated as follows: DPS = (Zx + 0.5Ax)/(Vx + Ax + Zx) (Thayer and Björkman, 1990).

Determination of Phytohormones

Phytohormone contents (ABA, *t*-Z, IPA, 2-IP, ZR, GA_1, GA_3, GA_4, and GA_7) were determined by UPLC-MS/MS as described in Müller and Munné-Bosch (2011). The extraction was carried out as described in the previous section, with the addition of deuterium-labeled internal standards at the beginning of the process. Quantification was carried out using the recovery rate of the labeled hormones and by the construction of calibration curves for each analyte. To do so, the software Analyst (Applied Biosystems, Inc., California, United States) was used.

Statistical Analyses

A two-way mixed factorial analysis was conducted to assess the effects "*Time*" and "*Leaf type*" or "*Tissue*" depending on the comparison being performed. To assess the differences between the two types of leaves (non-senescent vs. senescent leaf) and between the two types of subterranean organs (root, rhizome), Tukey's *post-hoc* tests were carried out (*agricolae* package). Data were tested for homoscedasticity of variances using the Bartlett test and for normality using the Shapiro–Wilk test. For the data not in compliance with said conditions, the non-parametrical factorial analysis method *ART* (*ARTool* package) was used (Wobbrock et al., 2011). All data are represented as mean ± SE. Differences are considered statistically significant if $p < 0.05$. All statistical analyses were performed using the R statistical software (R Foundation for Statistical Computing, Vienna, Austria).

RESULTS

Low Temperature Induces Leaf Senescence in *Iris pseudacorus*

To describe the process of senescence that leaves of *I. pseudacorus* growing under natural conditions undergo in response to low temperatures, two leaves were selected per individual during November: one with a non-senescent phenotype, which was used as a control, and one with a senescent phenotype (**Figure 2**). The F_v/F_m showed a decrease between the non-senescent leaf (NSL, control) and the senescent leaf (SL) in November, with a mean value under 0.75 for the latter (0.699; **Figure 2B**). F_v/F_m further decreased to 0.633 for the SL in December, consistent with the decrease in temperatures experienced with the onset of winter, as both the maximum and minimum monthly temperatures registered by the closest meteorological station (**Figure 1B**) and the air and water temperatures measured on site declined in December compared to November (**Figure 1C**). Total chlorophyll contents (Chl a + b) showed a similar pattern. In November, Chl a + b contents in NSL were 45% higher than those of SL. In December, the same pattern occurred (40% decrease between leaf types), but there were not any significant differences due to *Time* (**Figure 2B**). The senescence phenotype did not affect the chlorophyll a-to-b ratio (Chl a/b), as values were very similar between NSL and SL (2.89 and 2.84, respectively). However, in December Chl a/b increased, suggesting that, together with the results from F_v/F_m, individuals were suffering more stress and leaves showed a more advanced senescent stage in December compared to November (**Figure 2B**).

Regarding the water status of *I. pseudacorus* leaves, there were no differences between NSL and SL neither in November nor in December. However, a significant decrease due to the *Time* factor was observed, as RWC decreased by 7% in the NSL group and by 6% in SLs in December compared to November. There were no significant differences in H between leaf types neither in November ($p = 0.257$ for the post-hoc analysis) nor in December ($p = 0.327$). However, it is noteworthy that, in November, rhizomes showed significantly lower H than the root, yet in December both organs showed similar H (**Figure 2C**). Visual observations revealed that there was no re-greening of senescing leaves after winter stress and all aboveground organs in the next season were new sprouts.

ABA Contents Increase in Senescing Leaves and in Rhizomes

Abscisic acid levels in the senescent leaf group were 73 and 75% higher than in the non-senescent one in November and December, respectively. The highest ABA contents recorded in this study belong to the SL from individuals sampled in November, with 3.6 nmol/g DW (**Figure 3**). As it can be seen in **Figure 3**, neoxanthin contents (Nx), an ABA precursor, did not vary significantly either between leaf types or times. However, values for the SL group tended to be lower than those of NSLs in average. Contrastingly, violaxanthin contents (Vx), another precursor of ABA biosynthesis, decreased in SL compared to NSL, by 50% in November and by 44% in December (**Figure 3**). The de-epoxidation state of the xanthophyll cycle (DPS), a parameter that quantifies the conversion of violaxanthin (Vx) to antheraxanthin (Ax) and zeaxanthin (Zx), was significantly higher in SL compared to NSL. Furthermore, there was a significant decrease due to *Time*, which is consistent with a more advanced senescent stage (**Figure 3**). Most notably, Ax and Zx contents, the de-epoxidated forms of the xanthophyll cycle, did not vary between both leaf types, thus indicating that the increase in DPS was caused by a decrease in Vx rather than by an increase of either Ax or Zx.

Rhizomes showed significantly higher ABA content compared to roots (**Figure 3**). This organ showed the highest mean values recorded in the experiment, with 1.2 nmol/g DW in December. HPLC quantification of carotenoids in roots and rhizomes showed that contents for these compounds were not detectable (data not shown), thus indicating that ABA accumulation in these tissues may not occur due to local synthesis from xanthophylls.

Cytokinin Contents Decrease in Response to Reduced Temperatures in Winter

To describe the last stage of the developmental program of *I. pseudacorus* leaves, we carried out a UPLC-MS/MS quantification of the contents of CKs, which have been reported to act antagonistically to ABA in regulating senescence. Total CK levels did not show variations due to the *Tissue* factor, as means for the leaves were 20.5 ng/g DW for the SL group and 31.6 ng/g DW for the NSL group, and for the subterranean organs, 34.9 ng/g DW and 31.2 for the root and rhizome, respectively (**Figure 4**). Nonetheless, levels decreased significantly in December compared to November (by 2-fold in NSL, SL, and rhizomes; and by 1.5-fold in roots), as individuals were suffering from greater stress given that temperatures declined at the start of winter. The ABA-to-CKs ratio (ABA/CKs) reflected these changes, as the ratio increased in December for the subterranean organs, reaching its maximum in rhizomes (average of 236.2). As could be expected, SL levels were higher than in NSL, despite these changes not being significant in the data from November. ABA/CKs in rhizomes were also significantly higher compared to roots (**Figure 4**).

trans-Zeatin (*t*-Z) and 2-isopentenyladenine (2-iP) are the two main active forms of CKs, and their contents are displayed in **Figure 5**. A decrease in *t*-Z can be observed between leaf types in November; however, it is not statistically significant ($p = 0.134$). Besides that, the average contents for this hormone

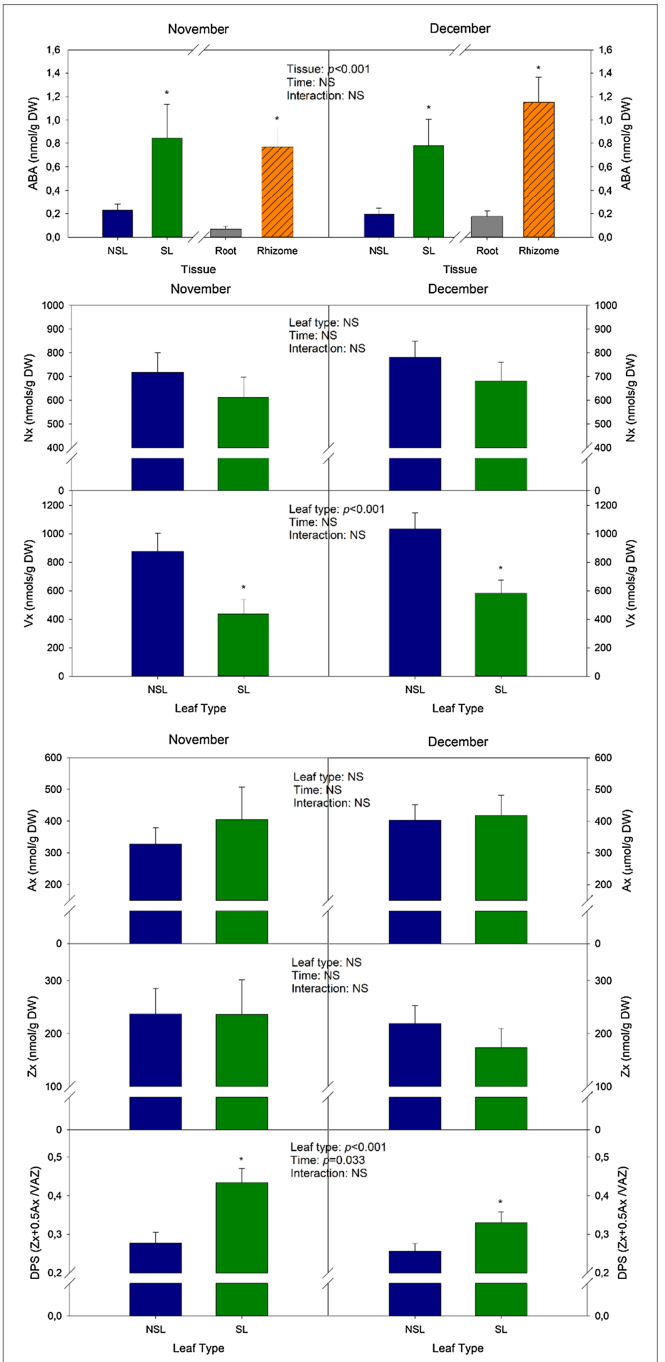

FIGURE 3 | Changes in abscisic acid (ABA) and carotenoid contents during cold-induced leaf senescence. ABA, violaxanthin (Vx), neoxanthin (Nx), antheraxanthin (Ax), zeaxanthin (Zx) contents, and the de-epoxidation state of the xanthophyll cycle (DPS) of senescent and non-senescent leaves. Values of *p* from the two-way mixed factorial analysis are shown, including the factor *Time*, *Leaf type/Tissue*, and their interaction. An asterisk indicates differences between leaf types or root tissue types. Data show the mean ± SE of $n = 12$ individuals. NSL, non-senescent leaf; SL, senescent leaf.

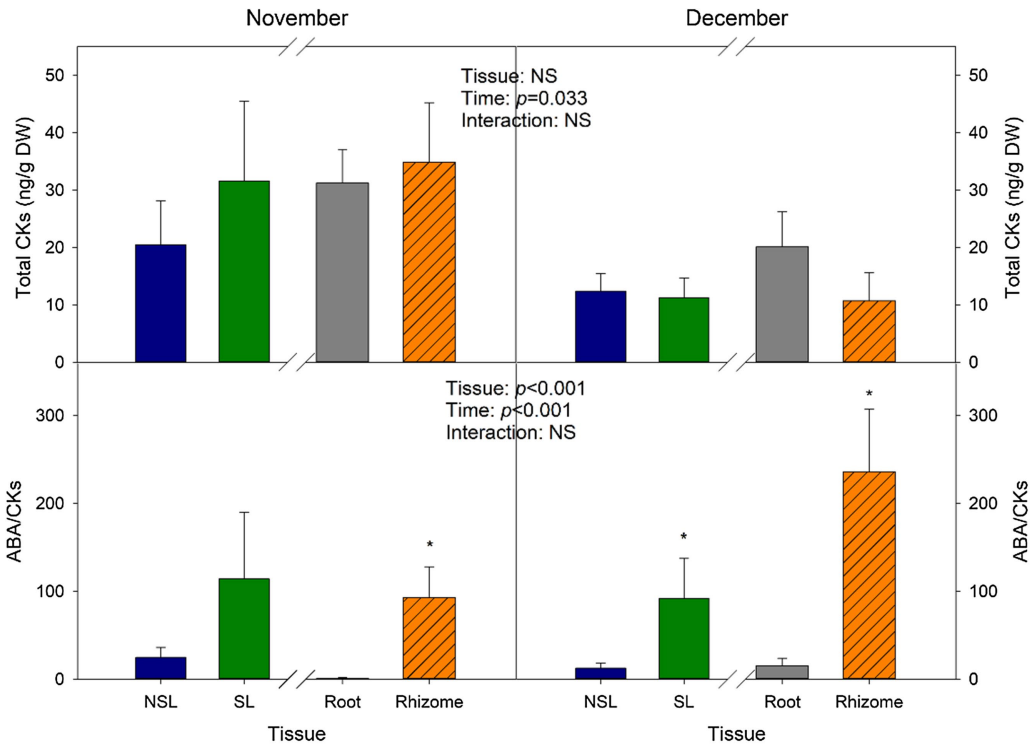

FIGURE 4 | Cytokinin variations with time and between leaf type and belowground organ type. Total cytokinin levels (Total CKs) and ABA/CKs ratio in leaves (SL, NSL) and subterranean organs (roots and rhizomes) from *I. pseudacorus* individuals growing in natural conditions. Values of *p* from the two-way mixed factorial analysis are shown, including the factor *Time*, *Leaf type/Tissue*, and their interaction. An asterisk indicates differences between leaf types or root tissue types. Data show the mean ± SE of $n = 12$ individuals. NSL, non-senescent leaf; SL, senescent leaf.

did not show many variations in *Time* or *Tissue*, as values ranged between 6 and 9 ng/g DW (**Figure 5**). However, 2-iP contents, although they ranged between 4 and 5 ng/g DW on leaves and 12 ng/g DW in subterranean organs in the samples from November, were not detectable in neither leaves nor belowground organs from December (**Figure 5**), suggesting that the decrease in temperature in this month had an effect on the content of this active CK. As for the non-active CKs, zeatin riboside (ZR) levels in roots were higher than the levels in rhizomes in both months, as rhizomes showed non-detectable contents. Contents in leaves remained low, with mean values below 3 ng/g DW (**Figure 5**). Isopentenyladenosine (iPA) showed differences caused by *Time*, since values from December were below 4.3 ng/g DW (**Figure 5**).

The ABA/GAs Ratio Increases in Rhizomes of Cold-Stressed Plants

The most abundant GA measured in rhizomes was GA_4, as contents were 20-fold higher than the other GAs (GA_1, GA_3, and GA_7). Although a trend can be observed as levels in December were lower than those of November, and rhizomes have higher contents than roots, these variations were not significant (**Figure 6**). Values for GA_4 ranged from 1,800 to 2,200 ng/g DW. GA_1 contents did not show any significant variation, although the mean in November was 92.9 ng/g DW for roots and 17 ng/g DW for rhizomes (**Figure 6**). GA_3 was the GA found in the lowest concentration, since mean values for all groups were below 30 ng/g DW. Lastly, GA_7 contents did not differ between tissues in November, but in December rhizome contents were significantly higher compared to roots (115.4 and 48.1 ng/g DW, respectively). No significant difference was observed in total GA contents (GA_{tot}) between roots and rhizomes. However, the ratio ABA/GAs in rhizomes was 93% higher than in roots, and this ratio further increased in December, as it increased by 68% in roots and by 48% in rhizomes.

DISCUSSION

Senescence represents the last phase of leaves, developmental program. It can be triggered by either internal or external factors, such as plant age or unfavorable environmental conditions. It allows plants to reallocate nutrients from photosynthetic tissues to various other organs such as younger leaves in vegetative development, or seeds during reproductive development in monocarpic plants. In perennial plants, when facing severe stress, one strategy that plants have evolved is to redistribute nutrients promoting storage in organs with meristematic tissues that remain viable and allow for regrowth once the adverse conditions are alleviated (Munné-Bosch, 2008). This is the case of *I. pseudacorus*, a perennial species that grows in wetlands and can reproduce

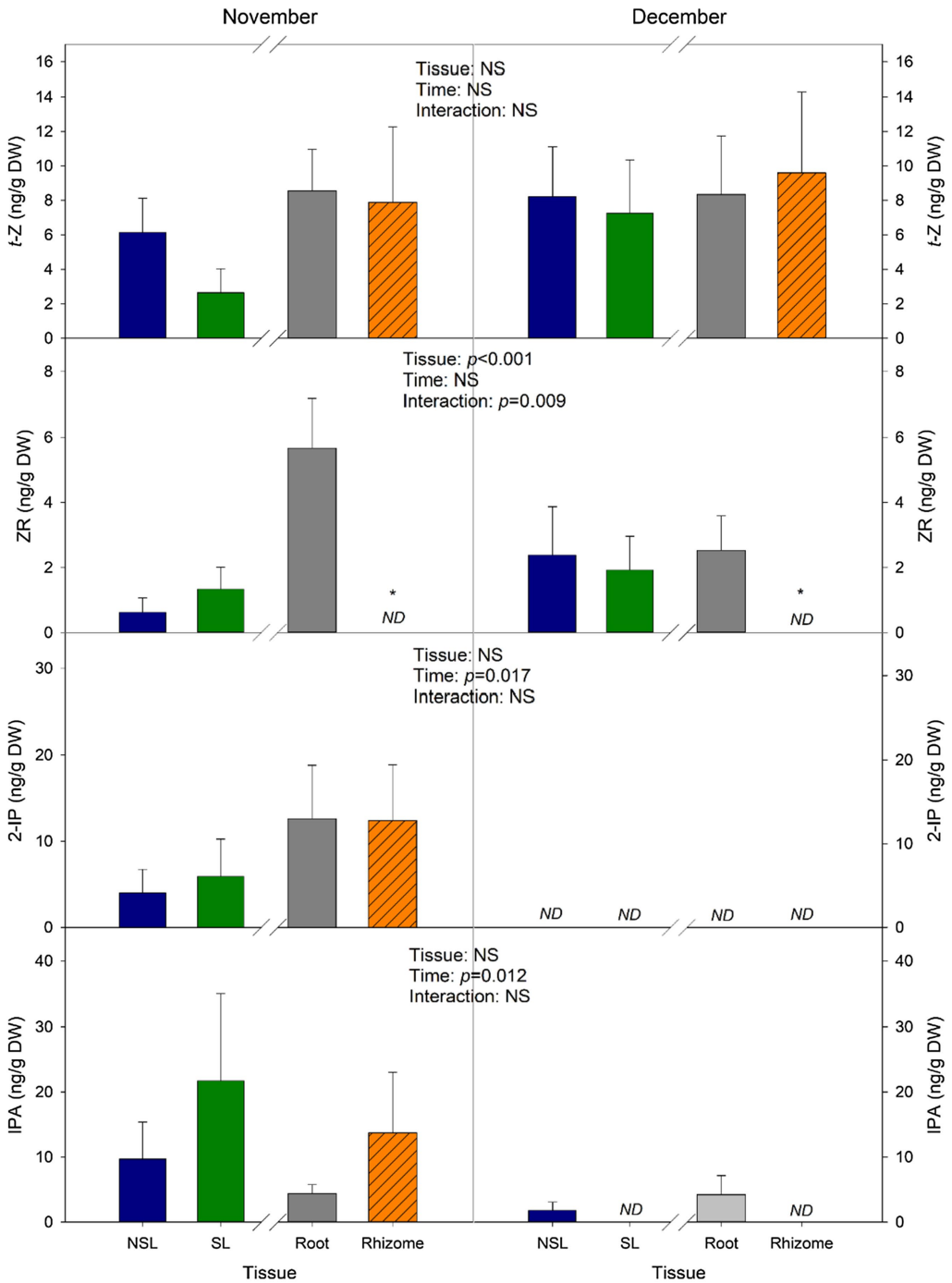

FIGURE 5 | Changes in the concentration of individual cytokinins. Measurements were performed in leaves and subterranean organs of *I. pseudacorus*. Values of *p* from the two-way mixed factorial analysis are shown, including the factor *Time*, *Leaf type/Tissue*, and their interaction. An asterisk indicates differences between leaf types or root tissue types. Data show the mean ± SE of $n = 12$ individuals. NSL, non-senescent leaf; SL, senescent leaf; 2-iP, isopentenyladenine; iPA, isopentenyladenosine; *t-Z*, *trans*-zeatin; and ZR, zeatin riboside.

vegetatively through its rhizomes. Leaf senescence is characterized by an organized and regulated dismantling of cellular structures and recycling of their components, with photosynthesis-related compounds being the first ones to be degraded (Matile et al., 1996). Therefore, photoinhibition and subsequent chlorophyll degradation are regarded as clear markers of leaf senescence. Coherently, in our study, maximum efficiency of PSII (F_v/F_m) was significantly lower in SL compared to NSL, and values declined in December, as temperatures decreased. Regarding total chlorophyll contents, a decrease of 45 and 40% was observed due to the

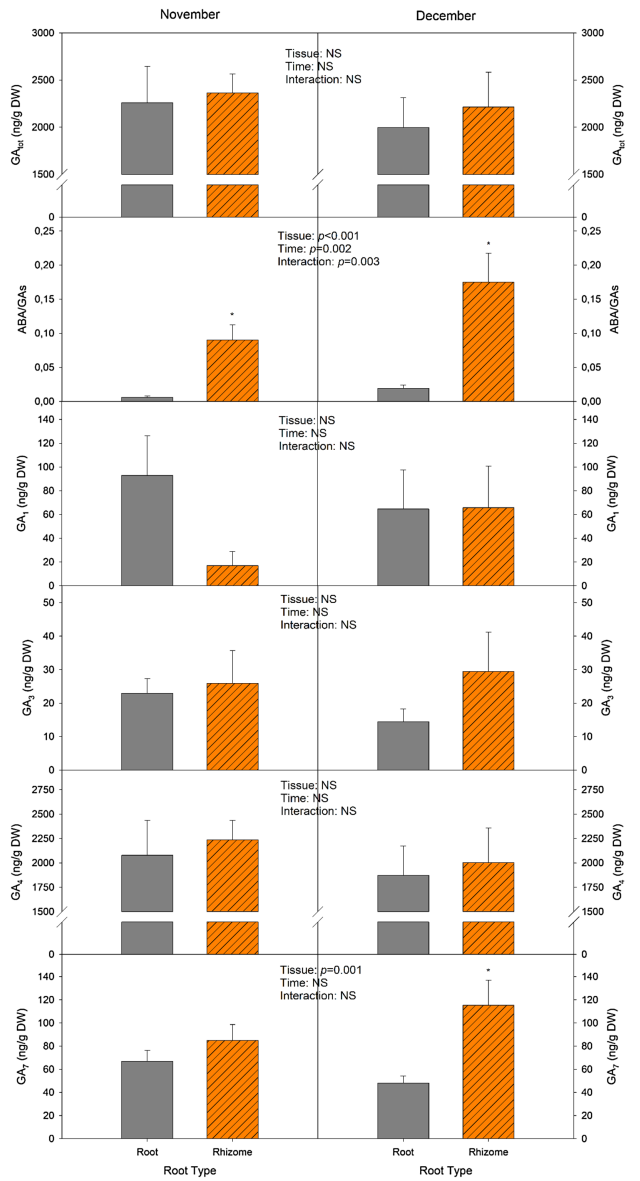

FIGURE 6 | Changes in total gibberellin (GA_{tot}) contents, ABA-to-GA ratio (ABA/GAs), and GA_1, GA_3, GA_4, and GA_7 concentrations. Measurements were performed in leaves and subterranean organs of *I. pseudacorus*. Values of *p* from the two-way mixed factorial analysis are shown, including the factor *Time*, *Leaf type/Tissue*, and their interaction. An asterisk indicates differences between leaf types or root tissue types. Data show the mean ± SE of $n = 12$ individuals. NSL, non-senescent leaf; SL, senescent leaf.

senescent phenotype in November and December, respectively. When SL from December was compared to NSL from November, which was used as controls, the Chl loss accounted for a 50%. This, together with the reduction in the F_v/F_m ratio and observational studies showing that leaves from this plant died during January, indicates a clear senescence phenotype for leaves. It is important to underline the fact that this senescent phenotype in aboveground organs does not indicate the plant as an organism was senescing, but only its aboveground organs, since rhizomes establish dormancy during winter and re-establish growth during the next spring. All aboveground organs senesce in a process mediated by low temperatures combined with reduced light intensity and changes in light quality. It should be noted that the parts of leaves closest to the rhizome were the ones experiencing an accelerated senescence phenotype, which suggests that low light intensity and an increased far red-to-red ratio may interact with low temperatures in triggering leaf senescence, as it occurs in other plant species (Lim et al., 2018).

Abscisic acid and CKs are considered to be key regulators of leaf senescence. ABA has been classically considered as a promoter of leaf senescence (Samet and Sinclair, 1980; An et al., 2021b). On the other hand, studies proving CKs involvement on inhibiting chlorophyll degradation in excised leaves date back to the 1950s (Richmond and Lang, 1957). Furthermore, treatment with a mixture of CKs (zeatin and its riboside along with others) through the xylem inhibits the degradation of photosynthetic proteins and pigments in oat and wheat seedlings (Badenoch-Jones et al., 1996). Additionally, receptors such as AHK3 and CK response factors have been identified as key regulators promoting leaf longevity in response to endogenous CK accumulation in the model plant *Arabidopsis thaliana* (Kim et al., 2006; Zwack et al., 2013). Here, we observed a significant increase in the ABA/CKs ratio in senescent leaves of *I. pseudacorus* under natural conditions, most notably during December, when mean monthly maximum and minimum air temperatures decreased around 4°C relative to values recorded 1 month earlier. ABA contents increased by 72% between leaf phenotypes in November and by 75% in December. On the other hand, consistent with the literature, total cytokinin contents were lower in December than in November. Furthermore, contents of the active CK and 2-iP were non-detectable in December. Interestingly, a recent study in another species shows that exogenous application of 2-iP is effective in delaying leaf senescence (Hallmark and Rashotte, 2020), which further supports the idea that in our study leaf senescence induced by low temperatures in winter was not only modulated by increased ABA contents, but also by reduced ABA/CKs ratios, 2-iP specifically playing a role among CKs, an aspect that deserves further studies at the molecular level.

Abscisic acid is synthesized from carotenoids by the NCED enzyme. In our study, a significant decrease in the xanthophyll, violaxanthin (Vx) was observed in senescent leaves, while neoxanthin contents did not vary, suggesting that Vx was, among these two xanthophylls in leaves, the one preferentially used for ABA synthesis. Furthermore, despite rhizome accumulating ABA, the results from HPLC carotenoid quantification in subterranean organs showed non-detectable contents of ABA precursors, which suggests a carotenoid mobilization from aboveground organs (such as leaves) towards the rhizome. A study by Manzi et al. (2016) showed the inability of detached citrus roots to accumulate ABA in response to water stress, while roots of intact plants were able to do so, suggesting that ABA accumulation in subterranean organs is dependent on aerial supply. Rhizomes showed ABA contents of 0.77 and 1.15 nmol/g DW in November and December, respectively. Given that there is no re-greening of senescing organs and all aboveground organs in the next season are new sprouts and that the rhizome is responsible for leaf regrowth in spring, ABA accumulation could be providing cold tolerance in rhizomes during

winter in *I. pseudacorus*, since it is known that this phytohormone induces the activation of the *cold-regulated* (COR) genes in *A. thaliana* in one of the most well-known cold-signaling pathways (Xiong et al., 2001).

Abscisic acid has been shown to play a key role in the regulation of dormancy of seeds, buds, bulbs, and tubers, in some cases interacting with gibberellins (Michalczuk, 2005; Pan et al., 2021), but no studies have focused thus far on the study of rhizome dormancy in wetland plants growing in their natural habitat. Furthermore, ABA is known to confer cold stress tolerance (Huang et al., 2017; An et al., 2021a), while gibberellins may even play a negative regulatory role, as shown by using gibberellin deficient mutants, which showed greater low temperature stress tolerance, as constitutive expression of cold-induced transcriptional activator *CBF1/DREB1b* conferred freezing tolerance as well as promoting DELLA protein accumulation in transgenic *A. thaliana* plants (Achard et al., 2008). In our study, ABA increased in roots, while gibberellin contents did not vary between root and rhizome nor between months. The only difference for gibberellins was observed in December, when rhizomes showed significantly higher GA_7 contents than roots. In any case, the ABA-to-gibberellin ratio was always significantly higher in rhizome than roots, indicating that increasing ABA contents may be the key to overcoming low temperatures during winter. Indeed, the ratio ABA/GAs was 93% higher in rhizomes than in roots, and it further increased in December, as this ratio increased by 68% in roots and by 48% in rhizomes. These results indicate that a steep increase in ABA coupled with constant GA levels might be involved in the ability of rhizomes to sustain potential damage stemming from low temperatures and to stay viable in order to initiate the re-growth process of leaves when conditions ameliorate during the next spring.

Altogether, results from our study suggest an interplay between leaf senescence, plant developmental program, and the stress response in yellow flag plants growing in a natural wetland, in which the hormonal response below and aboveground is finely regulated and both biochemically and physiologically interconnected at the whole-plant level. It appears that ABA plays a major role both above- and belowground, not only in the regulation of leaf senescence but also in the establishment of cold tolerance in rhizomes, two processes that appear to be intimately interconnected. As rhizomes accumulated large amounts of ABA during winter, while roots did not, and neither roots nor rhizomes accumulated 9-*cis*-epoxycarotenoids, it is possible that ABA accumulation in belowground organs results from phloem transport from senescing leaves, an aspect that requires further investigation.

DATA AVAILABILITY STATEMENT

The original contributions presented in the study are included in the article/supplementary material; further inquiries can be directed to the corresponding author.

AUTHOR CONTRIBUTIONS

VC, AC, and SM-B conceived the experiment. VC and AC performed the experiment and biochemical analyses. VC performed the statistical analyses and wrote the manuscript with the help of SM-B. All authors contributed to the article and approved the submitted version.

FUNDING

This research was supported by the Spanish Government through the PID2019-110335GB-I00 grant.

ACKNOWLEDGMENTS

We are grateful to Tania Mesa for her help in the sampling procedures and to Erola Fenollosa for her aid in the statistical analysis process. We thank Serveis Científico-Tècnics of the University of Barcelona for their assistance during the phytohormone analyses and Paula Muñoz for her assistance in the phytohormone quantification process.

REFERENCES

Achard, P., Gong, F., Cheminant, S., Alioua, M., Hedden, P., and Genschika, P. (2008). The cold-inducible CBF1 factor-dependent signaling pathway modulates the accumulation of the growth-repressing DELLA proteins via its effect on gibberellin metabolism. *Plant Cell* 20, 2117–2129. doi: 10.1105/tpc.108.058941

An, J.-P., Xu, R.-R., Liu, X., Su, L., Yang, K., Wang, X.-F., et al. (2021a). ABI4 interacts with ICE1 and JAZ proteins to regulate abscisic acid signaling-mediated cold tolerance in apple. *J. Exp. Bot.* doi: 10.1093/jxb/erab433 [Epub ahead of print].

An, J.-P., Zhang, X.-W., Liu, Y.-J., Zhang, J.-C., Wang, X.-F., You, C.-X., et al. (2021b). MdABI5 works with its interaction partners to regulate abscisic acid-mediated leaf senescence in apple. *Plant J.* 105, 1566–1581. doi: 10.1111/tpj.15132

Badenoch-Jones, J., Parker, C. W., Letham, D. S., and Singh, S. (1996). Effect of cytokinins supplied via the xylem at multiples of endogenous concentrations on transpiration and senescence in derooted seedlings of oat and wheat. *Plant Cell Environ.* 19, 504–516. doi: 10.1111/j.1365-3040.1996.tb00384.x

Daszkowska-Golec, A., and Szarejko, I. (2013). Open or close the gate—stomata action under the control of phytohormones in drought stress conditions. *Front. Plant Sci.* 4:138. doi: 10.3389/fpls.2013.00138

Fischer, A. (2012). The complex regulation of senescence. *Crit. Rev. Plant Sci.* 31, 124–147. doi: 10.1080/07352689.2011.616065

Gan, S., and Amasino, R. M. (1997). Making sense of senescence: molecular genetic regulation and manipulation of leaf senescence. *Plant Physiol.* 113, 313–319. doi: 10.1104/pp.113.2.313

Gepstein, S., and Thimann, K. V. (1980). Changes in the abscisic acid content of oat leaves during senescence. *Proc. Natl. Acad. Sci.* 77, 2050–2053. doi: 10.1073/pnas.77.4.2050

Hallmark, H. T., and Rashotte, A. M. (2020). Cytokinin isopentenyladenine and its glucoside isopentenyladenine-9G delay leaf senescence through activation of cytokinin-associated genes. *Plant Direct* 4:e00292. doi: 10.1002/pld3.292

Huang, X., Shi, H., Hu, Z., Liu, A., Amombo, E., Chen, L., et al. (2017). ABA is involved in regulation of cold stress response in Bermudagrass. *Front. Plant Sci.* 8:1613. doi: 10.3389/fpls.2017.01613

Joshi, S., Choukimath, A., Isenegger, D., Panozzo, J., Spangenberg, G., and Kant, S. (2019). Improved wheat growth and yield by delayed leaf senescence

using developmentally regulated expression of a cytokinin biosynthesis gene. *Front. Plant Sci.* 10:1285. doi: 10.3389/fpls.2019.01285

Kim, H. J., Ryu, H., Hong, S. H., Woo, H. R., Lim, P. O., Lee, I. C., et al. (2006). Cytokinin-mediated control of leaf longevity by AHK3 through phosphorylation of ARR2 in Arabidopsis. *Proc. Natl. Acad. Sci. U. S. A.* 103, 814–819. doi: 10.1073/pnas.0505150103

Lichtenthaler, H. K., and Wellburn, A. R. (1983). Determinations of total carotenoids and chlorophylls a and b of leaf extracts in different solvents. *Biochem. Soc. Trans.* 11, 591–592. doi: 10.1042/bst0110591

Lim, J., Park, J.-H., Jung, S., Hwang, D., Nam, H. G., and Hong, S. (2018). Antagonistic roles of PhyA and PhyB in far-red light-dependent leaf senescence in *Arabidopsis thaliana*. *Plant Cell Physiol.* 59, 1753–1764. doi: 10.1093/pcp/pcy153

Manzi, M., Lado, J., Rodrigo, M. J., Arbona, V., and Gómez-Cadenas, A. (2016). ABA accumulation in water-stressed citrus roots does not rely on carotenoid content in this organ. *Plant Sci.* 252, 151–161. doi: 10.1016/j.plantsci.2016.07.017

Masclaux-Daubresse, C., Purdy, S., Lemaitre, T., Pourtau, N., Taconnat, L., Renou, J.-P., et al. (2007). Genetic variation suggests interaction between cold acclimation and metabolic regulation of leaf senescence. *Plant Physiol.* 143, 434–446. doi: 10.1104/pp.106.091355

Matile, P., Hortensteiner, S., Thomas, H., and Krautler, B. (1996). Chlorophyll breakdown in senescent leaves. *Plant Physiol.* 112, 1403–1409. doi: 10.1104/pp.112.4.1403

Michalczuk, L. (2005). Hormonal control of dormancy. *Int. J. Fruit Sci.* 5, 59–73. doi: 10.1300/J492v05n01_06

Müller, M., and Munné-Bosch, S. (2011). Rapid and sensitive hormonal profiling of complex plant samples by liquid chromatography coupled to electrospray ionization tandem mass spectrometry. *Plant Methods* 7:37. doi: 10.1186/1746-4811-7-37

Munné-Bosch, S. (2008). Do perennials really senesce? *Trends Plant Sci.* 13, 216–220. doi: 10.1016/j.tplants.2008.02.002

Munné-Bosch, S., and Alegre, L. (2000). Changes in carotenoids, tocopherols and diterpenes during drought and recovery, and the biological significance of chlorophyll loss in Rosmarinus officinalis plants. *Planta* 210, 925–931. doi: 10.1007/s004250050699

Munné-Bosch, S., and Alegre, L. (2004). Die and let live: leaf senescence contributes to plant survival under drought stress. *Funct. Plant Biol.* 31, 203–216. doi: 10.1071/FP03236

Novák, J., Cerny, M., Roignant, J., Skalak, J., Saiz-Fernández, I., Luklova, M., et al. (2021). Limited light intensity and low temperature: can plants survive freezing in light conditions that more accurately replicate the cold season in temperate regions? *Environ. Exp. Bot.* 190:104581. doi: 10.1016/j.envexpbot.2021.104581

Pan, W., Liang, J., Sui, J., Li, J., Liu, C., Xin, Y., et al. (2021). ABA and bud dormancy in perennials: current knowledge and future perspective. *Gene* 12:1635. doi: 10.3390/genes12101635

Richmond, A. E., and Lang, A. (1957). Effect of kinetin on protein content and survival of detached xanthium leaves. *Science* 125, 650–651. doi: 10.1126/science.125.3249.650-b

Roitsch, T., and Ehneß, R. (2000). Regulation of source/sink relations by cytokinins. *Plant Growth Regul.* 32, 359–367. doi: 10.1023/A:1010781500705

Samet, J. S., and Sinclair, T. R. (1980). Leaf senescence and abscisic acid in leaves of field-grown soybean. *Plant Physiol.* 66, 1164–1168. doi: 10.1104/pp.66.6.1164

Schwartz, S. H., Tan, B. C., Gage, D. A., Zeevaart, J. A. D., and McCarty, D. R. (1997). Specific oxidative cleavage of carotenoids by VP14 of maize. *Science* 276, 1872–1874. doi: 10.1126/science.276.5320.1872

Sutherland, W. J. (1990). Iris Pseudacorus L. *J. Ecol.* 78:833. doi: 10.2307/2260902

Sutherland, W. J., and Walton, D. (1990). The changes in morphology and demography of Iris pseudacorus L. at Different Heights on a saltmarsh. *Funct. Ecol.* 4:655. doi: 10.2307/2389733

Thayer, S. S., and Björkman, O. (1990). Leaf xanthophyll content and composition in sun and shade determined by HPLC. *Photosynth. Res.* 23, 331–343. doi: 10.1007/BF00034864

Thiele, A., and Krause, G. H. (1994). Xanthophyll cycle And thermal energy dissipation In photosystem II: relationship between zeaxanthin formation, energy-dependent fluorescence quenching and Photoinhibition. *J. Plant Physiol.* 144, 324–332. doi: 10.1016/S0176-1617(11)81194-6

Washington State Noxious Weed Control Board (2013). Written findings of the Washington State Noxious Weed Control Board. Available at: http://nas.er.usgs.gov/plants/docs/ir_pseud.htm (Accessed June 7, 2021).

Welti, R., Li, W., Li, M., Sang, Y., Biesiada, H., Zhou, H. E., et al. (2002). Profiling membrane lipids in plant stress responses: role of phospholipase Dα in freezing-induced lipid changes in arabidopsis. *J. Biol. Chem.* 277, 31994–32002. doi: 10.1074/jbc.M205375200

Wobbrock, J. O., Findlater, L., Gergle, D., and Higgins, J. J. (2011). "The Aligned Rank Transform for nonparametric factorial analyses using only ANOVA procedures." in *Conference on Human Factors in Computing Systems—Proceedings*; May 7–12, 2011; 143–146.

Xiong, L., Ishitani, M., Lee, H., and Zhu, J.-K. (2001). The Arabidopsis LOS5/ABA3 locus encodes a molybdenum cofactor sulfurase and modulates cold stress– and osmotic stress–responsive gene expression. *Plant Cell* 13, 2063–2083. doi: 10.1105/tpc.010101

Zwack, P. J., Robinson, B. R., Risley, M. G., and Rashotte, A. M. (2013). Cytokinin response factor 6 negatively regulates leaf senescence and is induced in response to cytokinin and numerous abiotic stresses. *Plant Cell Physiol.* 54, 971–981. doi: 10.1093/pcp/pct049

Conflict of Interest: The authors declare that the research was conducted in the absence of any commercial or financial relationships that could be construed as a potential conflict of interest.

Publisher's Note: All claims expressed in this article are solely those of the authors and do not necessarily represent those of their affiliated organizations, or those of the publisher, the editors and the reviewers. Any product that may be evaluated in this article, or claim that may be made by its manufacturer, is not guaranteed or endorsed by the publisher.

Advantages of publishing in Frontiers

OPEN ACCESS
Articles are free to read for greatest visibility and readership

FAST PUBLICATION
Around 90 days from submission to decision

HIGH QUALITY PEER-REVIEW
Rigorous, collaborative, and constructive peer-review

TRANSPARENT PEER-REVIEW
Editors and reviewers acknowledged by name on published articles

Frontiers
Avenue du Tribunal-Fédéral 34
1005 Lausanne | Switzerland

Visit us: www.frontiersin.org
Contact us: frontiersin.org/about/contact

REPRODUCIBILITY OF RESEARCH
Support open data and methods to enhance research reproducibility

DIGITAL PUBLISHING
Articles designed for optimal readership across devices

FOLLOW US
@frontiersin

IMPACT METRICS
Advanced article metrics track visibility across digital media

EXTENSIVE PROMOTION
Marketing and promotion of impactful research

LOOP RESEARCH NETWORK
Our network increases your article's readership